Siegfried Peer
Hannes Gruber
Editors

Atlas of Peripheral Nerve Ultrasound

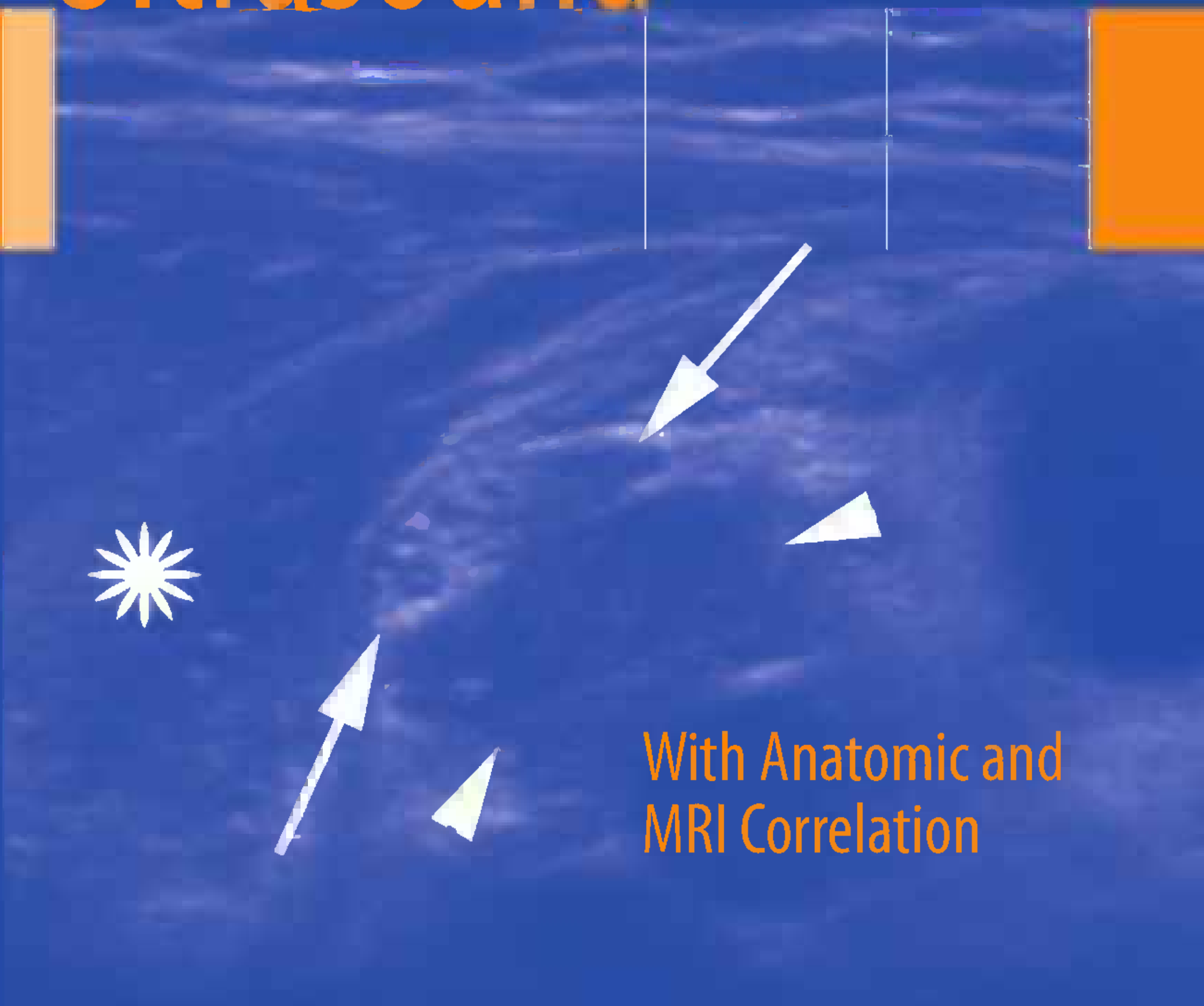

With Anatomic and MRI Correlation

Springer

Atlas of Peripheral Nerve Ultrasound

Siegfried Peer • Hannes Gruber
Editors

Atlas of Peripheral Nerve Ultrasound

With Anatomic and MRI Correlation

Springer

Editors
Siegfried Peer
CTI GesmbH
Klostergasse 4
Innsbruck
Austria

Hannes Gruber
Department of Radiology
Innsbruck Medical University
Innsbruck
Austria

ISBN 978-3-642-25593-9 ISBN 978-3-642-25594-6 (eBook)
DOI 10.1007/978-3-642-25594-6
Springer Heidelberg New York Dordrecht London

Library of Congress Control Number: 2013931946

Printed on acid-free paper

Springer is part of Springer Science+Business Media (www.springer.com)

Preface

The first publication on peripheral nerve ultrasound dates back to 1988 with Bruno Fornage's article *Peripheral nerves of the extremities: Imaging with US* published in Radiology. Afterwards peripheral nerve ultrasound has been performed only by very few specialists around the world. During the last years, we have seen a tremendous increase of publications concerning diagnostic and interventional sonography of the peripheral nervous system, especially the technique of sonography-guided regional anesthesia, and pain therapy is getting widespread acceptance.

Especially the latter applications of sonography ask for a profound knowledge of the local topographic anatomy of peripheral nerves. The local topography often is rather complex. As peripheral nerves are small structures, typical landmarks may help to find them with sonography. The same is true for MRI, which is the second imaging modality for diagnosis of peripheral nerve disease.

For daily clinical practice, a resource, which offers side by side presentation of topographic anatomy with correlative sonograms and MR images, allows for quick recapitulation of typical regional features. This is important to succeed with peripheral nerve diagnosis and intervention. Like our old anatomy teacher always said: “doctors without knowledge of anatomy are like moles, they roam in the dark and their daily task are piles of soil!” To prevent that, we provide you with this book, which is based on our extensive experience in nerve imaging.

Innsbruck, Austria — Siegfried Peer, Hannes Gruber

How to Use This Book

Why an *Atlas of Peripheral Nerve Ultrasound*? Well actually there are two reasons: first, until now a book like that simply did not exist. Second, during congresses, seminars, and workshops, we were often asked by participants "How do you do that," "I simply don't get the results, you achieve, when imaging nerves with ultrasound," and "How can I become more efficient in sonography of the peripheral nerve?" Well, probably the best thing is to attend a dedicated workshop and to volunteer in a department, where peripheral nerve ultrasound is done, but what, if in your area a possibility like that simply does not exist? In addition people attending workshops still tell us "once I am at home things do not turn out that easy, when I am confronted with an individual patient!" This is the most important reason why we decided to provide you with this atlas.

What this atlas is not: it is not an attempt to show you sonography of *all* peripheral nerves and especially not how to perform peripheral nerve intervention. This atlas covers the nerves which allow for diagnostic ultrasound, and this is a huge difference. While you may, for example, perform ultrasound-guided intervention of the third occipital nerve, this nerve is hardly affected by pathological changes, which may be diagnosed with ultrasound, and therefore it is not covered in this atlas. Peripheral nerve intervention may often be achieved based on landmark techniques, without visualizing the nerve itself – think of infiltration of lumbar spinal nerve roots! So if you are interested in interventional procedures, please refer to other textbooks, like the *Atlas of Ultrasound Guided Procedures in Interventional Pain Management* by Samer Narouze et al., which is highly recommendable.

What this atlas should be: an up-to-date source on diagnostic strategies for identification and diagnosis of peripheral nerves with ultrasound. The format of this atlas relies on our concept of "landmark-based imaging" of peripheral nerves: nerves are complex structures and travel a long way before reaching their end organ. Along a nerve's course, there may be segments, where it is very difficult to identify because of a complicated local anatomical situation. In the case of coexisting hematoma or edema, identification may sometimes be nearly impossible. But the good news is: for every nerve certain regions exist, where the local anatomy is very typical and the nerve is more easily identified due to its intimate relationship with surrounding "landmarks" such as bony ridges, muscles, tendons, and vascular structures. This atlas is organized according to these typical anatomical regions and provides a set of four images for every typical nerve topography: a photograph showing how to

place the transducer in order to see the structures in the corresponding ultrasound image, an anatomical cross section, and T1-weighted MR image in the same plane with the ultrasound scan. These images are exclusively oriented in a strictly transverse orientation to make them easier to understand compared with more complex oblique or longitudinal planes. Remember the focus of this atlas is to help you identify the nerve! Once you did that, a more oblique scan plane together with additional longitudinal imaging may sometimes be more suited for diagnostic evaluation of the nerve! We decided to put all the anatomical labeling exclusively on the anatomical cross section and only mark the nerve in the ultrasound and MRI in order to have you visually compare the structures in the images with the anatomical cross section, which asks your brain to work and as we believe enhances visual learning. In addition to this set of four images, on every page – which is dedicated to one nerve in one typical anatomical region – we provided one or two extra images, which may either be an additional longitudinal or panoramic sonogram of a normal nerve or a sonogram of a typical disease process such as compression neuropathy!

We hope this format achieves what it was designed for: to enable you with a "how to find the nerve guide" according to the individual need of your patients.

Acknowledgement

A book like this would not be possible without the help of a lot of people. Apart from the authors several colleagues contributed substantially and shall not go unmentioned.

Our special thanks goes to the Innsbruck Medical University Department of Anatomy, Histology and Embryology (chairwoman Prof. Dr. Helga Fritsch) Section for Clinical and Functional Anatomy for provision of the human corpse and the anatomical cross sections, in particular Gottfried Gstrein and Rupert Gstrein (autopsy assistants, production of cross sections), Romed Hörmann (photography), and Assistant Professor Dr. Karl-Heinz Künzel M.D. (anatomical advice). In this context, we also like to express our appreciation for all the people who donate their body for scientific studies. Without them basic medical education and research, as well as works like this, would not be possible.

Thanks to the Innsbruck Medical University Department of Radiology (chairman Prof. Dr. Werner Jaschke) for provision of all the sonographic and MRI images, the radiology technicians, who helped in the production of MRIs, and in particular Ingrid Messirek (photography).

The staff of Springer Verlag, Heidelberg, Germany, with excellent collaboration in editing, layout, and production. In particular Mrs. Corinna Schäfer, Associate Editor Clinical Medicine, for her help with all matters of communication and production, as well as Dr. Ute Heilmann, Editorial Director Clinical Medicine, for her trust in our work.

Contents

1 Introduction to High-Resolution Sonography of the Peripheral Nervous System: General Considerations and Examination Technique

Siegfried Peer

Contents

S. Peer
CTI GesmbH,
Klostergasse 4, 6020 Innsbruck, Tyrol, Austria
e-mail: info@siegfried-peer.at

Sonography of the peripheral nerve is not essentially new. As early as 1988, Bruno Fornage reported on the feasibility of peripheral nerve imaging (Fornage 1988). The progress of nerve sonography in the subsequent years, however, was slow, and this was mainly due to the fact that nerves are small structures and were not easy to approach with the then available technique. The lacking of high-resolution transducers was the main problem and therefore it took until the late 1990s and the first years of the new millennium for sonography of the peripheral nerve to experience a real boost, which still continues. While in the early era of peripheral nerve sonography actually only freaky guys were focusing on the then exotic area of nerve imaging – there were only very few groups worldwide really devoted to nerve sonography, such as the group around Carlo Martinoli and Stefano Bianchi in Genova, Italy, Leo Visser and Roy Beekman in the Netherlands, and our group in Innsbruck, Austria – meanwhile we experience a rising interest in peripheral nerve sonography from radiologists, neurologists, and anesthesiologists alike. This explosion of nerve sonography is also due to the fact that the unexpected technical progress of ultrasound scanners, transducers, and software development is amazing. Again, peripheral nerves are small and topographically complex structures and therefore a certain arsenal of tools is important to achieve constant high quality in diagnostic and interventional nerve ultrasound.

S. Peer, H. Gruber (eds.), *Atlas of Peripheral Nerve Ultrasound*,
DOI 10.1007/978-3-642-25594-6_1, © Springer-Verlag Berlin Heidelberg 2013

1.1 Ultrasound Scanner Hardware and Software Requirements

In the following sections, I will provide a two-level recommendation on the technical requirements for nerve sonography: one for the practitioner, who likes to integrate nerve sonography into his toolbox for examining the most common peripheral nerve pathologies, such as compression neuropathies, and one for the dedicated specialist, who is interested in imaging of smaller nerves, more complex pathologies (nerve trauma, inflammatory conditions), or ultrasound-guided intervention in the peripheral nervous system.

1.1.1 Hardware

I will not comment on the type of ultrasound scanner to be used, because there is a competition among the companies and many of them provide a top of the notch machine, which enables for high-end sonographic imaging. The choice of scanner therefore is open to personal preferences in terms of ergonomics and design. One thing to mention, however, is the general availability of fine portable ultrasound systems such as the Philips CX50 (Philips Healthcare) (Fig. 1.1a). While in the past many of these small systems were lacking software for high-resolution imaging or were not working with some high-resolution transducers, this has changed a lot during the last years. There are systems for the more generally

Fig. 1.1 (**a**) The Philips CX50 portable ultrasound system is one of the currently available high-quality systems especially suited for the guidance of nerve blocks and pain treatment. (**b**) The Philips Sparq ultrasound system, a very versatile point of care system, designed with an intuitive dynamic interface that eliminates knobs or buttons and a sealed, easy-to-clean, tempered glass control panel to facilitate disinfecting

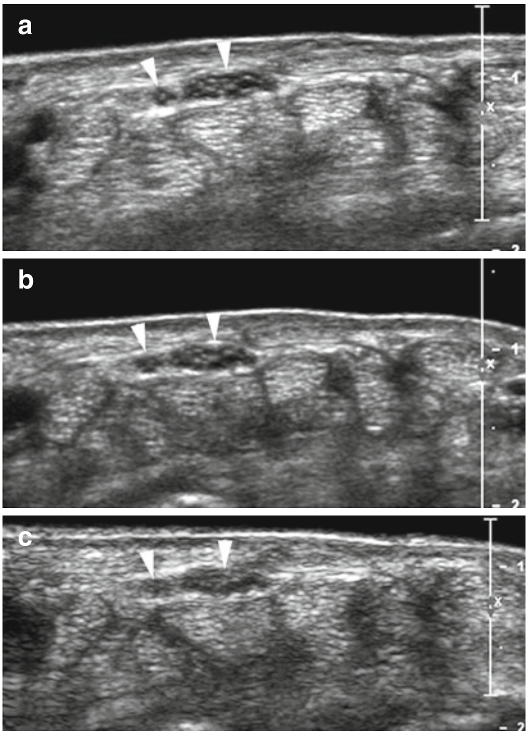

Fig. 1.2 Transverse ultrasound images through bifid median nerve (*arrowheads*) in a healthy volunteer taken with a 17 MHz (**a**), 12 MHz (**b**), and 9 MHz (**c**) transducer (all images taken on a Philips IU22 under the same preset). Note the difference in the discrimination of the fascicular nerve structure. In (**c**) the inner structure of the nerve is barely defined

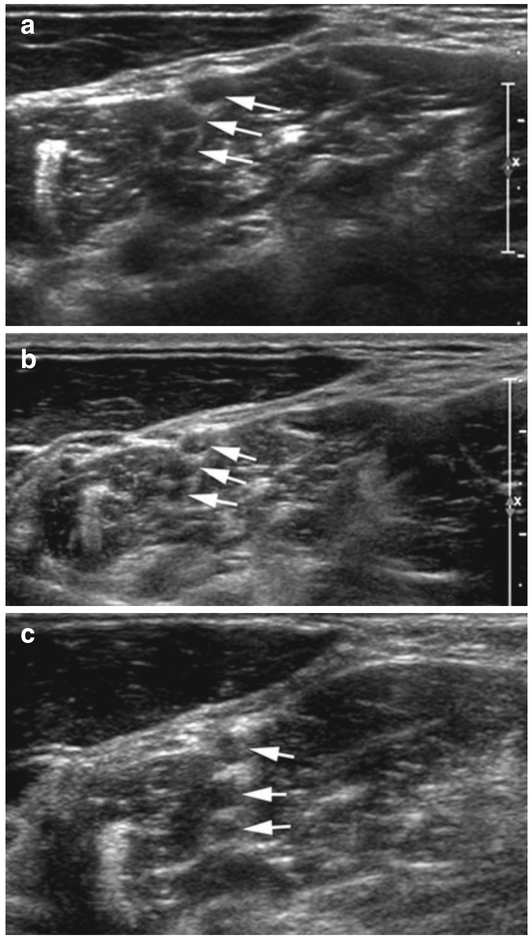

Fig. 1.3 Transverse ultrasound images through the brachial plexus (*arrows* plexus trunks) in a normal volunteer taken with a 17 MHz (**a**), 12 MHz (**b**), and 9 MHz (**c**) transducer (all images taken on a Philips IU22 under the same preset). Note that for deep-lying structures covered by thick soft tissues a 12 MHz or even 9 MHz transducer results in most acceptable image quality

interested user and dedicated systems for the specialist, such as the Philips Sparq (Philips Healthcare) (Fig. 1.1b), which is a small point of care system with a wide array of available transducers from curved arrays for general imaging to a 12 MHz wideband linear transducer especially suited for the anesthesiologist or pain physician performing guided nerve blocks.

Contrast and resolution are the basic physical principles that matter with sonography; therefore, high-resolution transducers are a must for nerve imaging. Currently available transducers for clinical imaging reach frequencies of up to18 MHz which results in an axial resolution of 250–500 μm. Such types of transducers are definitely needed for imaging of small nerves and for evaluation of inner nerve texture – for example, in sonography of nerves after nerve repair. Fine details such as small intraneural neuroma or partial dehiscence of a coaptation may go unnoticed with lower resolution transducers. For imaging of common compression neuropathies, a 12 MHz transducer usually suffices and for deep-lying nerves (e.g., sciatic nerve) or in obese patients a 9 MHz transducer may even be better suited (Figs. 1.2a–c and 1.3a–c). A recommendation on the type of transducer to be used depending on the nerve to be imaged and the clinical scenario is given in Table 1.1.

Table 1.1 Recommendation of transducers based on clinical context, type of nerve, and anatomical location

Transducer	Nerve	Clinical context
L9-3 MHz linear array or similar	Sciatic nerve (proximal), pudendal nerve, obturator nerve	Trauma
L12-5 MHz linear array or similar	Suited for most nerves, especially sciatic nerve (peripheral portion), extremity nerves, brachial plexus, etc.	Suited for almost all clinical scenarios, from compression neuropathy (measurement of nerve diameter and cross section), trauma to tumor imaging and especially suited for intervention
L17-5 MHz linear array or similar	Extremity nerves (median, ulnar, etc.) and peripheral branches of extremity nerves (superficial radial, posterior interosseous nerve, etc.), finger nerves	Compression neuropathy (evaluation of nerve texture, edema, etc.), trauma and postoperative lesions (scarring, partial dehiscence), neuritis
C9-4 MHz or C5-1 MHz curved array		Intervention in the cervical and lumbar spine

In general the smaller and more superficially situated a nerve is, the higher the transducer frequency should be

The future looks bright in terms of new hardware development with matrix arrays and improved crystal technology, but concerning transducer technology there is still a principal trade-off between rising frequency/improved resolution and depth of insonation.

1.1.2 Software

Various software tools are supplied with state-of-the-art ultrasound scanners. All of them attempt to improve image quality by management of the basic signal gained from reflection of sound waves inside the tissue. Generally speaking, these software tools – no matter what their name – improve image quality a lot and without them imaging of peripheral nerves would not have reached its current quality and status.

1.1.2.1 Compound Imaging

Meanwhile real-time image compounding has become a basic feature in state-of-the-art ultrasound scanners. One of the problems with conventional sonography is image degradation by coherent wave interference, known as "speckle." This shows as mottled superimpositions on images especially in regions with rather homogeneous tissue composition. The ultrasound companies use different names for the technique of image compounding, but basically the technique behind fancy names such as Sono-CT® (Philips), ApliPure® (Toshiba), or CrossXBeam® (GE) is somewhat similar: compound imaging averages several ultrasound frames in a single image. By use of the beam-steering software, the region of interest is scanned in different angles (frequencies or strain conditions), thus producing different artifact patterns (Fig. 1.4); averaging the single views results in improved definition of "real" tissue structures with marked reduction of artifacts (Piccoli et al. 2000). Newer developments enable the user to change the compound mode and to switch between modes for more enhancement of the region of interest and a quick overview mode. By reduction of image noise, speckle, dropout, or refractive shadowing, a better definition of tissue interfaces is achieved (Fig. 1.5a, b). Especially in peripheral nerve imaging, the details of a nerve and the discrimination of the epineurial/perineurial tissue are improved, which is why we generally perform nerve sonography with image compounding.

1.1.2.2 Harmonic Imaging

In "normal" B-mode sonography, a broad band of low frequencies is transmitted to the tissue inside the body. The reflected signal – which is detected by the transducer and produces the visible image – resonates off tissue in the body and has then a broad range of signal frequencies compared to the originally transmitted signal. Simply speaking, the sound waves travel into the body and back; therefore, they pass tissue interfaces twice and

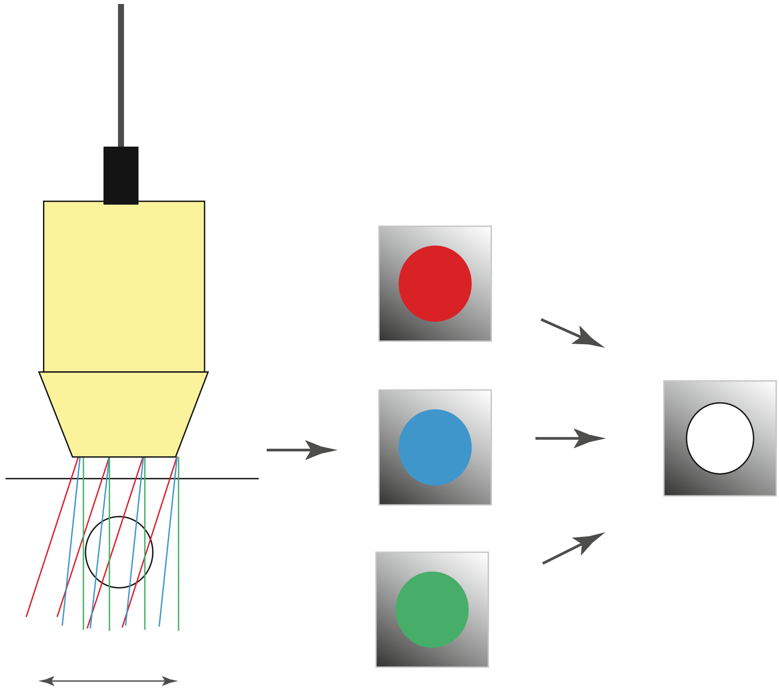

Fig. 1.4 Schematic drawing of compound imaging technique. The target is scanned from different view angles and the individual images from every angle (with different artifact pattern) are combined to one single image

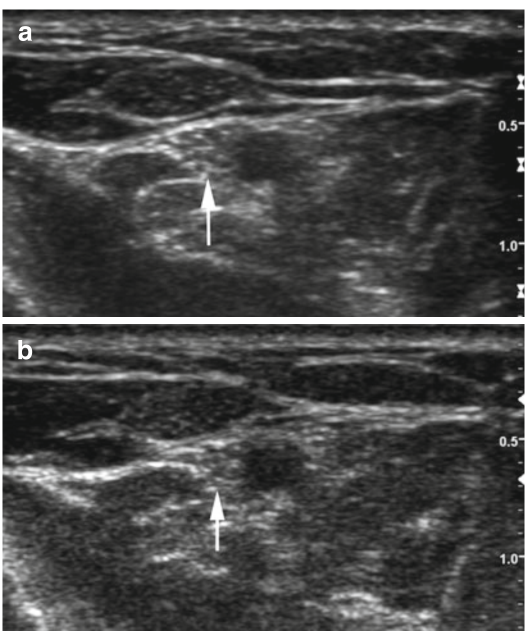

Fig. 1.5 Transverse ultrasound images through a median nerve (*arrow*) of a healthy volunteer taken with a 15 MHz transducer on a GE Logiq9 with (**a**) and without (**b**) image compounding. Note the improved detail in the compound image (distinct echoic inner and outer epineurium)

artifacts increase and sound energy decays exponentially. The physical principle of tissue harmonic imaging is actually quite simple: while travelling through the body, sound waves compress tissue, which results in a fractional increase of tissue density, a change in the sound speed, and distortion of the shape of the initial waveform. The angular components of the latter are the overtones or harmonics. These signals can be selected for imaging and have some advantages: they travel only one way toward the transducer; they are less prone to artifacts and lower in reverberations, which results in improved tissue contrast. As usual there is also a problem with this technique: harmonics are substantially less intense than the fundamental sound waves and therefore signal volume drops markedly. When harmonic imaging is used in a system with a good dynamic range, it results in exceptionally sharp images. This has proven of great benefit in abdominal imaging (Burns et al. 1996), but quite interestingly not so much for soft tissue imaging. The latter is especially true for the imaging of peripheral nerves (Fig. 1.6a, b). According to our experience, using

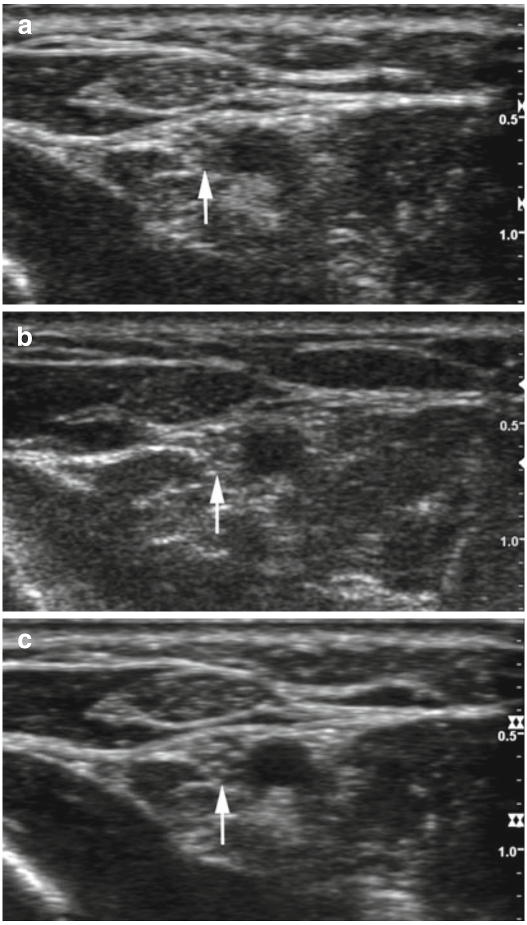

Fig. 1.6 Transverse ultrasound images through median nerve (*arrow*) in a healthy volunteer taken with a 15 MHz transducer on a GE Logiq9 with (**a**) and without (**b**) tissue harmonic imaging. In contrast to the effect of compounding (Fig. 1.5), there is only minimal change in the image quality by the use of harmonic imaging. The addition of image compounding to the harmonic image (**c**) results in the best image quality in this series of images

harmonic imaging does hardly improve image quality in high-resolution nerve scanning but even reduce image intensity. In any case tissue harmonic imaging should not be used without adding image compounding; the combination of both techniques gives in some cases added value, as it results in better quality than application of any of the two techniques alone (Fig. 1.6c)!

1.1.2.3 Extended Field of View Imaging

SieScape®, extended field of view imaging, panoramic imaging: different names for the same. During a longitudinal sweep of the transducer, a continuous registration of reflections takes place and dedicated software is used to build a longitudinal scan along the course of the sweep (Fig. 1.7). While initially only signals at the edge of a transducer were used for image construction, meanwhile special pattern recognition software is applied, which is responsible for the smoothness and resolution of a panoramic image. With application of the latter technique, the user can even easily adjust a sweep by moving back and forth to correct, for example, the loss of a target. The value of the technique lies mainly in the demonstration of complex lesions, documentation of the true extent of a lesion in one single image (Fig. 1.8), and size measurements which is especially appreciated by clinicians because of the better depiction of the local situation.

1.1.2.4 High-Resolution Imaging

Different software is used by the ultrasound providers to further enhance image quality and

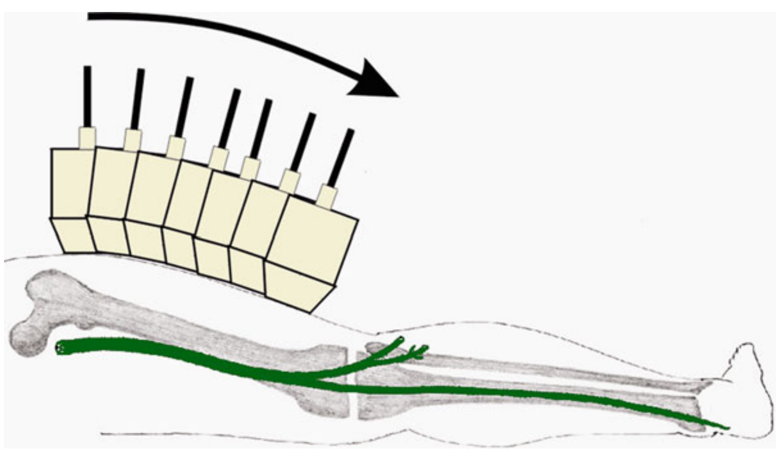

Fig. 1.7 Schematic drawing of extended field of view imaging: during a longitudinal sweep of the transducer along an area of interest, the image is continuously registered and subsequently calculated to one single image along the distance of the sweep

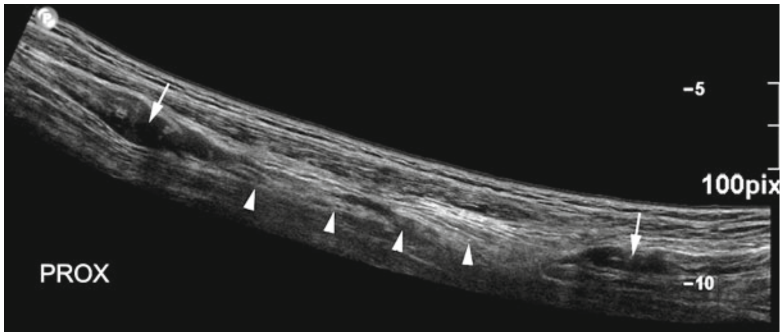

Fig. 1.8 Extended field of view image along the dorsal thigh in a patient with complete rupture of the sciatic nerve in a motor vehicle accident. Both ends of the nerve are thickened (*arrows*) with stump neuroma at the proximal end. Between the stumps there is a gap of almost 20 cm (*arrowheads*)

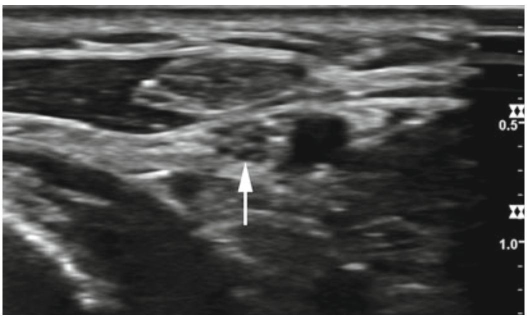

Fig. 1.9 Transverse ultrasound images through median nerve (*arrow*) in a healthy volunteer taken with a 15 MHz transducer on a GE Logiq9: addition of the company's proprietary image-enhancing software provided on the machine to an image with harmonics and compounding results in further improvement of image with exceptional clarity of tissue interfaces and profound artifact suppression (cf Figs. 1.5 and 1.6)

reduce artifacts. Most of that relies on some kind of pixel analysis, pattern recognition, and other dedicated analyses of the raw data of an ultrasound image. Afterward, a variety of image enhancing processes is used, with the general goal of image quality improvement by reduction of noise, speckles, and artifacts. While some companies have this software in the background as a simple turn "on" or "off" feature, some vendors allow for interactive changes of various settings. For the clinical sonographer, this means to spend some time and work at the scanner and know the "knobology": he has to accustom himself with the type of features that can be chosen on his scanner and to run a series of imaging trials to look for the best setting for the individual region of interest, examination task, and his personal preferences. We generally recommend these features, because they result in sharper tissue interfaces, borders, and margins (Fig. 1.9). Keep in mind that different body regions/imaging tasks and also patients (skinny patients, obese patients) may ask for different settings.

1.2 General Technique of Sonographic Nerve Examination

As it is the case for sonographic examinations in general, nerves must be imaged in two perpendicular planes; however, we recommend starting the exam in a transverse plane. Nerves are tubular structures with hypoechoic fascicular bundles interspersed by echoic connective tissue (Graif et al. 1991; Martinoli et al. 1996). This is why on longitudinal scans nerves are not easily distinguished from close-lying muscle tissue or tendons (Fig. 1.10). On transverse scans, this is much easier achieved, as nerves run along fascial planes embedded in fat and connective tissue – often together with vessels – and the honeycomb appearance of a nerve on a transverse scan is quite characteristic and easily distinguished from other anatomical structures. If there is a problem in distinguishing nerves and tendons on a transverse scan, we recommend tilting of the transducer to look for a signal change caused by anisotropy effects (Fig. 1.11): while tendons show a marked change of their signal from hyper- to hypoechoic, nerves show only a small change of signal with angled insonation. This is due to the fact that tendons have overlapping short fascicular elements, while nerves are long, continuous tubules.

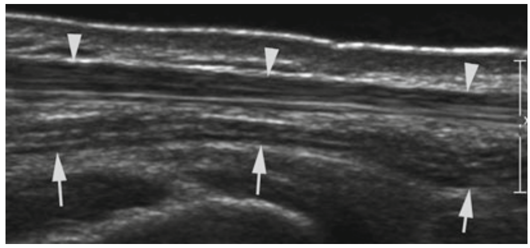

Fig. 1.10 Extended field of view image along the distal wrist with presentation of the ulnar nerve (*arrows*) and flexor tendons (*arrowheads*). Note the rather similar appearance of nerve and tendon on the longitudinal image, thus difficult differentiation

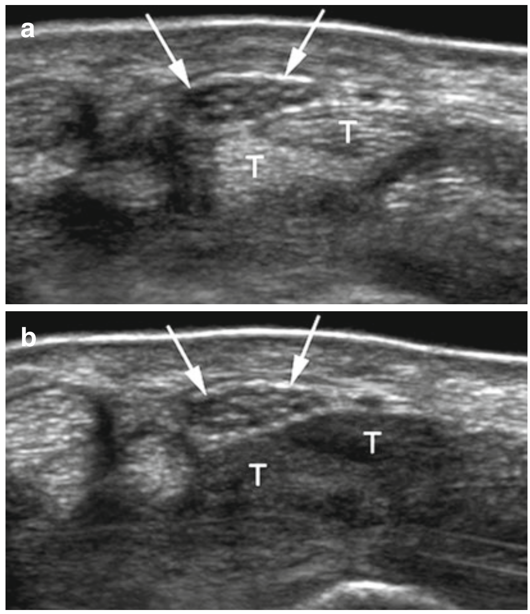

Fig. 1.11 Transverse ultrasound images through the median nerve (*arrows*) in a healthy volunteer taken with a 17 MHz transducer on a Philips IU22 with different transducer tilt position. Note the marked change of flexor tendon (*T*) signal from hyperechoic in (**a**) to hypoechoic in (**b**) but only minimal change of the median nerve

In general the presentation of nerves on high-resolution sonograms is exquisite and nicely correlates with the anatomical ultrastructure (Fig. 1.12) (Walker 2004). On transverse scans, you can experience the nerves' inner fascicular structure. Fascicles are the smallest structure to be discerned by modern sonography and are groups of nerve fibers surrounded by a common outer epi- and perineurial sheath (Silvestri et al. 1995; Maravilla and Bowen 1998). The single nerve fibers composed of axons, myelin sheaths, and Schwann cells are still beyond the resolution of sonographic imaging. An individual amount of fascicles comprises a peripheral nerve, which is surrounded by outer epineurium. How many fascicles combine to a peripheral nerve is variable and depends on the type of nerve (amount of motor and sensory fibers), its location in the body (distance from its origin, type of surrounding tissue), and its size. There is even a longitudinal variation of the amount of fascicles within a nerve, because fascicles repeatedly unite and divide along the course of the nerve, allowing the passage of axons from one fascicle to another. For the clinical sonographer, the fascicles and the epineurial tissue are important features, as changes in these two elements are the hallmark of distinct pathophysiological entities of peripheral nerve disease. Marked swelling of fascicles and loss of inner and outer hyperechoic epineurial borders, for example, may result from venous congestion and edema and are characteristic for

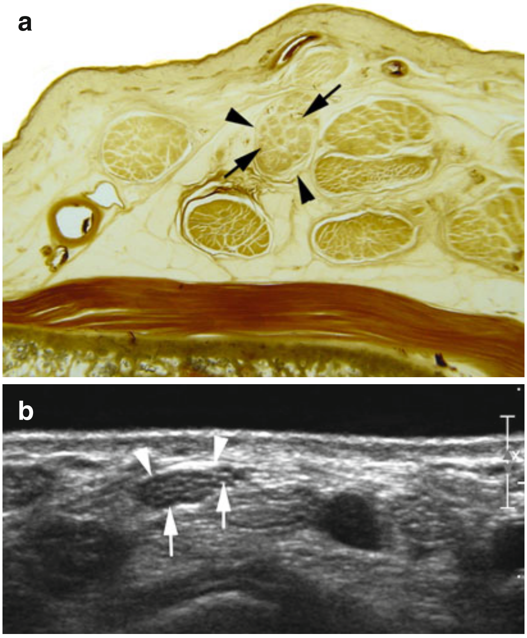

Fig. 1.12 Anatomical plastination specimen through wrist (**a**) with demonstration of median nerve ultrastructure (*arrowheads* outer epineurium, *arrows* fascicular bundle covered by inner epineurium). Corresponding ultrasound image (**b**) with demonstration of the same ultrastructural features

acute or subacute compression neuropathy (Buchberger et al. 1991; Chiou et al. 1998; Dahlin 1991). Thickening of a nerve and enlarged cross section but – in contrast to the aforementioned reaction – with hyperechoic thickening of the outer epineurium can be caused by chronic friction and thus are hallmarks of long-standing chronic neuropathy. So when performing peripheral nerve sonography, attention to the microanatomic texture of a nerve is important.

Especially with traumatic nerve injury, we often strive at the definition of nerve continuity (Bodner et al. 1999; Gruber et al. 2003, 2005; Peer et al. 2002). While the detection of complete transection is quite forward, the examination of injuries with incomplete severance of nerve fascicles or an attempt to define fascicular continuity after suturing has to be done with caution (Peer et al. 2001). The number of fascicles discerned by sonography does not always correspond to the real number of fascicles existing within a nerve. This is probably due to the coalescence of some adjacent fascicles in a single image. Keep also in mind that the number of fascicles seen on sonography decreases with reduced transducer resolution (reduction of frequency)!

Nerves are vascularized structures. Tiny nutrient vessels run along the nerve and penetrate it at frequent intervals along its course, communicating with the longitudinally oriented epineurial, interfascicular, perineurial, and intrafascicular arteries and arterioles. With state-of-the-art high-resolution transducers, these intraneural vessels are sometimes detected with duplex sonography; but up to date, we have only limited experience concerning what is normal and what is abnormal vasculature inside a nerve. There are reports on the presence of nerve hypervascularization in patients with compression neuropathies (Mallouhi et al. 2006; Ghasemi-Esfe et al. 2011), so analyzing a nerve's vascular state is potentially promising.

Nerves have a complex course and travel a long way from their exit at the spine until they reach their end organ. They form into bundles, exchange fibers, give way to small branches, and interconnect with each other. Therefore, imaging a peripheral nerve may be challenging. In many cases, however, the site of potential pathology is clear – as is the case for compression syndromes, which occur in distinct anatomical locations, where a nerve traverses through a narrow tunnel – and the exam is tailored directly to this region. As mentioned, this is the case for entrapment neuropathies, where the neural pathology is well localized, the local situation has typical anatomical features, and the nerve is easily found, measured, and diagnosed. For the evaluation of peripheral nerve trauma, however, the situation is more complex. Based on a neurological exam and/or electrophysiological studies, there may be a diagnosis of paralysis, motor weakness, or a nerve block, but the exact site of nerve compromise and its extent are less obvious in the case of a closed injury (such as traction). In addition hematoma or edema may obscure the local anatomy, by overshadowing or encasement of a nerve. In these cases a direct sonographic approach toward a presumed site of injury may turn out disappointing, even may result in misdiagnosis. For every nerve landmarks along its course, typical topographical relationships to close-lying bone, muscle, tendon, or vascular structures exist, which allow for an easy identification of a nerve at various sites. In clinical practice we therefore

strongly recommend the following approach for the examination of a traumatic nerve lesion:

- Identify the injured nerve at a site with distinct anatomical landmarks in a transverse scan (If possible this should be a site where no injury exists!).
- Starting from here, follow the nerve upward and downward along its course – still scanning in a transverse scan plane – until you reach the level of nerve damage or can rule out a substantial lesion.
- If a lesion exists, document it in transverse and additional longitudinal scans; the latter are better suited for the definition of nerve continuity and some measurements.

For neuropathies such as mononeuritis multiplex, vasculitic neuropathy, and similar lesions, mapping of a nerve along its complete course is recommended, as focal enlargement of a nerve at a single or at multiple levels may be found in these diseases (Beekman et al. 2005; Takato et al. 2007). Sonography is especially suited for such an attempt at nerve mapping, because the transducer can easily be steered along the complete course of a nerve. As we know now, several (possibly distinct) patterns of nerve enlargement along the course of peripheral nerves may exist in such neuropathies. Therefore, the examiner is advised to scan all large nerves in the extremities along their complete course in order to define the type of existing neuropathy.

1.3 Basic Technique of Peripheral Nerve Intervention Under Ultrasound Guidance

For a long time, fluoroscopy and computed tomography were the favorite imaging tools of many practitioners performing guided interventions also in the peripheral nervous system. In 1996 Dodd and colleagues called ultrasound the "undiscovered jewel" of interventional radiology (Dodd et al. 1996) and to a certain extent it still is. While the use of ultrasound for the guidance of regional anesthesia and pain management is increasing, it is still not widely used. This may be due to the fact that many pain therapists and radiologists alike lack the knowledge of topographic anatomy, which is needed to correctly identify peripheral nerves, but even more lack a formal training in ultrasound-guided procedures. Handling of the ultrasound transducer and needle during interventions is a task, which demands a rather high level of coordination and practice: not only coordination of hand and eye, but more so of right and left hand (Bradley 2001). This sounds trivial, but the coordination of the transducer and the needle in a three-dimensional environment may be quite tricky, depending on the local anatomy and the complexity of the procedure. In phantom studies with simulation of simple interventional tasks, such as the puncture of an olive buried inside a piece of meat, it is evident that 70 % of the examiners with little experience in ultrasound intervention lose control of their needle at some point during the procedure (Sites et al. 2004). This may be detrimental and lead to unintended puncture of nerves or close-lying vessels; lead to hemorrhage, nerve injury, and even persistent palsy; or cause injury in close-lying organs – such as an iatrogenic pneumothorax. The ability of a beginner to maintain the needle within the longitudinal ultrasound scan plane represents the most difficult aspect of ultrasound-guided procedures. Constant visualization of the needle tip is crucial to avoid complications and thus an unrivaled advantage of the modality also combined with its real-time procedure control. One step toward good needle control is the adherence to a simple rule: use in principle an in-plane needle approach (whenever possible).

1.3.1 How to Guide Your Needle

The old proverb, "all roads lead to Rome," holds some truth, but in terms of ultrasound-guided interventions, some of these roads may be hard travelled.

In principle we may perform ultrasound-guided injections in freehand technique or with the use of a mechanic needle guide. At first sight, the mechanic needle guide is tempting: it fixes the needle to the ultrasound transducer and thus holds it inside the scan plane at all time – without the operator having to care about the position of the needle in the lateral plane. Therefore, needle visibility is approximately

30 % better, if inexperienced trainees use such a needle guide. For the intervention the operator simply chooses the required angle to the target and advances the needle. For the beginner the use of a needle guide allows for reduction of procedure time, quick success, and good results; however, the fixed relationship of needle and transducer also restricts the range of motion of the needle within the scan plane: only certain puncture angles are possible and during complex interventions this may lead you into trouble.

The freehand technique requires the operator to steer the needle with one hand and maneuver the transducer with the other; please refrain from handling the needle only and have a colleague hold the transducer for you! This technique is outdated and intervention is not for the faint hearted, so be brave, do it yourself and the success is yours (as is the failure). The freehand technique asks for versatility in positioning the needle during its placement, which may sometimes be difficult even for the experienced interventionalist. Training with expert mentorship is mandatory and may be performed on commercially available phantoms or simple custom-made phantoms such as the "piece of meat model" mentioned before. When performing procedures in patients, start with the easy and only proceed toward the more complex procedures once you feel comfortable with the handling of superficial interventions.

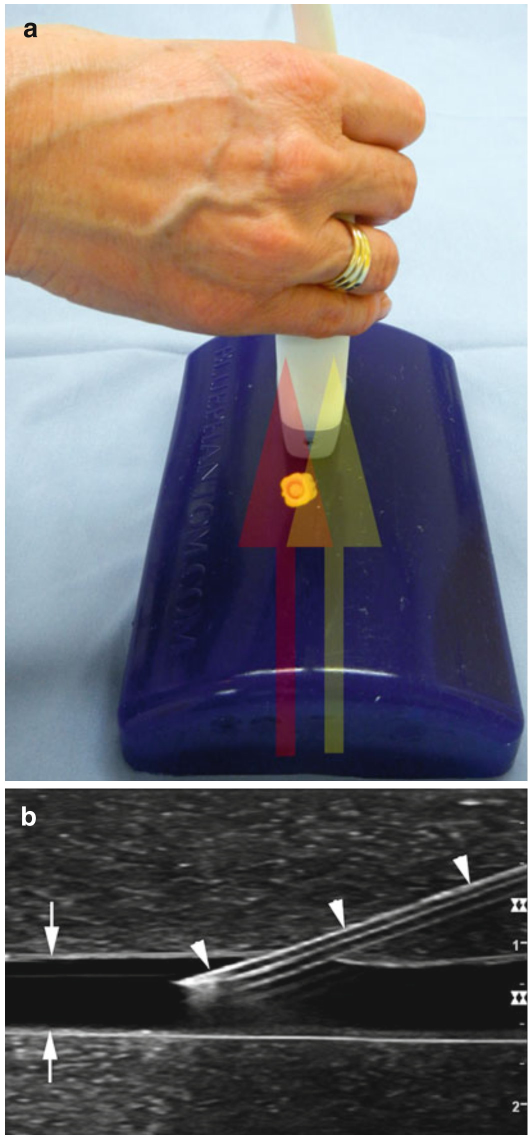

Fig. 1.13 (**a**) Simulated "in-plane needle approach" in a phantom: the needle is inserted on the small side of the probe and the needle path (*yellow arrow*) is in line with the scan plane of the transducer (*red arrow*). (**b**) Ultrasound image acquired with "in-plane needle approach" in a vessel phantom: the needle (*arrowheads*) is seen as a bright hyperechoic longitudinal reflex from its entrance into the scan plane until its bright tip enters the simulated vessel (*arrows*)

1.3.1.1 In-Plane Needle Approach

The "in-plane needle approach" is one of the classical techniques used for ultrasound-guided interventions and is especially suited for interventions at the peripheral nerve. The needle is inserted on the small side of the probe and advanced exactly in line with the scan plane (Fig. 1.13a). On the resulting ultrasound image, the needle is seen as a hyperechoic, bright, linear reflex (Fig. 1.13b) and along its whole extent from its entry into the scan plane to its tip. Depending on the type of transducer used and the distance from skin to target, even the entire needle path from skin to the target may be visualized. The in-plane needle approach is said to have some disadvantages:

- Longer path from skin to target and therefore more patient discomfort (in fact an in-plane approach requires about two to three times the needle length to reach the target compared to the out-of-plane approach).

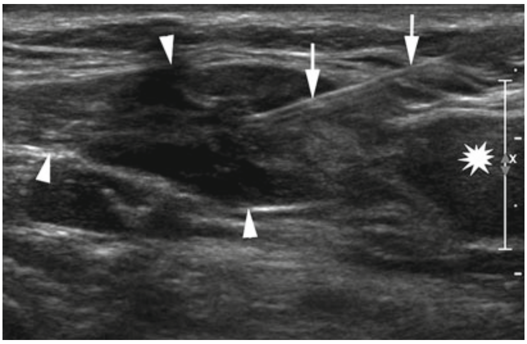

Fig. 1.14 Ultrasound-guided neurosclerosis in "in-plane needle approach." The needle (*arrows*) is inserted longitudinally to the scan plane into the neck of the peroneal nerve (*arrowheads*) above a terminal type neuroma (*asterisk*) for treatment of phantom pain with phenol injection

- Easy deviation of the needle from the narrow scan plane and therefore prolonged procedure time and need for frequent repositioning of the needle.
- Shadowing of structures lying deep under the echoic artifact produced by the needle.

With sufficient experience, however, control of the needle inside the tissue is outstanding (Fig. 1.14), which is why we generally recommend this technique.

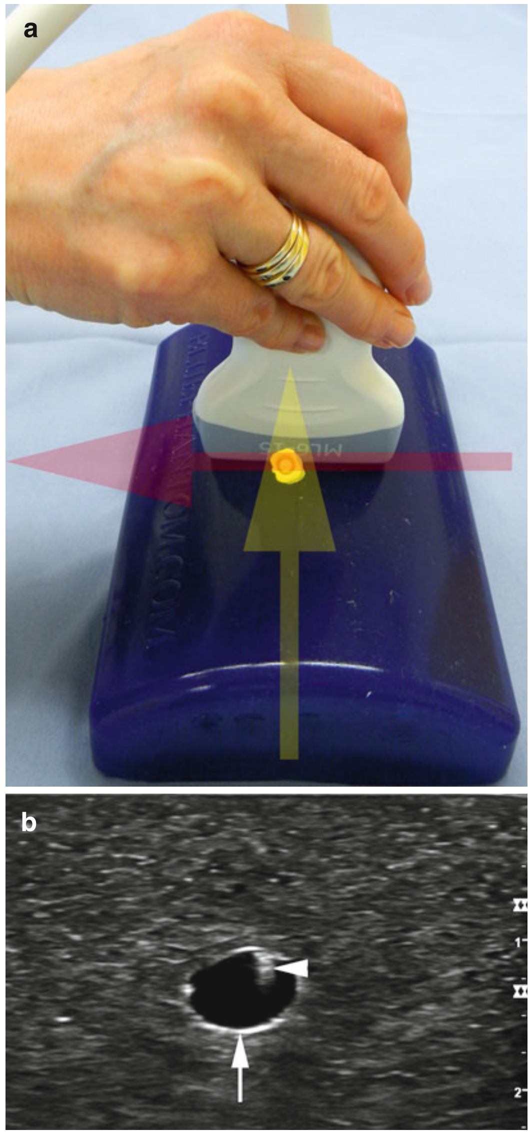

Fig. 1.15 (**a**) Simulated "out-of-plane needle approach" in a phantom: the needle is inserted on the broad side of the probe and the needle path (*yellow arrow*) is perpendicular to the scan plane of the transducer (*red arrow*). (**b**) Ultrasound image acquired with "out-of-plane needle approach" in a vessel phantom: the needle (*arrowheads*) is seen as a bright hyperechoic spot on the upper border of the simulated vessel (*arrows*), if this spot represented the needle tip entering the vessel or an obliquely imaged part of the shaft cannot be judged on this image

1.3.1.2 Out-of-Plane Needle Approach

The "out-of-plane needle approach" is the second commonly used technique for ultrasound-guided interventions and especially used by anesthesiologists or pain physicians for the guidance of nerve blocks. In this case the needle is inserted on the broad side of the probe and advanced perpendicularly to the scan plane (Fig. 1.15a). On the resulting ultrasound image, the needle is only seen as a bright spot (Fig. 1.15b); whether this spot represents the true needle tip or part of the needle shaft hit by the ultrasound beam from an oblique angle is very difficult to decide: this is the major disadvantage of the out-of-plane approach. Another equally important disadvantage is the need of constant angulations of the probe toward the needle tip while advancing the needle to its target. In rare cases the out-of-plane approach may be more feasible in cases where only limited space for probe coupling and needle positioning exists. This is, for example, the case for punctures in the neck region: this is an area where a lot of structures lie close together. Depending on the type of probe used, the broad edge of the transducer may cover a length of 4–5 cm, which restricts the maneuverability of a needle at a predefined angle toward a small target surrounded

by "don't touch structures." There is less freedom in the choice of a needle path toward the target and the handling of the needle may simply be hampered by the edge of the mandible interfering with the needle or the operator's hand. In such a case an out-of-plane approach allows for more choices of the puncture site on the skin and different angles toward the target (almost 360° around the target). So generally speaking, we prefer the "in-plane needle approach" whenever it is feasible, but an experienced operator should be able to switch between techniques to adapt to the specific interventional task.

1.3.2 Technical Factors Affecting Ultrasound-Guided Procedures

There is a wide range of technical factors affecting ultrasound-guided procedures, from the physical properties of sound waves, factors relating to the ultrasound scanner and its software, factors relating to the needle material, to factors relating to tissue capabilities and body composition. To cover all of them is beyond the scope of this introductory chapter and many have been covered in extent by other authors (Narouze 2010): as a general rule, however, we advice the novice interventionalist to get accustomed with his "toolbox." Adapt the ultrasound scanner settings to the task of intervention! Needle visibility is highly enhanced with dedicated settings and the normal settings used for diagnostic imaging may not be ideally suited for the visibility of needles inside tissue. Software features such as compound imaging generally result in better needle depiction; harmonic imaging does so on some scanners but not on others. You have to try things out, probably with use of a phantom first and fine-tuning of your setup later during a real interventional procedure.

There are specially designed needles for sonographic interventions, which should promise a brighter reflex, due to some fancy design features, such as small indentations or surface wrinkling resulting in better sound reflections from different angles (Hopkins and Bradley 2001). Quite interestingly there are reports that these needles do not result in a general improvement of needle visibility, but may be advantageous under special circumstances, such as very steep angulations of a needle.

The simplest advice still is the most versatile:

- Larger needles result in better visibility (at the trade-off of higher patient discomfort and a higher risk of complications).
- The insertion site and the angle of the procedure needle toward the skin and transducer footprint play a critical role: the steeper the angle of the needle toward the ultrasound beam, the lesser reflection you get, resulting in poor needle visibility.
- Remember the advantages/disadvantages of the in-plane and out-of-plane needle approach discussed earlier in this chapter: an in-plane approach generally results in a flatter puncture angle, while an out-of-plane approach naturally results in a steep angle.
- Try to insert your needle at an angle of 50–60° (Bradley 2001). Why not close to 90°? In principle this may result in optimal reflection, but in clinical practice to achieve such an angle is only partly feasible: to image a needle perpendicular to the sound beam, you must insert the needle too far from the edge of the transducer along a curve in the body surface (you may, for example, do that for injections to the lateral femoral cutaneous nerve with needle insertion from a lateral approach); however, this results in loss of needle visibility at the skin entrance.
- You can also perform a so-called heel-in maneuver to achieve a flatter angle: the transducer edge far from the needle insertion site is tilted away and firmly pressed into the skin and thus the sound beam is angled toward the needle insertion site. This is a quite clever approach especially for interventions with curvilinear probes but may result in additional patient discomfort because of transducer pressure on the soft tissues. This is hardly a problem when curved arrays are used, but with linear array probes the pressure of the outer transducer edge may be intolerable especially for chronic pain patients.

1.3.3 General Advice and Conclusion

The performance of interventions under ultrasound guidance is complex and requires training, optimization of all involved technical aspects

including management of the patient: interventions may be painful and need patient cooperation, so try to perform them in a comforting atmosphere and adequate environment.

Infections hardly occur in peripheral nerve interventions but nevertheless hygiene is of outmost importance, so the use of sterile equipment and sterile ultrasound gel is mandatory. This is especially important for interventions to deep-lying structures and joints.

Adequate training and experience are needed to constantly achieve good results with little complications. However, complications will occur so be prepared to handle them accordingly. There is a variety of substances to be used for injections and all have distinct properties, advantages, and disadvantages.

Modern ultrasound intervention does not stop at injection of corticoids or local anesthetics: cryoablation or radiofrequency ablation may be performed under ultrasound guidance, as may be the implantation of electrodes for peripheral nerve stimulation.

References

Beekman R, van den Berg LH, Franssen H et al (2005) Ultrasonography shows extensive nerve enlargements in multifocal motor neuropathy. Neurology 65:305–307

Bodner G, Huber B, Schwabegger A et al (1999) Sonographic detection of radial nerve entrapment within a humerus fracture. J Ultrasound Med 18:703–706

Bradley MJ (2001) An in-vitro study to understand successful free-hand ultrasound guided intervention. Clin Radiol 56:495–498

Buchberger W, Schoen G, Strasser K et al (1991) High resolution ultrasonography of the carpal tunnel. J Ultrasound Med 101:531–537

Burns PN, Powers JE, Hpe SD et al (1996) Harmonic imaging: principles and preliminary results. Angiology 47:63–69

Chiou HJ, Chou YH, Cheng SP et al (1998) Cubital tunnel syndrome: diagnosis by high resolution ultrasonography. J Ultrasound Med 17:643–648

Dahlin LB (1991) Aspects on pathophysiology of nerve entrapments and nerve compression injuries. Neurosurg Clin N Am 2:21–29

Dodd GGD, Esola CC, Memel DS et al (1996) Sonography: the undiscovered jewel of interventional radiology. Radiographics 16:1271–1288

Filler AG, Kliot M, Howe FA et al (1996) Application of magnetic resonance neurography in the evaluation of patients with peripheral nerve pathology. J Neurosurg 85:299–309

Fornage BD (1988) Peripheral nerves of the extremities: imaging with ultrasound. Radiology 167:179–182

Ghasemi-Esfe AR, Khalizadeh O, Vaziri-Bozorg SM et al (2011) Color and power Doppler US for diagnosing carpal tunnel syndrome and determining its severity: a quantitative image processing method. Radiology 261:499–506

Graif M, Seton A, Nerubali J et al (1991) Sciatic nerve: sonographic evaluation and anatomic pathologic considerations. Radiology 181:405–408

Gruber H, Kovacs P, Peer S, Marth R, Bodner G (2003) The ultrasonographic appearance of the femoral nerve and cases of iatrogenic impairment. J Ultrasound Med 22:163–172

Gruber H, Peer S, Meirer R, Bodner G (2005) Peroneal nerve palsy associated with knee luxation: evaluation by sonography-initial experiences. Am J Roentgenol 185:1119–1125

Hopkins RE, Bradley M (2001) In-vitro visualization of biopsy needles with ultrasound: a comparative study of standard and echogenic needles using an ultrasound phantom. Clin Radiol 56:499–502

Mallouhi A, Pülzl P, Trieb T, Pizza H, Bodner G (2006) Predictors of carpal tunnel syndrome: accuracy of gray-scale and color Doppler sonography. AJR Am J Roentgenol 186:1240–1245

Maravilla KR, Bowen BC (1998) Imaging of the peripheral nervous system: evaluation of peripheral neuropathy and plexopathy. AJNR Am J Neuroradiol 19: 1011–1023

Martinoli C, Serafini G, Bianchi S et al (1996) Ultrasonography of peripheral nerves. J Peripher Nerv Syst 1:169–174

Narouze NN (2010) Atlas of ultrasound-guided procedures in interventional pain management. Springer, New York. doi:10.1007/978-1-4419-1681-5

Peer S, Bodner G, Meirer R et al (2001) Evaluation of postoperative peripheral nerve lesions with high resolution ultrasound. AJR Am J Roentgenol 177:415–419

Peer S, Kovacs P, Harpf C et al (2002) High resolution sonography of lower extremity peripheral nerves: anatomic correlation and spectrum of pathology. J Ultrasound Med 21:315–322

Piccoli C, Merrit CRB, Forsberg F et al (2000) Real-time compound imaging of the breast. In: Presented at the annual meeting of the American Institute of Ultrasound in Medicine, San Francisco, April 2000

Silvestri E, Martinoli C, Derchi LE et al (1995) Echotexture of peripheral nerves: correlation between US and histologic findings and criteria to differentiate tendons. Radiology 197:291–296

Sites BD, Gallagher JD, Cravero J et al (2004) The learning curve associated with a simulated ultrasound-guided interventional task by inexperienced anesthesia residents. Reg Anesth Pain Med 29:544–548

Takato I, Masanori K, Takashi W et al (2007) Ultrasonography of the tibial nerve in vasculitic neuropathy. Muscle Nerve 35:379–382

Walker FO, Cartwright MS, Wiesler ER, Caress J (2004) Ultrasound of nerve and muscle. Clin Neurophysiol 115:495–507

Introduction to Magnetic Resonance Imaging of the Peripheral Nervous System: General Considerations and Examination Technique

2

Werner Judmaier

Contents

W. Judmaier
Department of Radiology, Innsbruck Medical University, Anichstrasse 35, 6020 Innsbruck, Tyrol, Austria
e-mail: werner.judmaier@i-med.ac.at

2.1 General Considerations on Peripheral Nerve MRI

Ever since magnetic resonance imaging (MRI) got introduced in the armamentarium of medical imaging methods, it received highest interest from neuroscience. This method's superb soft tissue contrast allowed for unprecedented imaging of nervous tissue and developed very quickly into a standard method of brain and spine imaging. Over the past few decades, MR scanners became a routine tool and a mass product within affordable cost and thus widely spread. At the same time, rapid technical advances of the method opened the door for even more detailed imaging and complete new applications: to date, scanners with a field strength of 1.5–3T can be considered standard and allow for even more detailed imaging within acceptable imaging time. Cross-sectional imaging of nervous tissue can today be combined with numerous complementary scanning schemes, such as depiction of the vasculature with various MR angiography methods, insight into the biochemistry of nervous tissue and its pathologies with spectroscopy, and observation of nerve tissue function by exploiting tissue perfusion and blood deoxygenation effects with functional MRI. A more recent development in MRI is the ability to assess the Brownian molecular motion of water molecules termed diffusion-weighted imaging (DWI). This method is routinely used for the early depiction of ischemic stroke where hypoxic injury of the neural tissue leads to a shift of free interstitial water into

S. Peer, H. Gruber (eds.), *Atlas of Peripheral Nerve Ultrasound*,
DOI 10.1007/978-3-642-25594-6_2,

swollen neurons (cytotoxic edema), thus reducing the free diffusibility of water molecules which results in a drop of the calculated diffusion coefficient. This imaging method is also used to facilitate the differentiation of dense cellular tumor tissue from inflammatory or infectious changes as well as scar tissue after tumor resection. Even more interestingly, DWI is also capable of assessing the foremost direction of free Brownian molecular motion, thus permitting the visualization of the nerve bundles' course within the spinal cord and cerebral tracts or, in case of injury, their anatomical or functional disruption.

Despite these fascinating capabilities of MRI, its use has so far mainly been focused on central nervous system diseases. The reasons for this are particularly numerous and diverse:

- Microsurgical procedures were not developed to the point to warrant a precise anatomical depiction of nerve injury.
- Electrophysiological studies were considered adequate to ascertain the clinical diagnosis.
- The distribution of mainly low- to midfield scanners with the at that time existing coil technology and scanning hardware and software did not allow for a reliable depiction of peripheral nerve structures.

MRI of the peripheral nervous system was mainly performed to rule out compression of neural bundles from surrounding structures, e.g., depiction of soft tissue tumors, hematomas, or cysts, as well as anatomical variants such as hypertrophic muscles and ligamentous restriction or impingement due to scarring upon a peripheral nerve: in most of these cases, it was sufficient to assess the course of the nerve in question without the need to precisely depict the nerve itself. Only in few instances as in the carpal tunnel syndrome, an effort was made to assess the diameter and the degree of flattening of the median nerve under the retinaculum. Also, the degree of edema with swelling and hyperintensity in T2-weighted images of the nerve proximal to its entry into the carpal canal was evaluated in these cases (Mesgarzadeh et al. 1989; Campagna et al. 2009) (Fig. 2.1). More often, the CTS syndrome being clinically clear and proven by electrophysiologic examinations, MRI was merely ordered to rule out tumorous or inflammatory reasons of nerve impingement.

Another indication for performing an MRI examination is the depiction, classification, and follow-up of primary neural tumors (Fig. 2.2). Especially in cases of hereditary neurofibromatosis where multiple peripheral nerve tumors need to be observed, MRI offers a variety of advantages: modern scanners allow for multiple scan regions within one examination so that eventual central nervous tumors as well as peripheral schwannomas and plexiform neurofibromas in various parts of the body can be evaluated and reliably monitored using a repetitive standard imaging technique and documentation. Comparison of the actual images with technically identical images of prior exams allows early to pinpoint tumors with tendency of proliferation and rule out eventual malignant transformation (Wasa et al. 2010). These repetitive and sometimes "whole-body exams" with MRI do not endanger the patient with lifelong accumulating ionizing radiation.

In cases of suspected solitary neural tumors, MRI might help in ascertaining its presence or absence as in patients with neuroma formation after limb amputation or in patients with Morton's neuroma. Although ultrasound plays a predominant role in demonstrating the neural origin of such a tumor, MRI is of great value for the surgeon providing a clear anatomical picture of the tumor and its surrounding structures in multiple planes. Thus, MRI greatly facilitates resection planning (Figs. 2.3, 2.4).

In posttraumatic nerve damage, MR is capable to reveal or rule out nerve root avulsion from the spinal cord. In more distally located nerve damage as in peripheral nerve traction injury, there are at times only subtle signal changes to be detected in the compromised section along the course of the nerve: overstretching of nerve fibers leads to edematous changes with subsequent swelling of the nerve. These changes can be observed by MRI by comparing the diameter of the injured nerve with the contralateral nerve or the portion of the same nerve proximal and distal to the site of injury and visualizing its water content by using heavily T2-weighted sequences with spectral fat suppression. These changes in

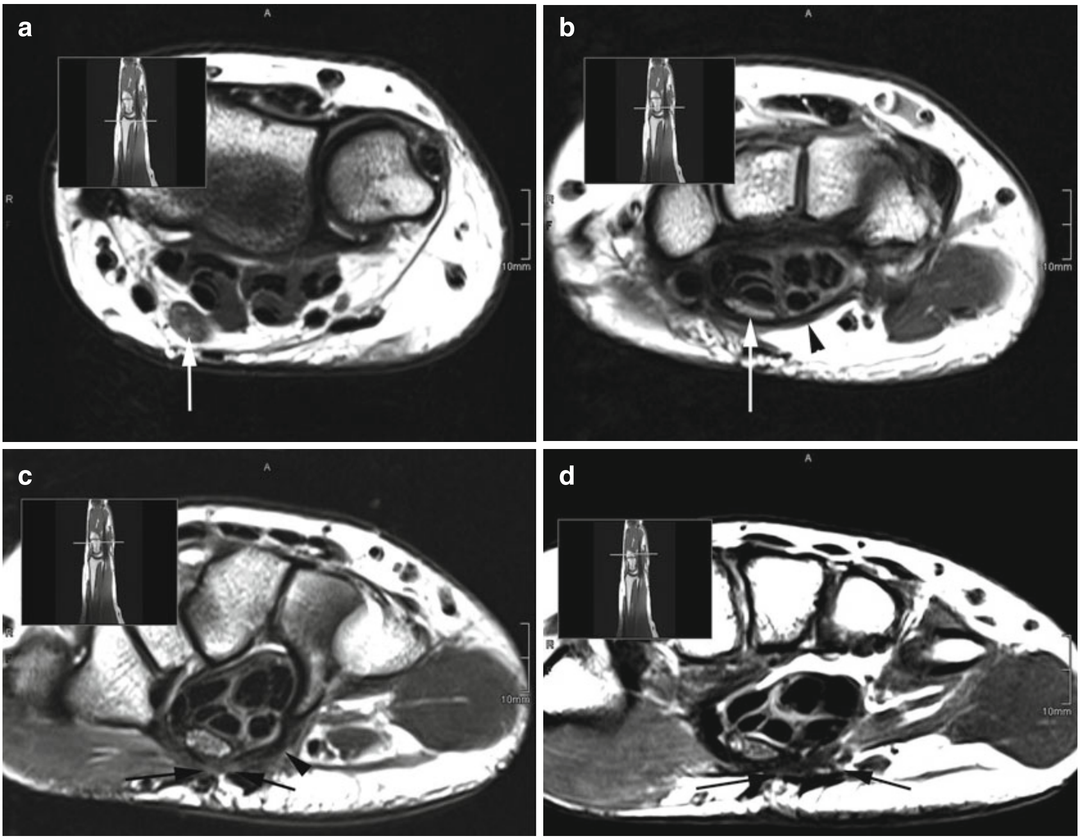

Fig. 2.1 Recurrent carpal tunnel syndrome (CTS) after insufficient dissection of the transverse carpal ligament. Axial T2-weighted images: (**a**) median nerve (*arrow*) at the level of the wrist joint before entering the carpal tunnel; the nerve is massively enlarged with increased signal intensity on T2 (higher than the signal of the adjacent musculature) indicating edematous changes of the nerve. (**b**) Marked flattening of the median nerve (*arrow*) at the entrance into the carpal tunnel due to the narrowed space between the flexor tendons and the portion of the transverse ligament left intact (*arrowhead*). (**c**) Dissected portion of the transverse ligament at the level of the carpal tunnel (*arrows*). Note the bowing of the ligament near its insertion at the hamate bone indicating its laxity (*arrowhead*). The median nerve is decompressed, albeit showing edematous changes with fluid collections in the epineural spaces surrounding the individual nerve fibers. (**d**) Typical and normal fibrotic changes after surgery in the subcutaneous fatty tissue of the palm of the hand (*arrows*). The edematous reaction of the median nerve due to the entrapment more proximally extends as far as its bifurcation

T2 values of the injured nerve and their time course have been shown to correlate with the observed functional deficits in an animal model of peripheral nerve traction injury (Shen et al. 2010). Clinically, this method is mainly used to assess injuries to the brachial or lumbosacral plexus: the individual nerve roots subsequently conjoin to form distinct nerve trunks. All of these possess a sufficiently large diameter to make them readily visible on MR images. These scans should always include coronal T2-weighted images with depiction of both sides of the plexus, so that the signal behavior of the affected area can be compared to the healthy contralateral side of a patient. Furthermore, MR is very sensitive to demonstrate collateral damages, like muscular edema or tears, bone fractures, hematomas, or diffuse edematous changes to the perineural fat indicating the site and severity of a sheer trauma.

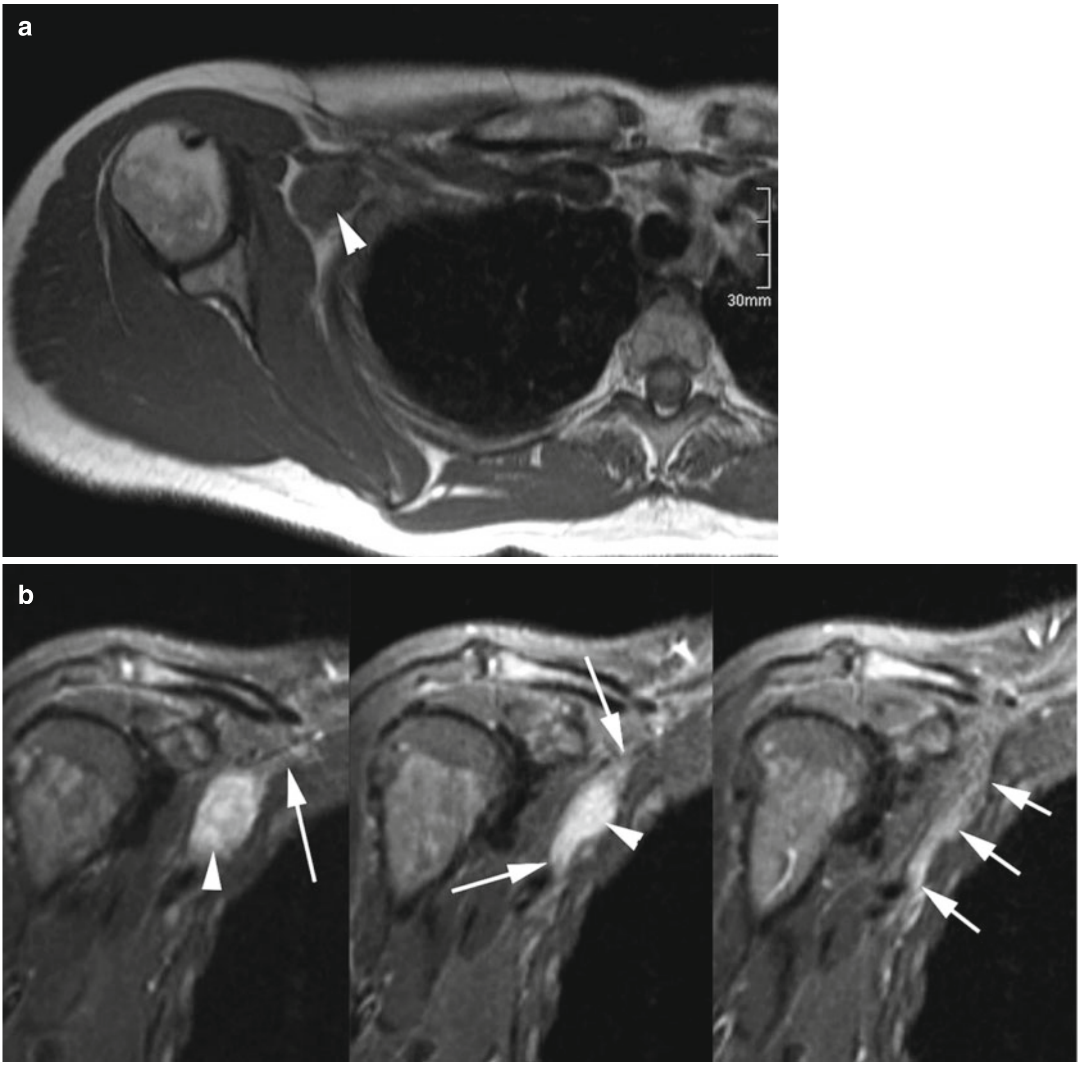

Fig. 2.2 (**a**) Axial T1-weighted image at the level of the right shoulder joint. A slightly oval mass of indeterminate origin (lymph node, primary soft tissue tumor) is noted in the axillary space (*arrowhead*). Note the progressive, cone like enlargement of the nerve at the proximal and distal margin of the tumor. (**b**) Coronal T2-weighted inversion recovery images (TIRM) show the mass (*arrowhead*) arising from the enlarged and swollen trunk of the brachial plexus (*arrows*) indicating a primary peripheral nerve tumor. The lesion was histologically classified as a schwannoma

Peripheral nerves can reliably be imaged in MRI down to a diameter of about 2 mm. In T1-weighted images, used for a detailed anatomic survey, nerve structures have intermediate signal intensity, comparable to peripheral musculature. In order to be able to separate nervous from muscle fibers, we therefore have to rely on tissue of different signal behavior that separates nervous structures from musculature or skeletal bones. This is well known from sagittal images of the spine where the nerve roots and ganglia can be easily identified within the neuroforamen at the level of the thoracic and lumbar spine due to the surrounding perineural fat. In the cervical spine, however, there is substantially less fatty tissue within the neuroforamen, so that the nerve root is less easily identifiable, especially in patients with low body mass index. In large nerves, there is always a sufficient amount of surrounding fat causing high signal in T1-weighted images to

make them easily identifiable. In even larger nerves, like the sciatic nerve, there is also adipose tissue interspersed between the perineural sheets of the individual fascicles which renders them visible. In smaller nerve fibers that abut musculature or have an intramuscular course the lack of surrounding fatty tissue impedes their detection, even when their diameter is substantially larger than the minimal resolution provided by the imaging sequence. Therefore, routine use of MRI in the peripheral nervous system is somewhat restricted: apart from the cervical-brachial and lumbosacral plexus, larger nerves of the upper extremity like the radial, ulnar, and median nerve down to the forearm and the median and ulnar nerve at the level of the wrist are routinely examined by MRI. In the lower extremity, the sciatic nerve as well as the tibial and peroneal nerves can be imaged down to the level of the lower leg (Maravilla and Bowe 1998).

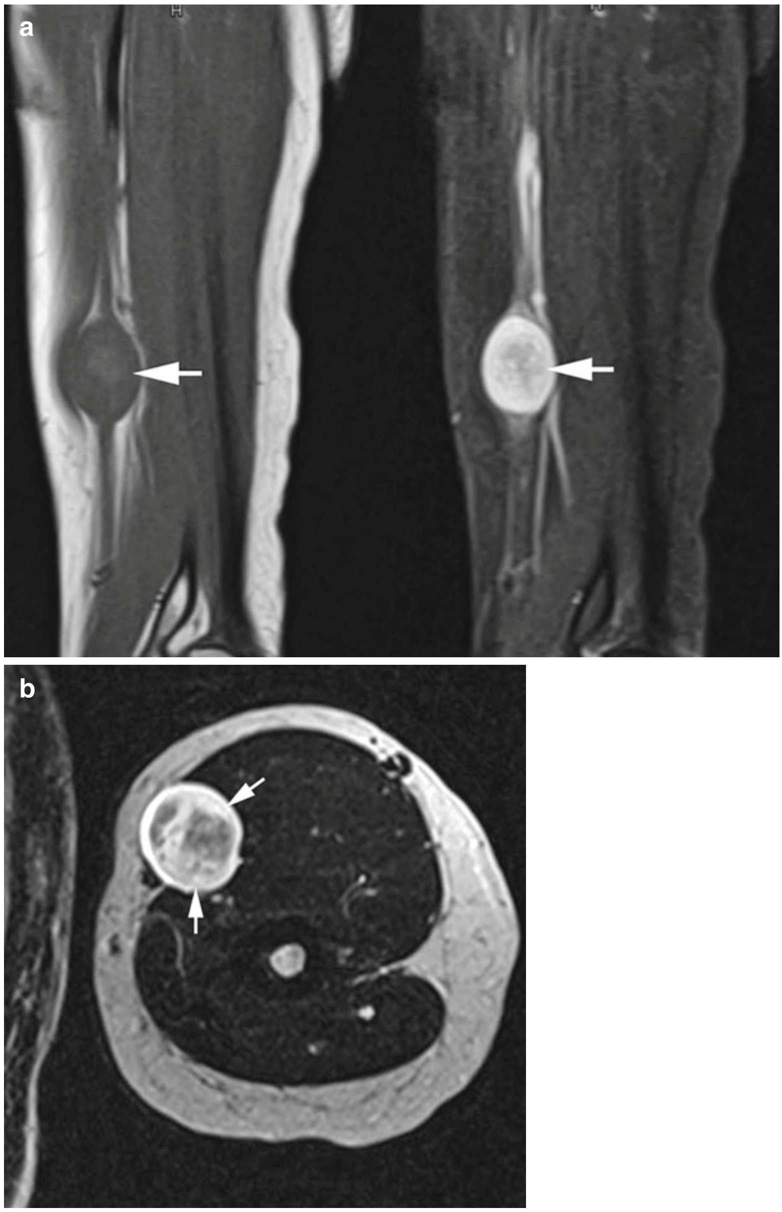

Fig. 2.3 (**a**) Sagittal T1-weighted (*left*) and T2-weighted inversion recovery image (TIRM – *right*) of the left upper arm showing a "tumor on a string" (*arrow*): the enlarged median nerve proximal and distal of the tumor can be clearly identified due to the surrounding fat in the T1-weighted image (*left*) and the bright edema on the T2-weighted image (*right*). Note the progressive, cone-like enlargement of the nerve at the proximal and distal to the tumor. (**b**) Axial T2-weighted image showing the extent of the tumor within the median bicipital groove and its internal inhomogeneity (*arrows*). (**c**) Series of axial T2-weighted images with spectral fat saturation: enlarged and abnormally bright median nerve (*arrowhead*) giving rise to the mass (*arrows*)

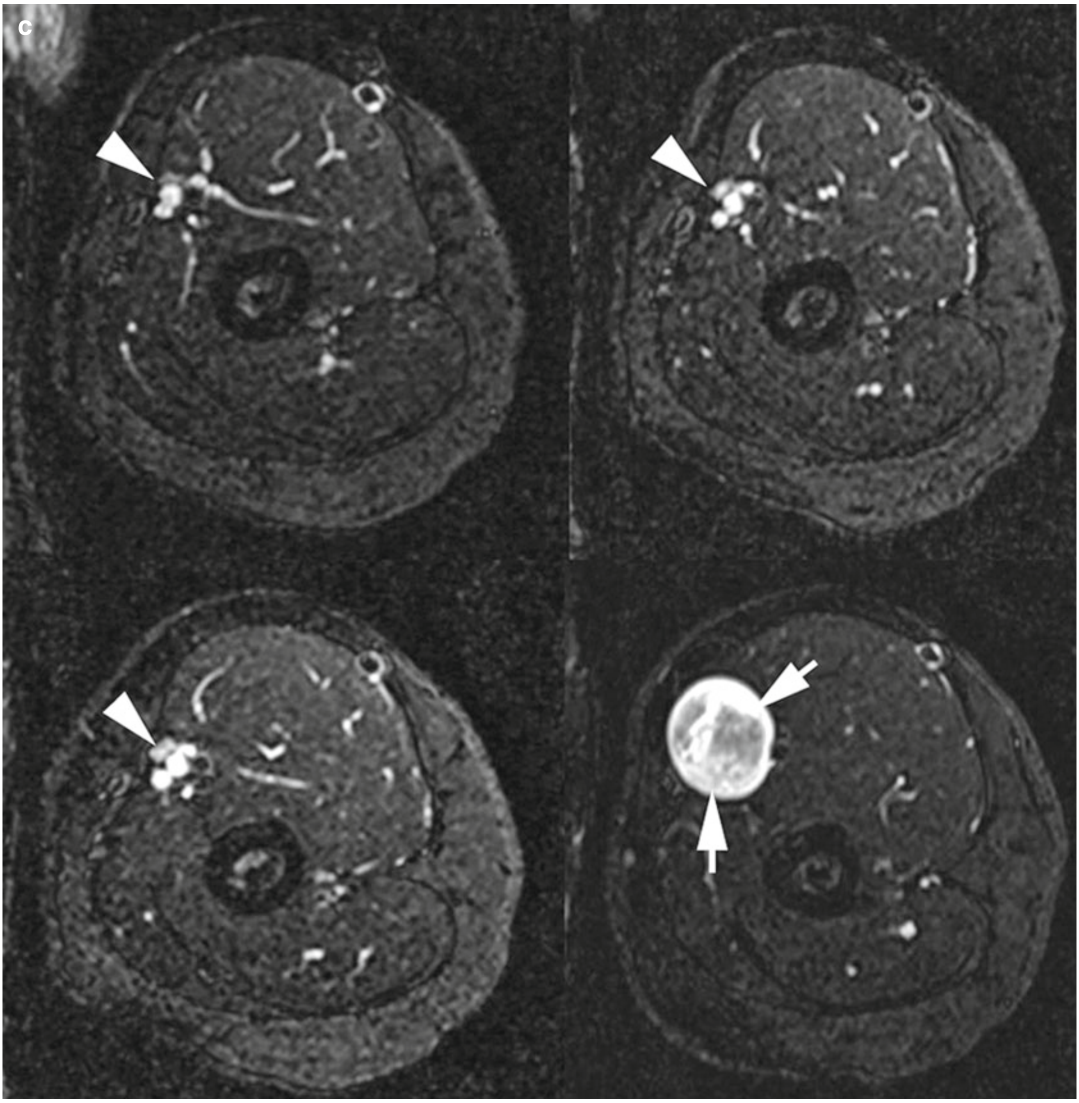

Fig. 2.3 (continued)

There are limitations in the assessment of pathologies of smaller nerves with MRI, especially in patients with degenerative nervous diseases. In these cases, there is only a very limited edematous reaction of the nerve secondary to the disease so that T2-weighted images fail to depict an enlarged and unusually hyperintense nerve. Contrast administration shows a markedly increased uptake in cases of acute inflammation; however, in chronic changes the inflammatory changes are much too subtle to reveal pathologic hyperperfusion. Nevertheless, MRI can be of great diagnostic value also in these cases: denervation of musculature causes signal changes in the muscle groups affected, which can readily be depicted by MR imaging. Muscle edema in early denervation and fatty degeneration and atrophy of the musculature at a later stage of a disease pinpoint the site of nervous damage, although the structural damage of the nerve itself cannot be visualized (Chhabrand and Andreisek 2012).

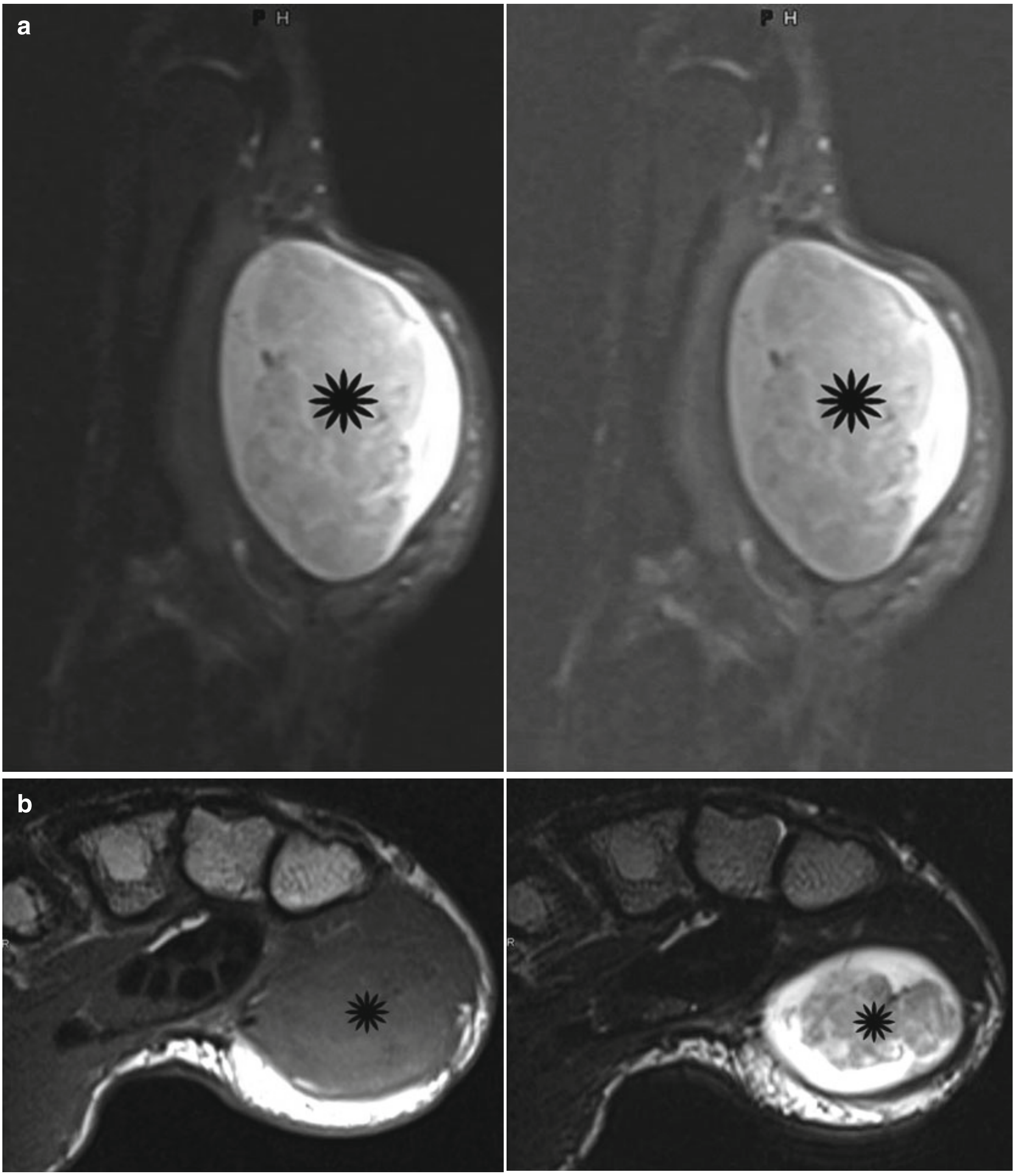

Fig. 2.4 Schwannoma (*asterisk*) of the ulnar nerve: (**a**) sagittal TSE T1 (*left*) and T2 TIRM (*right*) images of the hand. At the proximal end of the tumor, a portion of the ulnar nerve can be identified with a cone-shaped enlargement connected to the tumor: mass with "nervous tail." (**b**) Axial TSE T1- (*top*) and T2-weighted (*bottom*) images showing the extent and the inhomogeneous signal characteristics of the schwannoma (*asterisk*)

2.2 Measurement Sequences and Protocol Design

Imaging of peripheral nerves requires first of all a very detailed anatomical survey of the region of interest. This is best achieved by spin echo or turbo spin echo T1-weighted sequences. These images should be angulated along the direction of a nerve under investigation and, in a second plane, perpendicular to a nerves' course producing axial cross-sectional images. These sequences yield a high tissue signal thus allowing for very small imaging voxels with little background noise that would otherwise obscure image contrast. These sequences can be measured with almost all commercially available scanners; however, the stronger the static magnetic field, the higher the resonance signal gets. In lower-field scanners the same signal increase, and thus the ability to measure equally fine detailed images can be achieved by increasing the number of excitations: two excitations means that the same image plane is measured twice and the signal is internally averaged prior to image reconstruction. The gain in signal-to-noise ratio is unfortunately only by a factor of $\sqrt{2}$. However, an increase of the base magnetic field from 1.5T to 3T offers an approximately twofold signal gain. In order to achieve the same signal-to-noise ratio with the 1.5T scanner, four excitations would therefore be needed thus quadrupling imaging time: although lower-field scanners allow for adequately detailed anatomical imaging to assess the peripheral nervous system, time limitations could make such diagnostic procedures problematic in daily clinical practice.

Apart from the static magnetic field strength, coil technology is crucial for an optimal exploit of a resonance signal. Coils are antennas, picking up the resonance signal from within the patient's body. The smaller the coil, the better its signal gain; however, the overall scan area and the depth of penetration are at the same time reduced. Sophisticated multichannel array surface coils greatly facilitate high-resolution imaging by combining a set of smaller coils into one coil compound. This technology is quite demanding on scanner hardware and software and therefore cost intensive but allows for detailed imaging of more extensive areas of the patient's body while maintaining reasonable scan times.

The second set of sequences routinely used in imaging of peripheral nerves are turbo spin echo T2-weighted images with frequency-selective fat saturation. Alternatively, T2-weighted short TI inversion recovery images (STIR) can be measured – a comparable sequence where a different method to suppress the fat signal is used. These sequences are even more demanding for the scanner as they yield substantially less signal from the area under examination and the images can easily be obscured by background noise especially in low-field scanners. These images however are of high diagnostic interest: they mainly show the water content within anatomic structures and thus are very sensitive to edematous changes in any tissue. Whereas a normal, small peripheral nerve can be overlooked on these images, it is clearly shown as soon as it is enlarged due to an edema and its accordingly elevated water content (Fig. 2.5). This effect can equally be detected in cases of nerve entrapment or in posttraumatic lesions as in traction injury (mechanical edema), in infection (inflammatory edema), or in tumors where a combination of mechanical edema and inflammatory edema caused by an immunological reaction to the tumor growth occurs.

The use of contrast agents is generally not warranted in peripheral nervous imaging. Intravenous gadolinium should however be administered in patients with suspected infectious disease: inflammatory changes lead to a hyperperfusion of nerve bundles that can be visualized by "dying" the blood with a contrast agent. Inflammatory hyperpermeability of the endothelium also causes increased extravasation and thus accumulation of contrast agent in the extracellular space. To increase conspicuity, a fat-saturated T1 sequence should be used to cancel the bright signal from normal adipose tissue so that only the hyperintense signal from (hyper)perfused tissue remains. To distinguish contrast agent effects from normal bright structures in an image, it is mandatory to measure the exact same sequence before and after contrast administration.

Intravenous contrast agents should also be used in all cases where tumor formation is suspected. Gadolinium gives important information about the degree of vascularization of the tumor, helps to identify necrotic changes, and can at times aid in classifying the entity of the tumor.

Alternatively to fat-saturated spin echo or turbo spin echo T1 sequences, sometimes short TE volumetric 3D gradient echo sequences with either fat saturation or selective water excitation are used for pre- and postcontrast imaging. Although these sequences generally have a very high T1 contrast showing contrast agent accumulation in tissue with great conspicuity, their anatomical clarity is inferior and they are prone to produce various imaging artifacts.

Similarly, T2*-weighted 3D sequences can also be used instead or in adjunction to T2 or STIR sequences for the visualization of edematous changes of peripheral nerves. The use of such volumetric data acquisition methods is advantageous when secondary reconstructions of the acquired 3D data sets are needed. So, even a tortuous course of a nerve can be visualized in a single plane by calculating secondary curved reconstructions.

Apart from conventional imaging with T1- and T2-weighted spin echo or turbo spin echo sequences and 3D imaging, various modern and more sophisticated imaging techniques are presently under investigation for assessing peripheral nerves anatomically and possibly also functionally.

One of these novel approaches is called magnetization transfer imaging and emphasizes on the ratio and exchange rate of protein-bound and free water protons present in nerve tissue (Gambarota et al. 2012). Although the measured magnetization transfer ratio shows a physiologic variation between differently sized nerves (possibly due to differences in fascicle content), it seems to be sensitive for nerve damage within equally sized nerves or when compared to a healthy contralateral side. However, the value of this method has yet to be proven in daily clinical practice.

Diffusion-weighted imaging (DWI) on the other hand is a standard imaging scheme and widely used in central nervous system imaging. It has also been used to facilitate the detection of peripheral nerves in a whole-body MR examination (Yamashita et al. 2009). Apart from the intensity of the random microscopic motion (Brownian motion) of water molecules, their prevailing direction can also be assessed in diffusion-weighted sequences. Since the motion of

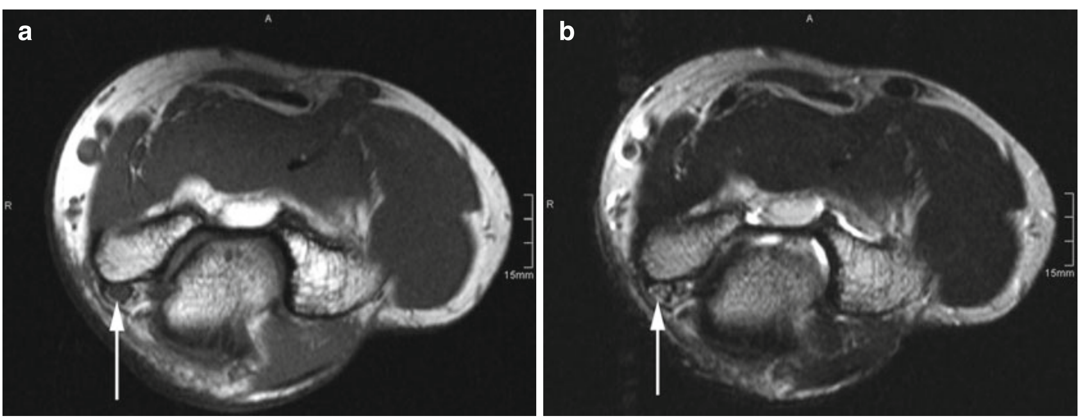

Fig. 2.5 (**a**) Axial T1-weighted image of the elbow at the level of the humeral condyle. The *arrow* indicates an enlarged ulnar nerve surrounded by perineural fat and abutting the bone. (**b**) Axial T2-weighted image demonstrating edematous changes within the swollen nerve (*arrow*). (**c**) Axial reconstructions of a 3D T2*-weighted sequence (DESS 3D) with selective water excitation: the ulnar nerve (*arrows*) can be easily followed in its course proximal, within, and distal to the ulnar nerve groove due to its bright signal (neural edema). (**d**) Single source image of the original 3D DESS data set in coronal orientation showing the portion of the ulnar nerve (*arrow*) running posterior to the medial humeral epicondyle

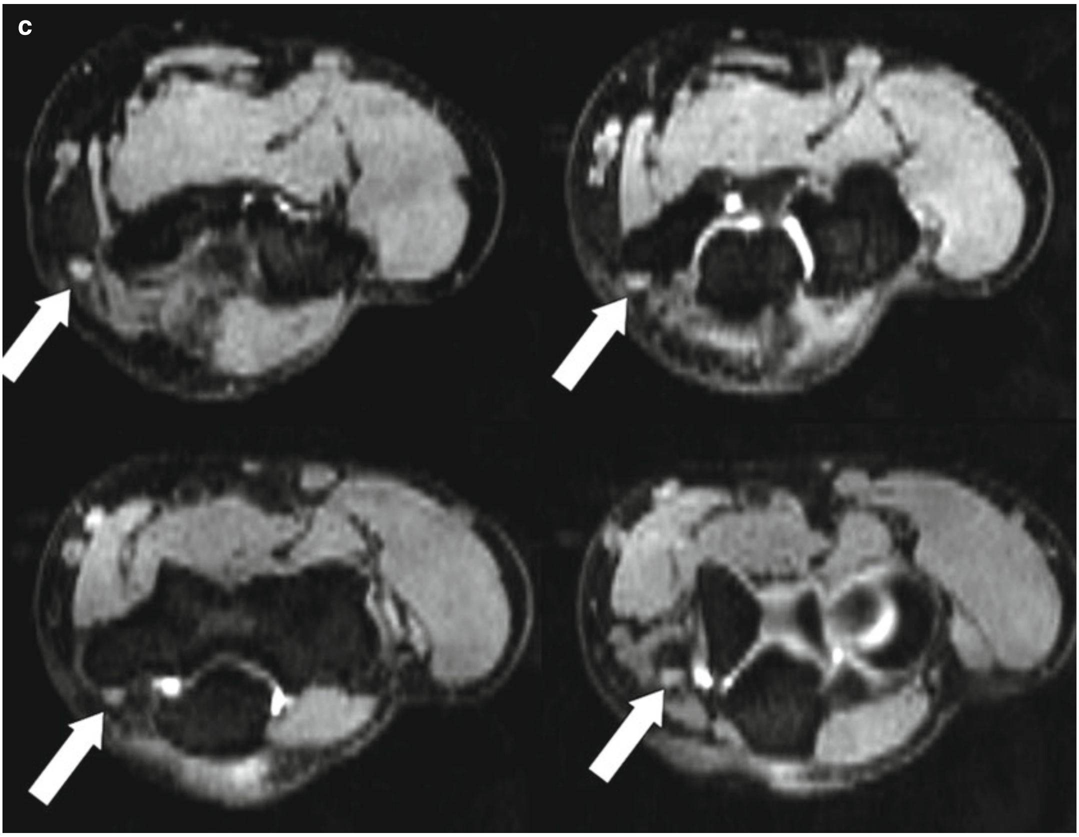

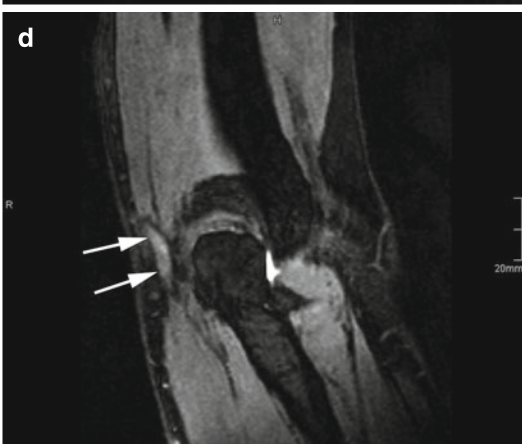

Fig. 2.5 (continued)

water molecules is impeded by membranes, its foremost direction follows the course of nerve bundles (Fig. 2.6). In the central nervous system, these anisotropic diffusion properties of nervous tracks are used to identify the course of nerve fibers within the medulla and the brain. One of its clinically important uses is to preoperatively help identify displaced tracts and thus permit to save their integrity when a space-occupying lesion needs to be resected. This variant of DWI is called diffusion tensor imaging (DTI) and shows promising results also for the peripheral nerve system, not only showing the nerve bundles themselves but also permitting to assess their integrity

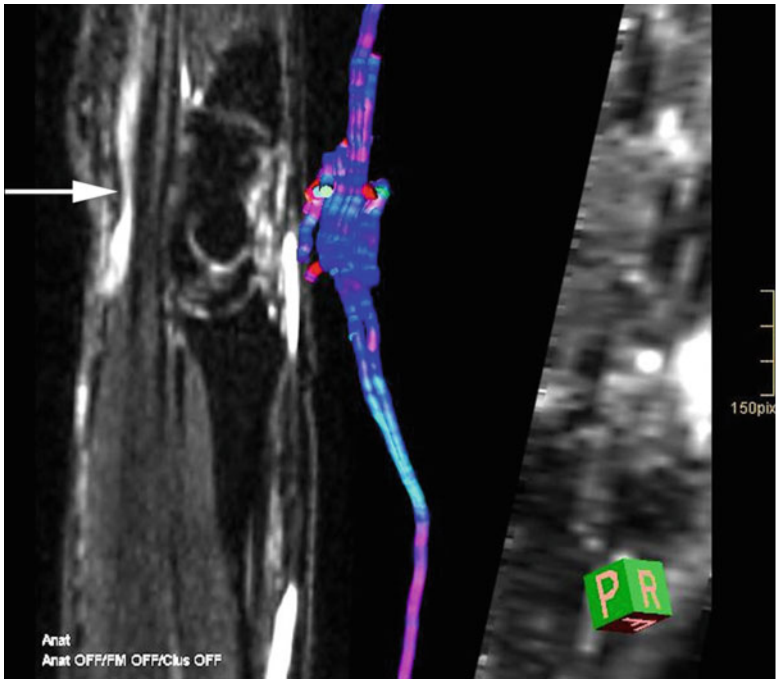

Fig. 2.6 Recurrent CTS (same patient as in Fig. 2.1). Direction-sensitive diffusion-weighted imaging called "diffusion tensor imaging" (DTI) allows for a 3D reconstruction of the molecular water motion within the nerve fascicles. Intact nerves can be followed by using seed points from where the computer generates images along a nerve's course and displays color coded its direction. Note the compression of the median nerve at its entrance into the carpal tunnel depicted on one of the sagittal source images (*arrow*)

(Skorpil et al. 2007; Kakuda et al. 2011). This measurement scheme, however, suffers from an inherent low signal-to-noise level. To obtain satisfactory images in small peripheral nerves, it is mandatory to use a high-performance gradient system and, preferably, a high-field MR scanner.

References

Campagna R et al (2009) MRI assessment of recurrent carpal tunnel syndrome after open surgical release of the median nerve. AJR Am J Roentgenol 193(3):644–650

Chhabrand A, Andreisek G (2012) Magnetic resonance neurography. Jaypee Brothers Medical Publishers, New Delhi

Gambarota G et al (2012) Magnetic resonance imaging of peripheral nerves: differences in magnetization transfer. Muscle Nerve 45:13–17

Kakuda T et al (2011) Diffusion tensor imaging of peripheral nerve in patients with chronic inflammatory demyelinating polyradiculoneuropathy: a feasibility study. Neuroradiology 53(12):955–960

Maravilla KR, Bowe BC (1998) Imaging of the peripheral nervous system: evaluation of peripheral neuropathy and plexopathy. AJNR Am J Neuroradiol 19:1011–1023

Mesgarzadeh M et al (1989) Carpal tunnel: MR imaging. Part II. Carpal tunnel syndrome. Radiology 171:749–754

Shen J et al (2010) MR neurography: T1 and T2 measurements in acute peripheral nerve traction injury in rabbits. Radiology 254(3):729–738

Skorpil M et al (2007) Diffusion-direction-dependent imaging: a novel MRI approach for peripheral nerve imaging. Magn Reson Imaging 25(3):406–411

Wasa J et al (2010) MRI features in the differentiation of malignant peripheral nerve sheath tumors and neurofibromas. AJR Am J Roentgenol 194(6):1568–1574

Yamashita T et al (2009) Whole-body magnetic resonance neurography. N Engl J Med 361:538–539

3 Nerves in the Neck

Verena Spiss, Siegfried Peer, Werner Judmaier,
and Erich Brenner

Contents

V. Spiss (✉) • W. Judmaier
Department of Radiology, Innsbruck Medical University, Anichstrasse 35, Innsbruck 6020, Tyrol, Austria
e-mail: verena.spiss@i-med.ac.at; werner.judmaier@i-med.ac.at

S. Peer
CTI GesmbH,
Klostergasse 4, 6020 Innsbruck, Tyrol, Austria
e-mail: info@siegfried-peer.at

E. Brenner
Division for Clinical and Functional Anatomy, Innsbruck Medical University,
Müllerstrasse 59, 6020 Innsbruck, Tyrol, Austria
e-mail: erich.brenner@i-med.ac.at

3.1 Introduction

Under the prerequisite of a good anatomical knowledge, even the nerves in the neck and the brachial plexus with its complex regional anatomic topography can be clearly visualized with high-resolution ultrasound (HRUS). The typical appearance of nerves has to be distinguished from other surrounding structures, which may be especially challenging in this delicate region because of the many different types of surrounding structures.

The 12 pairs of cranial nerves emerge from the basal skull. In order to reach their end organ, they mainly take their course through bony channels in the skull base. That is the reason why most of them are rarely accessible to sonography. Only some like the accessory and the vagus nerves can be visualized along their extracranial course.

The vagus nerve is the tenth of the 12 paired cranial nerves. It represents the strongest parasympathetic nerve in the human body. After leaving the medulla oblongata and running through the jugular foramen, it passes into the carotid sheath and heads down to the neck, chest, and abdomen between the internal carotid artery and the internal jugular vein.

The vagus nerve is detected best at the level of the carotid sinus, where it is situated in the posterior triangular space between the internal jugular vein and the common carotid artery.

The accessory nerve is formed by the fusion of a cranial and a cervical root. Like the vagus nerve, it also exits from the jugular foramen and divides

S. Peer, H. Gruber (eds.), *Atlas of Peripheral Nerve Ultrasound*,
DOI 10.1007/978-3-642-25594-6_3, © Springer-Verlag Berlin Heidelberg 2013

afterward into two branches, the external and the internal branches. The internal branch fuses with the vagus nerve. The external branch is mainly a motor nerve and arises from the C1 to C3 spinal root. It gets superficial right beneath the sternocleidomastoid muscle and takes its topographic course down the lateral cervical triangle, which is bordered by the sternocleidomastoid muscle, the trapezius muscle, and the clavicle. It enters the trapezius muscle at its ventral side and innervates this muscle together with some branches of the cervical plexus. Due to its relatively long superficial course, iatrogenic lesions of this nerve are common complications of standard surgical interventions in the neck, such as neck dissection, lymph node biopsy, and jugular vein cannulation. Also different types of cervical trauma, or even deep massage, are well-known causes of a spinal accessory nerve dysfunction or palsy, which results in pain, stiffness, and dropping of the shoulder ("winging of the scapula").

Damage to the cervical plexus and especially to the phrenic nerve is most commonly due to iatrogenic injury during cardiothoracic or neck surgery. The phrenic nerve originates mainly from the fourth cervical nerve and also receives contributions from the third and fifth cervical nerves. It arises in the neck and passes down to supply the diaphragm as well as the mediastinal pleura, the pericardium, and the bordering peritoneum. The phrenic nerve heads down close to the anterior scalene to get anterior to the subclavian artery and posterior to its accompanying vein to enter the chest. It descends in the ventral mediastinum between the mediastinal pleura and the pericardium. It supplies motor fibers to the diaphragm and sensory fibers to the fibrous pericardium and to the mediastinal, pleural, and diaphragmatic peritoneum.

The brachial plexus as a fine network of nerve fibers heading down from the spine consists of the ventral rami of the lower four cervical and the first thoracic nerve roots (C5–C8, T1) and emerges through the neck and proceeds through the axilla into the arm. It is responsible for the muscular and cutaneous innervation of the entire upper limb. Only the trapezius muscle is innervated by the spinal accessory nerve, and the skin area near the axilla is innervated by the intercostobrachial nerve. The brachial plexus is divided into different levels that consist of roots, trunks, divisions, cords, and branches. Its supraclavicular section is formed by the superior, the medial, and the inferior trunk. The three plexus fascicles, the medial, the lateral, and the posterior fascicle, are built by interchanging fibers between these trunks and are named according to their topographic relationship to the axillary artery. These fascicles generate the three main nerves of the upper extremity (the median, the ulnar, and the radial nerve) as well as the axillary nerve, the musculocutaneous nerve, and several cutaneous nerves. The visualization of the brachial plexus at the trunk level is attained best in a transverse plane through the interscalene gap with a slight cranial tilt of the transducer. Surrounded by loose connective and fatty soft tissue, the superior, the medial, and the inferior trunk arise as small hypoechoic nodules. An essential tool to identify and visualize the brachial plexus by ultrasonography at its root level is the transverse process of the vertebra C7; here, the anterior tubercle of the transverse process is missing. After defining this anatomic landmark, the transducer can be moved further cranially to detect the relevant root by simple counting of the transverse processes. In the final scan plane, the nerve roots can be identified as hypoechoic small nodules exiting the cervical spine anterior to the posterior tubercle of the transverse processes.

Brachial plexus lesions, more precisely traumatic brachial plexus injuries, are very common in young patients. The most reported cause of adult brachial plexus injuries is high-impact trauma, e.g., car, motorcycle, skiing, or mountaineer accidents. Brachial plexus injuries in children usually occur as a result of birth trauma.

A well known but rather rare compression syndrome of the neurovascular bundle at the thoracic outlet region is the "thoracic outlet syndrome" (TOS). It is usually caused by anatomical variations or abnormalities, like an additional cervical rib, or masses in the surrounding structures. Patients typically present with pain, numbness, paresthesia, Raynaud's syndrome, and muscle atrophy in the affected upper limb.

3.2 Nerves in the Neck: Topographic Overview

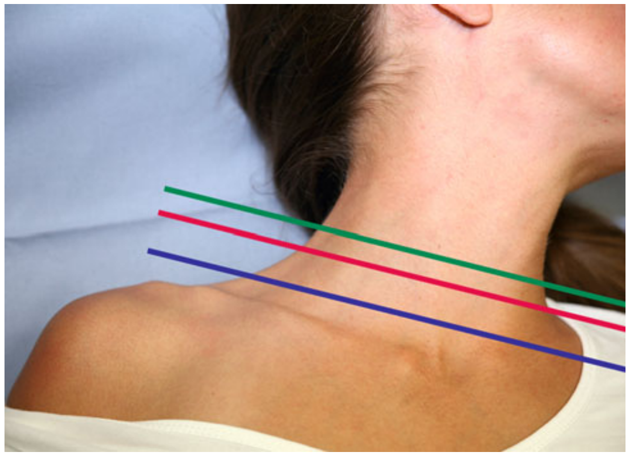

Fig. 3.1 General topographic overview of nerve anatomy in the neck. Localizer for anatomical cross sections (Fig. 3.2a–c). *Colored lines* correspond to level of cross sections

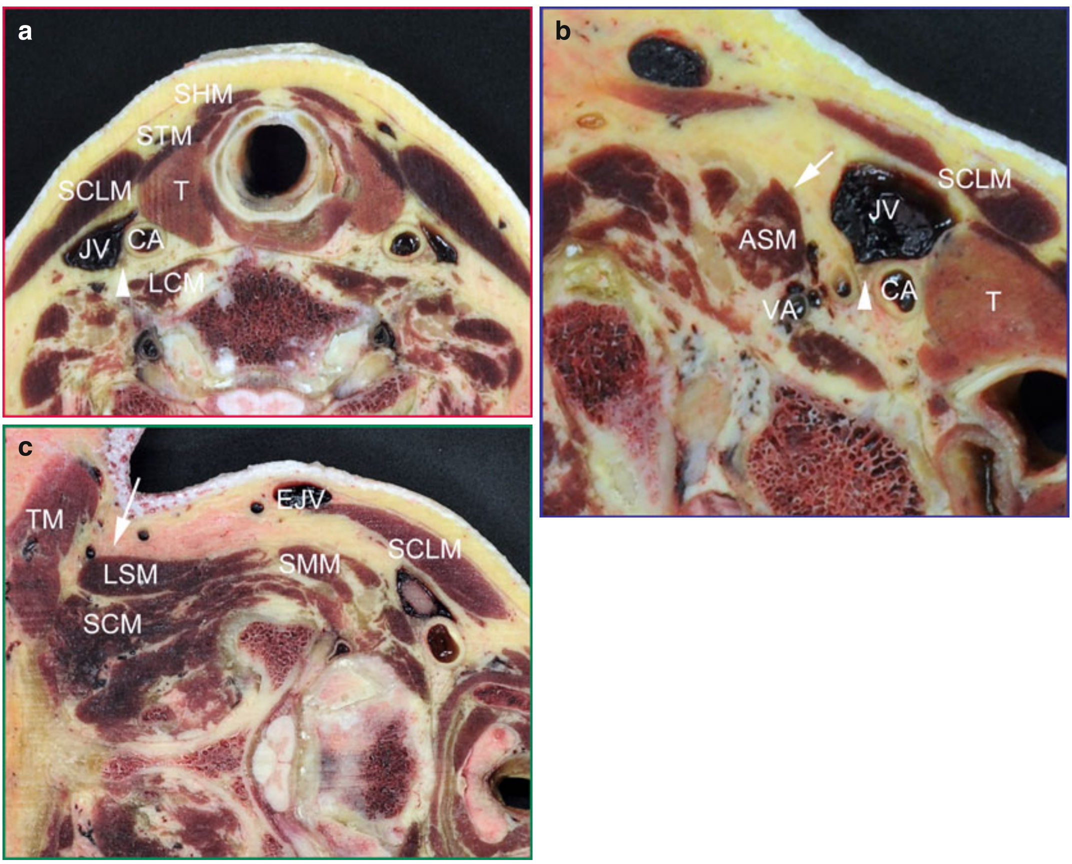

Fig. 3.2 (**a**) Anatomical cross section through the parathyroid region (*red line* in Fig. 3.1). Vagus nerve (*arrowhead*) in fat plane between carotid artery (*CA*) and internal jugular vein (*JV*) = "carotid space"; *SCLM* sternocleidomastoid muscle, *STM* sternothyroid muscle, *SHM* sternohyoid muscle, *LCM* longus colli muscle, *T* thyroid. (**b**) Anatomical cross section through the sternocleidomastoid region (*blue line* in Fig. 3.1). Vagus nerve (*arrowhead*); Phrenic nerve (*arrow*) alongside anterior scalene muscle (*ASM*); *SCLM* sternocleidomastoid muscle, *LCM* longus colli muscle, *CA* carotid artery, *JV* internal jugular vein, *VA* vertebral artery. (**c**) Anatomical cross section through lateral cervical triangle (*green line* in Fig. 3.1). Accessory nerve (*arrow*) is seen adjacent to edge of levator scapulae muscle (*LSM*) and anterior to trapezius muscle (*TM*). *SCM* splenius cervicis muscle, *SMM* scalenus medius muscle, *SCLM* sternocleidomastoid muscle, *EJV* external jugular vein

3.2.1 Parathyroid Region (Vagus Nerve)

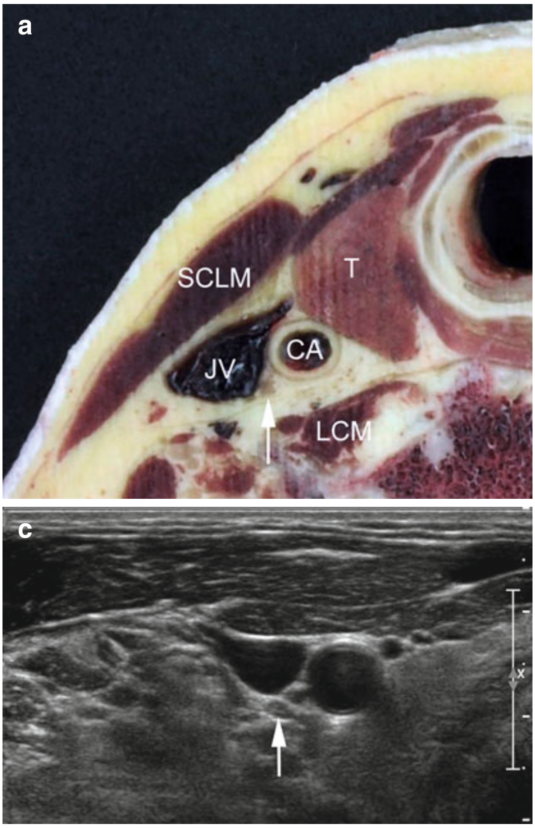

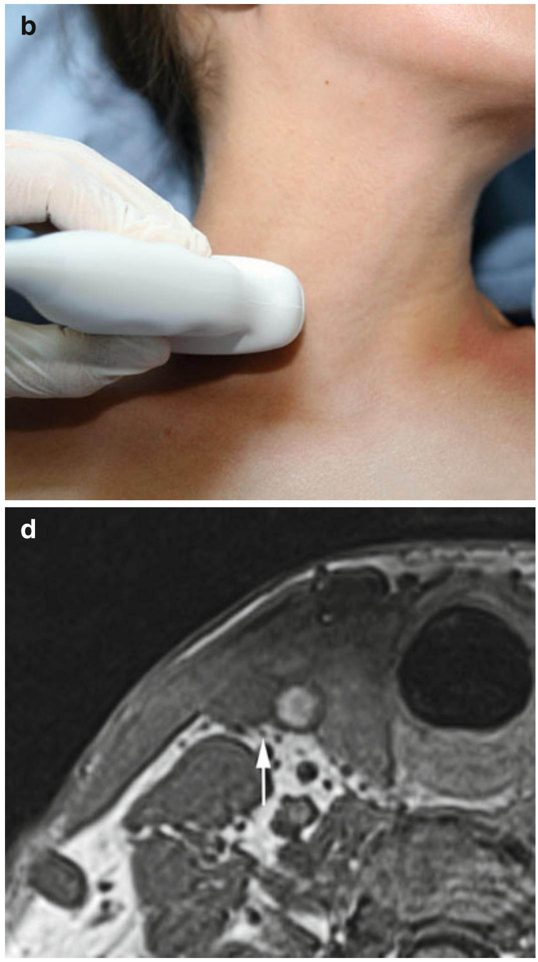

Fig. 3.3 (**a**) Anatomical cross section. (**b**) Transducer position. (**c**) Transverse sonogram. (**d**) Transverse T1-weighted MR image. Vagus nerve (*short arrow*) in triangle between internal jugular vein (*JV*) and carotid artery (*CA*); *SCLM* sternocleidomastoid muscle, *LCM* longus colli muscle, *T* thyroid.

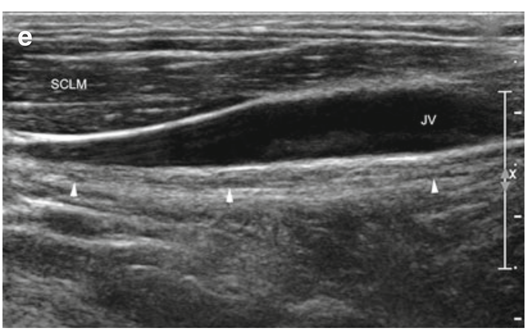

(**e**) Longitudinal sonogram of vagus nerve (*arrowheads*) lying underneath the sternocleidomastoid muscle (SCLM) and internal jugular vein (JV)

3.2.2 Sternocleidomastoid Region (Phrenic Nerve)

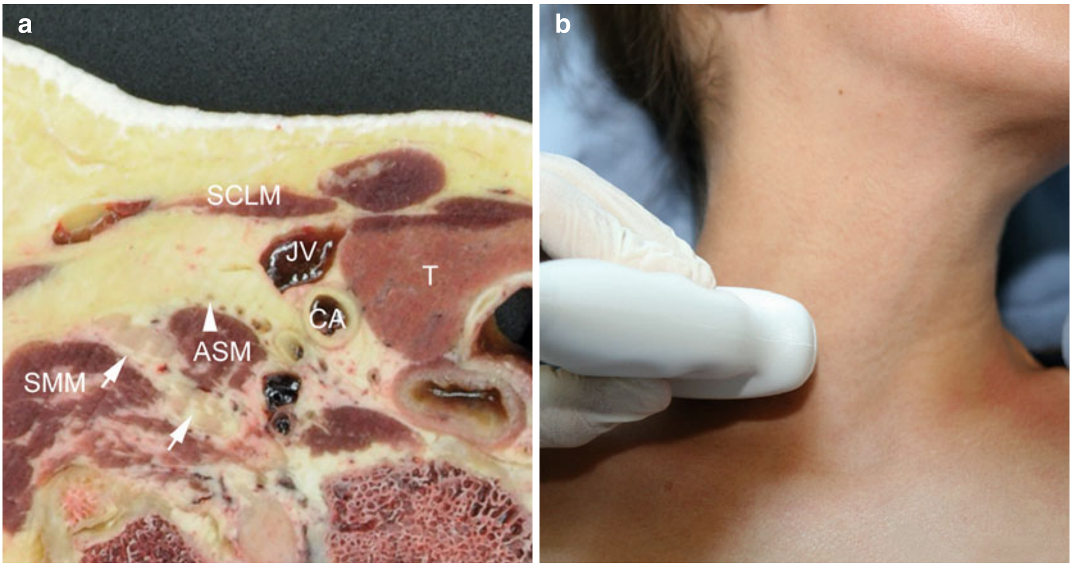

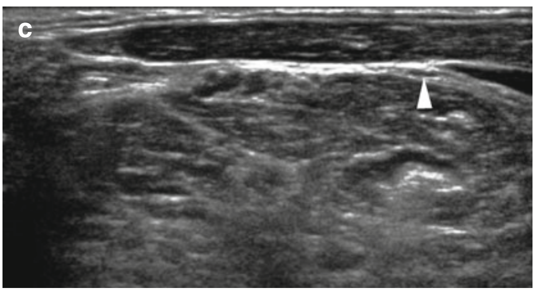

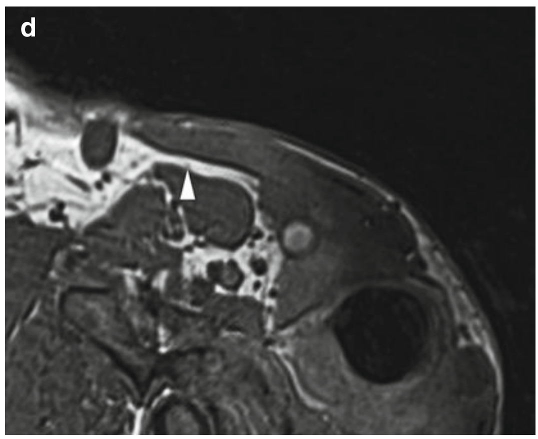

Fig. 3.4 (**a**) Anatomical cross section. (**b**) Transducer position. (**c**) Transverse sonogram. (**d**) Transverse T1-weighted MR-image. The phrenic nerve (*arrowhead*) is seen traversing on top of the anterior scalene muscle (*ASM*). *Arrows* interscalene portion of brachial plexus, *JV* internal jugular vein, *CA* carotid artery, *SCLM* sternocleidomastoid muscle, *SMM* scalenus medius muscle, *T* thyroid.

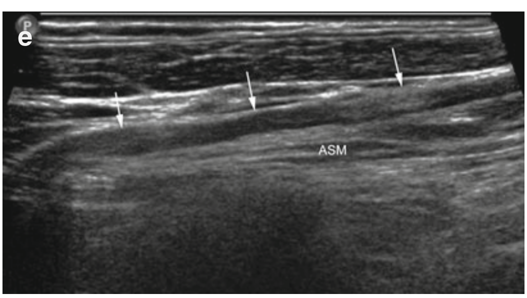

(**e**) Longitudinal sonogram of phrenic nerve (*arrows*) riding on top of the anterior scalene muscle (ASM)

3.2.3 Lateral Cervical Triangle (Accessory Nerve)

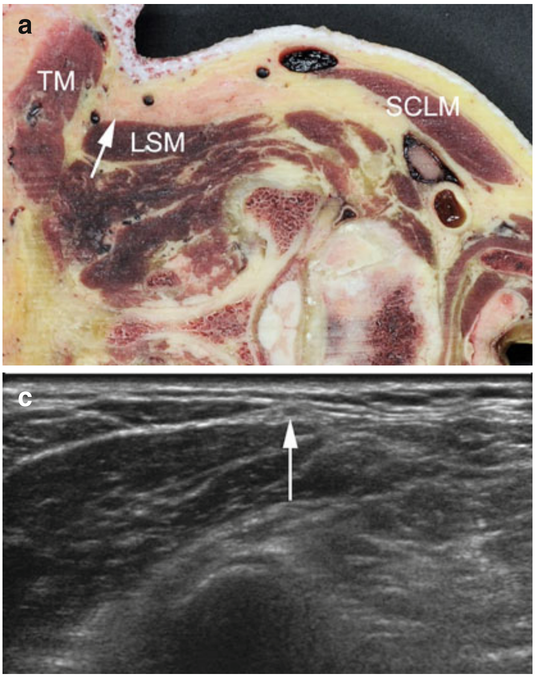

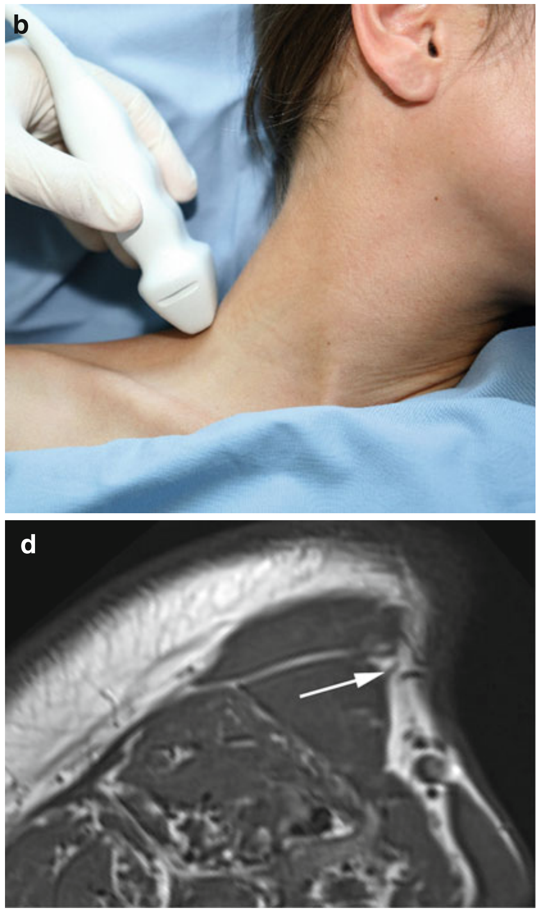

Fig. 3.5 (**a**) Anatomical cross section. (**b**) Transducer position. (**c**) Transverse sonogram. (**d**) Transverse T1-weighted MR image. The accessory nerve (*arrow*) is seen on top of the levator scapulae muscle (*LSM*). *SCLM* sternocleidomastoid muscle, *TM* trapezius muscle.

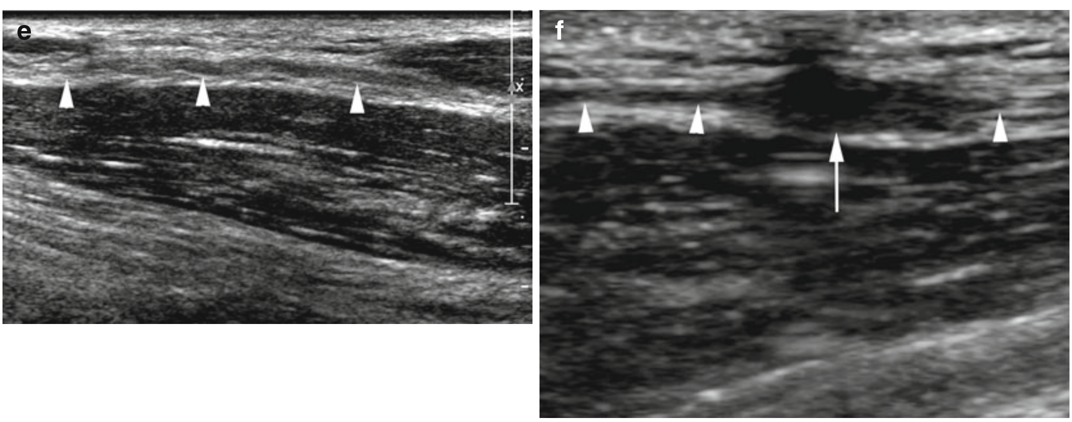

(**e**) Longitudinal view of a swollen accessory nerve (*arrowheads*) in a patient with accessory nerve palsy after carrying a heavy load on top of his shoulder. (**f**) Longitudinal view of fusiform accessory nerve (*arrowheads*) in another patient with accessory nerve palsy after cervical lymph node biopsy. The nerve is swollen and encased by scar formation (*arrow*)

3.3 The Brachial Plexus: Topographic Overview

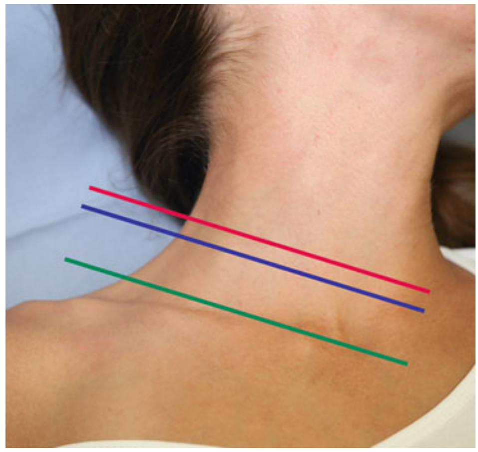

Fig. 3.6 General topographic overview of nerve anatomy in the brachial plexus. Localizer for anatomical cross sections (Fig. 3.7a–c). *Colored lines* correspond to level of cross sections

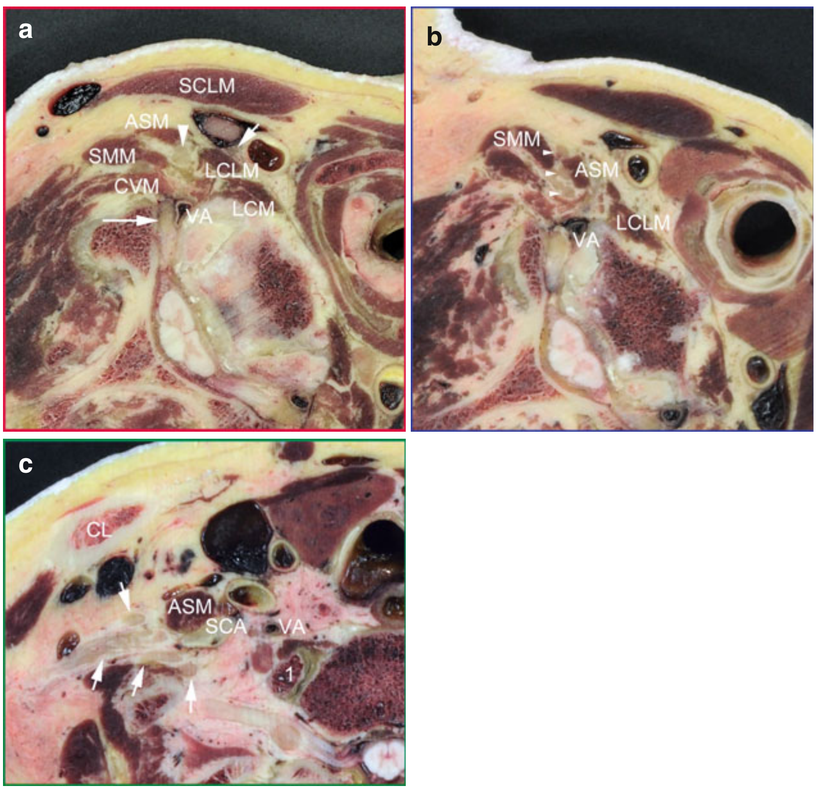

Fig. 3.7 (**a**) Anatomical cross section through the paravertebral region = root level of the brachial plexus (*red line* in Fig. 3.6). The cervical root C6 (*long arrow*) is seen exiting the neuroforamen next to the vertebral artery (*VA*). The C5 nerve root (*arrowhead*) is already entering the interscalene gap. *ASM* anterior scalene muscle, *SMM* scalenus medius muscle, *LCM* longus capitis muscle, *LCLM* longus colli muscle, *SCLM* sternocleidomastoid muscle, *CVM* cervical muscles (longissimus cervicis and iliocostalis cervicis muscle). Note vagus nerve (*small arrow*) inside the triangle formed by the common carotid artery and the jugular vein (see Sect. 3.2.1). (**b**) Anatomical cross section through the interscalene region (*blue line* in Fig. 3.6). The cervical nerve roots (*arrowheads*) traverse through the interscalene gap, where they exchange fibers to form the plexus trunks. *ASM* anterior scalene muscle, *SMM* scalenus medius muscle, *LCLM* longus colli muscle, *VA* vertebral artery. (**c**) Anatomical cross section through supraclavicular region (*green line* in Fig. 3.6). After exiting the interscalene gap, the cervical nerve roots (*arrows*) start to group along to the vascular bundle (*SCA* subclavian artery) and the lateral edge of the anterior scalene muscle (*ASM*). *CL* clavicle, *1* first costovertebral joint, *VA* vertebral artery

3.3.1 Localizing the Cervical Spinal Segments

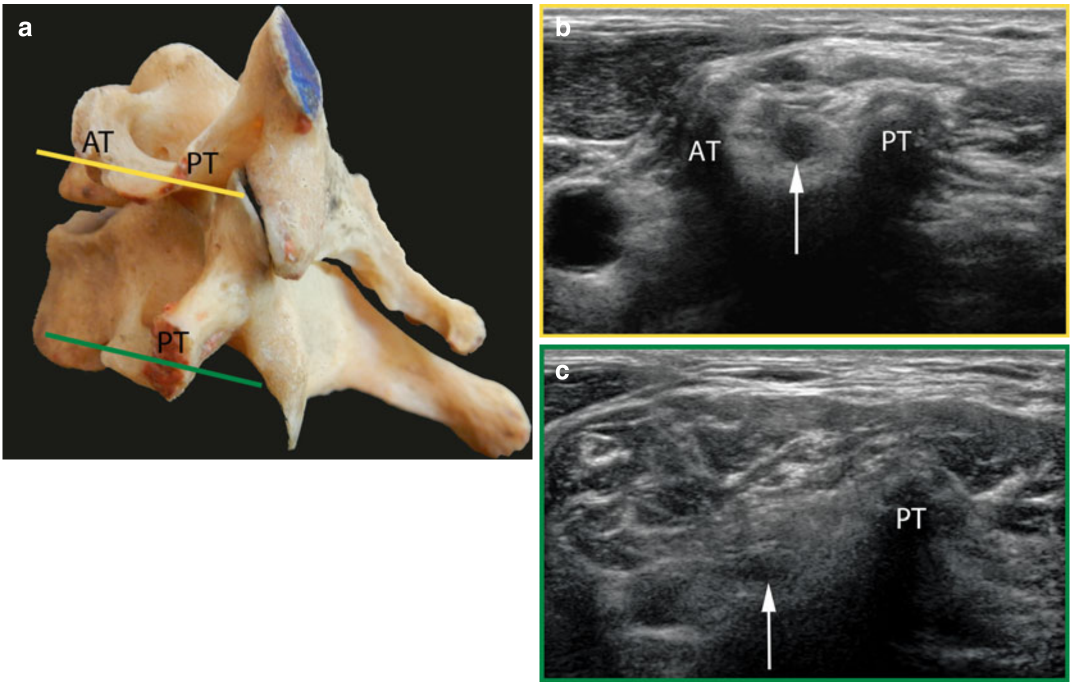

Fig. 3.8 (**a**) Anatomical specimen showing distinct features of transverse process at the level C6 with a big anterior (*AT*) and posterior (*PT*) bony tubercle and C7 with a missing anterior tubercle. *Colored lines* correspond to level of transverse sonograms. (**b**) Transverse sonogram through transverse process of the sixth cervical vertebra (*yellow line* in **a**) demonstrating the C6 nerve root (*arrow*) and anterior (*AT*) and posterior tubercle (*PT*). (**c**) Transverse sonogram through transverse process of the seventh cervical vertebra (*green line* in **a**) demonstrating the C7 nerve root (*arrow*) and only a posterior tubercle (*PT*)

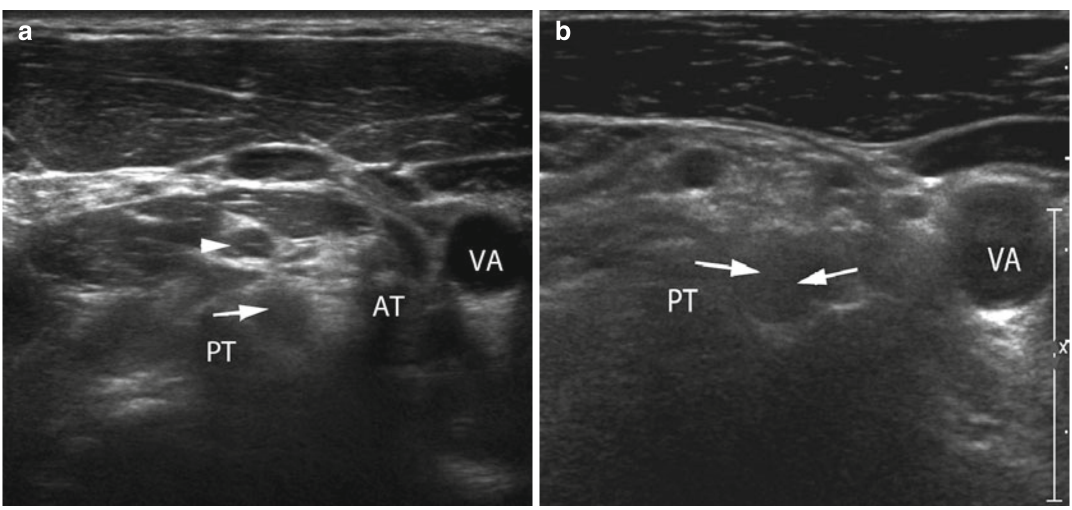

Fig. 3.9 (**a**) Transverse sonogram through transverse process of C6 in a patient with plexus palsy. The swollen and blurred nerve root (*arrow*) is identified as C6 because of presence of big anterior (*AT*) and posterior tubercle (*PT*); *arrowhead* C5 nerve root, *VA* vertebral artery. (**b**) In another patient with plexus palsy, the affected swollen and also blurred nerve root (*arrows*) is identified as C7 due to absence of anterior tubercle

3.3.2 Paravertebral Region (Brachial Plexus: Root Level)

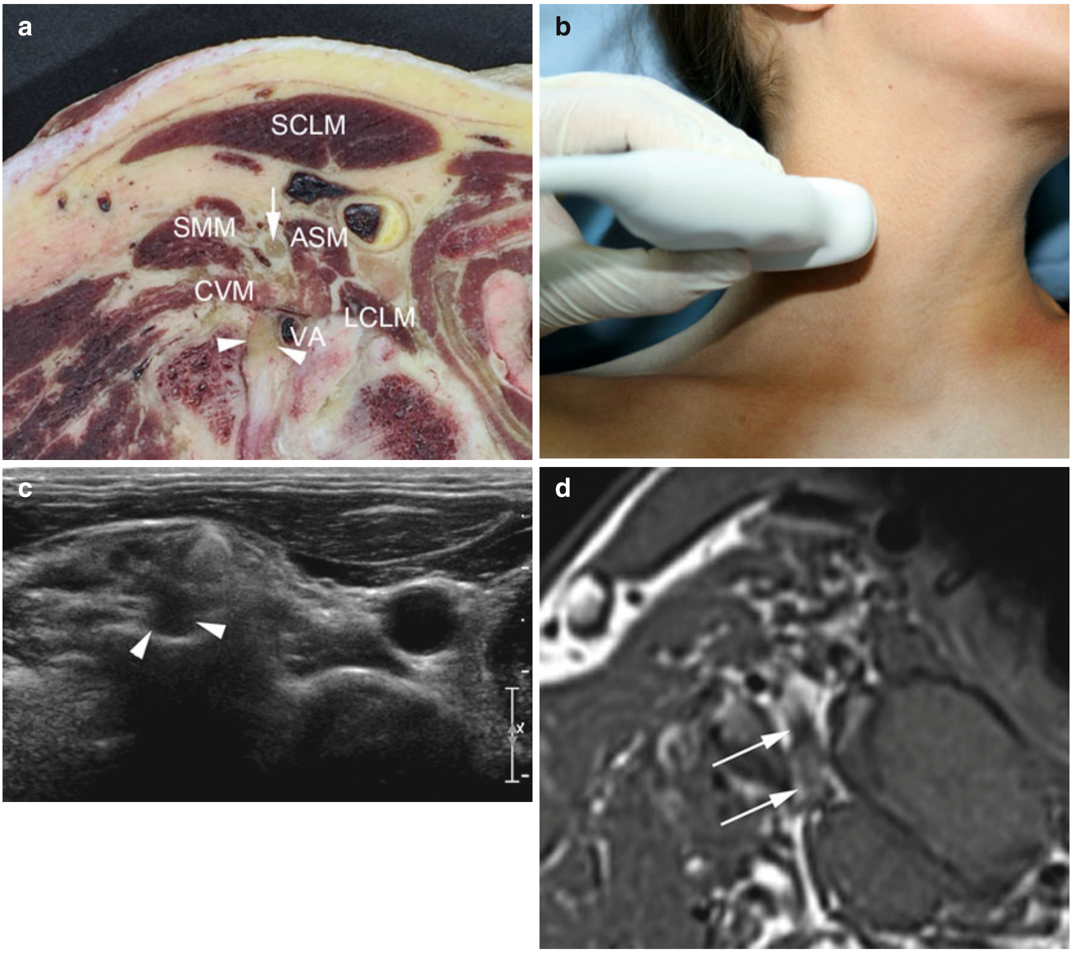

Fig. 3.10 (**a**) Anatomical cross section. (**b**) Transducer position. (**c**) Transverse sonogram. (**d**) Transverse T1-weighted MR image. The cervical root C6 (*arrowheads*) is seen exiting the neuroforamen close to the vertebral artery (*VA*). The C5 nerve root (*arrow*) is already close to entering the interscalene gap. *ASM* anterior scalene muscle, *SMM* scalenus medius muscle, *LCLM* longus colli muscle, *SCLM* sternocleidomastoid muscle, *CVM* cervical muscles (longissimus cervicis and iliocostalis cervicis muscle)

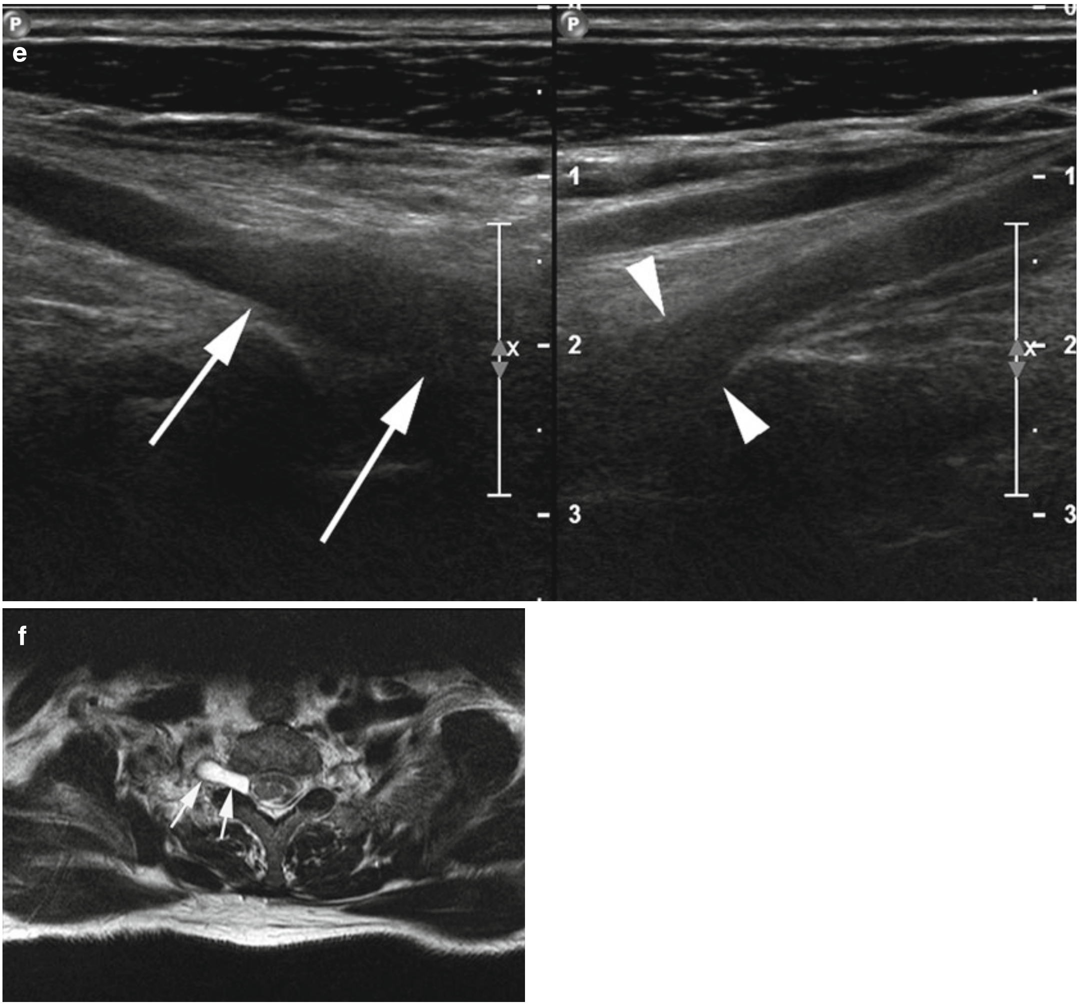

Fig. 3.10 (**e**) Longitudinal sonograms (**e**) of right and left paravertebral plexus showing an empty C7 root sleeve on the right (*arrows*) due to traumatic root avulsion (compare with normal root sleeve on the left *arrowheads* in **e**). (**f**) Corresponding axial T2-weighted MR image confirming foraminal root avulsion with a pseudomeningocele (*arrows*)

3.3.3 Interscalene Region (Brachial Plexus: Trunk Level)

Fig. 3.11 (**a**) Anatomical cross section. (**b**) Transducer position. (**c**) Transverse sonogram. (**d**) Transverse T1-weighted MR image. The brachial plexus trunks (*small arrows* C7 nerve root, *arrowheads* middle trunk, *long arrow* superior trunk) are seen on their passage through the interscalene gap (*arrowheads*). *ASM* anterior scalene muscle, *SMM* scalenus medius muscle, *SPM* scalenus posterior muscle, *LCLM* longus colli muscle

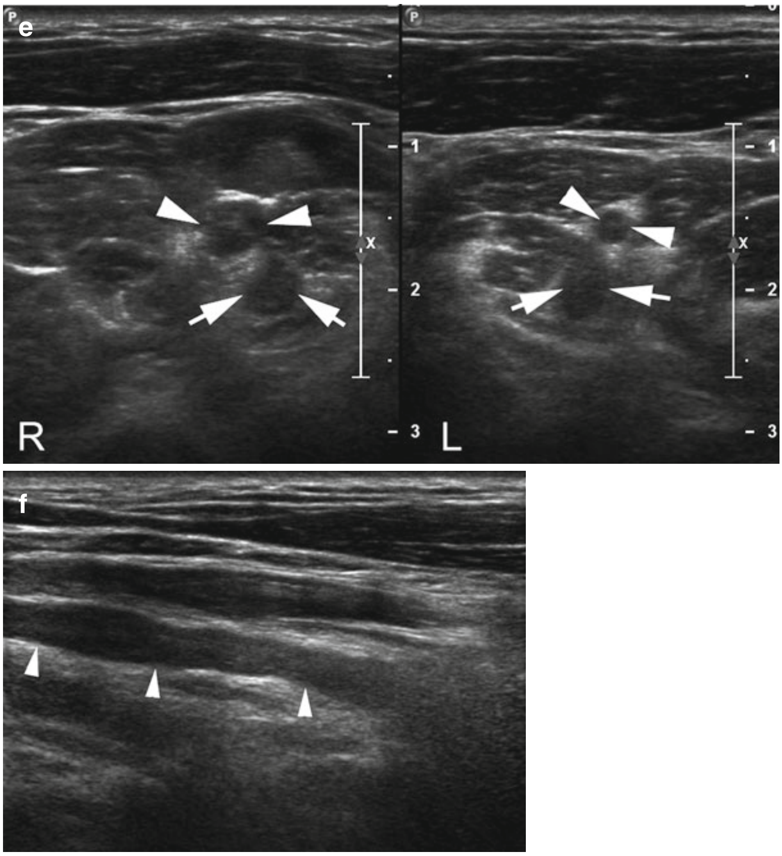

Fig. 3.11 (**e**, **f**) Transverse (**e**) and longitudinal (**f**) sonogram through interscalene region of a patient with a post-traumatic plexus palsy. In the side-by-side comparison, there is marked swelling of the C5 nerve root (*arrowheads*) within the interscalene gap on the right, while on the left the root is normal. Note normal appearance of C6 nerve root (*arrows*) on both sides. On the longitudinal view (**f**), the C5 nerve root (*arrowheads*) shows a wavy contour due to traction and edema

3.3.4 Supraclavicular Region (Brachial Plexus: Trunk Level)

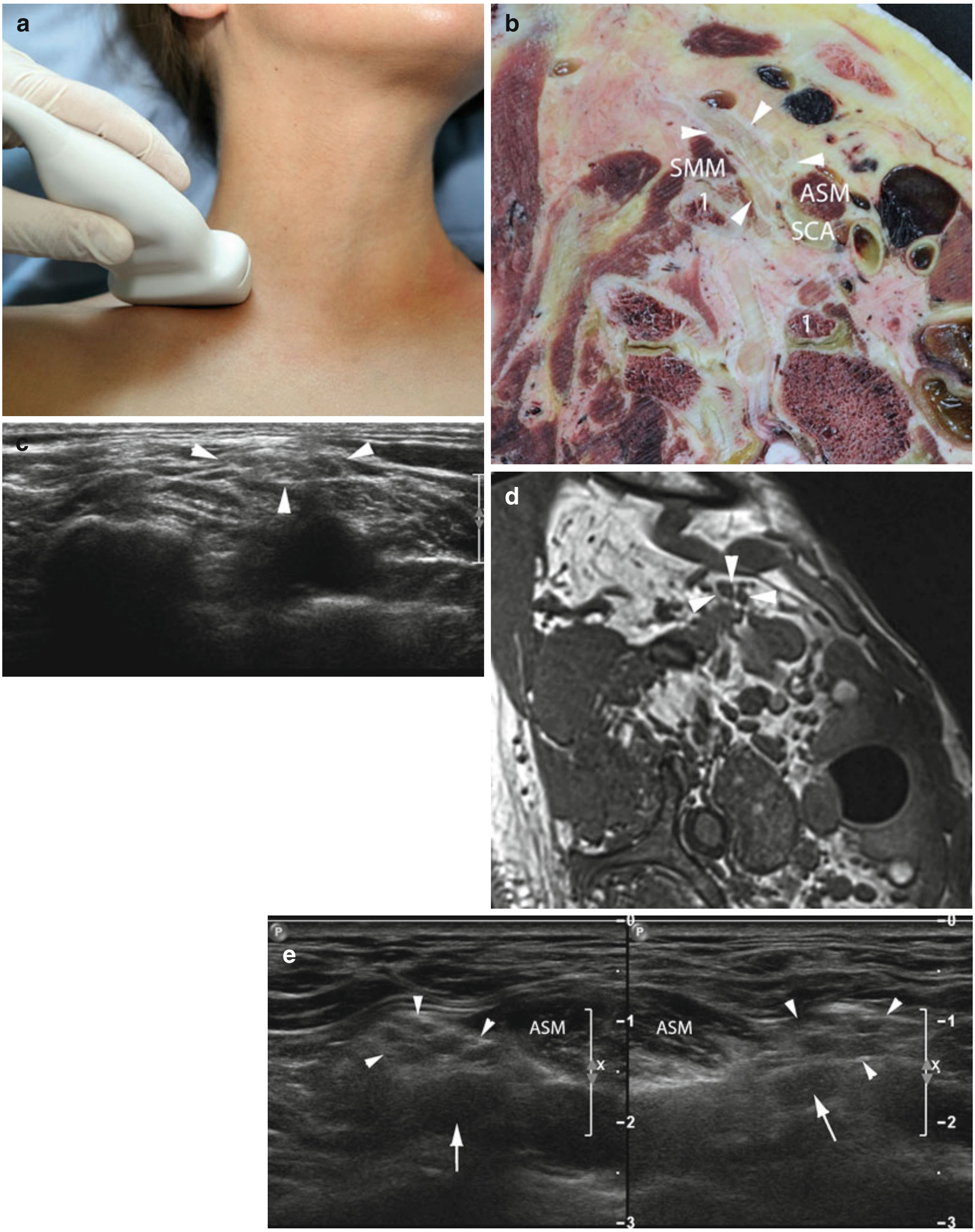

Fig. 3.12 (**a**) Anatomical cross section. (**b**) Transducer position. (**c**) Transverse sonogram. (**d**) Transverse T1-weighted MR image. The supraclavicular plexus (*arrowheads*) spreads after the plexus exits the interscalene gap. *ASM* anterior scalene muscle, *SMM* scalenus medius muscle, *SCA* subclavian artery, *1* medial and lateral part of first rib (dissected) (**e**) Transverse sonogram with side-by-side comparison of supraclavicular plexus shortly after exiting the interscalene gap (*arrowheads*). The C8 nerve root (*arrows*) is markedly thickened on the right side in this patient with right-sided posttraumatic incomplete plexus palsy

Bibliography

Agten A, Maes K et al (2012) Bortezomib partially protects the rat diaphragm from ventilator-induced diaphragm dysfunction. Crit Care Med 40(8):2449–2455

Ahmed AA (2012) Dysfunction of the diaphragm. N Engl J Med 366(21):2036–2037; author reply 2037

Armstrong JD 2nd (2012) Dysfunction of the diaphragm. N Engl J Med 366(21):2036; author reply 2037

Asquier C, Troussier B et al (1996) Femoral neuralgia due to degenerative spinal disease. A retrospective clinical and radio-anatomical study of one hundred cases. Rev Rhum Engl Ed 63(4):278–284

Beastrom N, Lu H et al (2011) mdx((5)cv) mice manifest more severe muscle dysfunction and diaphragm force deficits than do mdx mice. Am J Pathol 179(5): 2464–2474

Boczkowski J, Lisdero CL et al (1999) Endogenous peroxynitrite mediates mitochondrial dysfunction in rat diaphragm during endotoxemia. FASEB J 13(12): 1637–1646

Caron MA, Debigare R et al (2011) Diaphragm and skeletal muscle dysfunction in COPD. Rev Mal Respir 28(10): 1250–1264

Carvalho GA, Nikkhah G et al (1997) Diagnosis of root avulsions in traumatic brachial plexus injuries: value of computerized tomography myelography and magnetic resonance imaging. J Neurosurg 86(1):69–76

Goligher EC, Ferguson ND et al (2012) Ventilator-induced diaphragm dysfunction: from mice (hopefully) to men. Anesthesiology 117:463–464

Harpf C, Rhomberg M et al (1999) Iatrogenic lesion of the accessory nerve in cervical lymph node biopsy. Chirurg 70(6):690–693

Hudson MB, Smuder AJ et al (2012) Both high level pressure support ventilation and controlled mechanical ventilation induce diaphragm dysfunction and atrophy. Crit Care Med 40(4):1254–1260

Ishizaki M, Maeda Y et al (2011) Rescue from respiratory dysfunction by transduction of full-length dystrophin to diaphragm via the peritoneal cavity in utrophin/dystrophin double knockout mice. Mol Ther 19(7): 1230–1235

Kierner AC, Zelenka I et al (2000) Surgical anatomy of the spinal accessory nerve and the trapezius branches of the cervical plexus. Arch Surg 135(12):1428–1431

Kim WY, Suh HJ et al (2011) Diaphragm dysfunction assessed by ultrasonography: influence on weaning from mechanical ventilation. Crit Care Med 39(12): 2627–2630

Liss AG, af Ekenstam FW et al (1995) Changes in the spinal terminal pattern of the superficial radial nerve after a peripheral nerve injury. An anatomical study in cats. Scand J Plast Reconstr Surg Hand Surg 29(2): 117–131

McCool FD, Tzelepis GE (2012) Dysfunction of the diaphragm. N Engl J Med 366(10):932–942

Mirjalili SA, Muirhead JC et al (2012) Ultrasound visualization of the spinal accessory nerve in vivo. J Surg Res 175(1):e11–e16

Miyata K, Kitamura H (1997) Accessory nerve damages and impaired shoulder movements after neck dissections. Am J Otolaryngol 18(3):197–201

Mrozek S, Jung B et al (2012) Rapid onset of specific diaphragm weakness in a healthy murine model of ventilator-induced diaphragmatic dysfunction. Anesthesiology 117:560–567

Peer S, Bodner G (2008) High-resolution sonography of the peripheral nervous system. Springer, Berlin/Heidelberg

Perlmutter GS, Apruzzese W (1998) Axillary nerve injuries in contact sports: recommendations for treatment and rehabilitation. Sports Med 26(5):351–361

Peterson JM, Kline W et al (2011) Peptide-based inhibition of NF-kappaB rescues diaphragm muscle contractile dysfunction in a murine model of Duchenne muscular dystrophy. Mol Med 17(5–6): 508–515

Platzer W (2009) Taschenatlas Anatomie, Bewegungsapparat. Thieme-Verlag, Stuttgart

Resnick D, Niwayama G et al (1981) Spinal vacuum phenomena: anatomical study and review. Radiology 139(2):341–348

Smuder AJ, Min K et al (2012) Endurance exercise attenuates ventilator-induced diaphragm dysfunction. J Appl Physiol 112(3):501–510

Testelmans D, Maes K et al (2006) Rocuronium exacerbates mechanical ventilation-induced diaphragm dysfunction in rats. Crit Care Med 34(12): 3018–3023

Trepel M (2011) Neuroanatomie, 5. Auflage. Urban & Fischer-Verlag, Elsevier

van Hees HW, Schellekens WJ et al (2012) Titin and diaphragm dysfunction in mechanically ventilated rats. Intensive Care Med 38(4):702–709

Wiater JM, Bigliani LU (1999) Spinal accessory nerve injury. Clin Orthop Relat Res 368:5–16

Yang LJ, Chang KW et al (2012) A systematic review of nerve transfer and nerve repair for the treatment of adult upper brachial plexus injury. Neurosurgery 71(2):417–429

Upper Extremity Nerves

4

Michaela Plaikner, Hannes Gruber, Werner Judmaier, and Erich Brenner

Contents

M. Plaikner (✉) • H. Gruber • W. Judmaier
Department of Radiology,
Innsbruck Medical University, Anichstrasse 35,
6020 Innsbruck, Tyrol, Austria
e-mail: michaela.plaikner@-i.med.ac.at;
hannes.gruber@i-med.ac.at;
werner.judmaier@i-med.ac.at

E. Brenner
Division for Clinical and Functional Anatomy,
Innsbruck Medical University, Müllerstrasse 59,
6020 Innsbruck, Tyrol, Austria
e-mail: erich.brenner@i-med.ac.at

S. Peer, H. Gruber (eds.), *Atlas of Peripheral Nerve Ultrasound*,
DOI 10.1007/978-3-642-25594-6_4,

4.1 Introduction

The major nerves of the upper extremity include the axillary nerve, the musculocutaneous nerve, the medial brachial cutaneous nerve, the medial antebrachial cutaneous nerve, the radial nerve, the ulnar nerve, and the median nerve. A basic knowledge of regional anatomy and topography of these nerves and their major branches is an essential prerequisite for sonographic examinations. By means of landmarks the respective nerve can be easily localized in specific sections of its course. In addition, certain locations exist, where these nerves traverse through narrow tunnels or along bony ridges (such as the carpal tunnel, the ulnar sulcus, or the radial groove). These regions are especially prone for nerve compression or injury and have distinct anatomical features, which must be known to constantly achieve high-quality sonographic diagnoses.

The axillary nerve arises from the posterior fascicle originating from the C5 and C6 nerve root. This nerve runs deep, close to the shoulder joint capsule around the surgical neck of the humerus, where it passes through the lateral axillary hiatus and runs underneath the deltoid muscle until it reaches the muscles' front border. The axillary nerve contains several muscle branches for the deltoid muscle as well as for the teres minor and the long head of the triceps brachii muscle. It innervates the shoulder joint and provides sensory branches for the lateral skin of the shoulder. The axillary nerve may be injured in anterior-inferior dislocation of the shoulder joint or by a fracture of the surgical neck of the humerus. Based on our experience with high-resolution sonography of peripheral nerves, the axillary nerve may be best detected by sonography with eversion and abduction of the arm. Only with this type of positioning, the nerve may be visualized in the lateral axillary hiatus right beside the accompanying posterior circumflex humeral artery. The necessary examination position however is not reasonable for a patient after shoulder dislocation, and therefore, in the acute setting it is often quite difficult to clearly depict this tiny nerve, with its very complex course and location inside a thick bulk of (at least swollen) soft tissues.

The musculocutaneous nerve is a composite sensomotoric nerve and diverts from the lateral fascicle receiving its fibers from the C5 to C7 nerve roots. Along its course this nerve pierces the coracobrachial muscle, at the same time innervating the muscle by giving off muscular branches. Then the nerve bends to the anterior side of the upper arm, where it runs further downward between the brachial and the biceps muscle. The musculocutaneous nerve can easily be identified with sonography. It gives off branches to the flexors of the upper arm including the coracobrachial muscle, both bellies of the brachial biceps muscle and the brachial muscle. At the elbow level the nerve perforates the fascia and bifurcates in the lateral subcutaneous layer of the forearm, where it supplies the skin. In the antecubital fossa the musculocutaneous nerve is located next to local cephalic vein segments, and therefore, injury of the nerve during venous puncture in this area is not uncommon.

The medial brachial cutaneous nerve and the medial antebrachial cutaneous nerve are mere sensory nerves. They originate from the medial plexus fascicle. The medial brachial cutaneous nerve very often communicates with the intercostobrachial nerve. These nerves run downward in an epifascial and subcutaneous layer and supply the medial skin of the upper extremity. Since also the medial antebrachial cutaneous nerve has a very close relationship to subcutaneous veins, nerve injury during venous puncture may also occur. Because of their small size, sonographic identification of the medial brachial and antebrachial cutaneous nerve may be challenging.

The radial nerve arises from the posterior fascicle and is formed by the C5–C8 nerve roots. Initially the nerve runs into the axilla, from where it proceeds into the depth and in a spiral-shaped course around the humeral bone accompanied by the profound brachial artery and vein. Along this route the radial nerve stays in direct contact with the humerus for a long distance. At the distal upper arm, the nerve reaches the lateral flexor side, right above the antecubital fossa, lying between the brachial and the brachioradial muscle, shortly after the radial nerve divides into its both terminal branches at the level of the radial head: the deep and the superficial branch. The common radial nerve supplies the extensor

muscles of the whole upper extremity plus the dorsal skin. The mere sensitive superficial branch continues along the lower arm right next to the medial border of the brachioradial muscle toward the wrist being medially accompanied by the radial artery and veins. At the distal third of the forearm, it turns to the dorsal subcutaneous side and reaches the dorsum of the hand. The deep branch of the radial nerve crosses the supinator muscle through a small tendinous arch, the so-called arcade of Frohse. It gives off numerous muscular branches and ends in the very thin posterior antebrachial interosseous nerve, lying on the posterior surface of the interosseous membrane. The radial nerve is quite often injured in humeral shaft fractures due to its predisposed course in direct contact to the humerus. A damage of the radial nerve causes the characteristic "drop hand." Another particular location of radial nerve injury is the arcade of Frohse, where the deep branch of the radial nerve can be compressed.

The ulnar nerve originates from the roots C8 to Th1 and emerges from the medial fascicle. It heads directly downward to the elbow within the medial bicipital groove without releasing any branches. Approximately in the middle of the upper arm, it pierces the medial intermuscular septum and continues to the elbow level where the nerve bends around the lower margin of the medial epicondyle passing though the ulnar groove, an osteofibrous channel where the nerve has a very superficial and exposed location. Passing the groove the ulnar nerve lies between the two heads of the ulnar carpal flexor. Covered by this muscle it continues straight to the wrist. In the middle of the lower arm, the ulnar nerve gives off its sensory dorsal branch and in the distal part of the lower arm another sensory branch, the palmar branch of the ulnar nerve. In the distal part of the forearm, the ulnar nerve lies very superficially in the subcutaneous layer between the tendon of the ulnar carpal flexor muscle medially and the ulnar artery and veins laterally. At the wrist the ulnar nerve passes a loose fibrous channel – the so-called Guyon's channel – and divides into its end branches: the superficial and the deep branch. The ulnar nerve supplies several muscles of the lower arm including the ulnar carpal flexor muscle, the ulnar head of the flexor digitorum profundus muscle, the muscles of the hypothenar, and most of the short muscles of the middle hand. By means of the dorsal branch and the palmar branch as well as the residual superficial branch which ends in the paired proper palmar finger nerves, the ulnar nerve also occupies wide sensory innervation areas. The ulnar nerve can easily be identified with sonography along its course within the medial bicipital groove posterior to the brachial artery or also as the single structure within the ulnar groove and Guyon's channel. Another easy way to visualize the ulnar nerve is in the distal third of the forearm in its typical position between the tendon of the ulnar carpal flexor muscle and the ulnar artery. Common sites of ulnar nerve compression and injury – due to a superficial and exposed location – are the elbow region as well as the Guyon's channel. The leading symptom of a permanent lesion of the ulnar nerve is the claw hand.

The median nerve originates from the roots C6 to Th1, and it is formed by the lateral and medial fascicle of the brachial plexus (median loop). The median nerve runs distally to the elbow, lying in the medial bicipital groove located lateral to the brachial artery and distalward crossing anteriorly to run medial to the artery in the cubital fossa. The median nerve gives off an articular branch in the upper arm as it passes the elbow joint. In the cubital region one of the important median nerve branches is the anterior antebrachial interosseous nerve, which runs downward to the carpus directly on the interosseous membrane. It reaches the pronator muscle, supplying not only the last-mentioned muscle but also the long flexor of the thumb and the radial parts of the deep finger flexors. Then the median nerve usually passes between the two heads of the pronator teres muscle and continues on to the wrist being located between the flexor digitorum superficialis and the flexor digitorum profundus muscle. At the forearm level the median nerve gives off a lot of motor branches as well as sensory branches to the volar side of the hand. The palmar cutaneous branch of the median nerve arises at the distal part of the forearm and supplies sensory innervation for the lateral aspect also of the skin of the palm. At the wrist joint area the median nerve proceeds underneath the flexor muscle retinaculum into the carpal tunnel and divides into its end branches (common palmar digital nerves and proper palmar digital nerves).

The latter are directly positioned close to the tendons of the long finger flexors always right beside a close accompanying artery. The median nerve is the largest nerve of the upper arm and can easily be identified with sonography along its course within the medial bicipital groove ventral to the brachial artery or at a level of the carpal tunnel, where the nerve is lying directly underneath the flexor retinaculum. Due to its small caliber, the anterior antebrachial interosseous nerve is hardly visualized even by high-resolution sonography due to its size combined with its deep position (see Chap. 1). A very common syndrome is the compression of the median nerve within the carpal tunnel. Very seldom parts of the pronator teres muscle can restrict the median nerve which clinically results in an entrapment neuropathy.

4.2 Nerves in the Axillary Region and Upper Arm: Topographic Overview

Fig. 4.1 General topographic overview of nerve anatomy in the axilla and proximal upper arm. Localizer for anatomical cross sections (Fig. 4.2a–c). *Colored lines* correspond to level of cross sections

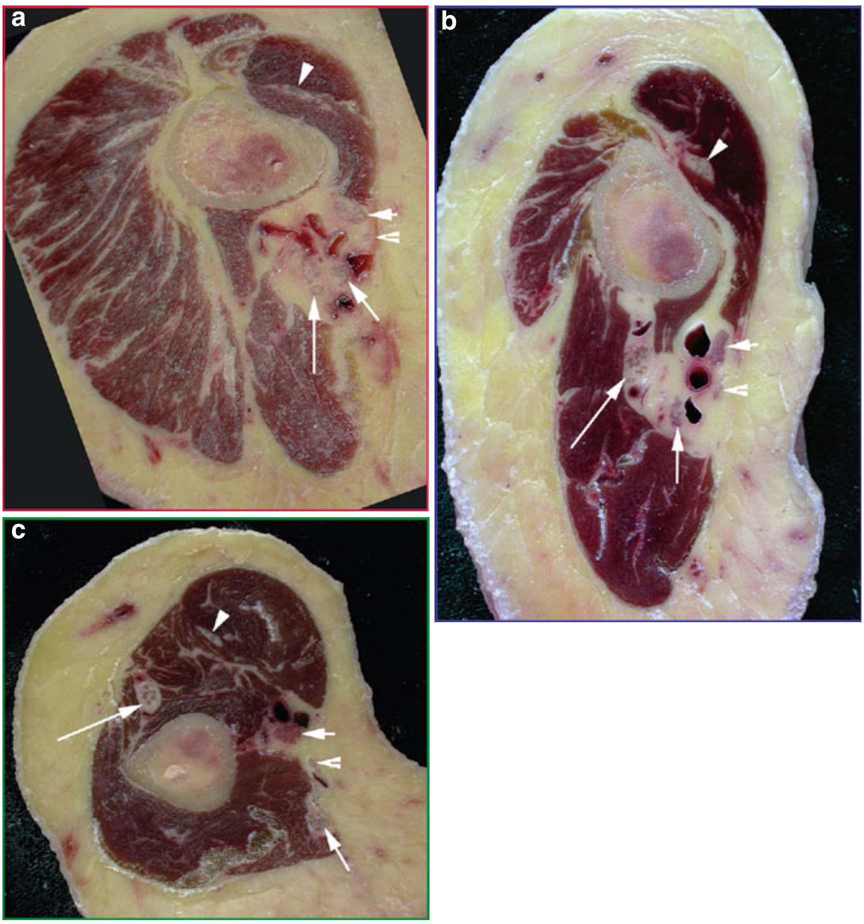

Fig. 4.2 (**a**) Anatomical cross section through the axillary region (*red line* in Fig. 4.1). Musculocutaneous nerve (*arrowhead*) inside short head of biceps muscle; median nerve (*short arrow*), cutaneous antebrachii medialis nerve (*slit arrow*), ulnar nerve (*medium arrow*), radial nerve (*long arrow*), surrounding the axillary vessels. (**b**) Anatomical cross section through the proximal upper arm (*blue line* in Fig. 4.1). Musculocutaneous nerve (*arrowhead*) inside short head of biceps muscle; median nerve (*short arrow*), cutaneous antebrachii medialis nerve (*slit arrow*), ulnar nerve (*medium arrow*) surrounding brachial artery and veins, and radial nerve (*long arrow*) between medial and lateral head of triceps muscle, accompanied by profound brachial artery. (**c**) Anatomical cross section through the middle upper arm (*green line* in Fig. 4.1). Musculocutaneous nerve (*arrowhead*) between biceps and brachial muscle; median nerve (*short arrow*), cutaneous antebrachii medialis nerve (*slit arrow*), ulnar nerve (*medium arrow*) close to medial head of triceps muscle, and radial nerve (*long arrow*) accompanied by profound brachial artery

4.2.1 Axillary Region (Origin of Upper Extremity Nerves)

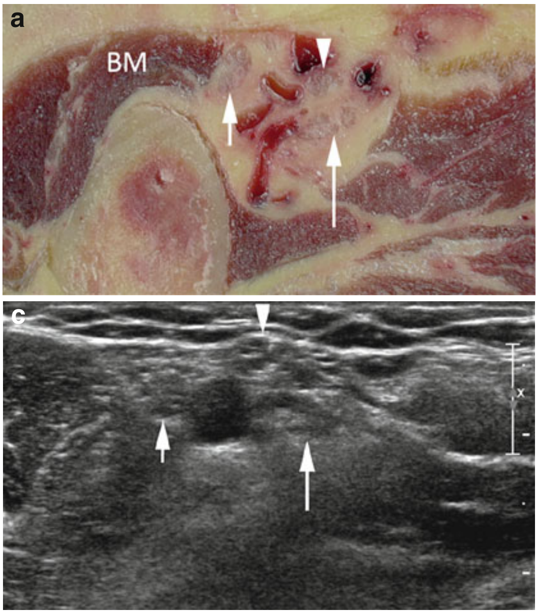

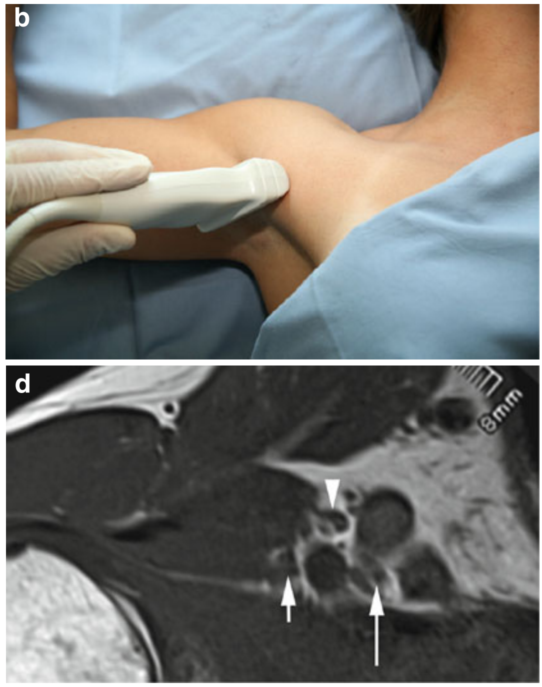

Fig. 4.3 (**a**) Anatomical cross section. (**b**) Transducer position. (**c**) Transverse sonogram. (**d**) Transverse T1-weighted MR image. Median nerve (*short arrow*), ulnar nerve (*arrowhead*), and radial nerve (*long arrow*) surrounding axillary vessels. *BM* biceps muscle

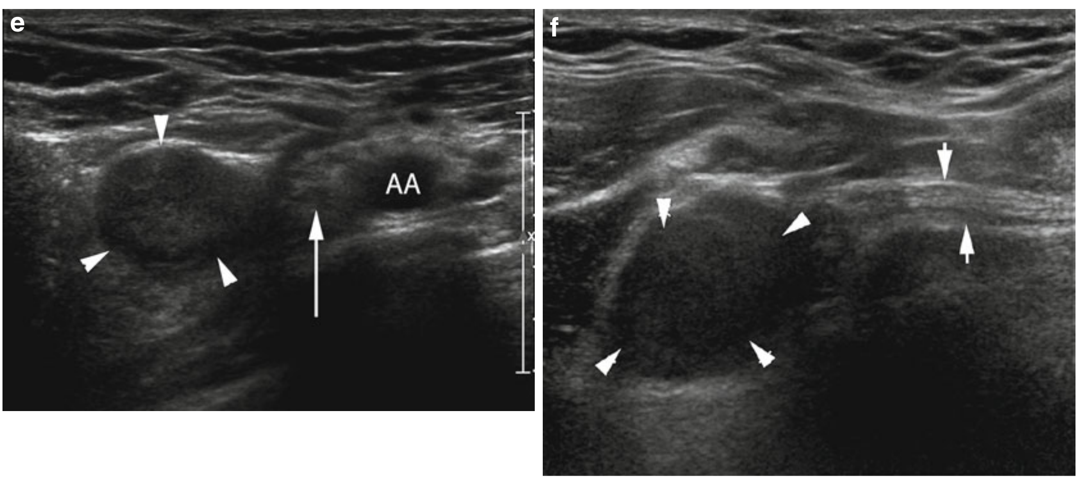

(**e**, **f**) Transverse (**e**) and longitudinal (**f**) sonogram through median nerve (*small arrows* in **f**) in the axillary region in a patient with median nerve schwannoma (histologically verified) (*arrowheads*). Long arrow ulnar nerve, *AA* axillary artery

4.2.2 Proximal Upper Arm (Median, Ulnar, and Radial Nerve)

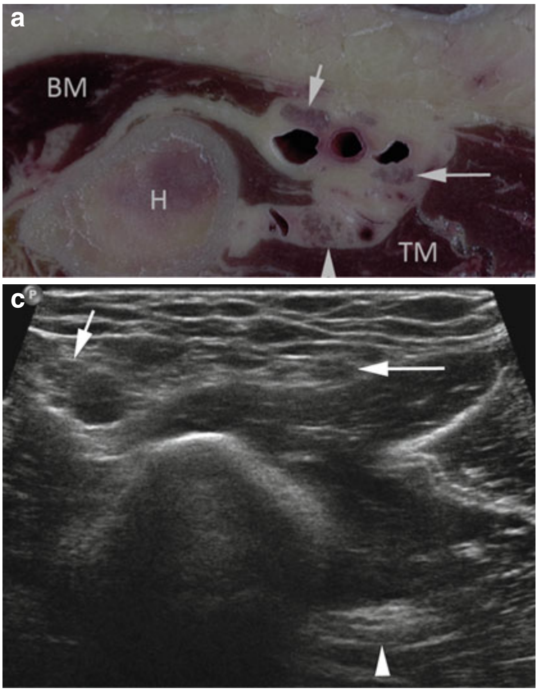

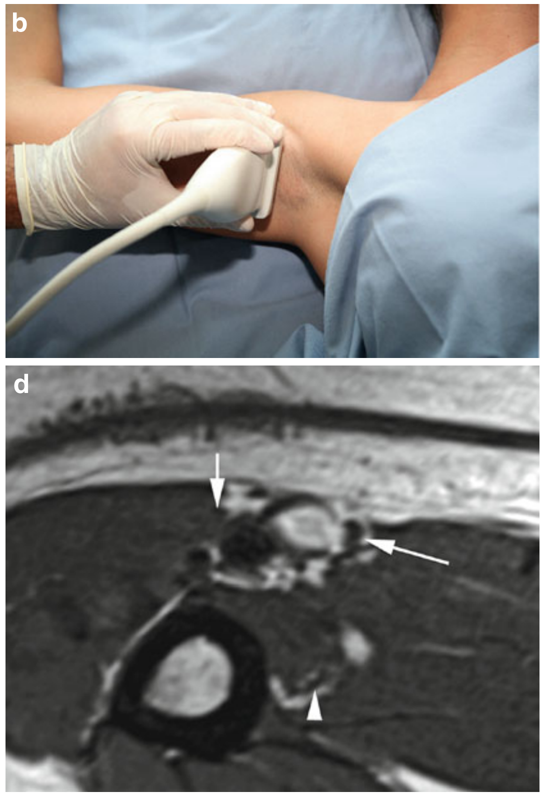

Fig. 4.4 (**a**) Anatomical cross section. (**b**) Transducer position. (**c**) Transverse sonogram. (**d**) Transverse T1-weighted MR image. Median nerve (*short arrow*), ulnar nerve (*long arrow*), and radial nerve (*arrowhead*) surrounding axillary vessels. *BM* biceps muscle, *TM* triceps muscle, *H* humerus

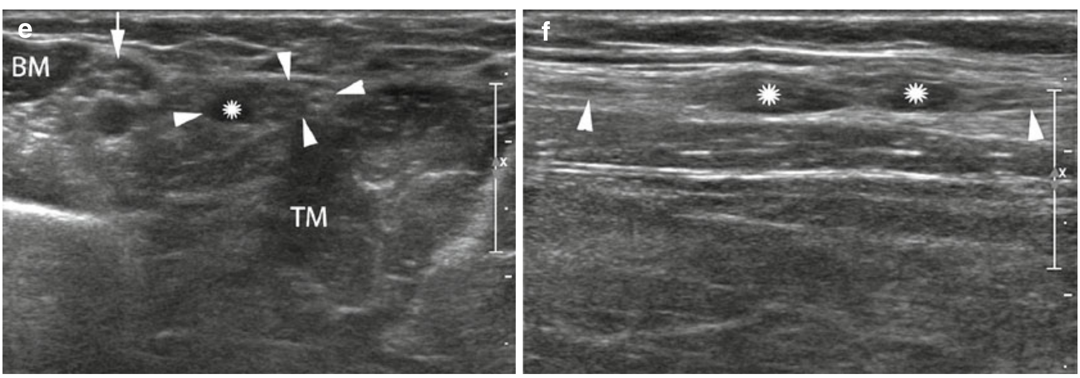

(**e**, **f**) Transverse (**e**) and longitudinal (**f**) sonogram through proximal upper arm in a patient with von Recklinghausen's disease. A small hypoechoic mass (*asterisk*) is seen connected to the otherwise normal ulnar nerve (*arrowheads*). Note that the neurofibroma is located inside the epineurial sheath of the ulnar nerve with enlargement of the outer nerve diameter (compare to normal median nerve = *arrow* in **e**). *BM* biceps muscle, *TM* triceps muscle. Two small neurofibromata are seen in the longitudinal scan (*asterisks* in **f**) in the course of the ulnar nerve (*arrowheads*)

4.2.3 Proximolateral Upper Arm on a Level with the Deltoid Muscle (Musculocutaneous Nerve)

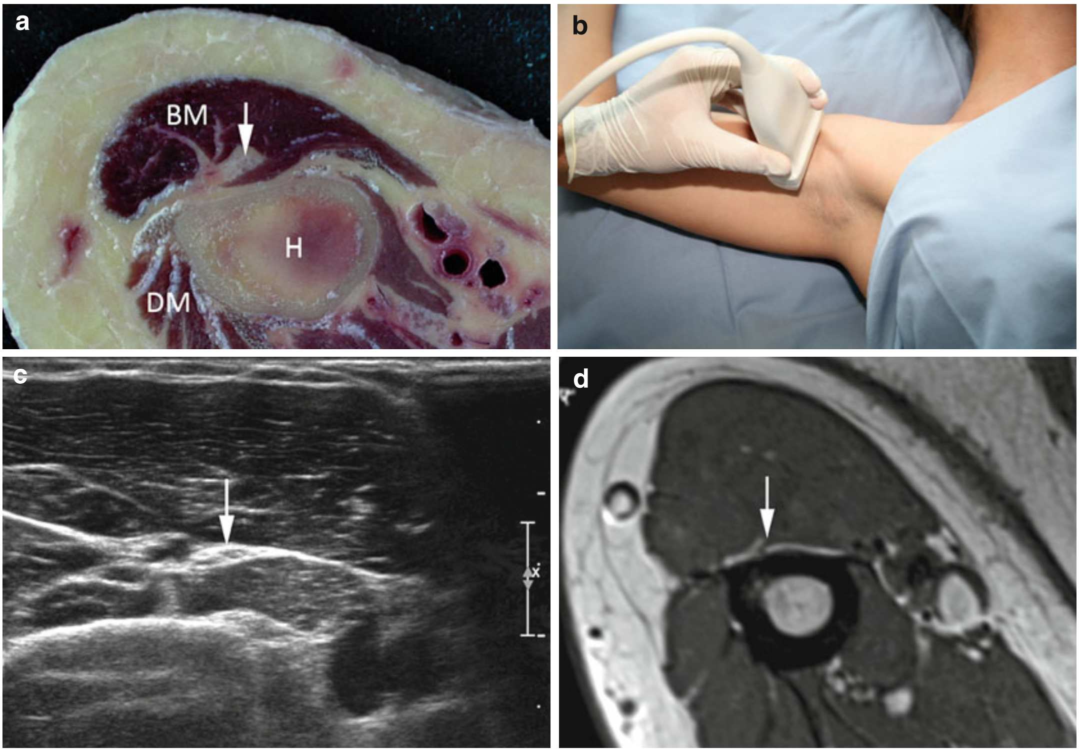

Fig. 4.5 (**a**) Anatomical cross section. (**b**) Transducer position. (**c**) Transverse sonogram. (**d**) Transverse T1-weighted MR image. Musculocutaneous nerve embedded in biceps muscle (*short arrow*). *BM* biceps muscle, *DM* deltoid muscle, *H* humerus

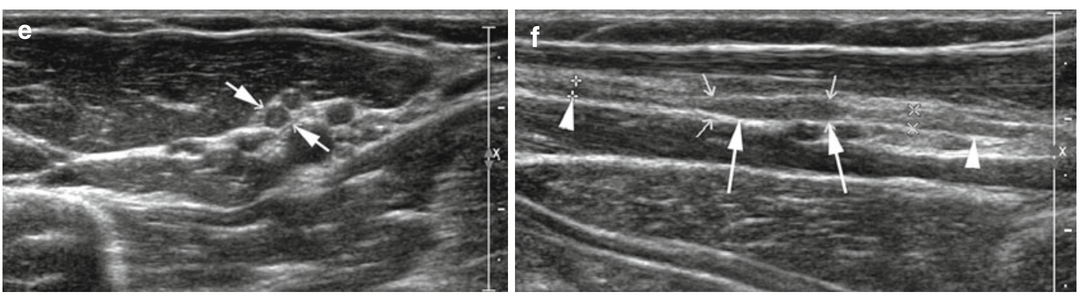

(**e**, **f**) Transverse (**e**) and longitudinal (**f**) sonogram through musculocutaneous nerve in a patient with posttraumatic paresthesia. The nerve (*arrowheads*) is continuous but demonstrates focal swelling with segmental thickening because of traction neuroma (*arrows*)

4.2.4 Ventrolateral Middle Upper Arm (Musculocutaneus Nerve)

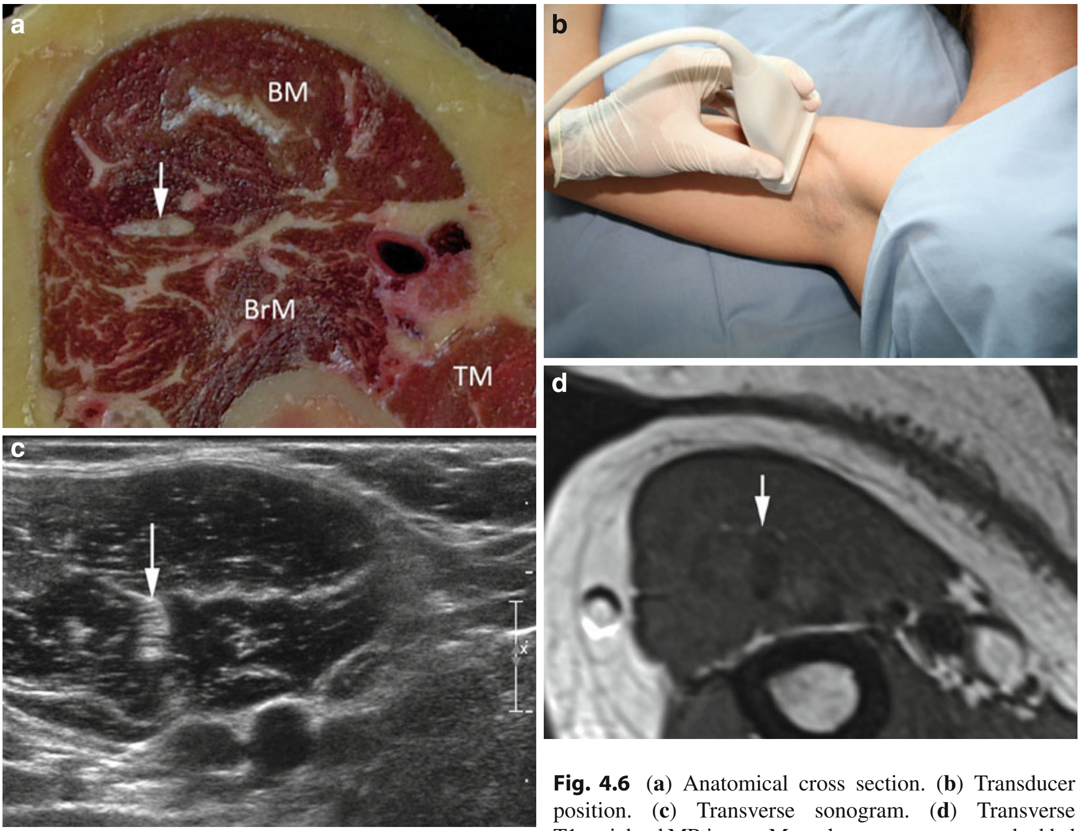

Fig. 4.6 (**a**) Anatomical cross section. (**b**) Transducer position. (**c**) Transverse sonogram. (**d**) Transverse T1-weighted MR image. Musculocutaneous nerve embedded in biceps muscle (*short arrow*). *BM* biceps muscle, *BrM* brachial muscle, *TM* triceps muscle

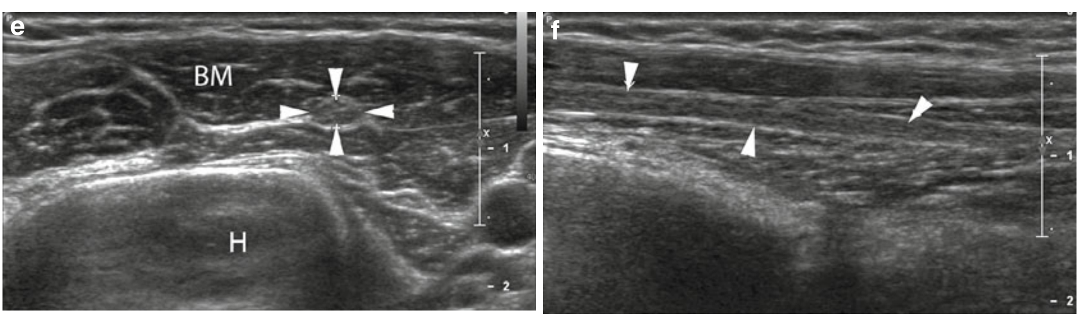

(**e**, **f**) Transverse (**e**) and longitudinal (**f**) sonogram through musculocutaneous nerve (*arrowheads*) in a patient with trauma to his upper arm and posttraumatic edema of the musculocutaneous nerve. *H* humerus

4.2.5 Bicipital Groove (Median, Ulnar, and Medial Cutaneous Antebrachial Nerve)

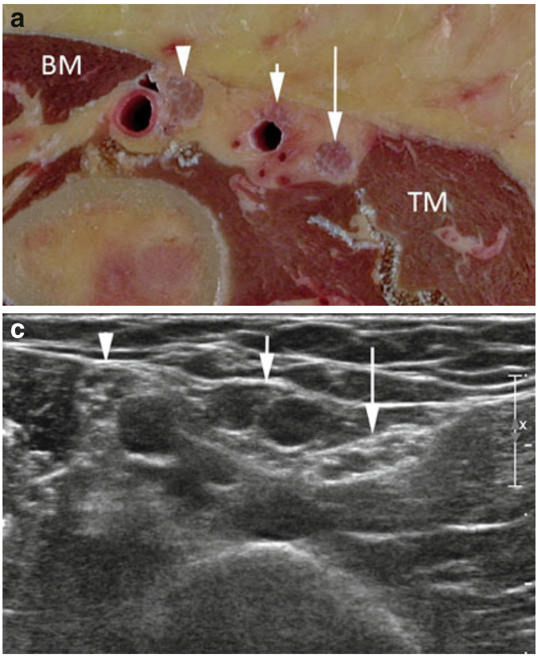

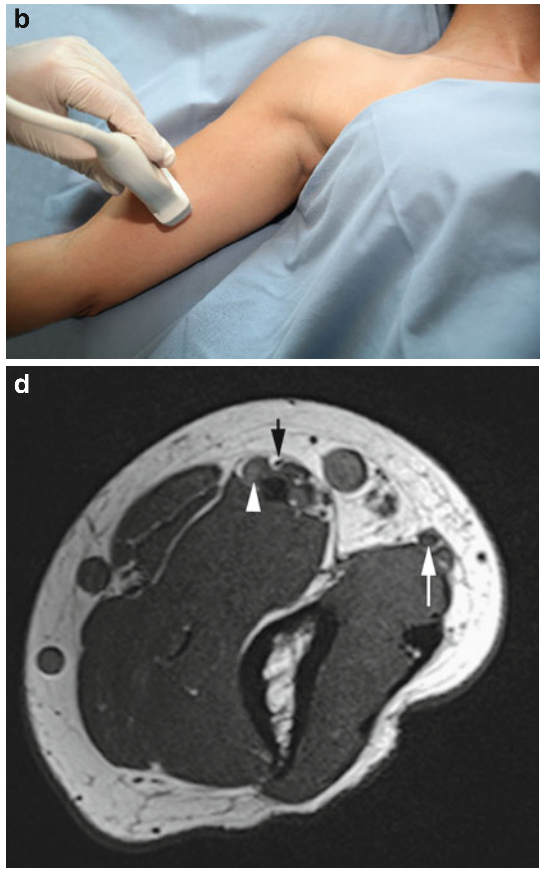

Fig. 4.7 (**a**) Anatomical cross section. (**b**) Transducer position. (**c**) Transverse sonogram. (**d**) Transverse T1-weighted MR image. Median nerve (*arrowhead*) close to brachial artery, medial cutaneous antebrachial nerve (*short arrow*) next to the basilic vein, and ulnar nerve (*long arrow*). *BM* biceps muscle, *TM* triceps muscle

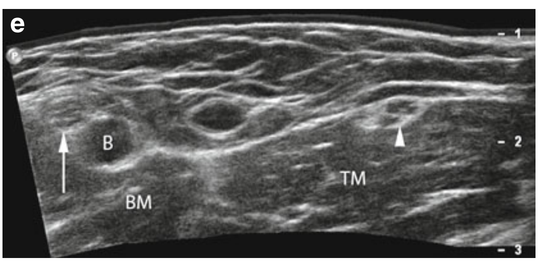

(**e**) Extended field of view sonogram through bicipital groove in a volunteer showing the relationship of median (*arrow*) and ulnar nerve (*arrowheads*) with brachial artery (*B*) and muscles (*BM* biceps muscle, *TM* triceps muscle)

4.2.6 Radial Sulcus (Radial Nerve)

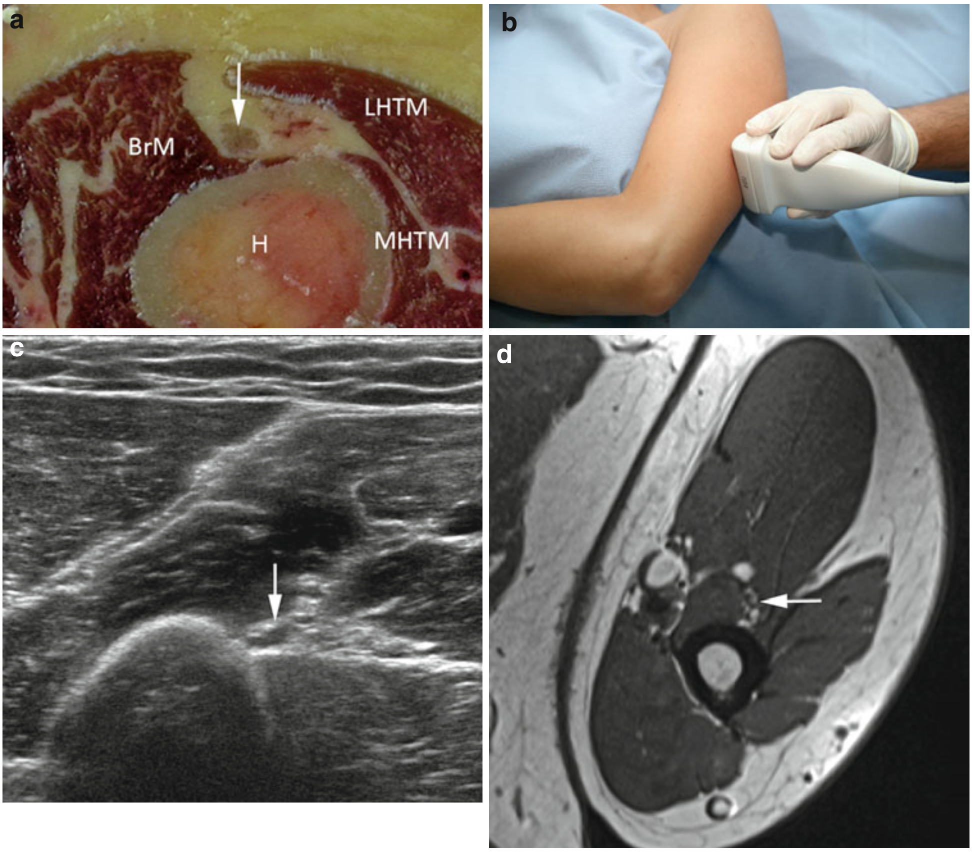

Fig. 4.8 (**a**) Anatomical cross section. (**b**) Transducer position. (**c**) Transverse sonogram. (**d**) Transverse T1-weighted MR image. Radial nerve (*arrow*) close to humerus (*H*) and brachial muscle (*BrM*). *LHTM* long head of triceps muscle, *MHTM* medial head of triceps muscle

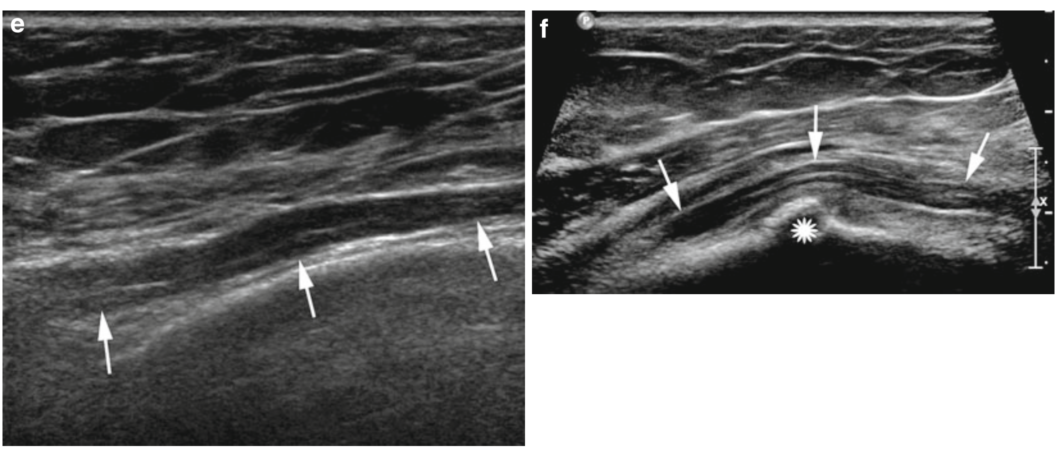

(**e**) Longitudinal sonogram through radial nerve inside radial sulcus in a patient with posttraumatic radial nerve palsy demonstrating mild traction edema with diffuse swelling of the nerve with incomplete fascicular masking (*arrows*). (**f**) Longitudinal sonogram through radial nerve inside radial sulcus in another patient with posttraumatic radial nerve palsy developing during consolidation of a humeral shaft fracture. Focal compression of the radial nerve (*arrows*) by bony callus (*asterisk*) is seen

4.3 Nerves in the Elbow Region: Topographic Overview

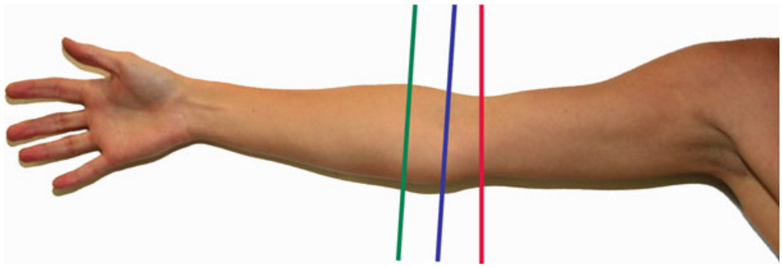

Fig. 4.9 General topographic overview of nerve anatomy in the elbow region. Localizer for anatomical cross sections (Fig. 4.10a–c). *Colored lines* correspond to level of cross sections

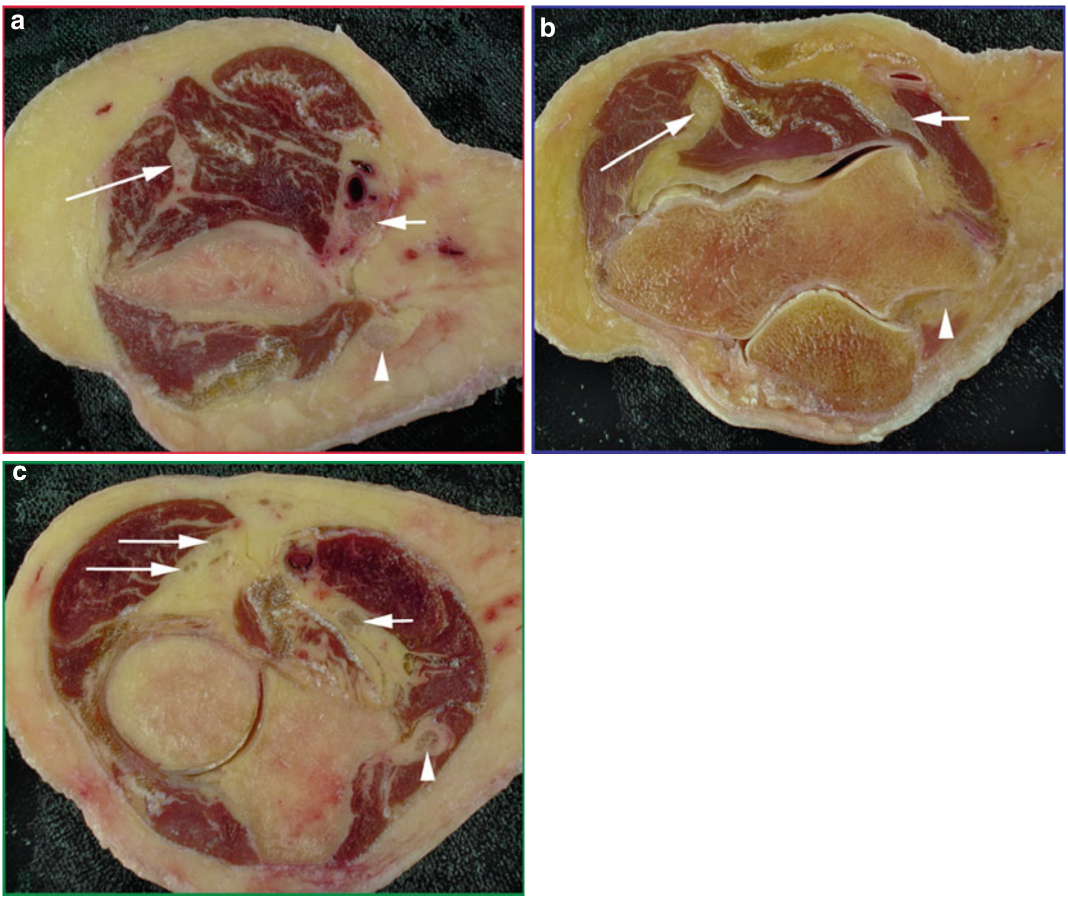

Fig. 4.10 (**a**) Anatomical cross section through the proximal elbow region (*red line* in Fig. 4.9). Ulnar nerve (*arrowhead*) close to medial head of triceps muscle; median nerve (*short arrow*) beside cubital artery; radial nerve (*long arrow*) between brachial and brachioradial muscle. (**b**) Anatomical cross section through the epicondylar region (*blue line* in Fig. 4.9). Ulnar nerve (*arrowhead*) inside ulnar sulcus; median nerve (*short arrow*) between humeral head of pronator teres muscle and brachial muscle; radial nerve (*long arrow*) between brachial and brachioradial muscle. (**c**) Anatomical cross section through the distal elbow region (*green line* in Fig. 4.9). Ulnar nerve (*arrowhead*) inside ulnar carpal flexor muscles; median nerve (*short arrow*); superficial and deep branch of radial nerve (*long arrows*) underneath brachioradial muscle

4.3.1 Anterior Cubital Region (Median Nerve above Elbow)

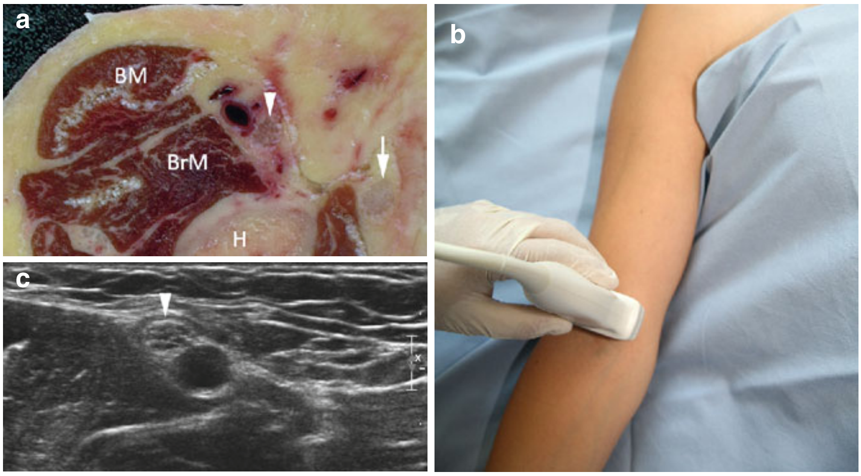

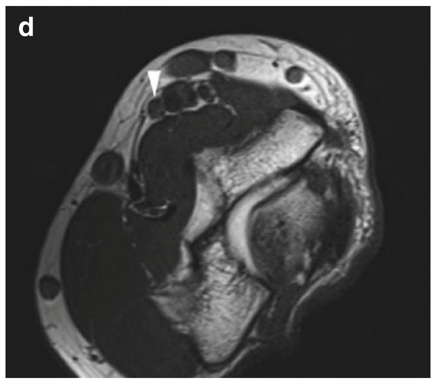

Fig. 4.11 (**a**) Anatomical cross section. (**b**) Transducer position. (**c**) Transverse sonogram. (**d**) Transverse T1-weighted MR image. Median nerve (*arrowhead*) next to the cubital artery, ulnar nerve (*short arrow*); *H* humerus, *BM* biceps muscle, *BrM* brachial muscle

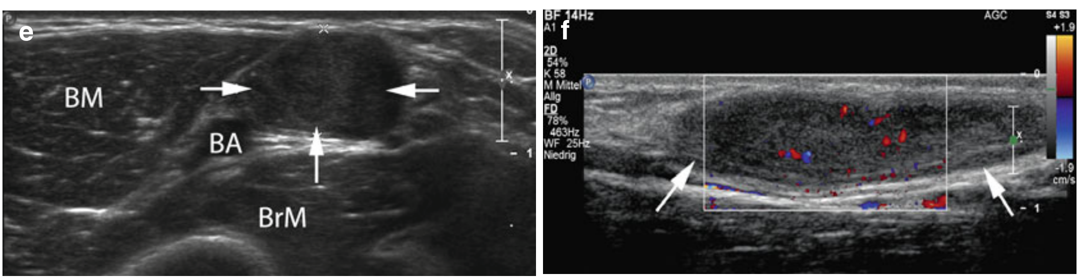

(**e**, **f**) Transverse (**e**) and longitudinal (**f**) sonogram of a median nerve schwannoma (*arrows*) in the cubital region (histologically verified). *BM* biceps muscle, *BrM* brachioradialis muscle, *BA* brachial artery. Note typical inner tumor vascularity

4.3.2 Anterior Cubital Region (Median Nerve below Elbow)

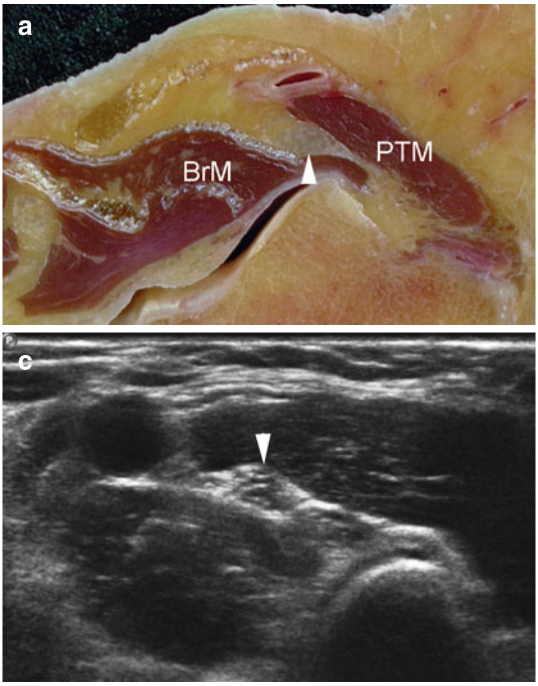

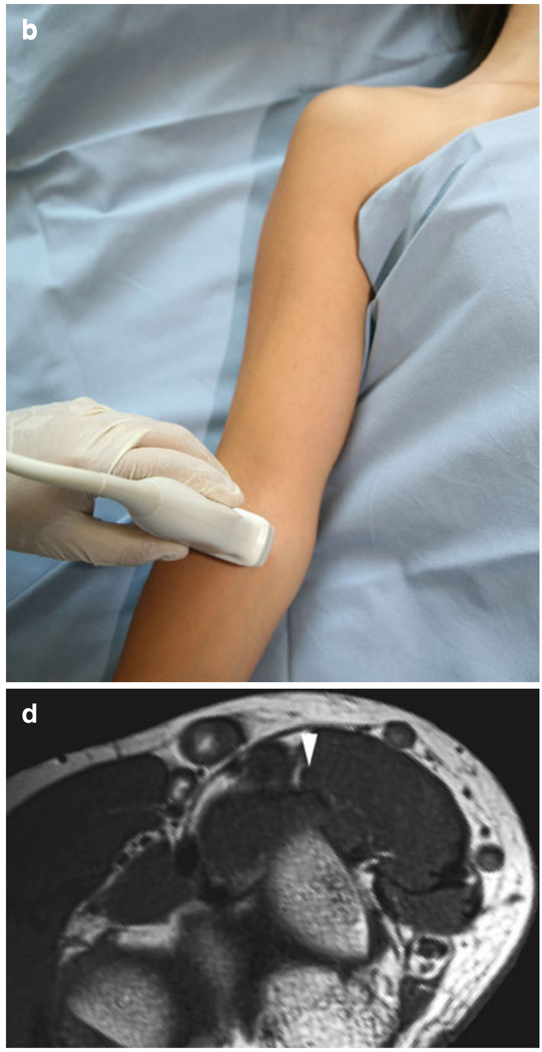

Fig. 4.12 (**a**) Anatomical cross section. (**b**) Transducer position. (**c**) Transverse sonogram. (**d**) Transverse T1-weighted MR image. Median nerve (*arrowhead*) between pronator teres muscle (*PTM*) and brachial muscle (*BrM*)

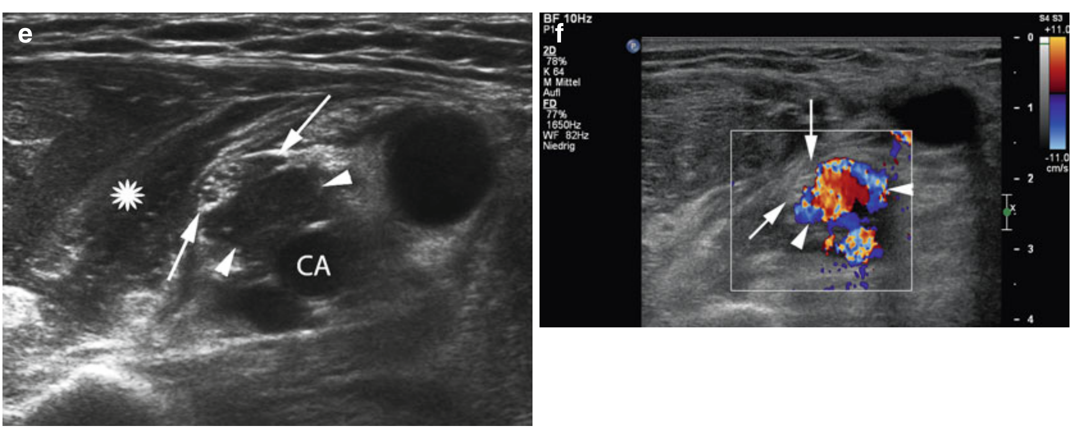

(**e**, **f**) Transverse sonogram (**e**) and color Doppler sonogram (**f**) of a patient with cubital artery injury (*CA*) and pseudoaneurysm (*arrowheads*) compressing the adjacent median nerve (*arrows*). *Asterisk* hematoma

4.3.3 Proximolateral Elbow (Division of Radial Nerve)

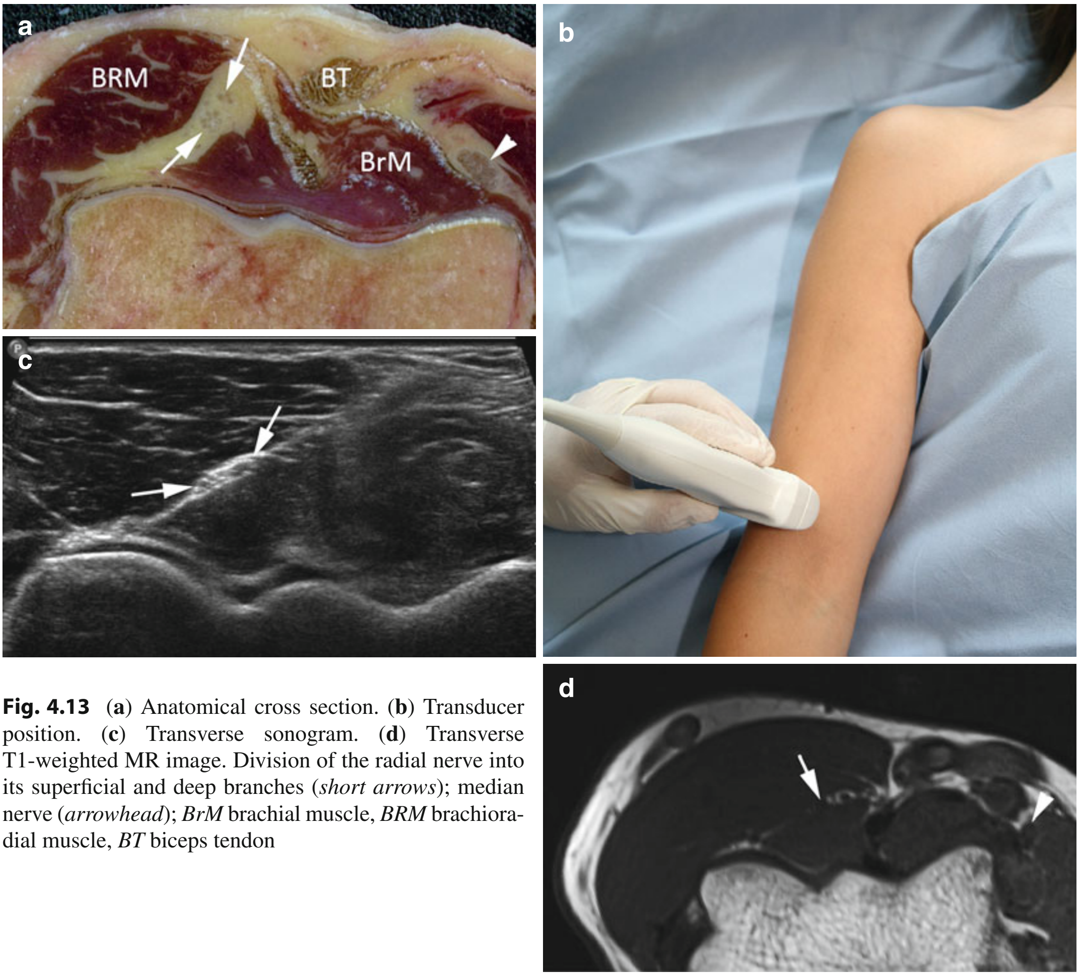

Fig. 4.13 (**a**) Anatomical cross section. (**b**) Transducer position. (**c**) Transverse sonogram. (**d**) Transverse T1-weighted MR image. Division of the radial nerve into its superficial and deep branches (*short arrows*); median nerve (*arrowhead*); *BrM* brachial muscle, *BRM* brachioradial muscle, *BT* biceps tendon

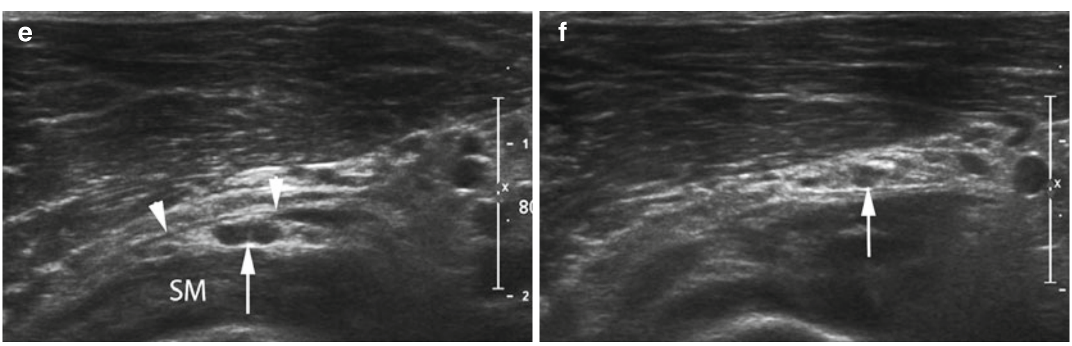

(**e**, **f**) Transverse sonogram through deep radial nerve branch (*arrow*) at the level of the arcade of Frohse (**e**) and at the radial nerve division (**f**) in a patient with PIN syndrome. Note marked thickening of deep branch underneath the arcade of Frohse (*arrowheads* in **e**) extending all the way up to the radial nerve division. *SM* supinator muscle

4.3.4 Anterior Cubital Region (Superficial Radial and Posterior Interosseus Nerve)

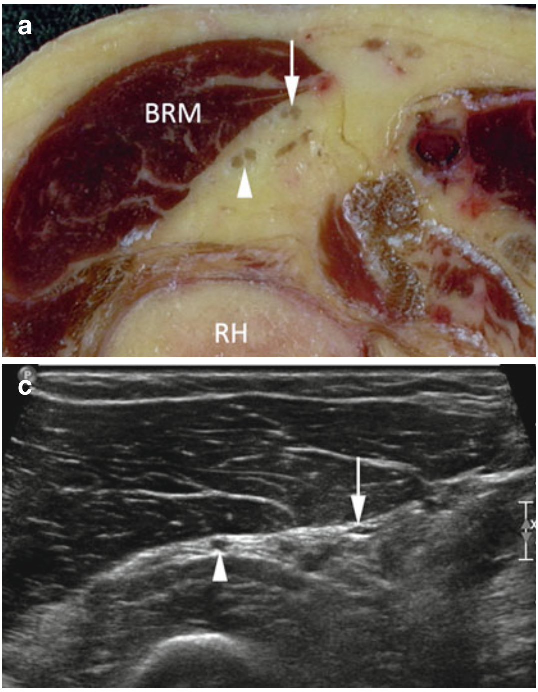

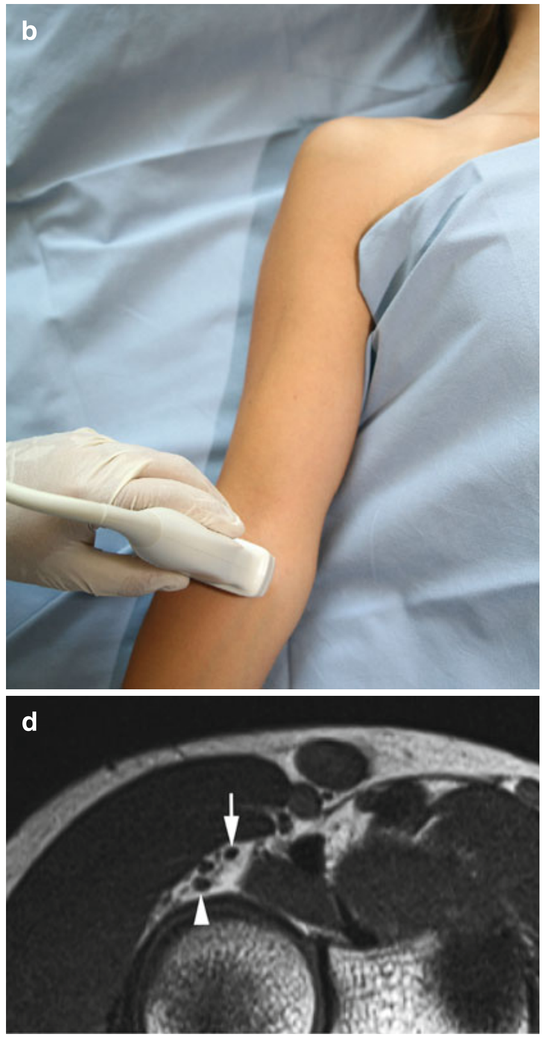

Fig. 4.14 (**a**) Anatomical cross section. (**b**) Transducer position. (**c**) Transverse sonogram. (**d**) Transverse T1-weighted MR image. Posterior interosseous nerve = deep branch of radial nerve (*arrowhead*); superficial branch of radial nerve (*arrow*); *BRM* brachioradial muscle, *RH* radial head

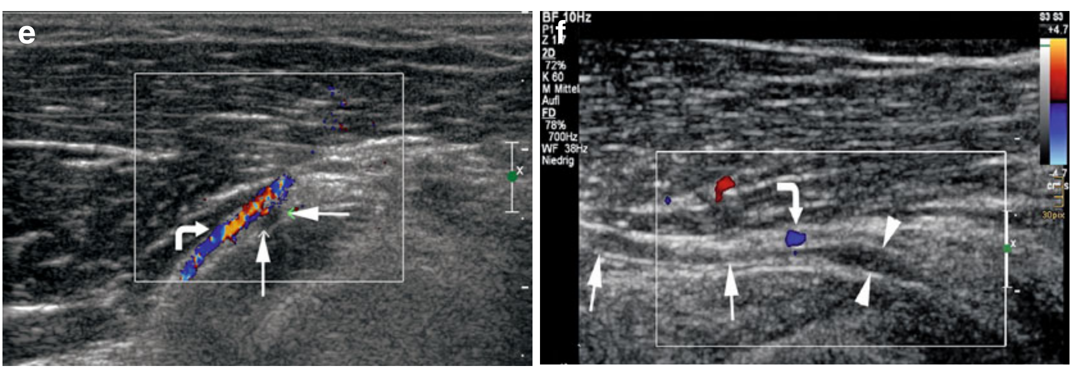

(**e**, **f**) Transverse and longitudinal sonogram through the posterior interosseous nerve (*arrows*) right distal to its origin in a patient with PIN syndrome. The nerve is thickened and hypoechoic (*arrowheads* in **f**) distal to the traversing recurrent radial artery (*curved arrow*) consistent with a "punched nerve syndrome"

4.3.5 Arcade of Frohse (Deep Branch of Radial Nerve)

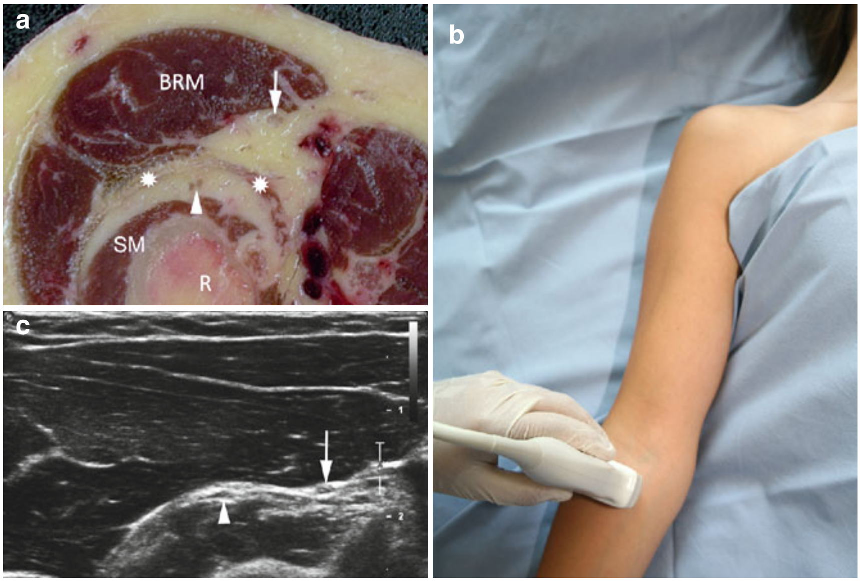

Fig. 4.15 (**a**) Anatomical cross section. (**b**) Transducer position. (**c**) Transverse sonogram. (**d**) Transverse T1-weighted MR image. Posterior interosseous nerve = deep branch of radial nerve (*arrowhead*); superficial branch of radial nerve (*arrow*); *BRM* brachioradial muscle, *SM* supinator muscle, *R* radius, *asterisk* arcade of Frohse

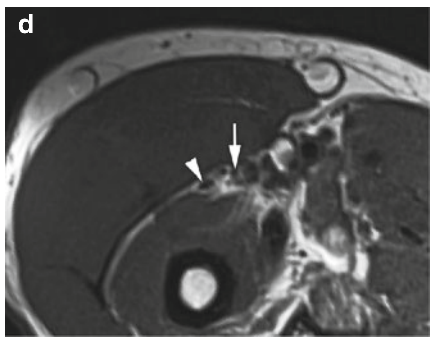

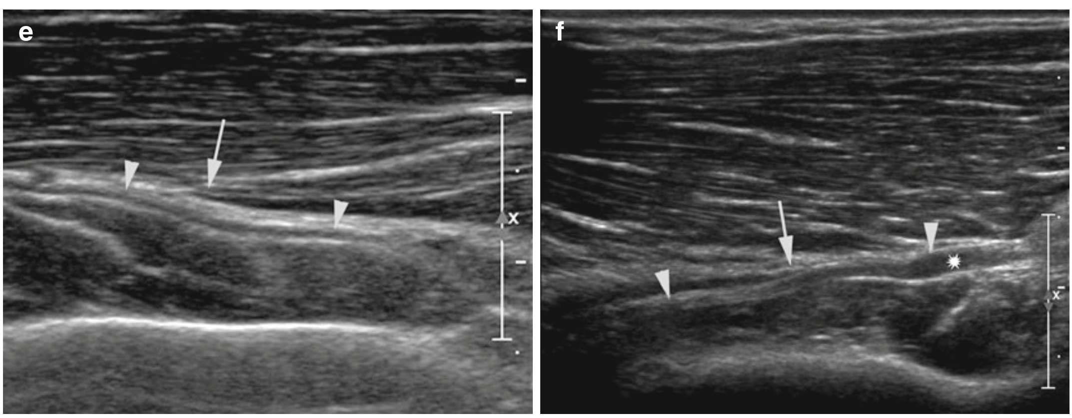

(**e**, **f**) Longitudinal ultrasound scan of posterior interosseous nerve (PIN) (*arrowheads*) at the arcade of Frohse (*arrow*). Normal volunteer (**e**), patient with PIN syndrome (**f**). Note edematous swelling of PIN proximal to its entrance under the supinator muscle (*asterisk*)

4.3.6 Cubital Tunnel Inlet (Ulnar Nerve)

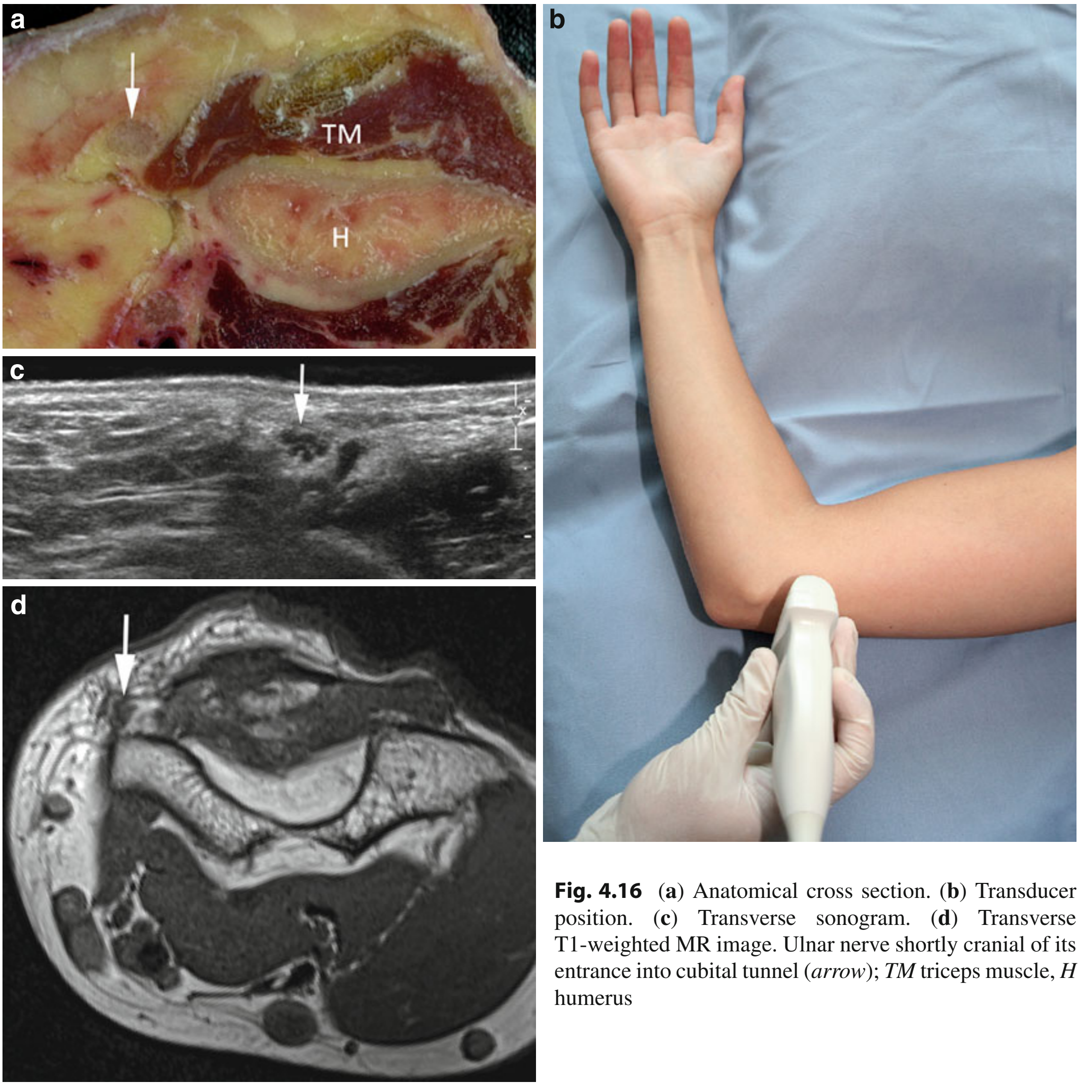

Fig. 4.16 (**a**) Anatomical cross section. (**b**) Transducer position. (**c**) Transverse sonogram. (**d**) Transverse T1-weighted MR image. Ulnar nerve shortly cranial of its entrance into cubital tunnel (*arrow*); *TM* triceps muscle, *H* humerus

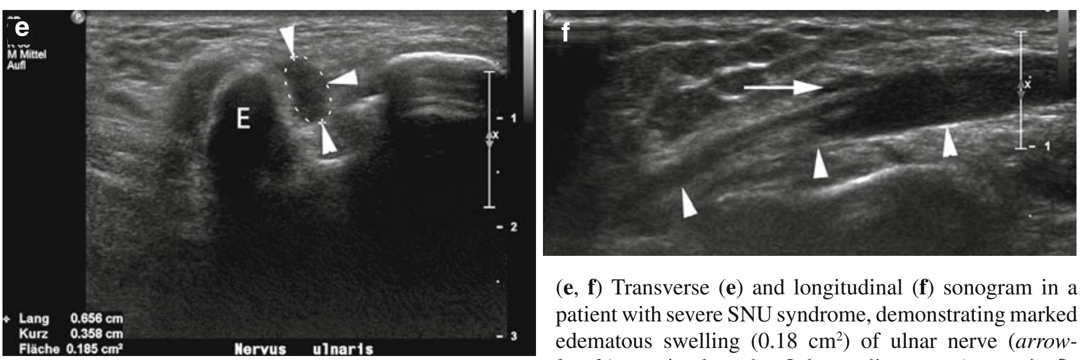

(**e**, **f**) Transverse (**e**) and longitudinal (**f**) sonogram in a patient with severe SNU syndrome, demonstrating marked edematous swelling (0.18 cm^2) of ulnar nerve (*arrowheads*) proximal to the Osborne ligament (*arrow* in **f**); *E* epicondyle

4.3.7 Cubital Tunnel (Ulnar Nerve)

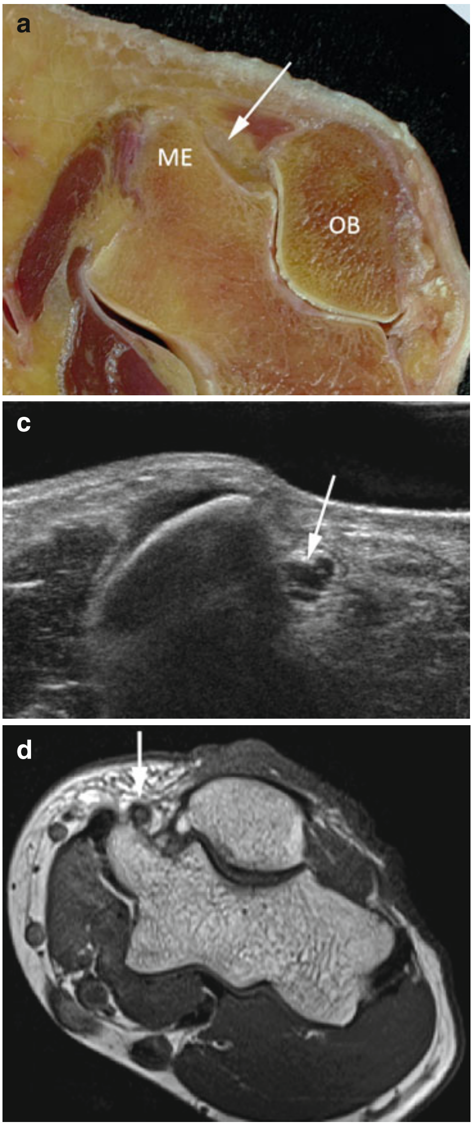

Fig. 4.17 (**a**) Anatomical cross section. (**b**) Transducer position. (**c**) Transverse sonogram. (**d**) Transverse T1-weighted MR image. Ulnar nerve (*arrow*) inside cubital tunnel right beside the medial epicondyle (*ME*); *OB* olecranon bone

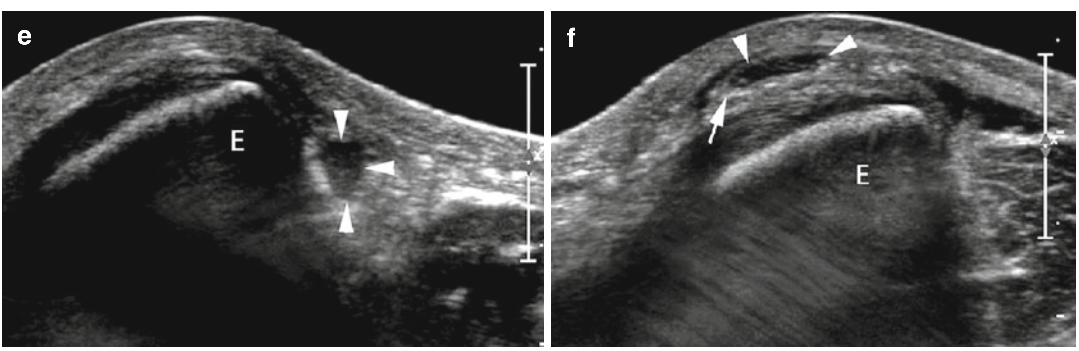

(**e**, **f**) Transverse sonogram of ulnar nerve (*arrowheads*) at the level of the medial epicondyle (*E*) in extension (**e**) and flexion (**f**) of the elbow in a patient with snapping ulnar nerve syndrome. Note dislocation of the nerve ventrally to the epicondyle in flexed position (**f**) and thickened hyper-echoic outer epineurium (*arrow* in **f**) due to chronic friction

4.3.8 Cubital Tunnel Outlet (Ulnar Nerve)

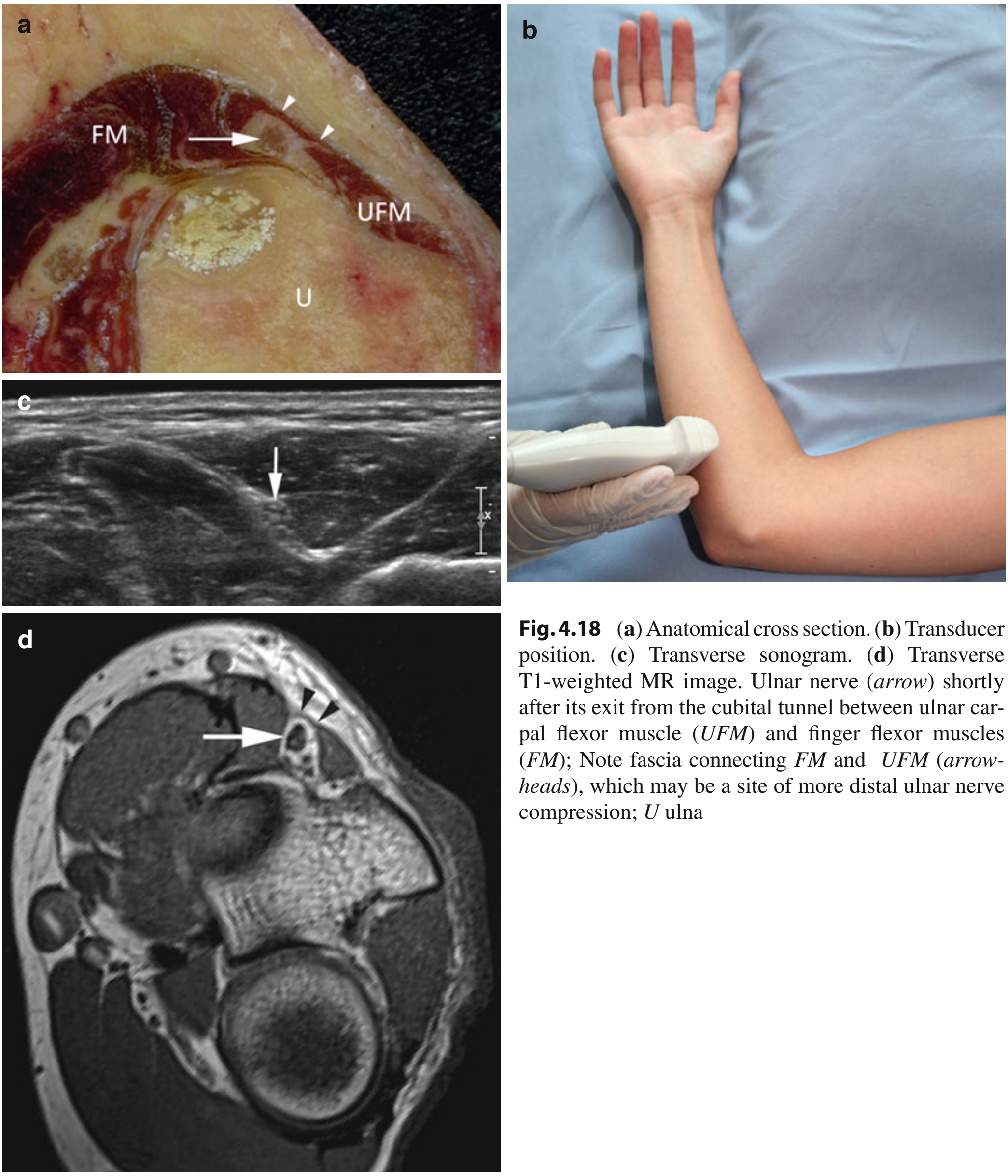

Fig. 4.18 (**a**) Anatomical cross section. (**b**) Transducer position. (**c**) Transverse sonogram. (**d**) Transverse T1-weighted MR image. Ulnar nerve (*arrow*) shortly after its exit from the cubital tunnel between ulnar carpal flexor muscle (*UFM*) and finger flexor muscles (*FM*); Note fascia connecting *FM* and *UFM* (*arrowheads*), which may be a site of more distal ulnar nerve compression; *U* ulna

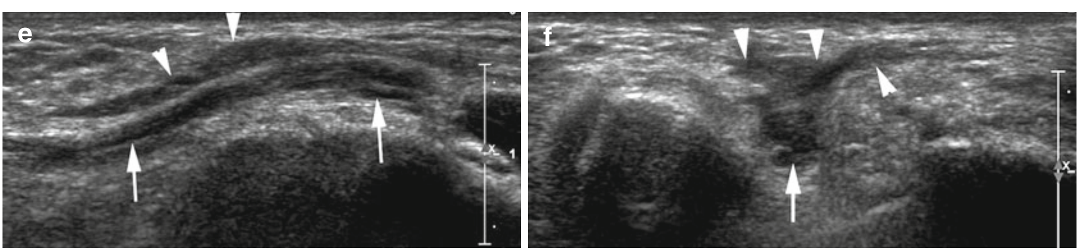

(**e**, **f**) Longitudinal (**e**) and transverse sonogram (**f**) through ulnar nerve (*arrows*) at cubital tunnel outlet in a patient with persisting ulnar neuropathy after cubital tunnel release due to compression of nerve by scar tissue (*arrowheads*)

4.4 Nerves in the Forearm and Hand: Topographic Overview

Fig. 4.19 General topographic overview of nerve anatomy in the forearm and hand region. Localizer for anatomical cross sections (Fig. 4.20a–d). *Colored lines* correspond to level of cross sections

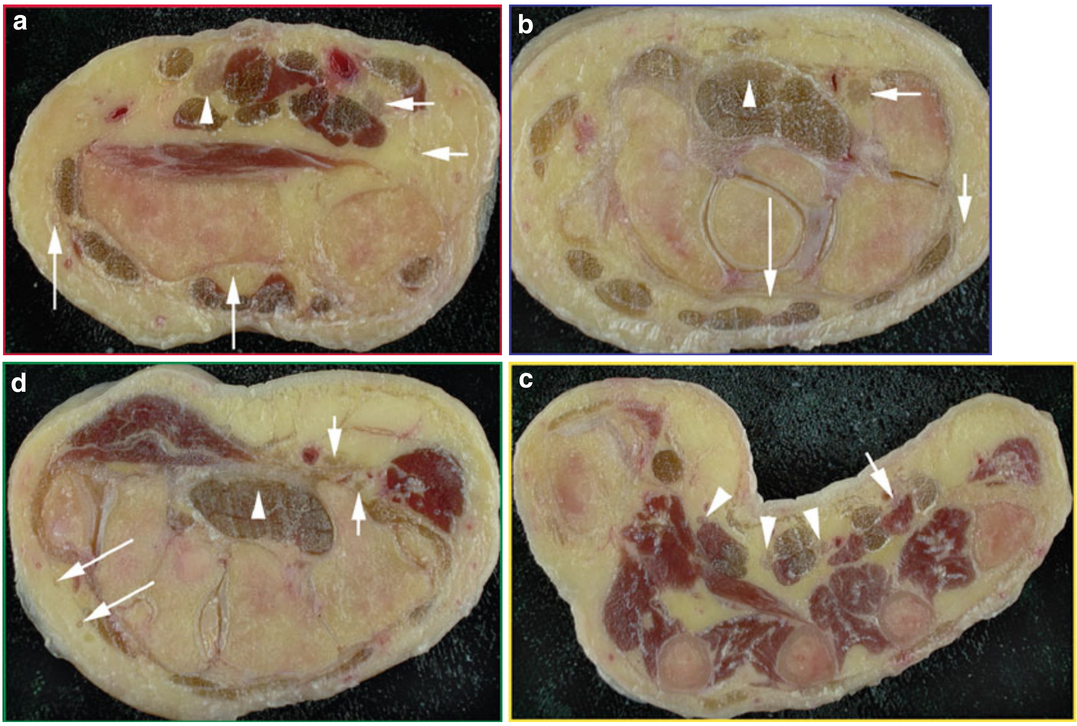

Fig. 4.20 (**a**) Anatomical cross section through the distal forearm region (*red line* in Fig. 4.19). Median nerve (*arrowhead*) between flexor tendons; ulnar nerve (next to ulnar artery) and its dorsal branch (*short arrows*) at the ulnar side of the forearm; superficial and deep branch of radial nerve (*long arrows*) at the radial and dorsal aspect of the distal forearm. (**b**) Anatomical cross section through the wrist area at the level of the carpal tunnel (*blue line* in Fig. 4.19). Median nerve (*arrowhead*) superficial to flexor tendons; ulnar nerve (next to ulnar artery) and its dorsal branch (*short arrows*) at the ulnar side of the forearm; deep branch of radial nerve (*long arrow*) at dorsal aspect of the distal forearm. (**c**) Anatomical cross section through the wrist area at the level of the hamulus of the hamate bone (*green line* in Fig. 4.19). Median nerve (*arrowhead*) superficial to flexor tendons at carpal tunnel outlet; ulnar nerve division – superficial and deep branch (*short arrows*) next to pisohamate ligament; terminal branches of superficial radial nerve (*long arrows*). (**d**) Anatomical cross section through the hand at the level of the metacarpal shafts (*yellow line* in Fig. 4.19). Common digital nerves of median nerve origin (*arrowheads*) and ulnar nerve origin (*short arrow*) next to flexor tendons, finger arteries, and lumbrical muscles

4.4.1 Distal Forearm on a Level with Pronator Quadratus (Median and Ulnar Nerve)

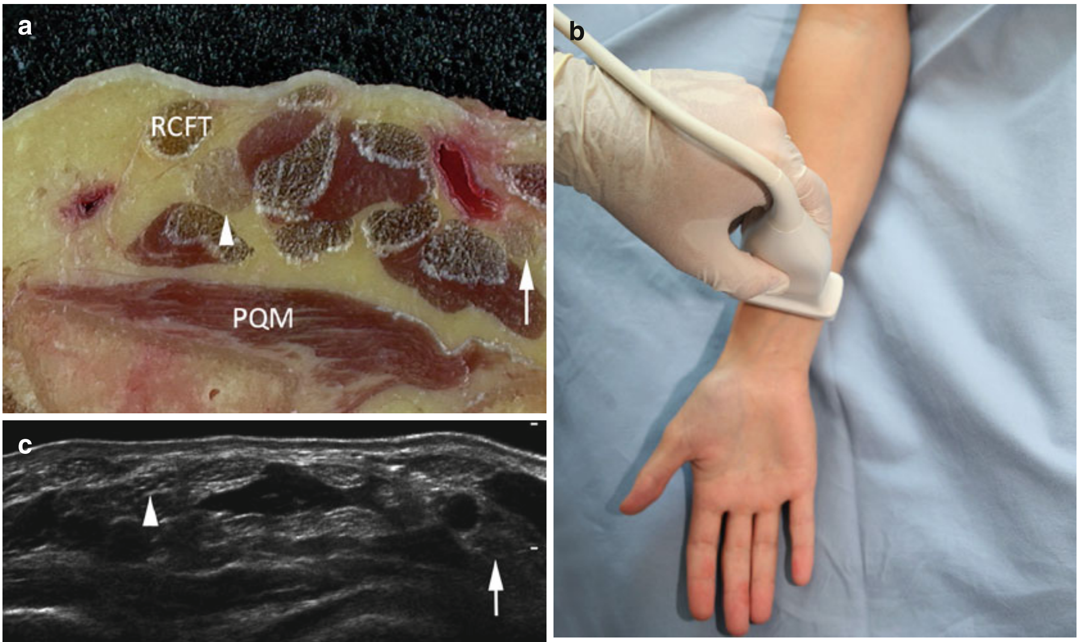

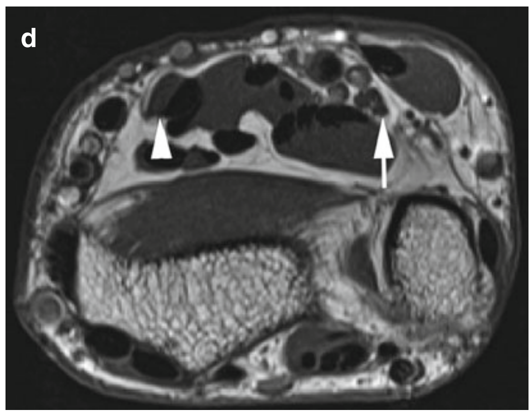

Fig. 4.21 (**a**) Anatomical cross section. (**b**) Transducer position. (**c**) Transverse sonogram. (**d**) Transverse T1-weighted MR image. Median nerve (*arrowhead*) next to radial carpal flexor tendon (*RCFT*) at the level of pronator quadratus muscle (*PQM*). Ulnar nerve (*short arrow*) beside ulnar artery

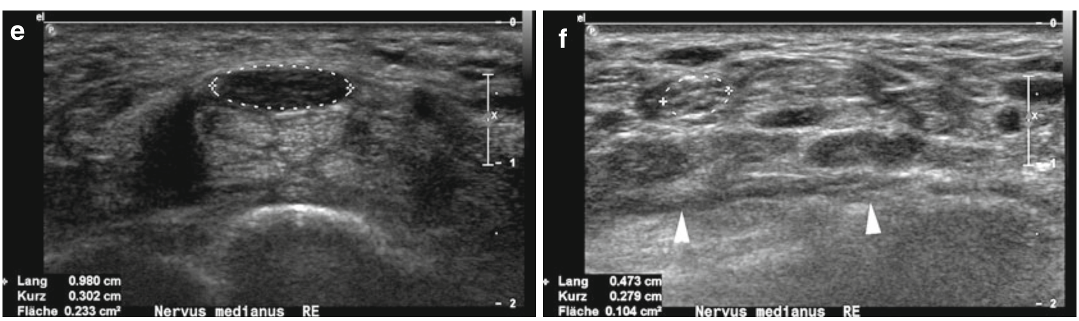

(**e**, **f**) Measurement of normal median nerve cross section area (0.10 cm^2) at reference location at the level of the pronator quadratus muscle (*arrowheads* in **e**) and increased cross section (0.23 cm^2) at carpal tunnel inlet (**f**) in a patient with carpal tunnel syndrome. Both values are used to calculate a wrist/forearm ratio (WFR); in this case highly abnormal with 2.3 (cutoff = 1.4)

4.4.2 Distal Forearm on a Level with Distal Radio-Ulnar Joint (Median and Ulnar Nerve)

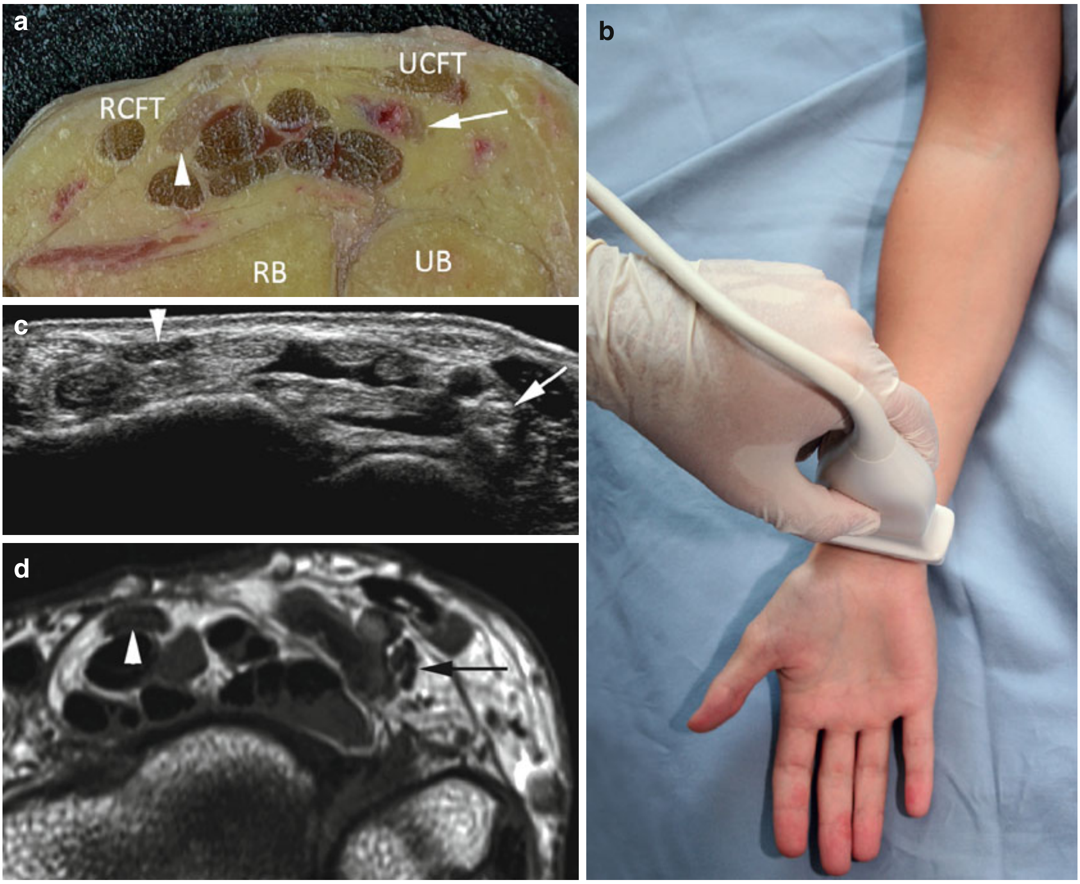

Fig. 4.22 (**a**) Anatomical cross section. (**b**) Transducer position. (**c**) Transverse sonogram. (**d**) Transverse T1-weighted MR image. Median nerve (*arrowhead*) next to radial carpal flexor (*RCFT*) and digital flexor tendons. Ulnar nerve (*short arrow*) beside ulnar artery underneath ulnar carpal flexor tendon (*UCFT*). *RB* radial bone, *UB* ulnar bone

(**e**) Extended field of view sonogram at the level of the distal radio-ulnar joint (*asterisk*) demonstrating median nerve (*arrow*) and ulnar nerve (*arrowhead*) in relationship to flexor tendons (*FT*) and ulnar artery (*U*)

4.4.3 Carpal Tunnel Inlet (Median Nerve)

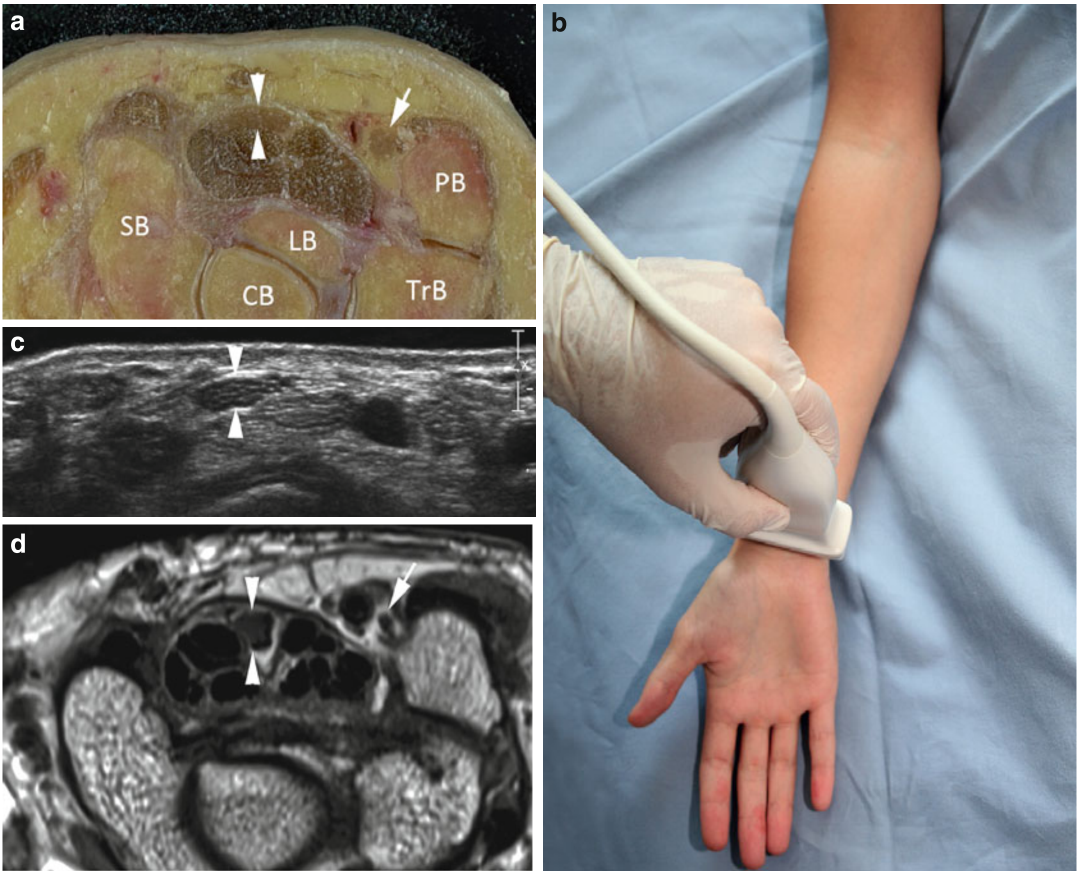

Fig. 4.23 (**a**) Anatomical cross section. (**b**) Transducer position. (**c**) Transverse sonogram. (**d**) Transverse T1-weighted MR image. Median nerve (*arrowheads*) inside carpal tunnel, underneath the flexor retinaculum. Ulnar nerve (*arrow*) inside Guyon's channel. *PB* pisiforme bone, *LB* lunate bone, *SB* scaphoid bone, *CB* capitate bone, *TrB* triquetral bone

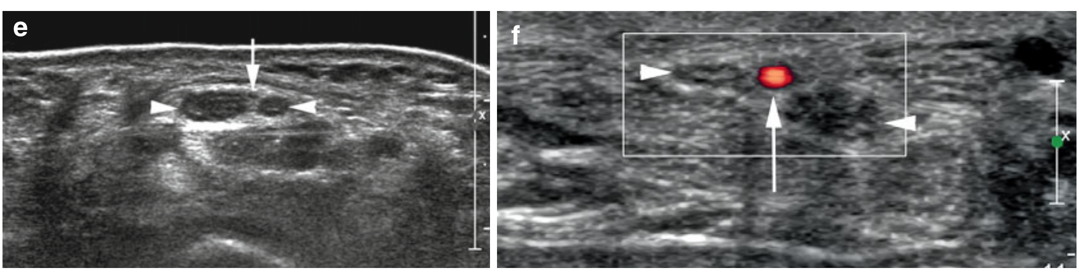

(**e**) Transverse sonogram through carpal tunnel inlet demonstrating bifid median nerve with a bigger and smaller branch (*arrowheads*) and an obliterated median artery (*arrow*). (**f**) Transverse power Doppler sonogram in another patient with bifid median nerve (*arrowheads*) and a perfused persisting median artery (*arrow*) lying between the median nerve branches

4.4.4 Carpal Tunnel Central Part (Median Nerve)

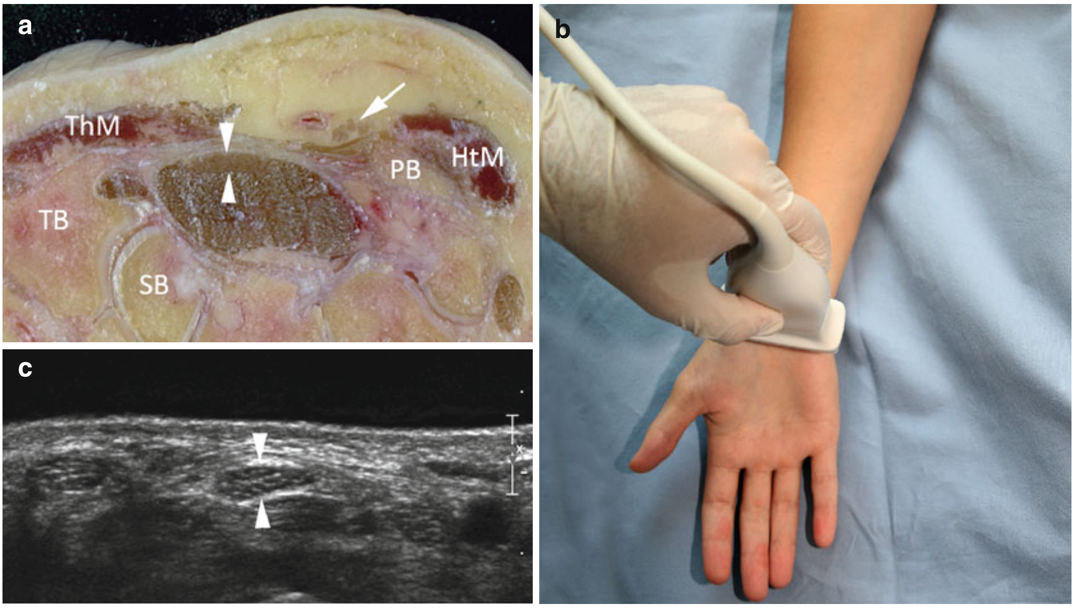

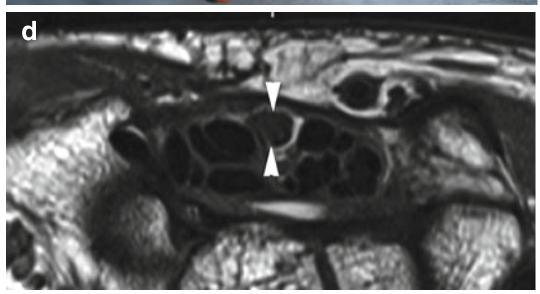

Fig. 4.24 (**a**) Anatomical cross section. (**b**) Transducer position. (**c**) Transverse sonogram. (**d**) Transverse T1-weighted MR image. Median nerve (*arrowheads*) inside carpal tunnel, underneath the flexor retinaculum. Ulnar nerve (*short arrow*) shortly proximal to its bifurcation. *PB* pisiforme bone, *SB* scaphoid bone, *TB* trapezium bone, *ThM* thenar muscles, *HtM* hypothenar muscles

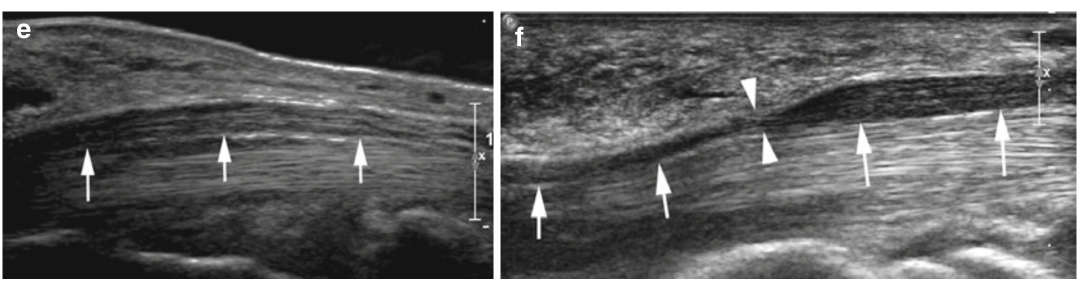

(**e**, **f**) Longitudinal sonograms through carpal tunnel in a normal volunteer (**e**) and patient with CTS (**f**) demonstrating normal median nerve (*arrows*) caliber in (**e**) and impressive caliber change at site of compression (*arrowheads*) in (**f**)

4.4.5 Carpal Tunnel Outlet (Median Nerve)

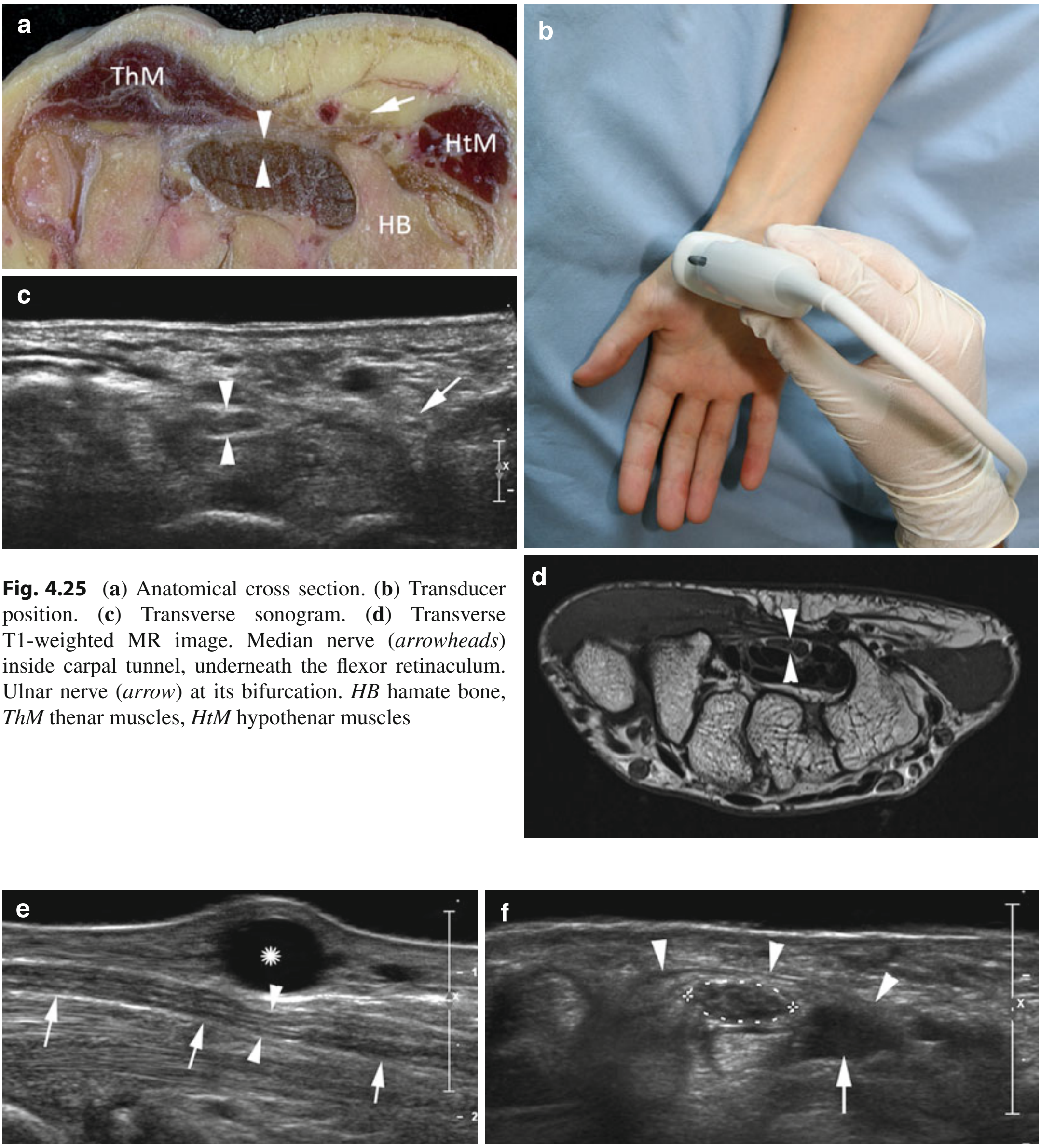

Fig. 4.25 (**a**) Anatomical cross section. (**b**) Transducer position. (**c**) Transverse sonogram. (**d**) Transverse T1-weighted MR image. Median nerve (*arrowheads*) inside carpal tunnel, underneath the flexor retinaculum. Ulnar nerve (*arrow*) at its bifurcation. *HB* hamate bone, *ThM* thenar muscles, *HtM* hypothenar muscles

(**e**) Longitudinal sonogram of median nerve inside carpal tunnel in a patient with CTS. Compression of the median nerve (*arrows*) by large fluid-filled ganglion cyst (*asterisk*) with indentation of median nerve (*arrowheads*) is demonstrated. (**f**) Transverse sonogram through carpal tunnel in a patient with median nerve paresthesia during dorsiflexion of the wrist. A small hypoechoic elongated muscle belly (*arrow*) is noted adjacent to the median nerve. *Arrowheads* flexor retinaculum

4.4.6 Distal Forearm: Palmar Branch of Median Nerve

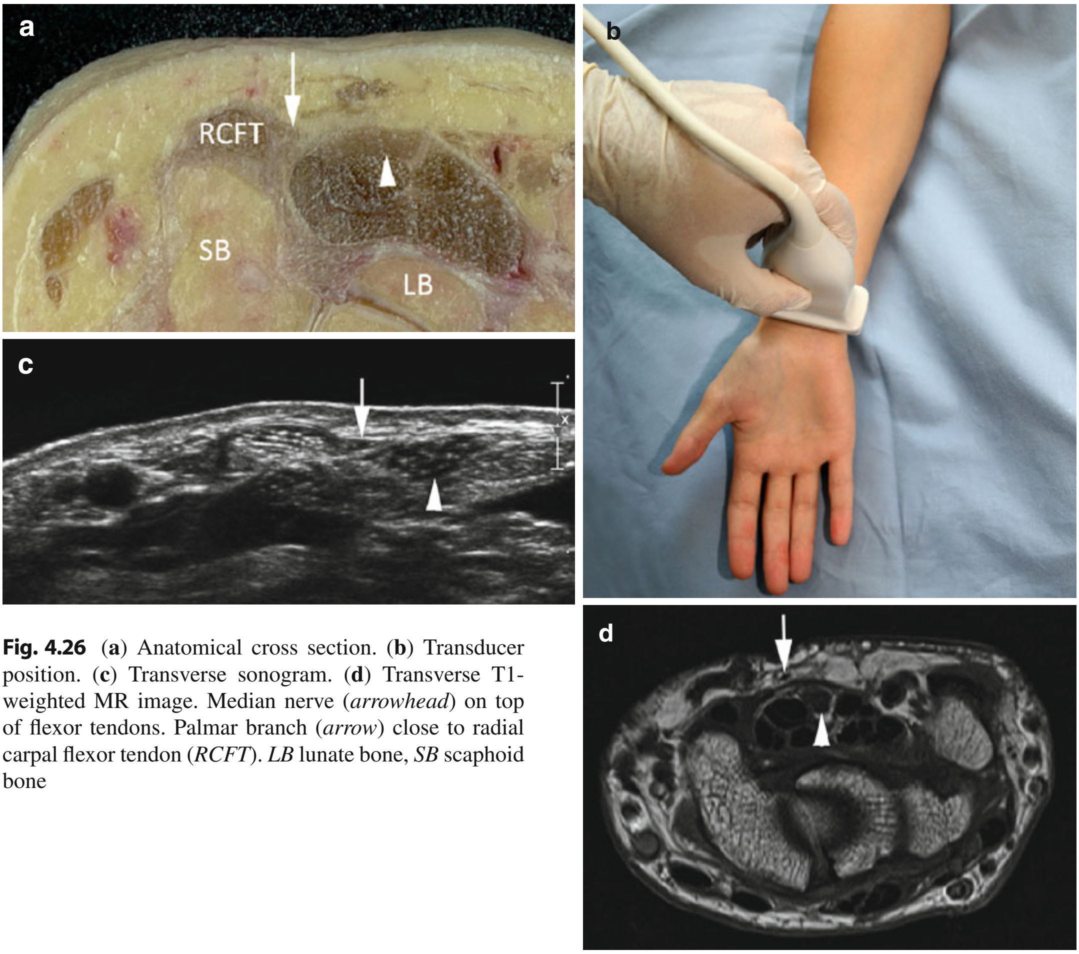

Fig. 4.26 (**a**) Anatomical cross section. (**b**) Transducer position. (**c**) Transverse sonogram. (**d**) Transverse T1-weighted MR image. Median nerve (*arrowhead*) on top of flexor tendons. Palmar branch (*arrow*) close to radial carpal flexor tendon (*RCFT*). *LB* lunate bone, *SB* scaphoid bone

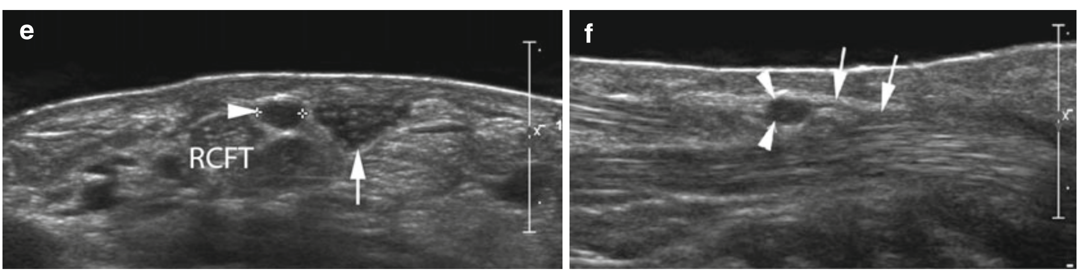

(**e**, **f**) Transverse (**e**) and longitudinal (**f**) sonogram through palmar branch in a patient with sharp trauma (knife wound) to his wrist. A small neuroma (*arrowheads*) is seen in the palmar branch (*arrow* in **f**). *RCFT* radial carpal flexor tendon, *arrow* main branch of median nerve

4.4.7 Carpal Tunnel: Thenar Branch of Median Nerve

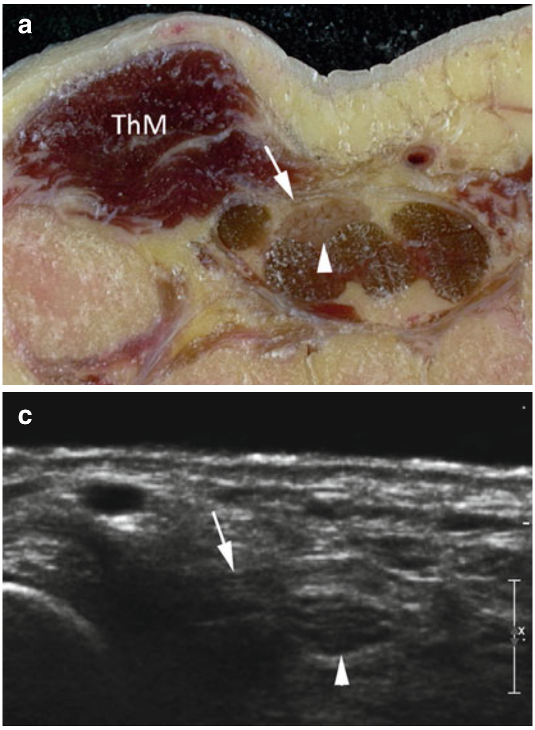

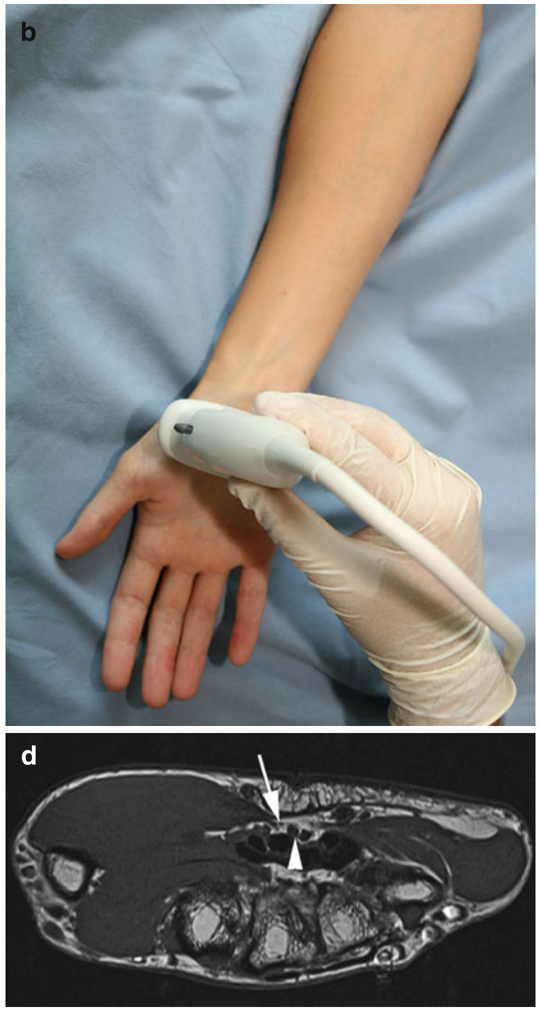

Fig. 4.27 (**a**) Anatomical cross section. (**b**) Transducer position. (**c**) Transverse sonogram. (**d**) Transverse T1-weighted MR image. Median nerve (*arrowhead*) on top of flexor tendons. Thenar branch (*arrow*) close to edge of flexor retinaculum, radial to main stem of median nerve. *ThM* thenar muscles

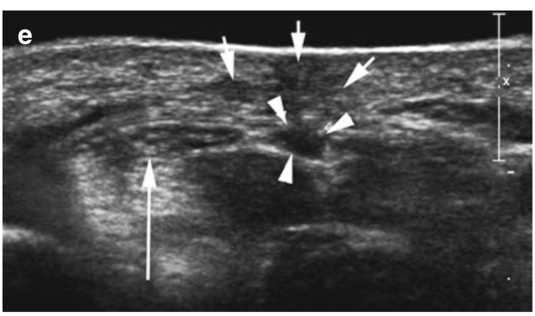

(**e**) Transverse sonogram through carpal tunnel in a patient with paresthesia and numbness in the thumb after carpal tunnel release. The thenar branch is thickened due to small neuroma (*arrowheads*) and scar compression (*small arrows*). Note normally appearing main branch of median nerve (*long arrow*)

4.4.8 Metacarpal Section of Hand (Common Digital Nerves)

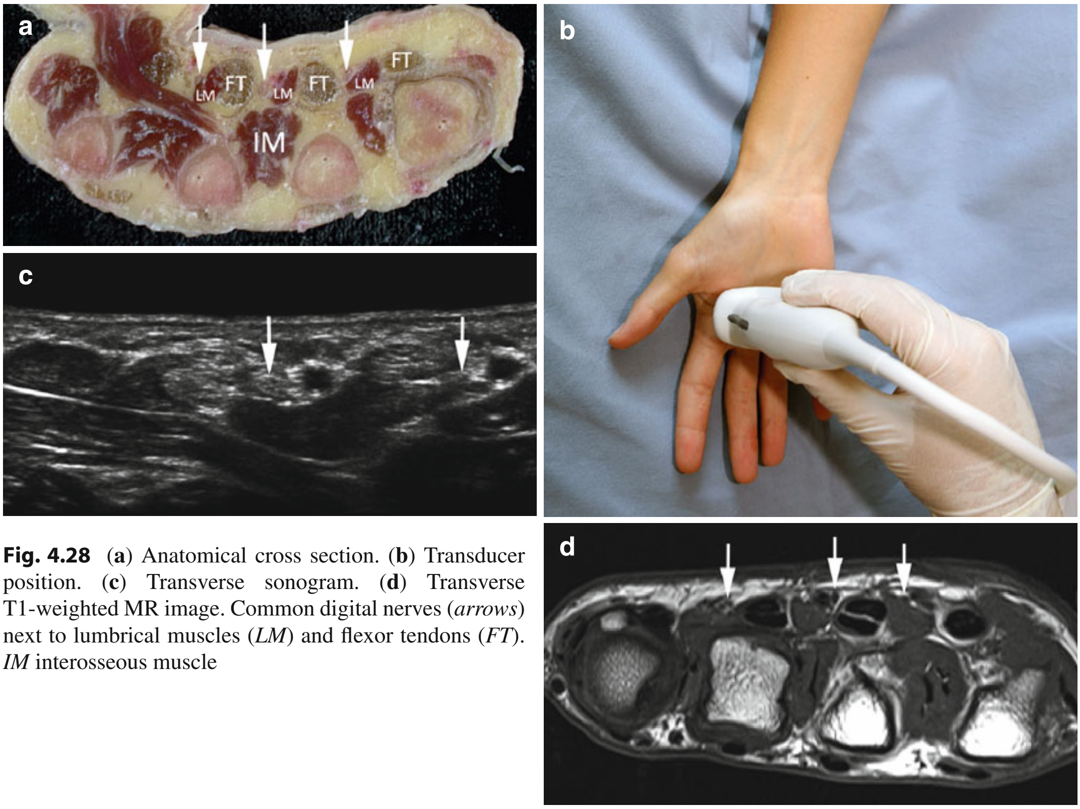

Fig. 4.28 (**a**) Anatomical cross section. (**b**) Transducer position. (**c**) Transverse sonogram. (**d**) Transverse T1-weighted MR image. Common digital nerves (*arrows*) next to lumbrical muscles (*LM*) and flexor tendons (*FT*). *IM* interosseous muscle

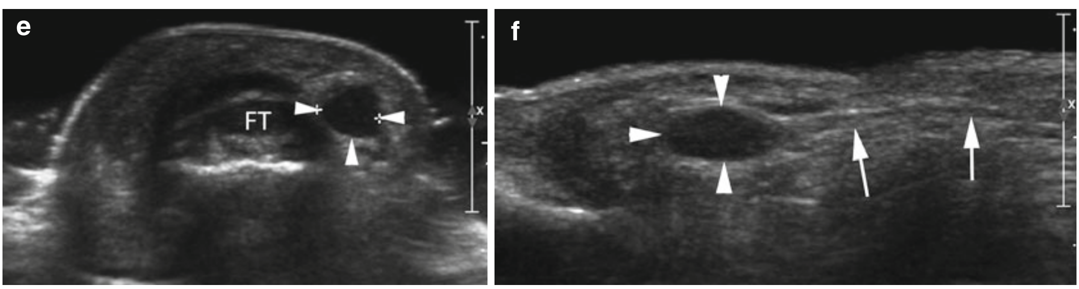

(**e**, **f**) Transverse (**e**) and longitudinal (**f**) sonogram in a patient with laceration of common digital nerve (*arrows* in **f**) and formation of terminal type neuroma (*arrowheads*). *FT* flexor tendon

4.4.9 Digital Section of Hand (Proper Digital Nerves)

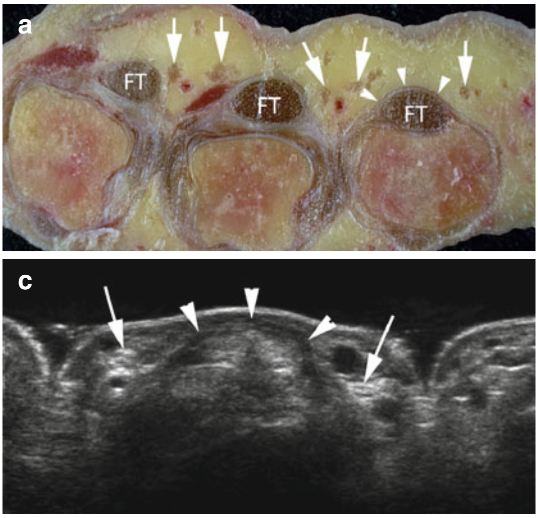

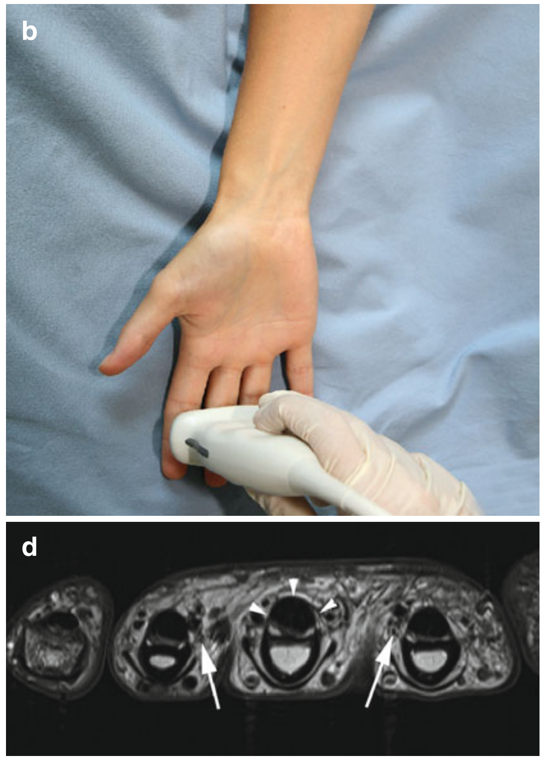

Fig. 4.29 (**a**) Anatomical cross section. (**b**) Transducer position. (**c**) Transverse sonogram. (**d**) Transverse T1-weighted MR image. Proper digital nerves (*arrows*) on both sides of finger arteries and flexor tendons (*FT*). *Arrowheads* anular pulley

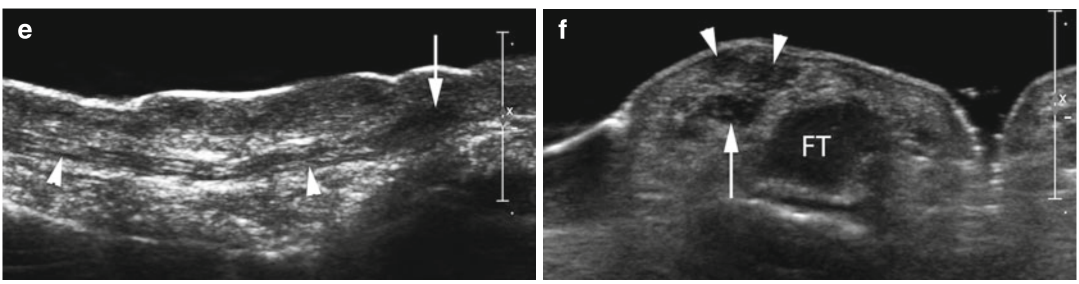

(**e**, **f**) Longitudinal (**e**) and transverse (**f**) sonogram in a patient with dissection of third proper digital nerve on radial side of index finger. The nerve (*arrowheads* in **e**) shows a wavy course and a small hypoechoic terminal type neuroma (*arrow* in **e**). On the transverse plane the neuroma (*arrow*) is seen adjacent to an inhomogeneous subcutaneous scar formation (*arrowheads*). *FT* flexor tendon

4.4.10 Proximal Forearm (Superficial Branch of Radial Nerve)

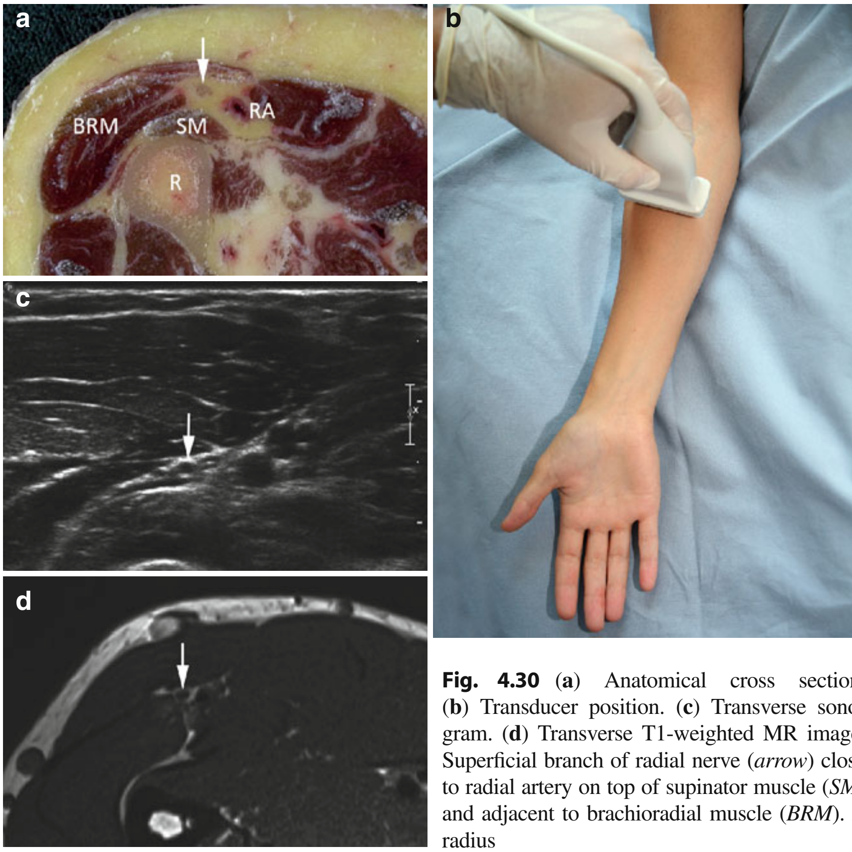

Fig. 4.30 (**a**) Anatomical cross section. (**b**) Transducer position. (**c**) Transverse sonogram. (**d**) Transverse T1-weighted MR image. Superficial branch of radial nerve (*arrow*) close to radial artery on top of supinator muscle (*SM*) and adjacent to brachioradial muscle (*BRM*). *R* radius

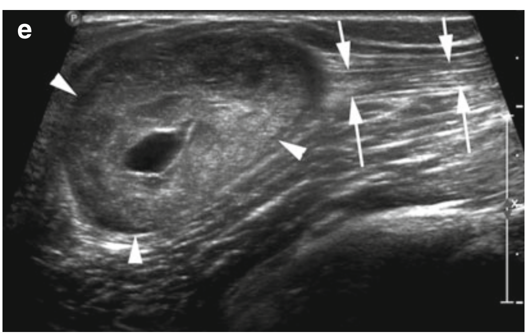

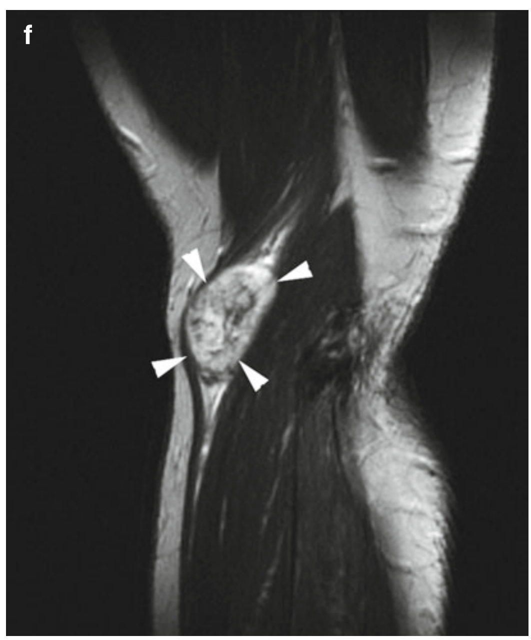

(**e**, **f**) Longitudinal sonogram (**e**) and parasagittal T1-weighted MR image after Gadolinium contrast application (**f**) in a patient with a histologically verified schwannoma (*arrowheads*) of the superficial radial nerve (*arrows* in **e**) immediately after the radial nerve bifurcation. Note marked but inhomogeneous contrast uptake in MRI ("salt-and-pepper"-appearance) and cystic inner fluid collection in the ultrasound image, which are typical features of schwannoma

4.4.11 Distal Forearm (Superficial Branch of Radial Nerve)

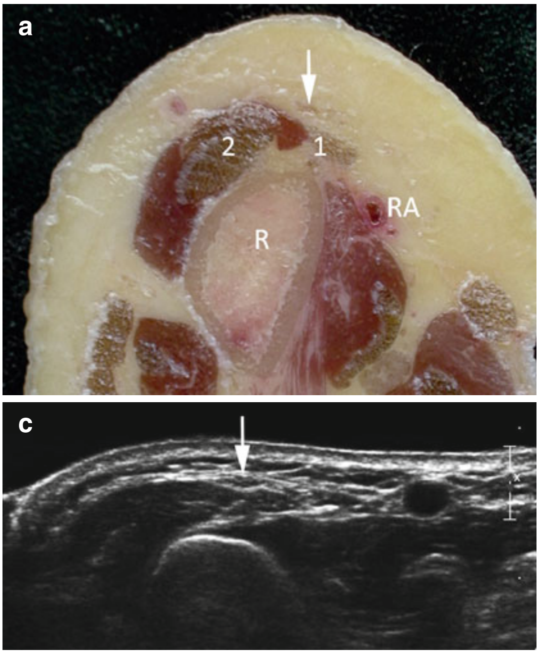

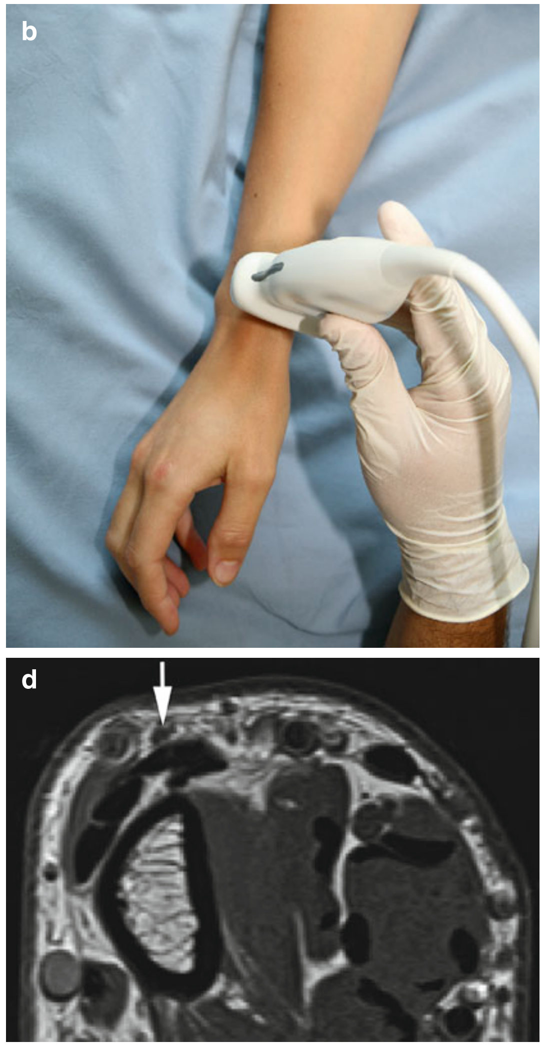

Fig. 4.31 (**a**) Anatomical cross section. (**b**) Transducer position. (**c**) Transverse sonogram. (**d**) Transverse T1-weighted MR image. Superficial branch of radial nerve (*arrow*) crossing to the dorsal aspect of the wrist. *1*, *2* first and second extensor tendon compartment. *R* radius, *RA* radial artery

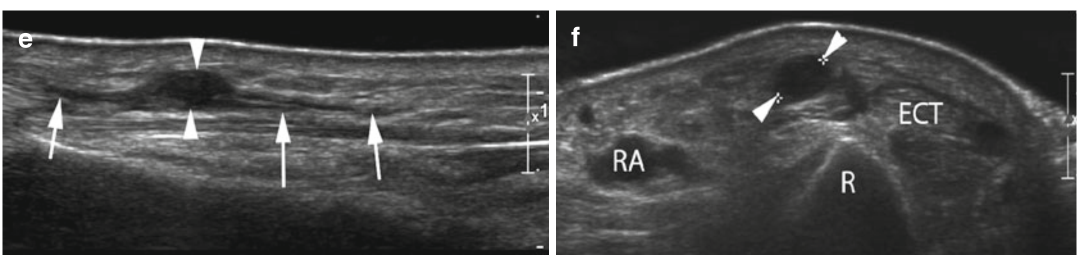

(**e**, **f**) Longitudinal (**e**) and transverse (**f**) sonogram through superficial radial nerve (*arrows*) at distal forearm in a patient with dissection of the nerve and neuroma formation (*arrowheads*). *RA* radial artery, *R* radius, *ECT* extensor carpi radialis longus tendon

4.4.12 First Extensor Tendon Compartment (Superficial Branch of Radial Nerve)

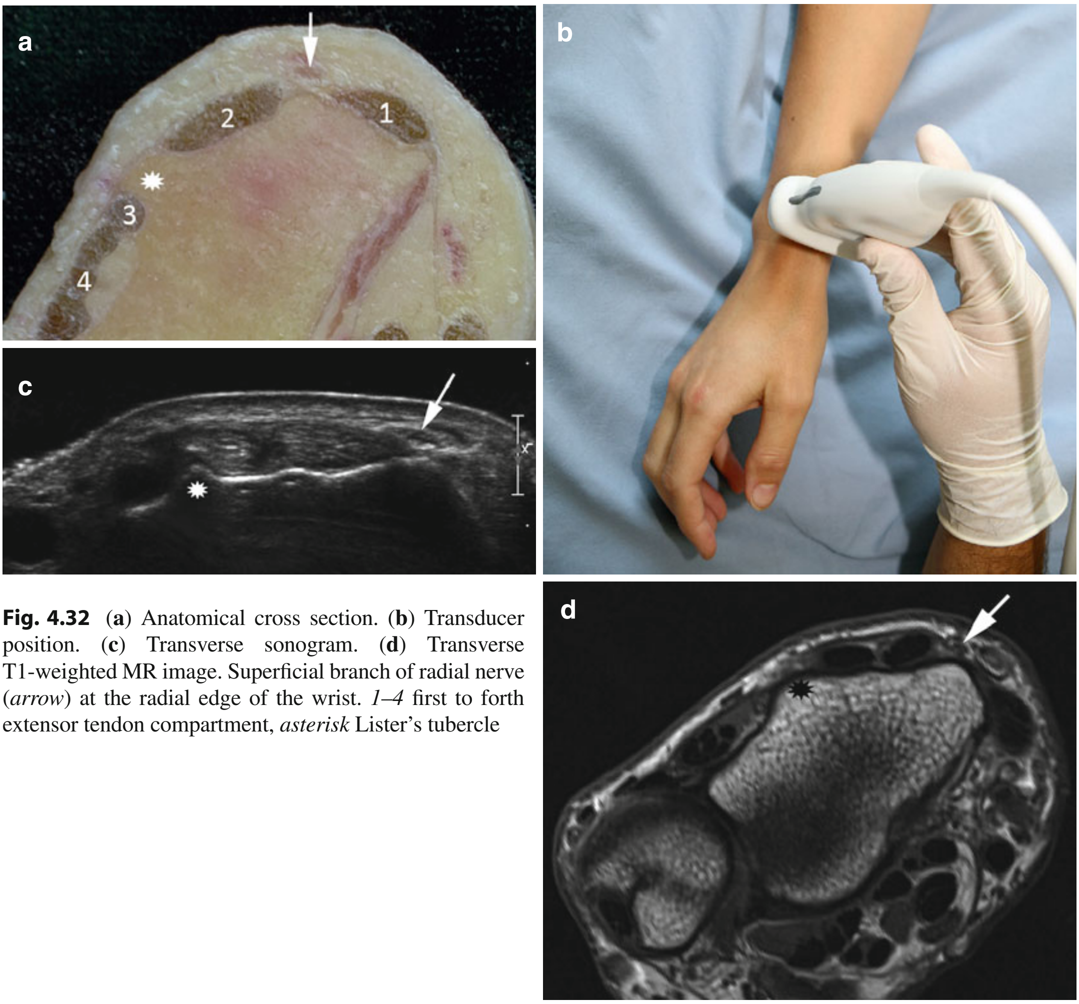

Fig. 4.32 (**a**) Anatomical cross section. (**b**) Transducer position. (**c**) Transverse sonogram. (**d**) Transverse T1-weighted MR image. Superficial branch of radial nerve (*arrow*) at the radial edge of the wrist. *1–4* first to forth extensor tendon compartment, *asterisk* Lister's tubercle

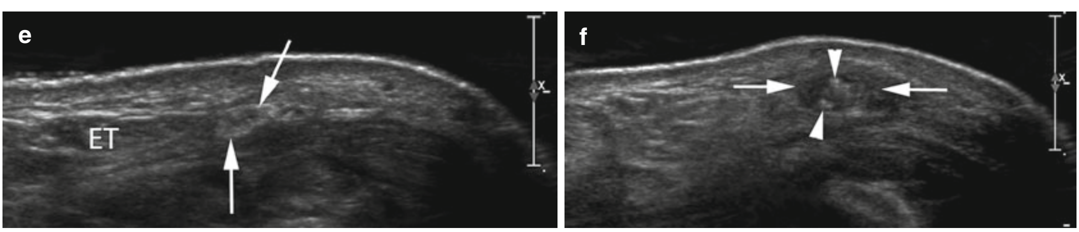

(**e**, **f**) Transverse sonogram at the level of the first extensor compartment (**e**) showing the normal superficial radial nerve (*arrows* in **e**). *ET* extensor tendons (2nd compartment). Slightly proximal (**f**) the nerve is thickened at the site of nerve repair (arrows in **f**) with demonstration of small hyperechoic suture artifacts (*arrowheads*) inside the nerve

4.4.13 Dorsum of the Hand (Superficial Branch of Radial Nerve)

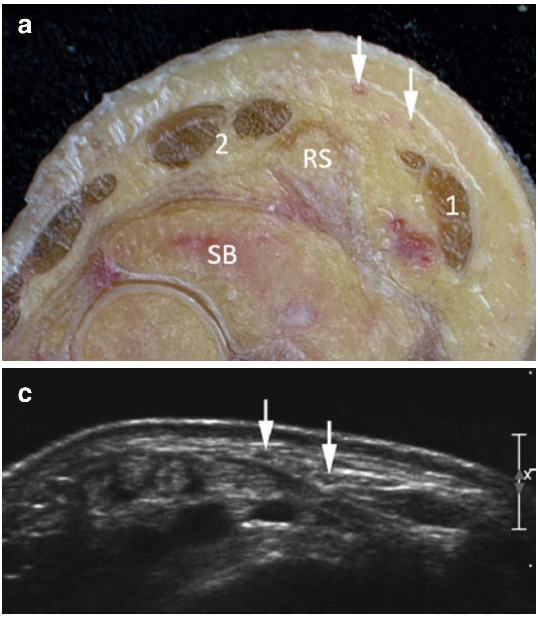

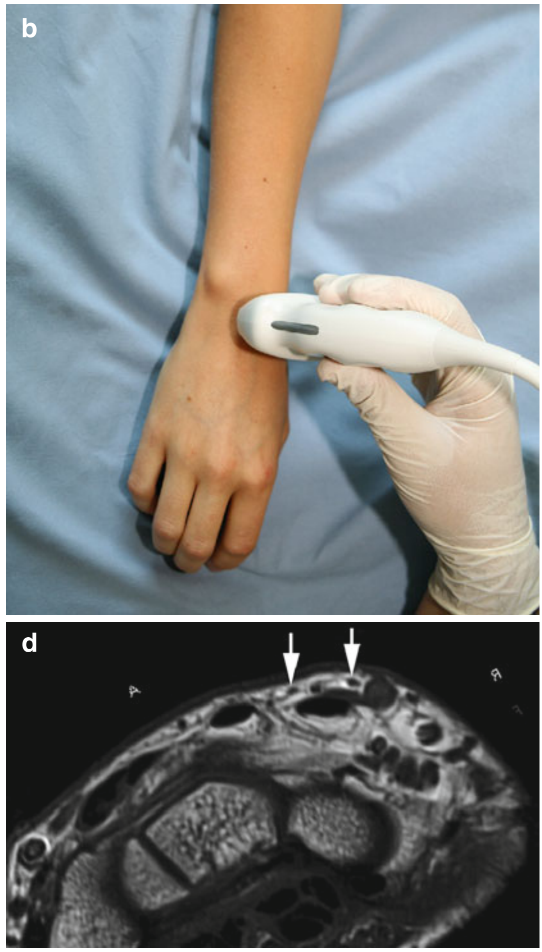

Fig. 4.33 (**a**) Anatomical cross section. (**b**) Transducer position. (**c**) Transverse sonogram. (**d**) Transverse T1-weighted MR image. Terminal division of superficial branch of radial nerve (*arrows*) on the dorsum of the hand. *1*, *2* first and second extensor tendon compartment, *RS* radial styloid, *SB* scaphoid bone

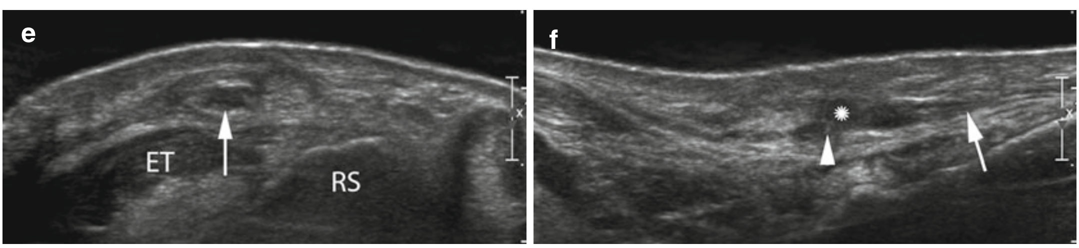

(**e**, **f**) Transverse (**e**) and longitudinal (**f**) sonogram through superficial radial nerve (*arrow*) on dorsum of the hand in a patient with dissection of the nerve and suturing. Note tiny hyperechoic dots corresponding with suture artifact (*arrowhead* in **f**) and globular thickening of nerve due to neuroma (*asterisk* in **f**) at the site of adaptation

4.4.14 Wrist Area (Deep Branch of Radial Nerve)

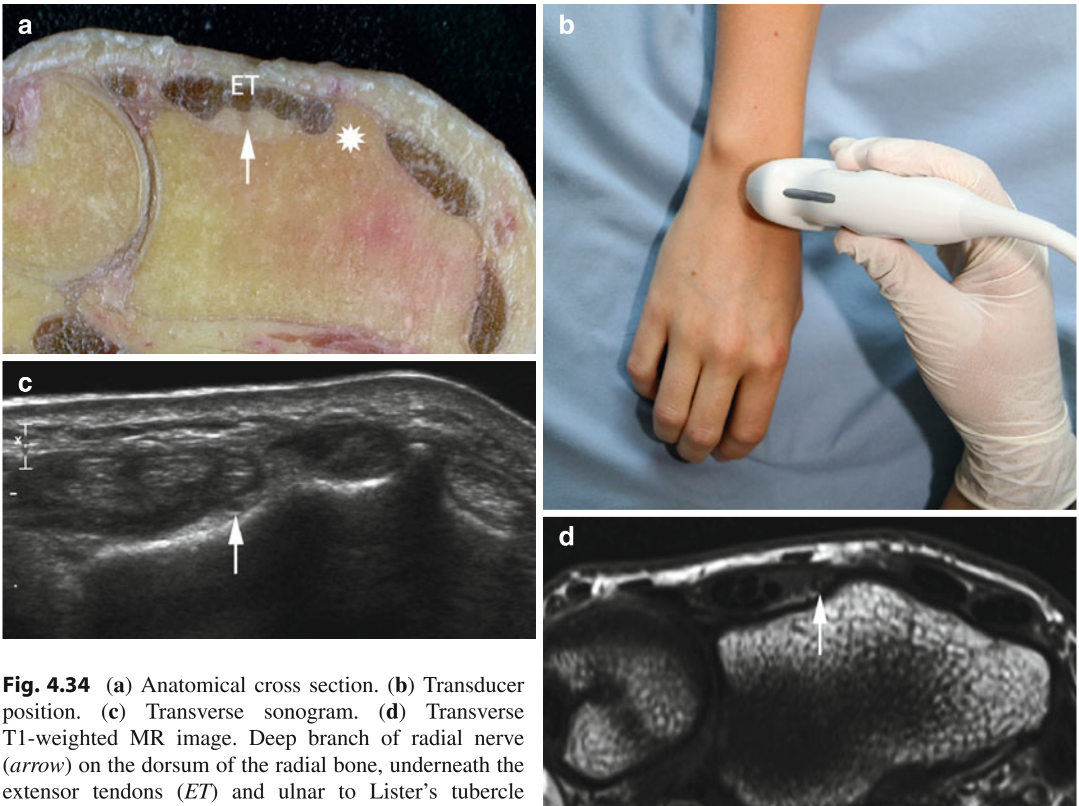

Fig. 4.34 (**a**) Anatomical cross section. (**b**) Transducer position. (**c**) Transverse sonogram. (**d**) Transverse T1-weighted MR image. Deep branch of radial nerve (*arrow*) on the dorsum of the radial bone, underneath the extensor tendons (*ET*) and ulnar to Lister's tubercle (*asterisk*).

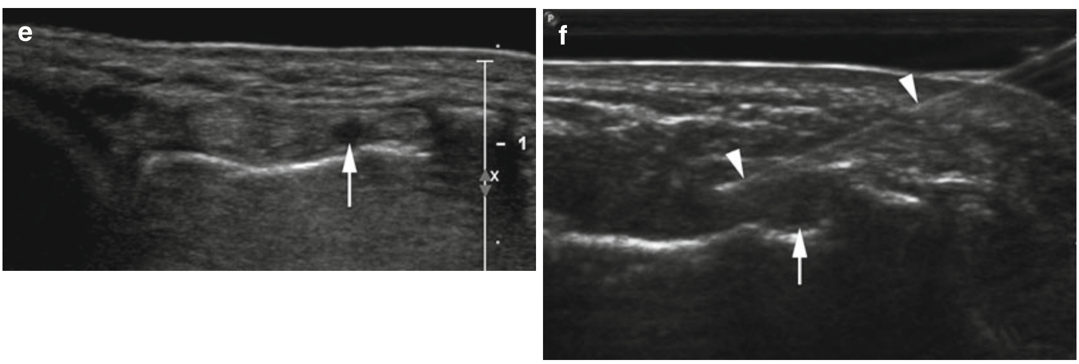

(**e**) Transverse sonogram through dorsal wrist in a patient with instability of the wrist and chronic dorsal pain. Note thickening and edema of deep radial nerve (*arrow*). (**f**) Transverse sonogram during ultrasound-guided injection of the nerve (*arrow*) with local anesthetic and corticoid. *Arrowheads* needle

4.4.15 Ulnar Side, Distal Third of Forearm (Dorsal Branch of Ulnar Nerve)

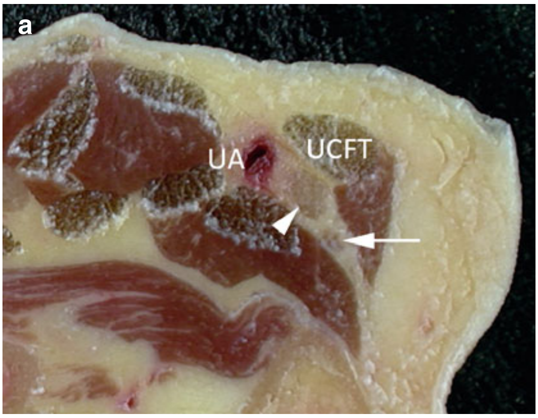

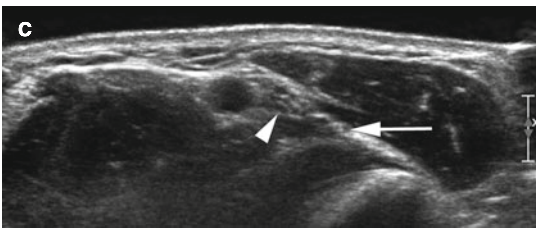

Fig. 4.35 (**a**) Anatomical cross section. (**b**) Transducer position. (**c**) Transverse sonogram. (**d**) Transverse T1-weighted MR image. Ulnar nerve (*arrowhead*) and dorsal branch (*arrow*) shortly after its origin. *UCFT* ulnar carpal flexor tendon, *UA* ulnar artery.

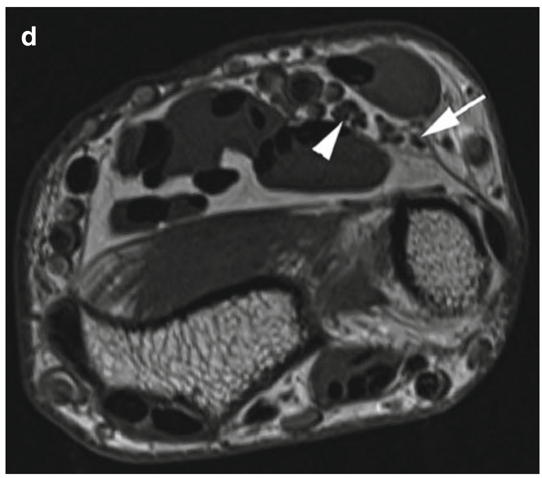

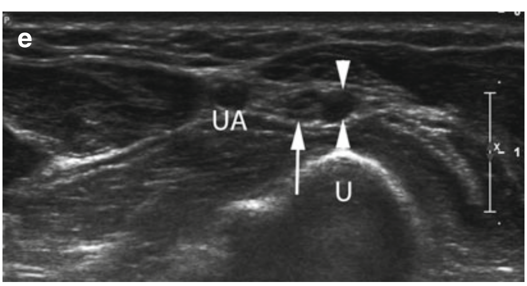

(**e**) Transverse sonogram in a patient with paresthesia of the ulnar nerve (dorsal branch) due to compression of the nerve by a crutch with development of a small neuroma (*arrowheads*) directly at the takeoff of the dorsal branch of the ulnar nerve (*arrows*). *UA* ulnar artery, *U* ulna

4.4.16 Guyon's Channel (Ulnar Nerve)

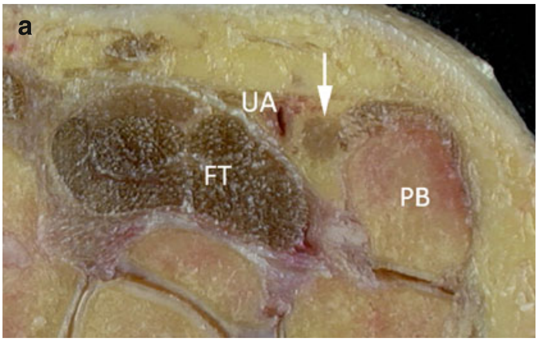

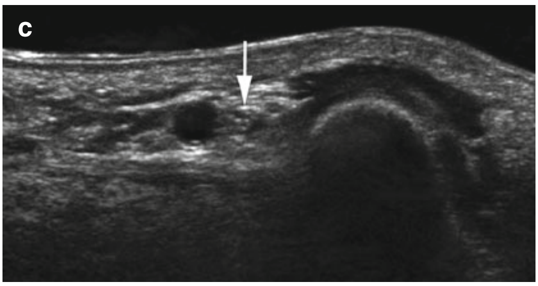

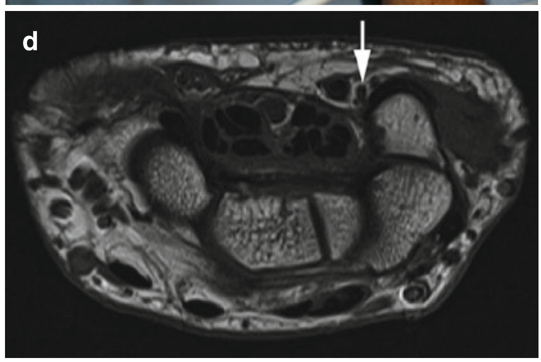

Fig. 4.36 (**a**) Anatomical cross section. (**b**) Transducer position. (**c**) Transverse sonogram. (**d**) Transverse T1-weighted MR image. Ulnar nerve inside Guyon's channel (*arrow*) underneath palmar carpal ligament. *UA* ulnar artery, *FT* flexor tendons, *PB* pisiforme bone

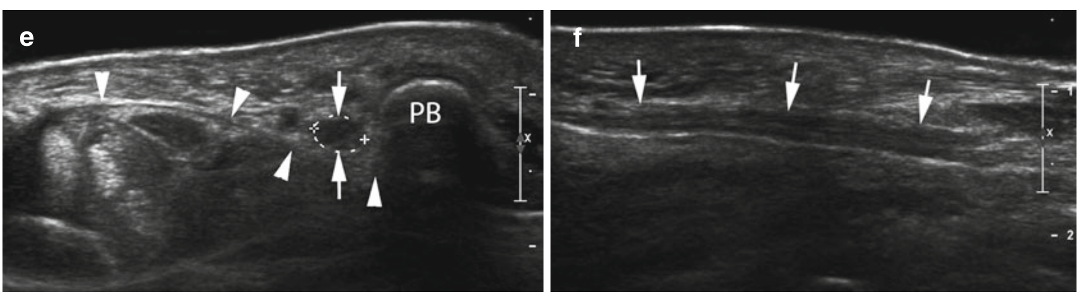

Transverse (**e**) and longitudinal (**f**) sonogram through ulnar nerve (*arrowheads*) at inlet of Guyon's channel in a patient with ulnar neuropathy. The ulnar nerve (*arrows*) is thickened (0.06 cm^2) with reduced fascicular texture due to edema. *PB* pisiforme bone, *arrowheads* retinaculum flexorum

4.4.17 Guyon's Channel Outlet (Ulnar Nerve Division)

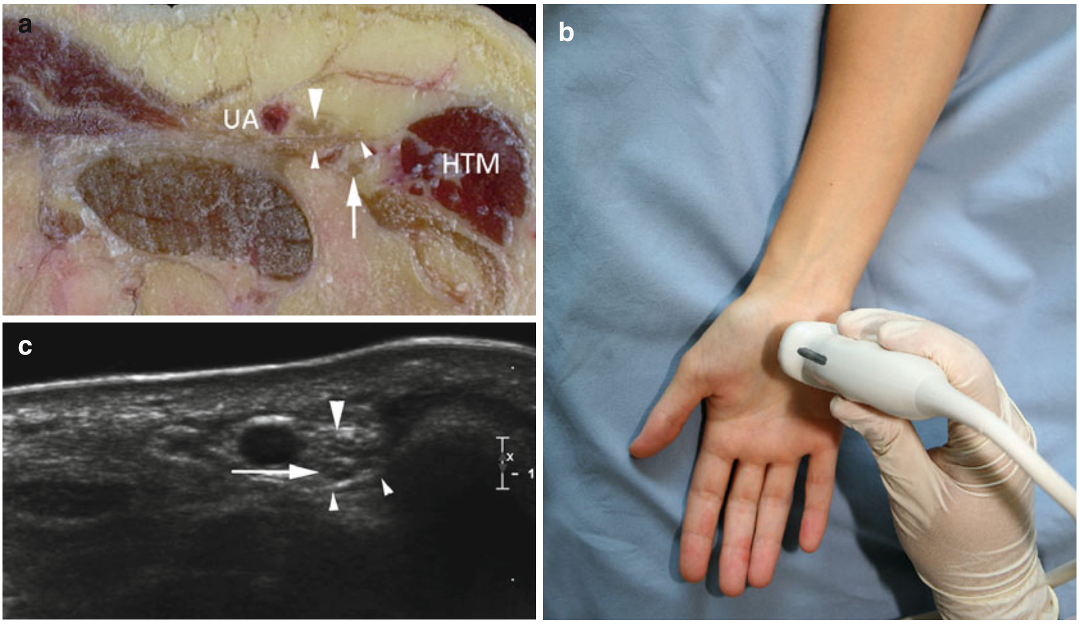

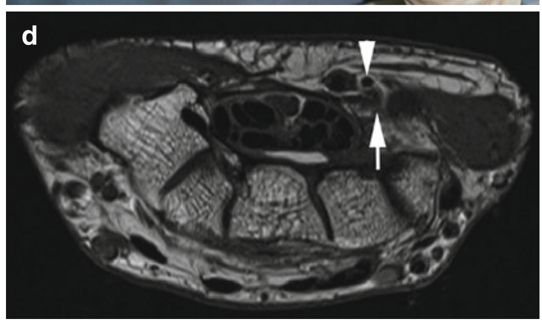

Fig. 4.37 (**a**) Anatomical cross section. (**b**) Transducer position. (**c**) Transverse sonogram. (**d**) Transverse T1-weighted MR image. Ulnar nerve division into superficial (*large arrowhead*) and deep (*arrow*) branch and the between lying pisohamate ligament (*small arrowheads*). *HTM* hypothenar muscles, *UA* ulnar artery

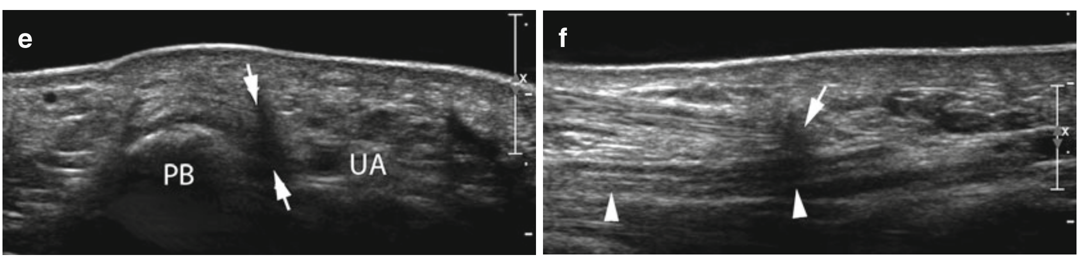

Transverse (**e**) and longitudinal (**f**) sonogram through ulnar nerve (*arrowheads*) inside Guyon's channel immediately above its division. In the transverse sonogram the nerve is not distinguished, because of overlying scar (*small arrows*). On the longitudinal sonogram continuity of the nerve can be confirmed. *UA* ulnar artery

Bibliography

Altinok MT, Baysal O, Karakas HM, Firat AK (2004) Sonographic examination of the carpal tunnel after provocative exercises. J Ultrasound Med 23:1301–1306

Bargalló X, Carrera A, Sala-Blanch X, Santamaría G, Morro R, Llusá M, Gilabert R (2010) Ultrasound-anatomic correlation of the peripheral nerves of the upper limb. Surg Radiol Anat 32(3):305–314

Bodner G, Huber B, Schwabegger A et al (1999) Sonographic detection of radial nerve entrapment within a humerus fracture. J Ultrasound Med 18:703–706

Bodner G, Harpf C, Gardetto A, Kovacs P, Gruber H, Peer S, Mallhoui A (2002) Ultrasonography of the accessory nerve. Normal and pathological findings in cadavers and patients with iatrogenic accessory nerve palsy. J Ultrasound Med 21:1159–1163

Buchberger W, Schoen G, Strasser K et al (1991) High resolution ultrasonography of the carpal tunnel. J Ultrasound Med 101:531–537

Chiou HJ, Chou YH, Cheng SP et al (1998) Cubital tunnel syndrome: diagnosis by high resolution ultrasonography. J Ultrasound Med 17:643–648

De Laat EA, Visser CP, Coene LN, Pahlplatz PV, Tavy DL (1994) Nerve lesions in primary shoulder dislocations and humeral neck fractures. A prospective clinical and EMG study. J Bone Joint Surg Br 76:381–383

Duncan I, Sullivan P, Lomas F (1999) Sonography in the diagnosis of carpal tunnel syndrome. AJR Am J Roentgenol 173:681–684

Fornage BD (1988) Peripheral nerves of the extremities: imaging with ultrasound. Radiology 167:179–182

Gassner E, Schocke M, Peer S, Schwabegger A, Jaschke W, Bodner G (2002) Persistent median artery in the carpal tunnel – color Doppler ultrasonographic findings. J Ultrasound Med 21:455–461

Hunderfund AN, Boon AJ, Mandrekar JN, Sorenson EJ (2011) Sonography in carpal tunnel syndrome. Muscle Nerve 44(4):485–491

Jacobson JA, Fessell DP, Lobo Lda G, Yang LJ (2010) Entrapment neuropathies I: upper limb (carpal tunnel excluded). Semin Musculoskelet Radiol 14(5):473–486

Linda DD, Harish S, Stewart BG, Finlay K, Parasu N, Rebello RP (2010) Multimodality imaging of peripheral neuropathies of the upper limb and brachial plexus. Radiographics 30(5):1373–1400

Loewy J (2002) Sonoanatomy of the median, ulnar and radial nerves. Can Assoc Radiol J 53(1):33–38

Martinoli C, Serafini G, Bianchi S et al (1996) Ultrasonography of peripheral nerves. J Peripher Nerv Syst 1:169–174

Miller TT, Reinus WR (2010) Nerve entrapment syndromes of the elbow, forearm, and wrist. AJR Am J Roentgenol 195(3):585–594

Prevel CD, Matloub HS, Zhong Y et al (1993) The extrinsic blood supply of the ulnar nerve at the elbow: an anatomic study. J Hand Surg 18A:433–438

Riffaud L, Morandi X, Godey B et al (1999) Anatomic basis for the compression and neurolysis of the deep branch of the radial nerve in the radial tunnel. Surg Radiol Anat 21:229–233

Sarria L, Cabada T, Cozcolluela R, Martinez-Berganza T, Garcia S (2000) Carpal tunnel syndrome: usefulness of sonography. Eur Radiol 10:1920–1925

Sheppard DG, Iyer RB, Fenstermacher MJ (1998) Brachial plexus: demonstration at US. Radiology 208:402–406

Silvestri E, Martinoli C, Derchi LE et al (1995) Echotexture of peripheral nerves: correlation between US and histologic findings and criteria to differentiate tendons. Radiology 197:291–296

Thomas SJ, Yakin DE, Parry BR, Lubahn JD (2000) The anatomical relationship between the posterior interosseous nerve and the supinator muscle. J Hand Surg [Am] 25: 936–941

Walker FO, Cartwright MS, Wiesler ER, Caress J (2004) Ultrasound of nerve and muscle. Clin Neurophysiol 115: 495–507

Lower Extremity Nerves

5

Verena Spiss, Hannes Gruber, Werner Judmaier, and Erich Brenner

Contents

V. Spiss (✉) • H. Gruber • W. Judmaier
Department of Radiology, Innsbruck Medical University, Anichstrasse 35, 6020 Innsbruck, Tyrol, Austria
e-mail: verena.spiss@i-med.ac.at; hannes.gruber@i-med.ac.at; werner.judmaier@i-med.ac.at

E. Brenner
Division for Clinical and Functional Anatomy, Innsbruck Medical University, Anichstrasse 59, 6020 Innsbruck, Tyrol, Austria
e-mail: erich.brenner@i-med.ac.at

5.1 Introduction

The sensory and motor innervation of the entire lower extremity derives from the lumbosacral plexus. According to its clinical significance, the major nerves of this anatomic region include the sciatic, the femoral with the saphenous nerve, the tibial nerve, and the common fibular nerve. These nerves or some of their branches may be affected by blunt or sharp trauma and by compression/entrapment or tumors and tumor like lesions, such as nerve sheath tumors, schwannomas, and

S. Peer, H. Gruber (eds.), *Atlas of Peripheral Nerve Ultrasound*,
DOI 10.1007/978-3-642-25594-6_5, © Springer-Verlag Berlin Heidelberg 2013

neurofibromas. Initial presumptive diagnoses of such lesions are based on clinical diagnostics, but high-resolution ultrasound (HRUS) proves high potential for a direct visualization and definition of relevant pathologies.

The femoral nerve is one of the largest peripheral nerves of the human body. It arises from the dorsal division of the ventral rami of the first to fourth lumbar nerves and contains the fascicles for the motor function and sensibility of a major part of the ventral to medial aspect of the lower extremity. It descends next to the psoas muscle passing down to the groin within the iliopsoas groove always underneath the iliac fascia. Laterally to the femoral artery and vein, it exits the pelvis through the muscles' lacuna to enter the thigh dividing into an anterior and posterior section. On its way through the muscles' lacuna, it is separated from the femoral artery only by a fibrous band, the iliopectineal arch, which is part of the inguinal ligament complex. Heading down the lower limb, the femoral nerve runs parallel to the sartorius muscle. It spreads into several terminal branches such as the ventral and medial cutaneous nerve branches and the motor branches which supply the ventral and medial muscles of the thigh.

While a complete failure of the femoral nerve caused by direct trauma is rather rare, it is prone to iatrogenic damage during orthopedic hip replacement, inguinal hernia repair, or gynecological procedures.

The largest branch of the femoral nerve is the saphenous nerve. It supplies the knee and the medial aspect of the lower leg including the medial foot with sensory fibers. In the middle of the thigh, it approaches the superficial femoral artery ventrally, passes through the adductor channel, and pierces the vasto-adductor membrane to get subcutaneous. It passes down the tibial side of the calf together with the accompanying greater saphenous vein within the same fascia duplication. Due to its close relationship with the greater saphenous vein, it is obvious that surgical procedures such as stripping of the saphenous vein may result in damage to this nerve. Especially peri-patellar branches but also the main stem of the nerve are frequently affected by surgery such as knee arthroplasty, focal compression or stretch injuries, or even direct impact.

The sciatic nerve, the largest human nerve originating from the lumbar plexus, leaves the retro- and subperitoneal space through the major sciatic foramen. It runs distalward into the subgluteal space directly laterally to the sciatic tuber neighbored by the inferior gluteal vessels to take its course down the thigh underneath its leading structures, the femoral biceps, and the semitendinosus and the semimembranosus muscle. The sciatic nerve actually consists of actually two nerves encased by one common perineural sheath: the fibular and the tibial nerve which form differently sized portions even dividing at different levels.

The fibular nerve is derived from the fifth lumbar to the second sacral segment. It passes down the dorsum of the thigh laterally to the tibial nerve (lateral portion of sciatic nerve) to the popliteal fossa, where it leaves the alliance to wind around the head of the fibula and to enter the fibular muscles. It has to be noted that the location of the division of the sciatic nerve has a rather high variability with a typical division in the lower part of the thigh or popliteal fossa in only about 75 % of subjects. In the latter 25 %, the nerve may divide in the upper thigh, the gluteal region, or even shortly after exiting the gluteal region. The fibular nerve divides into the deep and the superficial fibular nerve directly after passing the fibular neck. The more dorsally positioned deep fibular nerve enters the space between the dorsal long and the ventral short fibular muscle and heads for the extensor digitorum longus muscle inferomedially. Medially to the accompanying anterior tibial vessels, it heads downward to the dorsum of the foot where it runs underneath the anterior tibial muscle and the long extensor hallucis muscle on the interosseous membrane.

The more ventrally positioned superficial fibular nerve runs downward to the shank between the fibular muscles and the long digital extensor muscle. Crossing the tendons of the ventral extensor muscles, it gets subcutaneous and divides into its terminal sensory cutaneous branches: the medial, the dorsal, and the intermediate cutaneous

nerve and the intermediate dorsal cutaneous nerve at the dorsum of the foot.

The most frequent causes of compression neuropathy of the common fibular nerve are ganglions arising from the tibiofibular joint, osteophytes of the fibular neck, malaligned fibular head fractures, or different kinds of stretching injuries. A typical but rather rare compression neuropathy of the superficial fibular nerve is located at the level of its penetration point through the crural fascia. Also the deep fibular nerve may suffer compression on its way to the dorsum of the foot passing beneath the inferior extensor retinaculum, which is known as anterior tarsal tunnel syndrome.

The tibial nerve takes its course in the dorsal shank entering the space between the two heads of the gastrocnemius muscles to pass the arch of the soleus muscle. Before undercrossing this "soleus arch," it usually releases a number of cutaneous and muscular branches for the shank: the main subcutaneous branch – the sural nerve – of the dorsal shank passes downward next to the small saphenous vein aiming for the posterior region of the outer ankle. Together with its accompanying vessels, the posterior tibial artery, and vein, the tibial nerve runs more medially heading for the posterior medial malleolar region. Usually the nerve is positioned posterior to the posterior tibial vessels, the long digital flexor, and the posterior tibial muscle.

Even though the tibial nerve can be compressed all along its course down the limb, its affection on the way through the posterior tarsal tunnel has highest probability – known as the posterior tarsal tunnel syndrome.

The nerves of the foot are the terminal branches of the fibular and the tibial nerve: the dorsal ones comprise the intermediate dorsal cutaneous nerve, the medial dorsal nerve, the sural nerve, and the deep fibular nerve and their terminal branches. For the foot, the tibial nerve divides into the medial and lateral plantar nerve at the posterior third of the plantar region corresponding to the exit of the tarsal tunnel. The common plantar digital nerve of the medial plantar nerve splits into three common digital nerves and each into two proper digital branches. The common plantar digital nerve of the lateral plantar nerve usually communicates with a branch of the third common digital nerve and divides finally into two proper digital nerves.

A well-known, typical hypoechoic, fusiform nerve enlargement of the proper digital nerve in the intermetatarsal space is Morton's neuroma, which is esteemed to be a pseudotumor formed due to chronic, focal friction and compression of the nerve.

5.2 Nerves in the Groin and Thigh: Topographic Overview

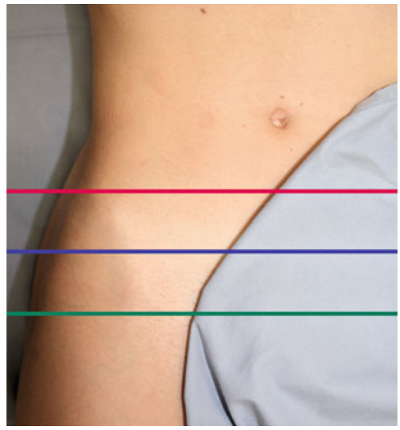

Fig. 5.1 General topographic overview of nerve anatomy in the groin and thigh. Localizer for anatomical cross sections (Fig. 5.2a–c)

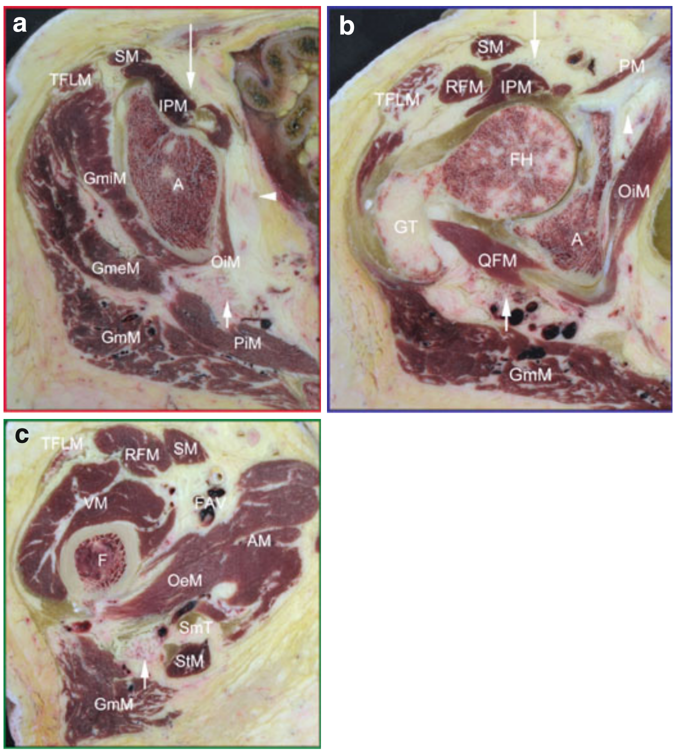

Fig. 5.2 (**a**) Anatomical cross section through the pelvic outlet (*red line* in Fig. 5.1). Femoral nerve (*long arrow*) lying on top of iliopsoas muscle (*IPM*). Sciatic nerve located (*small arrow*) between posterior edge of obturator internus muscle (*OiM*) and piriformis muscle (*PiM*). Obturator nerve (*arrowhead*) medial to obturator internus muscle (*OiM*). *A* acetabular roof, *SM* sartorius muscle, *TFLM* tensor fasciae latae muscle, *GmiM* glutaeus minimus muscle, *GmeM* glutaeus medius muscle, *GmM* glutaeus maximus muscle. (**b**) Anatomical cross section through the groin (*blue line* in Fig. 5.1). Femoral nerve (*long arrow*) lying on top of iliopsoas muscle (*IPM*). Sciatic nerve (*small arrow*) located between quadratus femoris muscle (*QFM*) and *GmM* glutaeus maximus muscle. Obturator nerve (*arrowhead*) ventral to obturator internus muscle (*OiM*) and posterior to pectineus muscle (*PM*). *SM* sartorius muscle, *RFM* rectus femoris muscle, *TFLM* tensor fasciae latae muscle, *A* acetabulum, *FH* femoral head, *GT* greater trochanter (**c**) Anatomical cross section through the gluteal region/proximal thigh (*green line* in Fig. 5.1). Sciatic nerve (*small arrow*) located close to semitendinosus muscle (*Stm*) and glutaeus maximus muscle (*GmM*). *SmT* semimembranosus tendon, *OeM* obturator externus muscle, *AM* adductor muscles, *VM* vastus muscles, *TFLM* tensor fasciae latae muscle, *RFM* rectus femoris muscle, *SM* sartorius muscle, *FAV* femoral artery and vein, *F* femur

5.2.1 Inguinal Region (Femoral Nerve Pelvic Outlet)

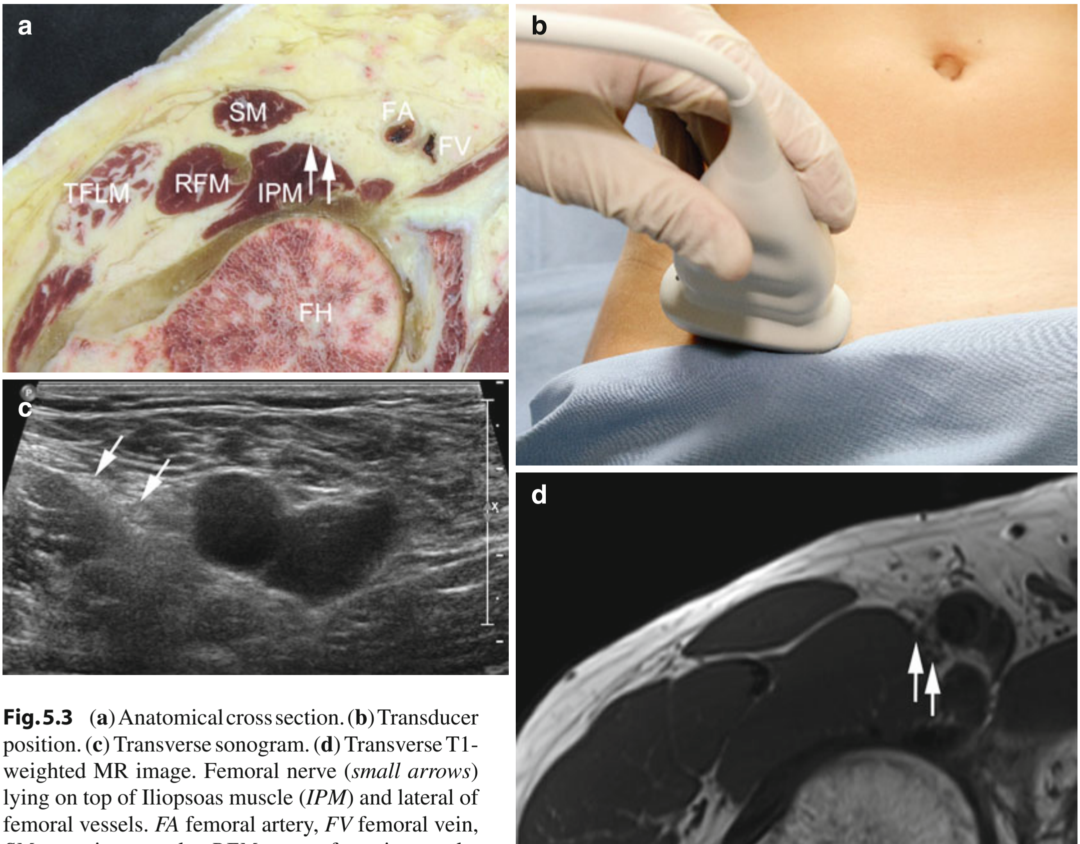

Fig. 5.3 (**a**) Anatomical cross section. (**b**) Transducer position. (**c**) Transverse sonogram. (**d**) Transverse T1-weighted MR image. Femoral nerve (*small arrows*) lying on top of Iliopsoas muscle (*IPM*) and lateral of femoral vessels. *FA* femoral artery, *FV* femoral vein, *SM* sartorius muscle, *RFM* rectus femoris muscle, *TFLM* tensor fasciae latae muscle, *FH* femoral head

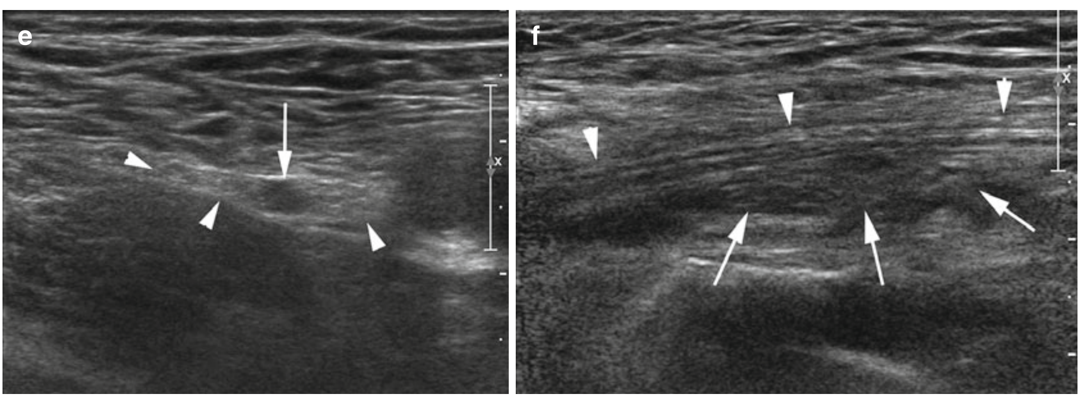

(**e**) Transverse sonogram in a patient with partial femoral nerve palsy after total hip arthroplasty. Note small traction neuroma (*arrow*) inside the otherwise normal femoral nerve (*arrowheads*). (**f**) Longitudinal sonogram in a patient with transient femoral nerve paresthesias after a femoral nerve block – "Winnie's block." Note indistinct outer epineurium of otherwise normal nerve (*arrowheads*) and focal fluid accumulation (*arrows*) deep to the femoral nerve

5.2.2 Inguinal Channel (Femoral Nerve Inguinal Channel)

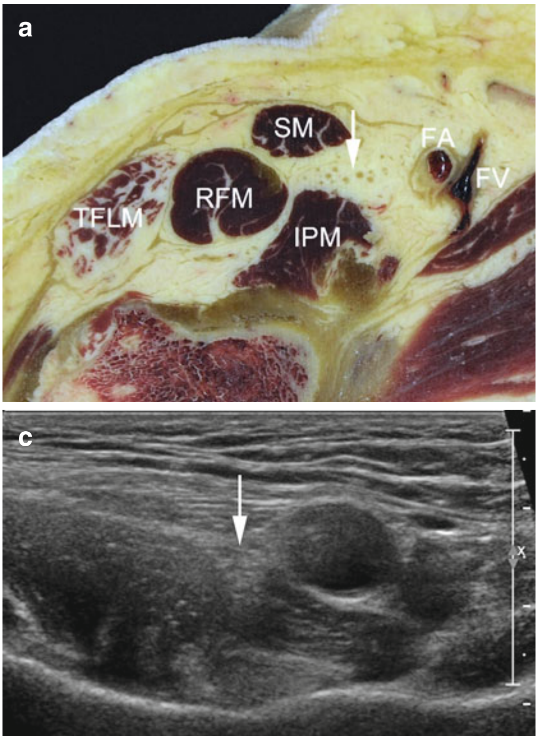

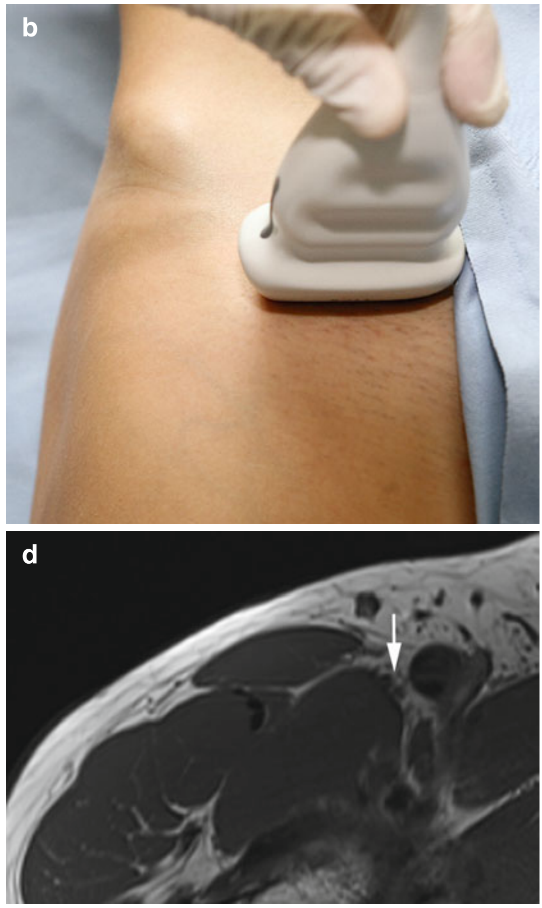

Fig. 5.4 (**a**) Anatomical cross section. (**b**) Transducer position. (**c**) Transverse sonogram. (**d**) Transverse T1-weighted MR image. Femoral nerve (*small arrow*) located in a groove between the Iliopsoas muscle (*IPM*) and the femoral artery (*FA*). *FV* femoral vein, *SM* sartorius muscle, *RFM* rectus femoris muscle, *TFLM* tensor fasciae latae muscle

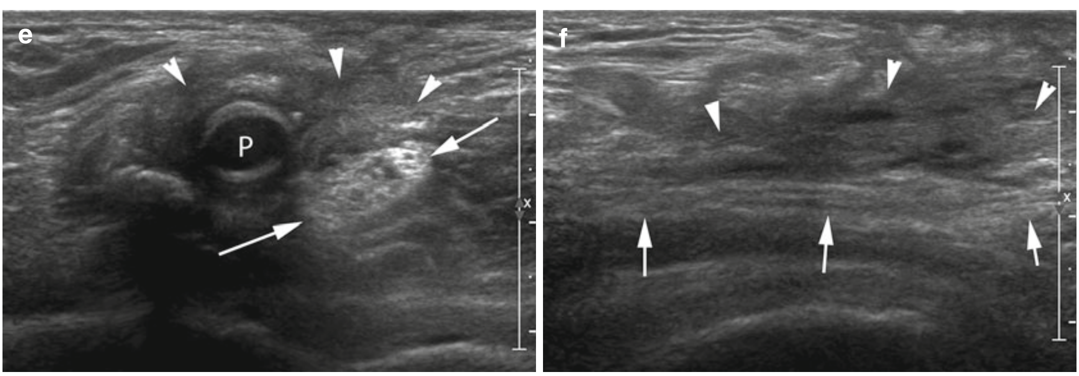

(**e**, **f**) Transverse (**e**) and longitudinal (**f**) sonogram in a patient with partial femoral nerve palsy after femoral artery reconstruction. Note tight scar tissue (*arrowheads*) surrounding the vascular prosthesis (*P*) and the femoral nerve (*arrows*)

5.2.3 Proximal Thigh (Femoral Nerve Division)

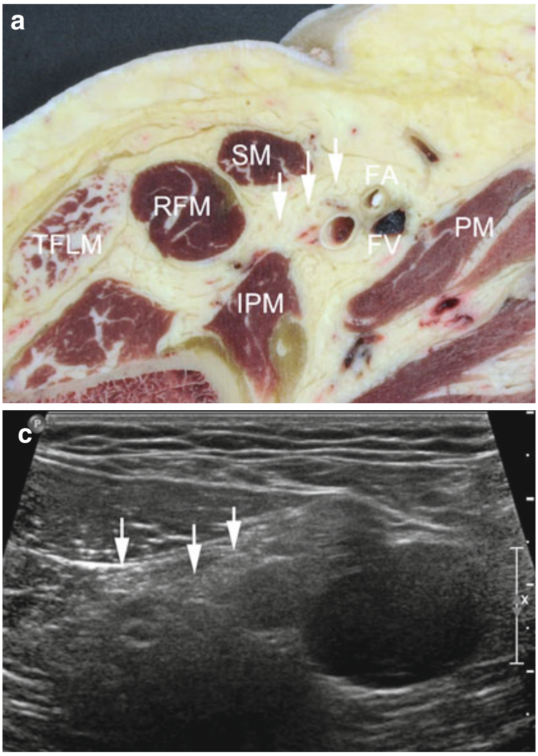

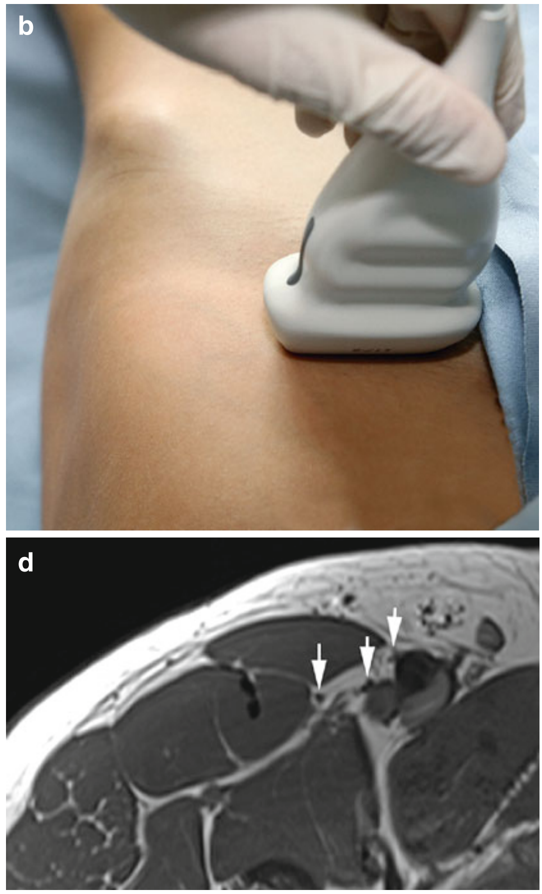

Fig. 5.5 (**a**) Anatomical cross section. (**b**) Transducer position. (**c**) Transverse sonogram. (**d**) Transverse T1-weighted MR image. Femoral nerve branches (*small arrows*) lying medial to iliopsoas muscle (*IPM*) and underneath sartorius muscle (*SM*) adjacent to femoral vessels. *FA* femoral artery, *FV* femoral vein, *SM* sartorius muscle, *RFM* rectus femoris muscle, *TFLM* tensor fasciae latae muscle, *PM* pectineus muscle

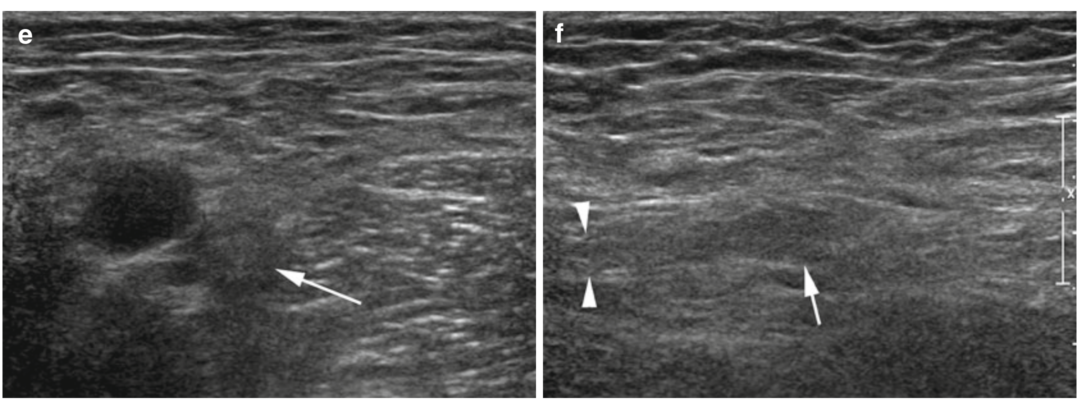

(**e**, **f**) Transverse (**e**) and longitudinal (**f**) sonogram of femoral nerve after its division demonstrating a small stump neuroma (*arrow*) of a femoral nerve branch (*arrowheads*)

5.2.4 Gluteal Region (Sciatic Nerve)

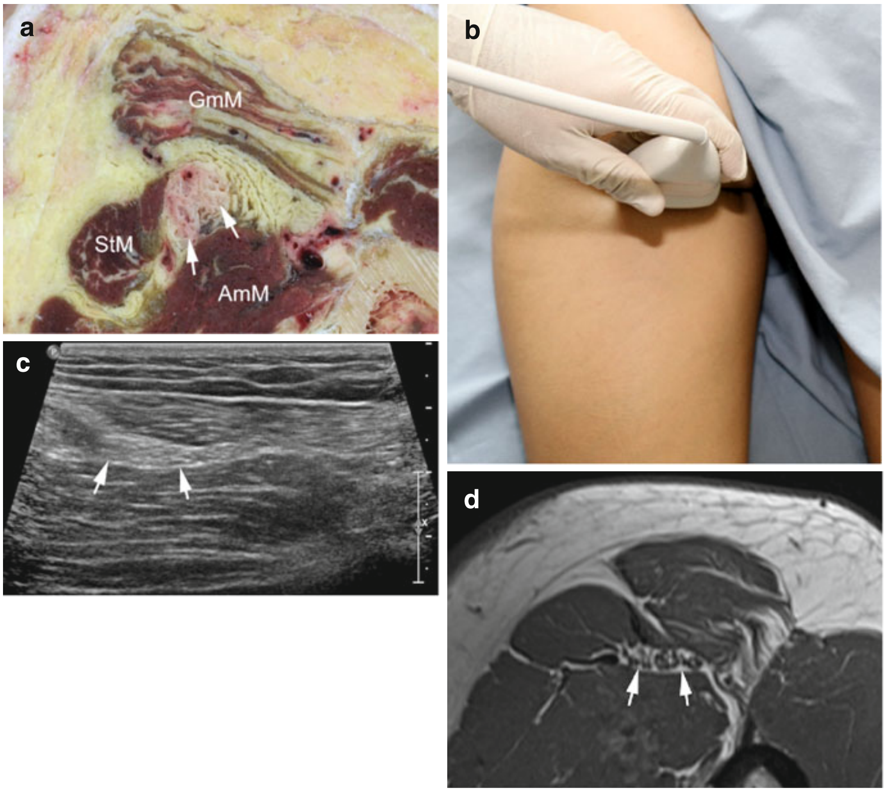

Fig. 5.6 (**a**) Anatomical cross section. (**b**) Transducer position. (**c**) Transverse sonogram. (**d**) Transverse T1-weighted MR image. Sciatic nerve (*arrows*) lying between gluteus maximus muscle (*GmM*) and adductor magnus muscle (*AmM*). *StM* semitendinosus muscle

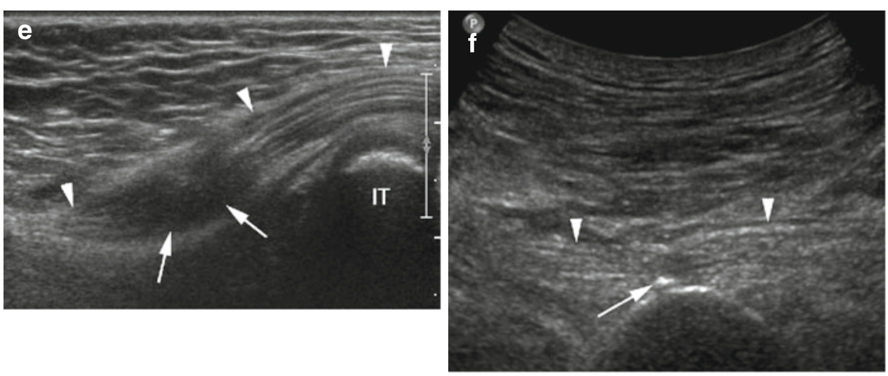

(**e**) Longitudinal sonogram of sciatic nerve (*arrowheads*) in the gluteal region close to the ischial tuberosity (*IT*) in a pediatric patient with partial sciatic nerve lesion after vaccination. Note marked swelling and indistinct fascicular texture (*arrows*) due to direct injection of the nerve. (**f**) Longitudinal sonogram of sciatic nerve (*arrowheads*) in the gluteal region in a patient with sciatic nerve palsy developing immediately after wire fixation of a periprosthetic femoral shaft fracture. Note the superficial indentation and loss of fascicular structure and metallic artifact (*arrow*) representing the wire traversing the nerve

5.3 Nerves Above the Knee: Topographic Overview

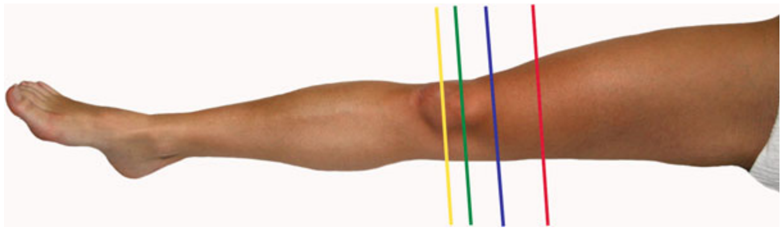

Fig. 5.7 General topographic overview of nerve anatomy in the distal thigh and above the knee. Localizer for anatomical cross sections (Fig. 5.8a–d). *Colored lines* correspond to level of cross sections

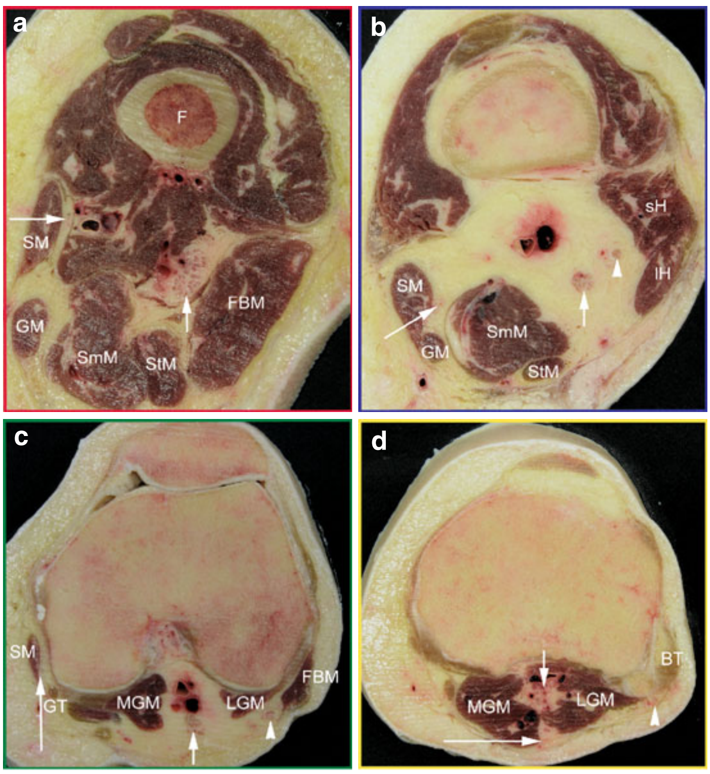

Fig. 5.8 (**a**) Anatomical cross section through the distal thigh (*red line* in Fig. 5.7). Sciatic nerve (*short arrow*) positioned close to long head of femoral biceps muscle (*FBM*). Saphenous nerve (*long arrow*) adjacent to sartorius muscle (*SM*). *GM* gracilis muscle, *SmM* semimembranosus muscle, *StM* semitendinosus muscle, *F* femur. (**b**) Anatomical cross section through adductor channel/proximal popliteal fossa (*blue line* in Fig. 5.7). Sciatic nerve is already divided into tibial nerve (*short arrow*) and common fibular nerve (*arrowhead*) running adjacent to the popliteal vessels. Saphenous nerve (*long arrow*) runs adjacent to the sartorius muscle. *GM* gracilis muscle, *SmM* semimembranosus muscle, *StM* semitendinosus muscle, *sH/lH* short head/long head of femoral biceps muscle. (**c**) Anatomical cross section through popliteal fossa (*green line* in Fig. 5.7). Tibial nerve (*short arrow*) close to popliteal artery and vein and common fibular nerve (*arrowhead*) running between lateral gastrocnemius muscle (*LGM*) and femoral biceps muscle (FBM). Saphenous nerve (*long arrow*) runs adjacent to the sartorius muscle. *GT* gracilis muscle tendon, *SM* sartorius muscle, *MGM* medial gastrocnemius muscle. (**d**) Anatomical cross section at level of tibial plateau (*yellow line* in Fig. 5.7). Tibial nerve (*short arrow*) close to popliteal artery and vein and common fibular nerve (*arrowhead*) running close to biceps tendon (*BT*). Sural nerve (*long arrow*) runs adjacent to *MGM* medial gastrocnemius muscle. *LGM* lateral gastrocnemius muscle

5.3.1 Posterior Thigh (Sciatic Nerve Division Proximal Level)

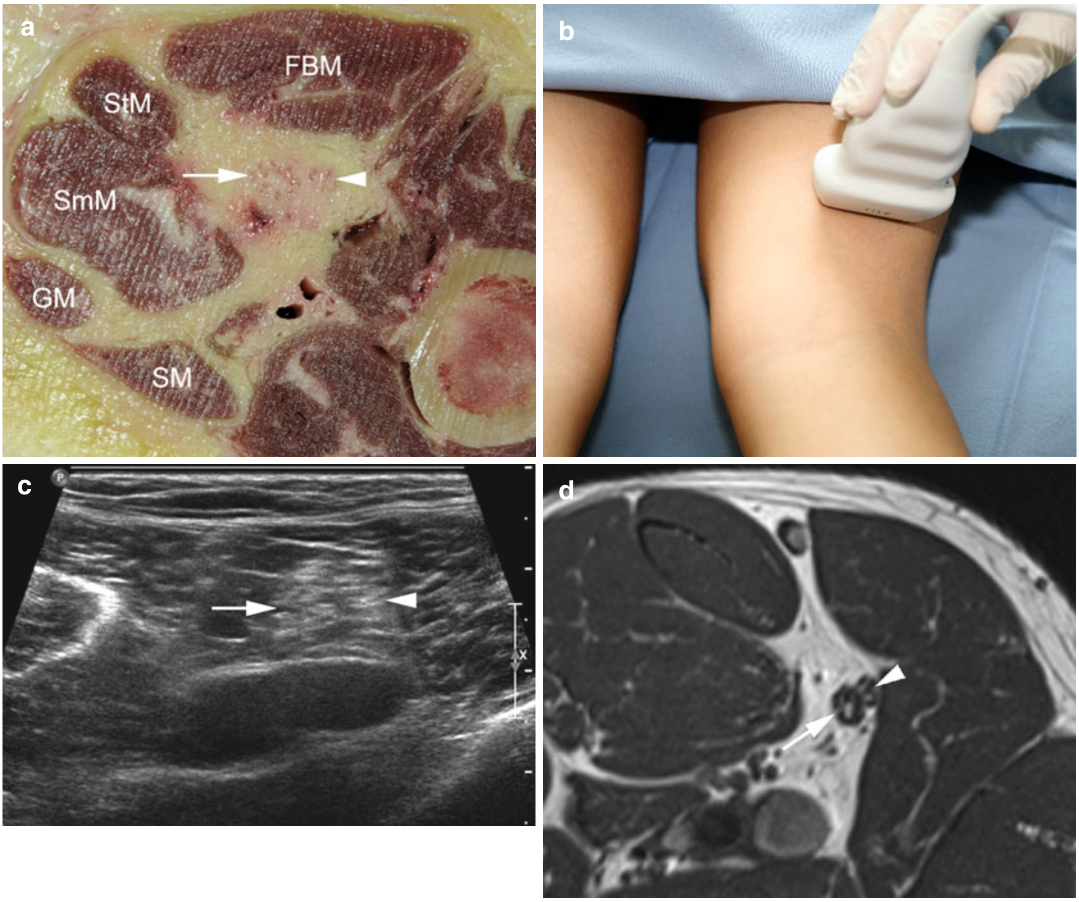

Fig. 5.9 (**a**) Anatomical cross section. (**b**) Transducer position. (**c**) Transverse sonogram. (**d**) Transverse T1-weighted MR image. Sciatic nerve with distinct differentiation of tibial (*small arrow*) and fibular portion (*arrowhead*) but still surrounded by a common outer nerve sheath. *FBM* femoral biceps muscle, *StM* semitendinosus muscle, *SmM* semimembranosus muscle, *GM* gracilis muscle, *SM* sartorius muscle

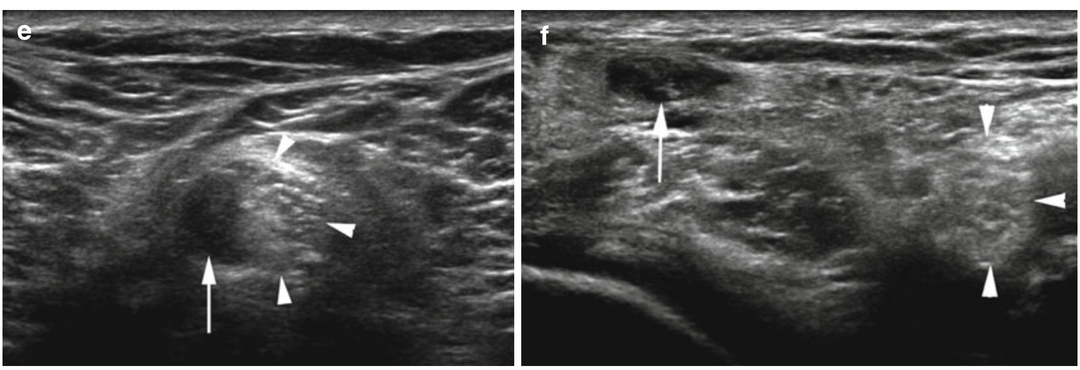

(**e**, **f**) Transverse sonogram through sciatic nerve division (**e**) and a few centimeters below (**f**) demonstrating a traction neuroma of the peroneal nerve (*arrow*) extending into the sciatic nerve. Note normal appearance of tibial nerve fascicles inside the sciatic nerve (*arrowheads* in **e**) and common tibial nerve (*arrowheads* in **f**)

5.3.2 Popliteal Fossa Inlet (Sciatic Nerve Division Middle Level)

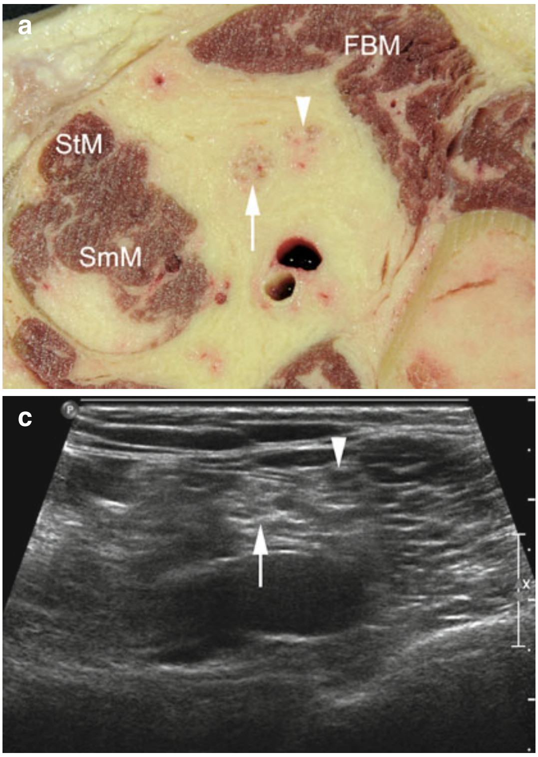

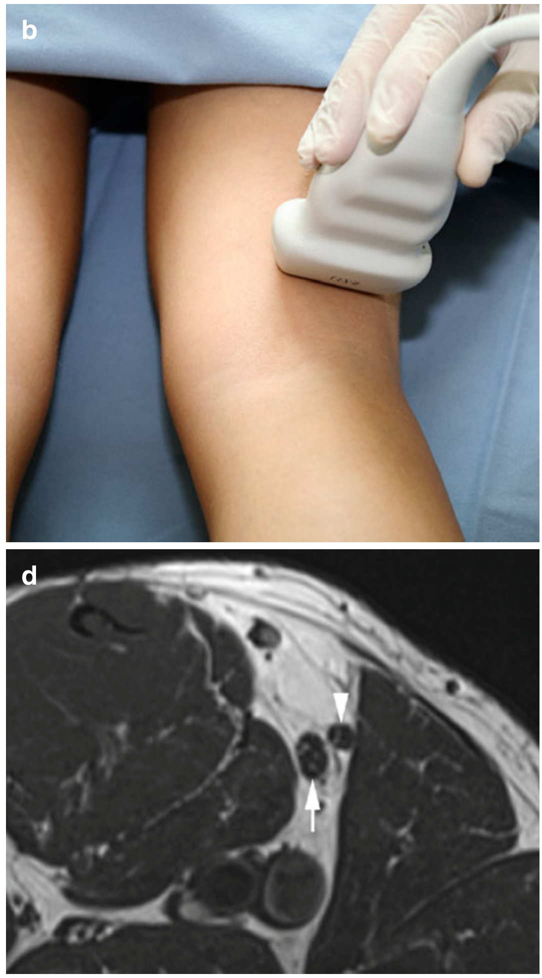

Fig. 5.10 (**a**) Anatomical cross section. (**b**) Transducer position. (**c**) Transverse sonogram. (**d**) Transverse T1-weighted MR image. Sciatic nerve with distinct differentiation of tibial (*small arrow*) and fibular portion (*arrowhead*) now each with an individual outer nerve sheath. *FBM* femoral biceps muscle, *StM* semitendinosus muscle, *SmM* semimembranosus muscle

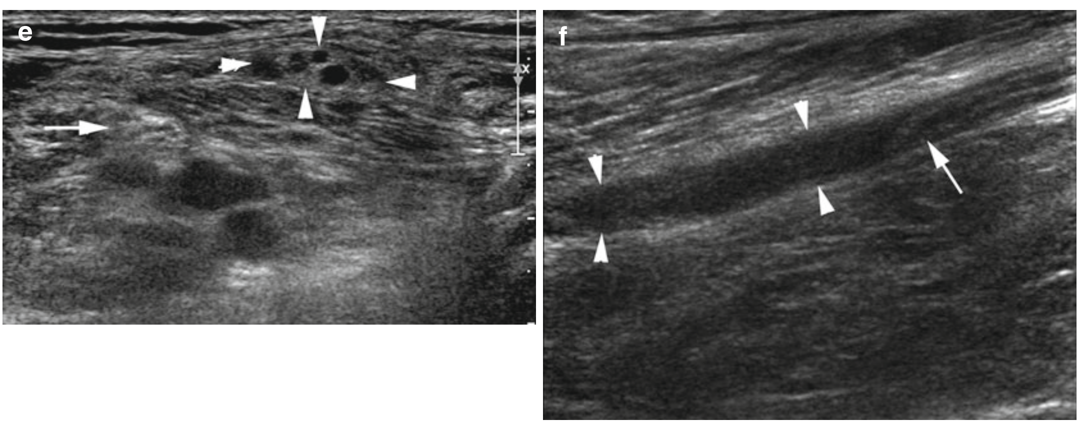

(e, f) Transverse **(e)** and longitudinal **(f)** sonogram of common fibular nerve at the inlet of the popliteal fossa in a patient with peroneal nerve palsy after dislocation of the knee. Note inconspicuous tibial nerve (*arrow* in **e**) and swollen fascicles of enlarged common fibular nerve (*arrowheads* in **e**)**.** On the longitudinal sonogram and empty epineural sleeve (*arrowheads* in **f**) and a retracted peroneal nerve stump (*arrow* in **f**) are seen

5.3.3 Popliteal Fossa (Sciatic Nerve Division Lower Level)

Fig. 5.11 (**a**) Anatomical cross section. (**b**) Transducer position. (**c**) Transverse sonogram. (**d**) Transverse T1-weighted MR image. Common tibial nerve (*small arrow*) and common fibular nerve (*arrowhead*). *StM* semitendinosus muscle, *SmM* semimembranosus muscle, *sH/lH* short head/long head of femoral biceps muscle

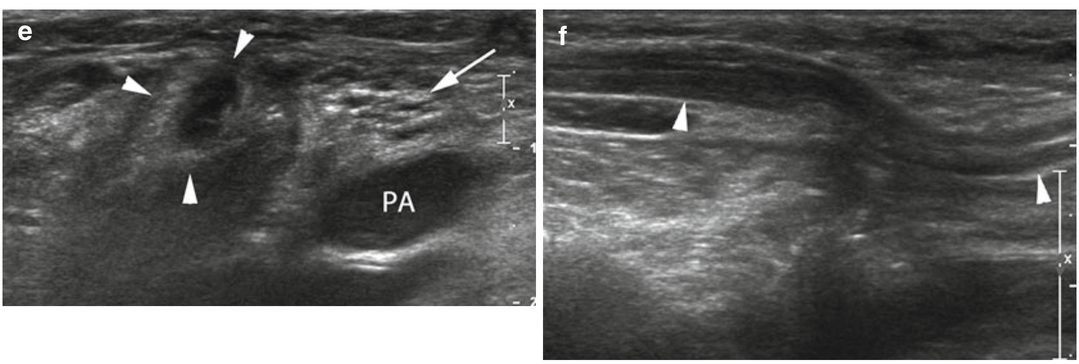

(**e**, **f**) Transverse (**e**) and longitudinal (**f**) sonogram through common fibular nerve in the lower aspect of the popliteal fossa. The nerve (*arrowheads*) is markedly thickened with hypoechoic edema proximal to the level of compression. The close-lying common tibial nerve (*arrow* in **e**) is normal. *PA* popliteal artery

5.3.4 Adductor Channel Inlet (Saphenous Nerve Middle Thigh)

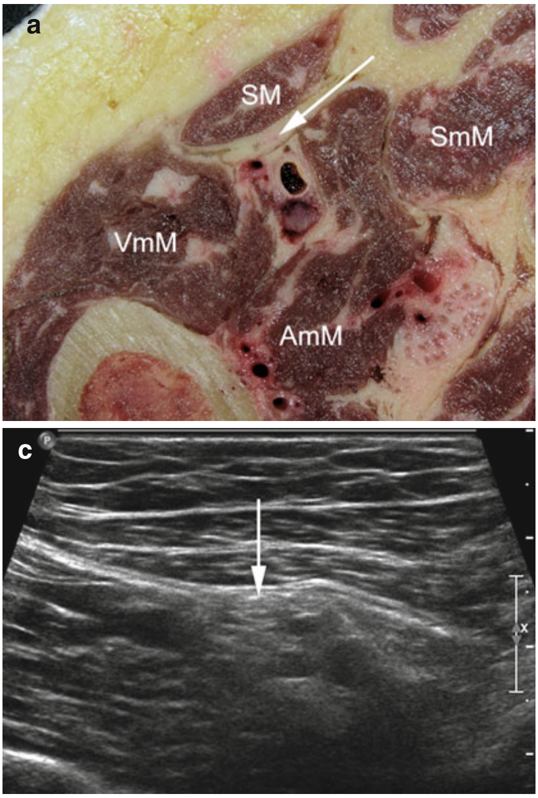

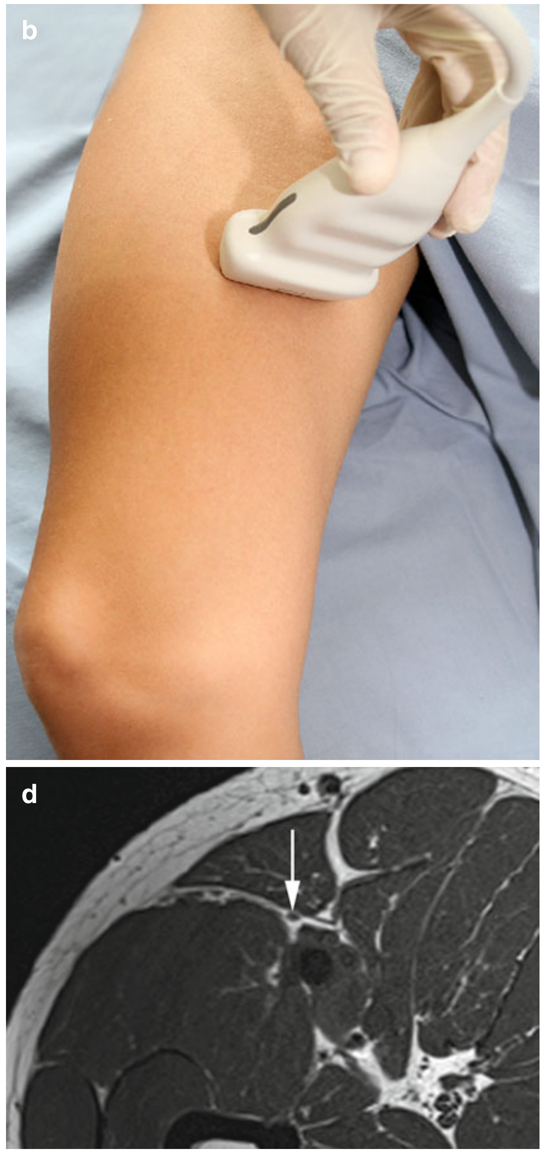

Fig. 5.12 (**a**) Anatomical cross section. (**b**) Transducer position. (**c**) Transverse sonogram. (**d**) Transverse T1-weighted MR image. Saphenous nerve (*long arrow*) close to sartorius muscle (*SM*) and femoral vessels. *SmM* semimembranosus muscle, *VmM* vastus medialis muscle, *AmM* adductor magnus muscle

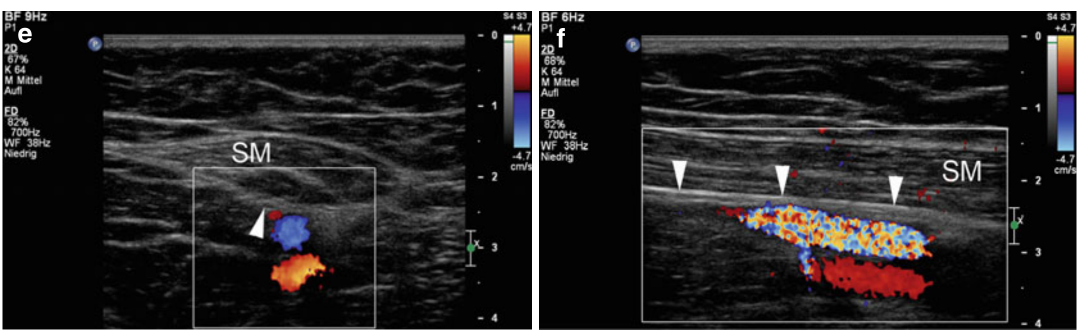

(**e**, **f**) Transverse (**e**) and longitudinal (**f**) color Doppler sonogram through adductor channel inlet, demonstrating the relationship of the saphenous nerve (*arrowheads*) to the femoral vessels. These may be a helpful landmark for identification of the nerve in this area. *SM* sartorius muscle

5.3.5 Adductor Channel Outlet (Saphenous Nerve)

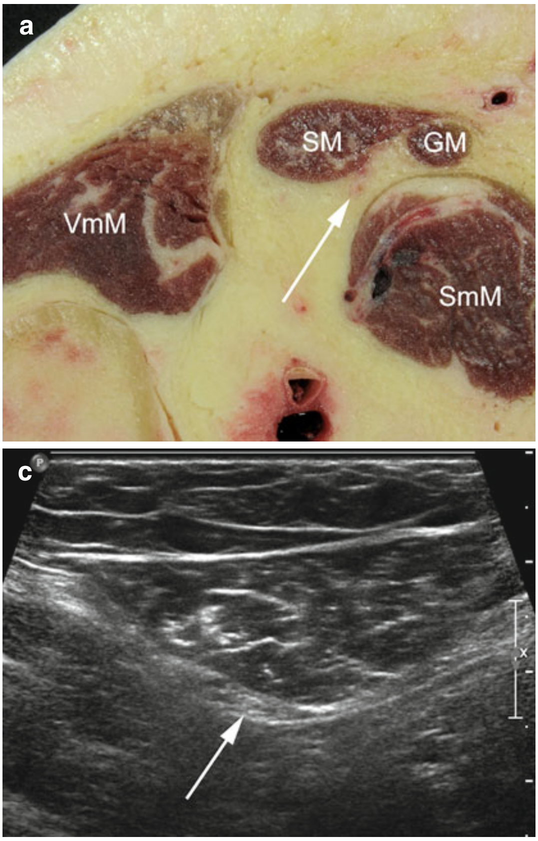

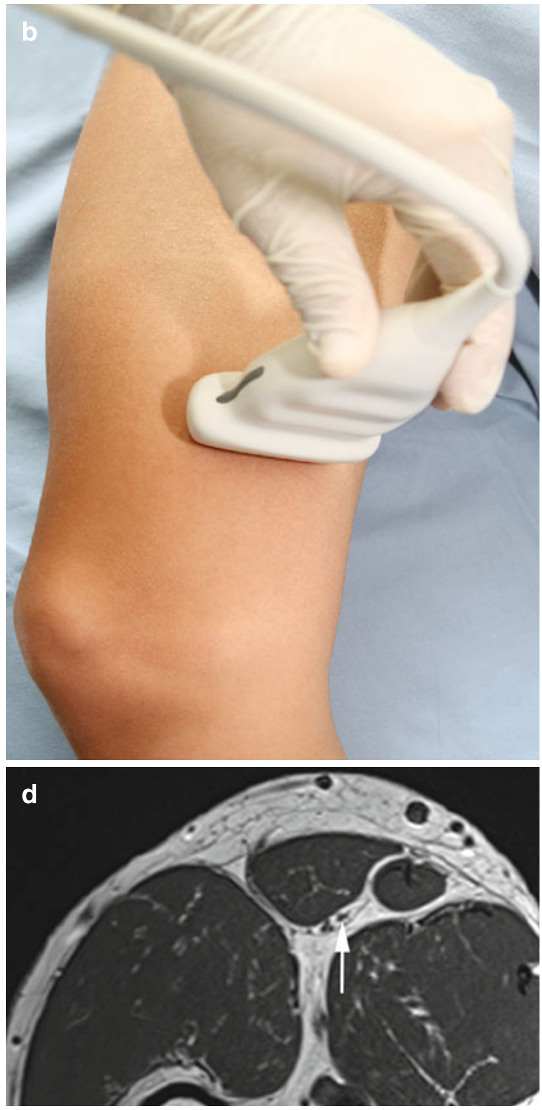

Fig. 5.13 (**a**) Anatomical cross section. (**b**) Transducer position. (**c**) Transverse sonogram. (**d**) Transverse T1-weighted MR image. Saphenous nerve (*long arrow*) close to sartorius muscle (*SM*). *GM* gracilis muscle, *SmM* semimembranosus muscle, *VmM* vastus medialis muscle

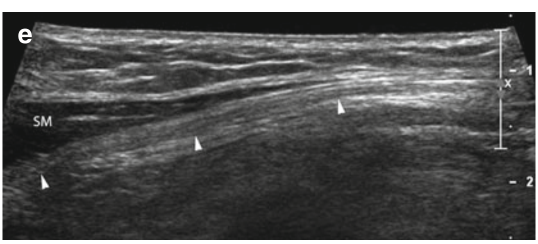

(**e**) Longitudinal sonogram of saphenous nerve (*arrowheads*) at the adductor channel outlet. *SM* sartorius muscle

5.3.6 Posteromedial Edge of Knee (Saphenous Nerve)

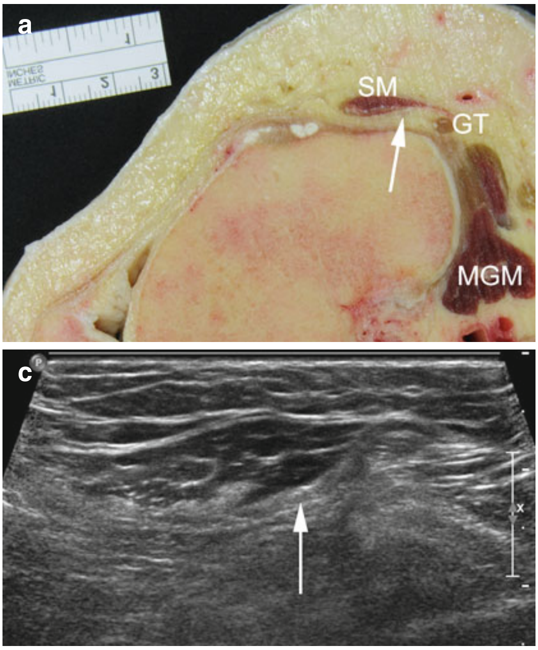

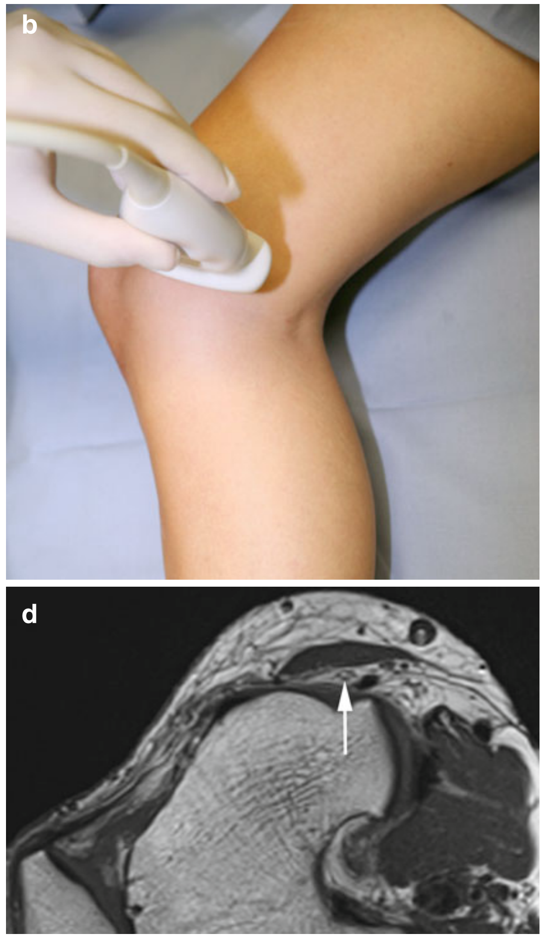

Fig. 5.14 (**a**) Anatomical cross section. (**b**) Transducer position. (**c**) Transverse sonogram. (**d**) Transverse T1-weighted MR image. Saphenous nerve (*long arrow*) close to sartorius muscle (*SM*). *GT* gracilis muscle tendon, *MGM* medial gastrocnemius muscle

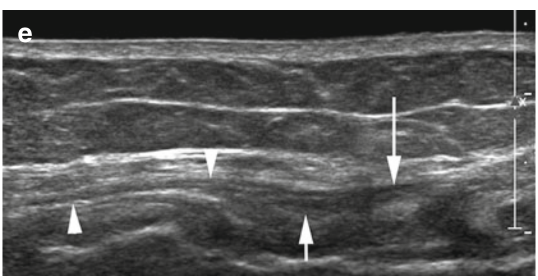

(**e**) Longitudinal sonogram through saphenous nerve (*arrowheads*) in the posteromedial knee region in a patient with saphenous nerve lesion after knee trauma. Note swelling of the nerve (*arrow*) above the level of rupture (*long arrow* proximal stump)

5.3.7 Posterior Tibial Plateau (Sural Nerve)

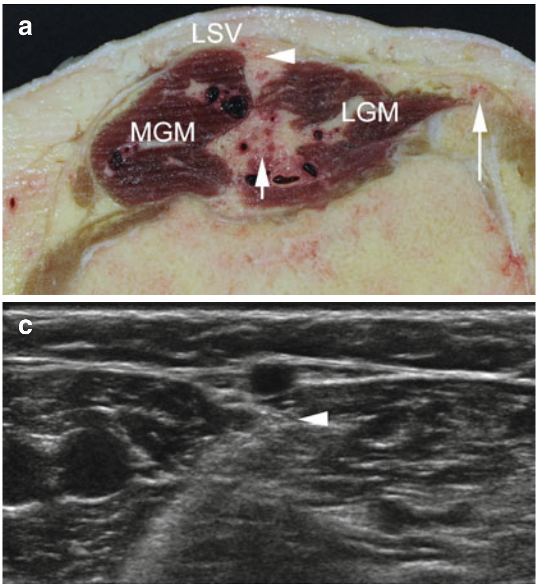

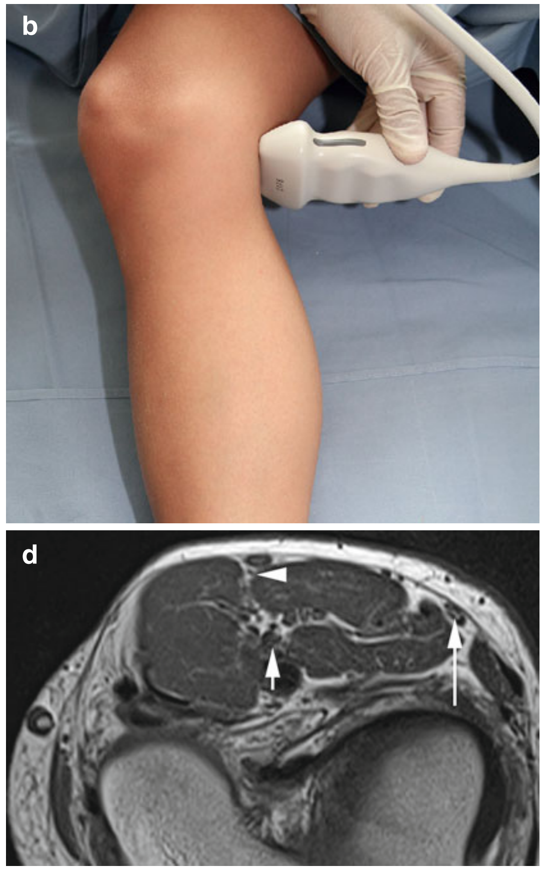

Fig. 5.15 (**a**) Anatomical cross section. (**b**) Transducer position. (**c**) Transverse sonogram. (**d**) Transverse T1-weighted MR image. Sural nerve (*arrowhead*) close to lesser saphenous vein (*LSV*). *MGM* medial gastrocnemius muscle, *LGM* lateral gastrocnemius muscle, tibial nerve (*short arrow*), common fibular nerve (*long arrow*)

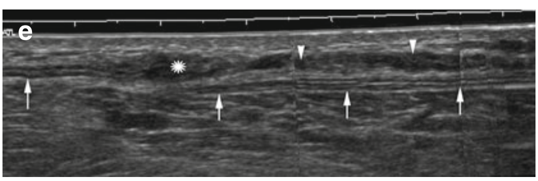

(**e**) Extended field of view sonogram of a sural nerve (*arrows*) in a patient with dissection of the nerve during stripping of the lesser saphenous vein. Note enlarged proximal nerve stump (*asterisk*) and longitudinal hematoma in the sheath of the lesser saphenous vein (*arrowheads*)

5.3.8 Nerves Below the Knee: Topographic Overview

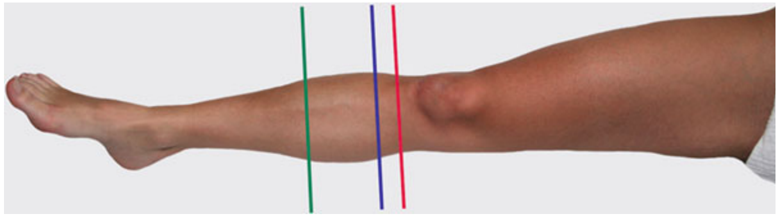

Fig. 5.16 General topographic overview of nerve anatomy below the knee and in the proximal shank. Localizer for anatomical cross sections (Fig. 5.8a–d). *Colored lines* correspond to level of cross sections

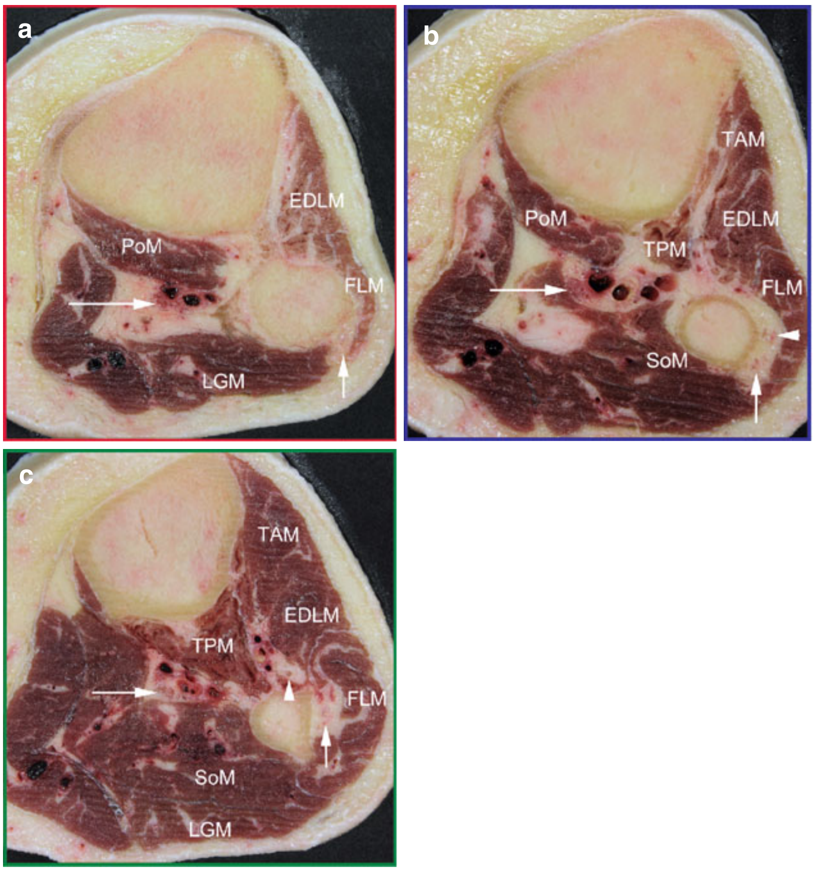

Fig. 5.17 (**a**) Anatomical cross section at the level of the fibular head (*red line* in Fig. 5.16). Common fibular nerve (*arrow*) positioned close to the cortical surface of fibular head (FH). Tibial nerve (*long arrow*) accompanies posterior tibial artery and veins. *EDLM* extensor digitorum longus muscle, *FLM* fibularis longus muscle, *PoM* popliteus muscle, *LGM* lateral gastrocnemius muscle. (**b**) Anatomical cross section at the level of the fibular neck/fibular nerve division (*blue line* in Fig. 5.16). Fibular nerve is already divided into posteriorly positioned superficial (*short arrow*) and anteriorly positioned deep branch (*arrowhead*). Tibial nerve (*long arrow*) runs close to posterior tibial artery and veins and popliteus muscle (*PoM*). *TAM* tibialis anterior muscle, *TPM* tibialis posterior muscle, *EDLM* extensor digitorum longus muscle, *FLM* fibularis longus muscle, *SoM* soleus muscle (**c**) Anatomical cross section through middle of shank (*green line* in Fig. 5.16). Deep fibular nerve (*arrowhead*) accompanies anterior tibial vessels coursing underneath tibialis anterior (*TAM*) and extensor digitorum longus muscle (*EDLM*). Superficial fibular nerve (*short arrow*) travels close to the fibular bone underneath the fibularis longus muscle. Tibial nerve (*long arrow*) runs close to posterior tibial artery and veins. *LGM* lateral gastrocnemius muscle, *SoM* soleus muscle

5.3.9 Posterolateral Edge of Knee (Common Fibular Nerve)

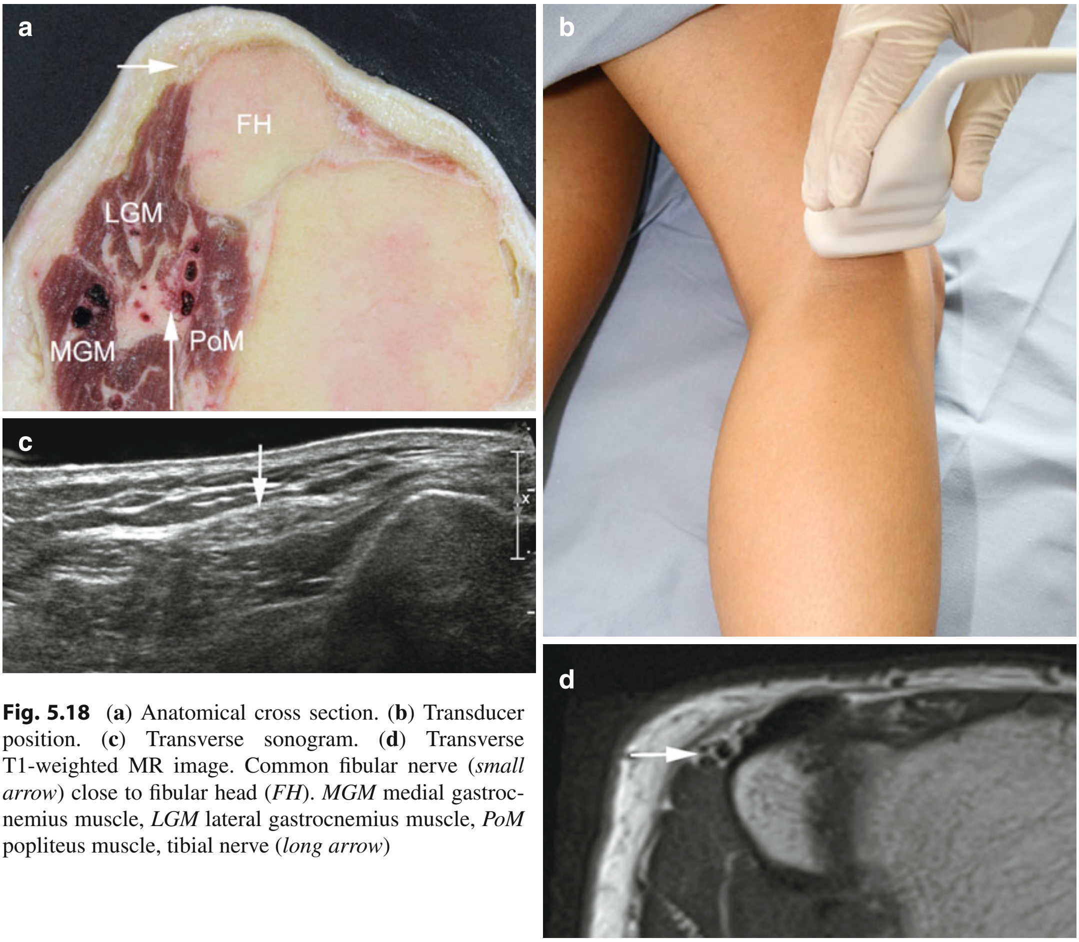

Fig. 5.18 (**a**) Anatomical cross section. (**b**) Transducer position. (**c**) Transverse sonogram. (**d**) Transverse T1-weighted MR image. Common fibular nerve (*small arrow*) close to fibular head (*FH*). *MGM* medial gastrocnemius muscle, *LGM* lateral gastrocnemius muscle, *PoM* popliteus muscle, tibial nerve (*long arrow*)

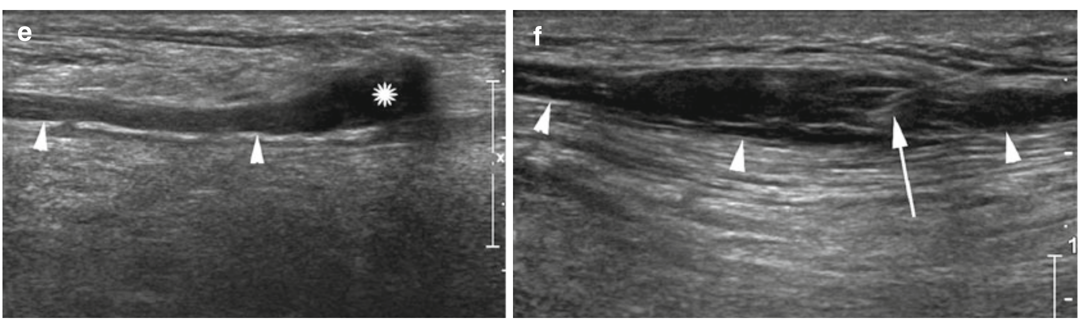

(**e**, **f**) Longitudinal sonograms through common fibular nerve (*arrowheads*) in a patient with phantom limb pain after traumatic amputation of the shank in a road accident. (**e**) A small terminal type neuroma (*asterisk*) is seen in the severed fibular nerve. (**f**) Injection of the nerve with phenolic solution for pain treatment shortly cranial to the neuroma under ultrasound guidance (*arrow* needle tip). Note swelling of nerve due to the injectant

5.3.10 Fibular Neck (Common Fibular Nerve)

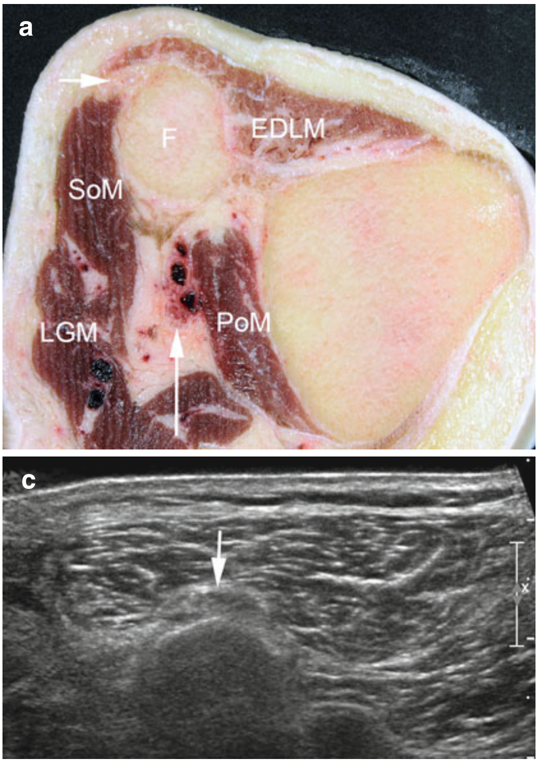

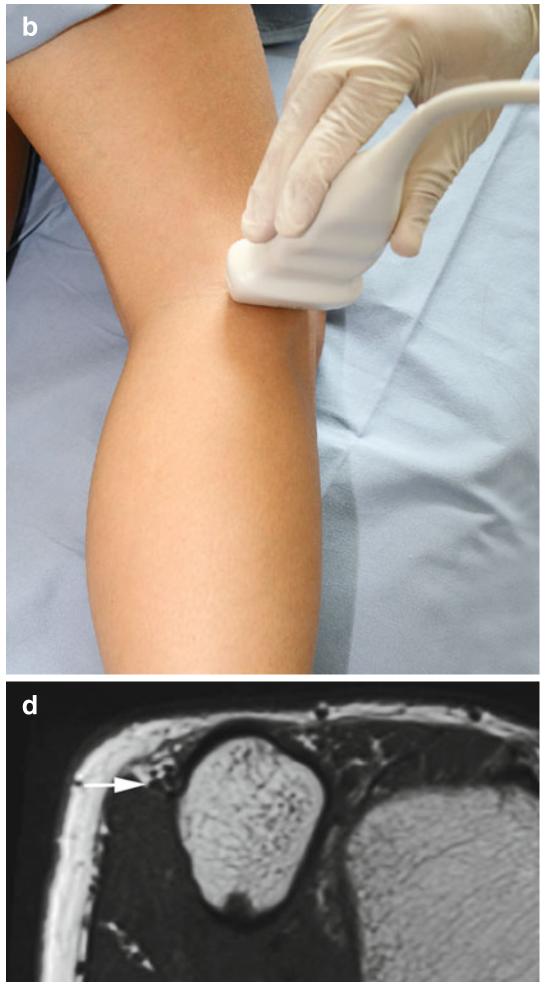

Fig. 5.19 (**a**) Anatomical cross section. (**b**) Transducer position. (**c**) Transverse sonogram. (**d**) Transverse T1-weighted MR image. Common fibular nerve (*small arrow*) close to fibula (*F*). *SoM* soleus muscle, *LGM* lateral gastrocnemius muscle, *PoM* popliteus muscle, *EDLM* extensor digitorum longus muscle, tibial nerve (*long arrow*)

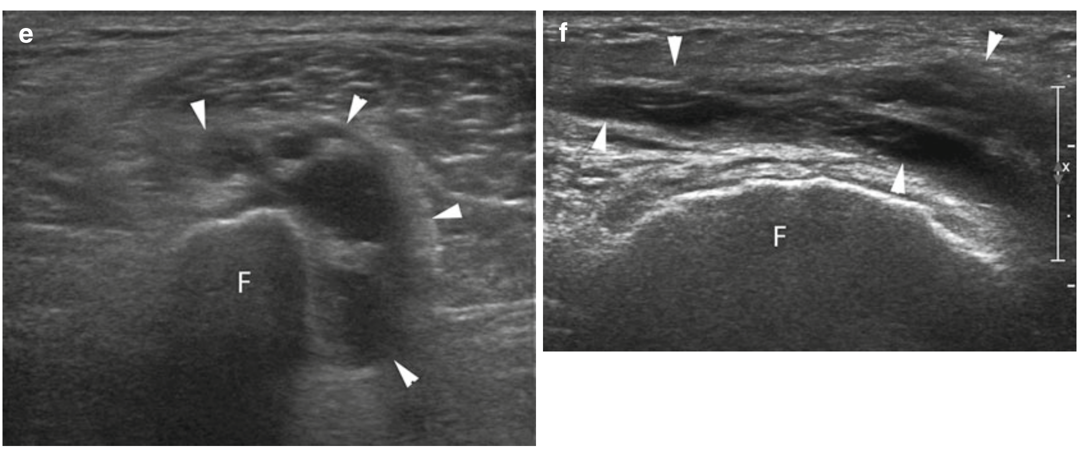

(**e**, **f**) Transverse (**e**) and longitudinal (**f**) sonogram of common fibular nerve at the level of the fibular neck. On the transverse sonogram (**e**) the fibular nerve (*arrowheads*) appears markedly enlarged by multiple internal cyst-like lesions. On the longitudinal sonogram (*F*) the nerve's outer border is hardly appreciated (*arrowheads*), and longitudinal internal ganglion is seen

5.3.11 Fibular Neck (Fibular Nerve Division)

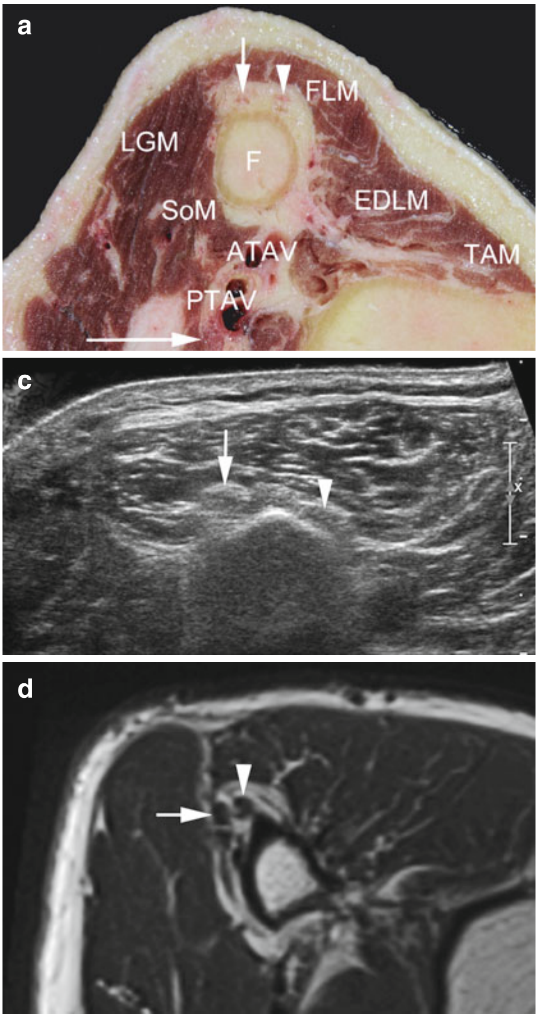

Fig. 5.20 (**a**) Anatomical cross section. (**b**) Transducer position. (**c**) Transverse sonogram. (**d**) Transverse T1-weighted MR image. Superficial fibular nerve (*small arrow*) and deep fibular nerve branch (*arrowhead*) close to fibula (*F*) and underneath fibularis longus muscle (*FLM*). *LGM* lateral gastrocnemius muscle, *SoM* soleus muscle, *EDLM* extensor digitorum longus muscle, *TAM* tibialis anterior muscle, *ATAV* anterior tibial artery and vein, *PTAV* posterior tibial artery and vein, tibial nerve (*long arrow*)

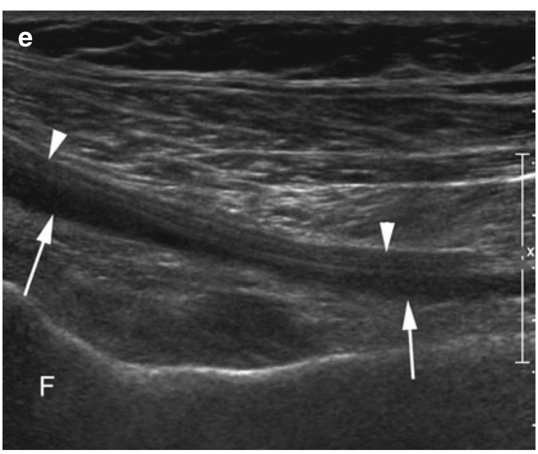

(**e**) Longitudinal sonogram through the proximal superficial peroneal nerve (*arrowheads*) at the level of the peroneal nerve division in a patient after knee trauma with peroneal nerve palsy. The nerve is slightly swollen and hypoechoic but continuous. Close to the nerve a fluid collection = hematoma is seen (*arrows*). *F* proximal fibula

5.3.12 Proximal Shank Lateral Compartment (Superficial Fibular Nerve)

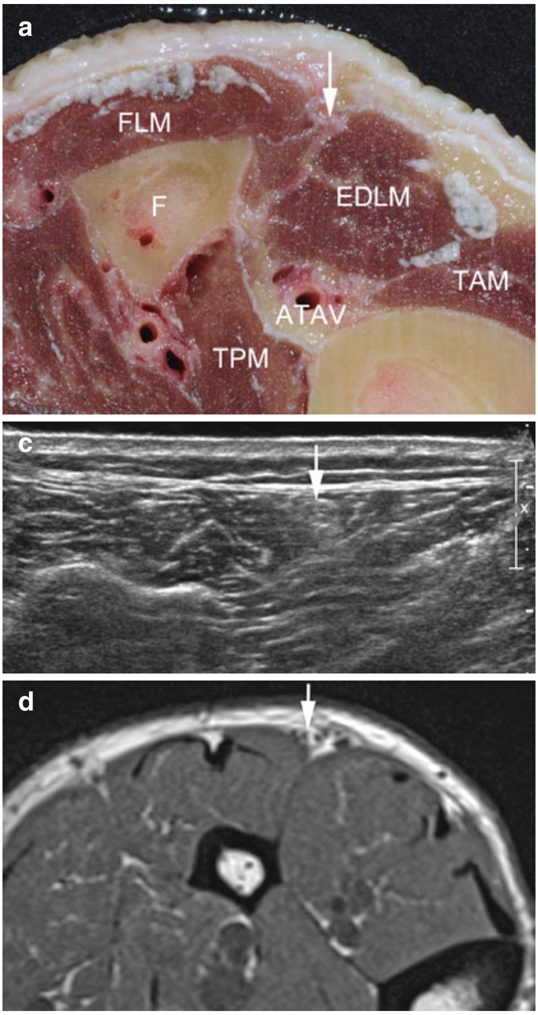

Fig. 5.21 (**a**) Anatomical cross section. (**b**) Transducer position. (**c**) Transverse sonogram. (**d**) Transverse T1-weighted MR image. Superficial fibular nerve (*arrow*) positioned between fibularis longus muscle (*FLM*) and extensor digitorum longus muscle (*EDLM*). *TAM* tibialis anterior muscle, *ATAV* anterior tibial artery and vein, *TPM* tibialis posterior muscle, *F* fibula

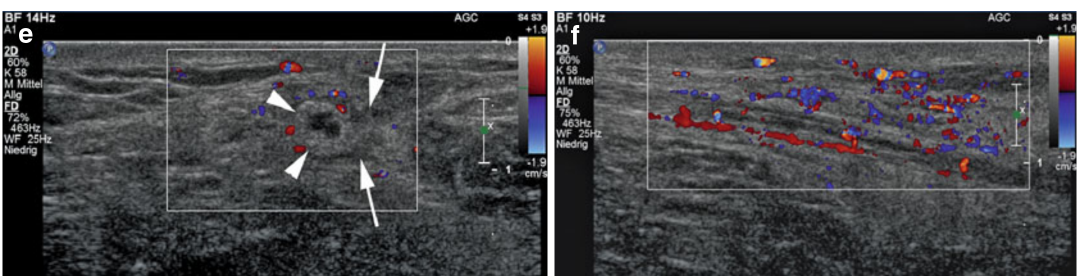

(**e**, **f**) Transverse (**e**) and longitudinal (**f**) color Doppler sonogram through proximal superficial fibular nerve in a patient with soft tissue trauma and local infection. The peroneal nerve is markedly thickened with echoic outer epineurium (*arrowheads*) and surrounding fluid collection (*arrows*). Intense inflammatory hypervascularization is evident in the longitudinal sonogram

5.3.13 Proximal Shank Medial Compartment (Tibial Nerve)

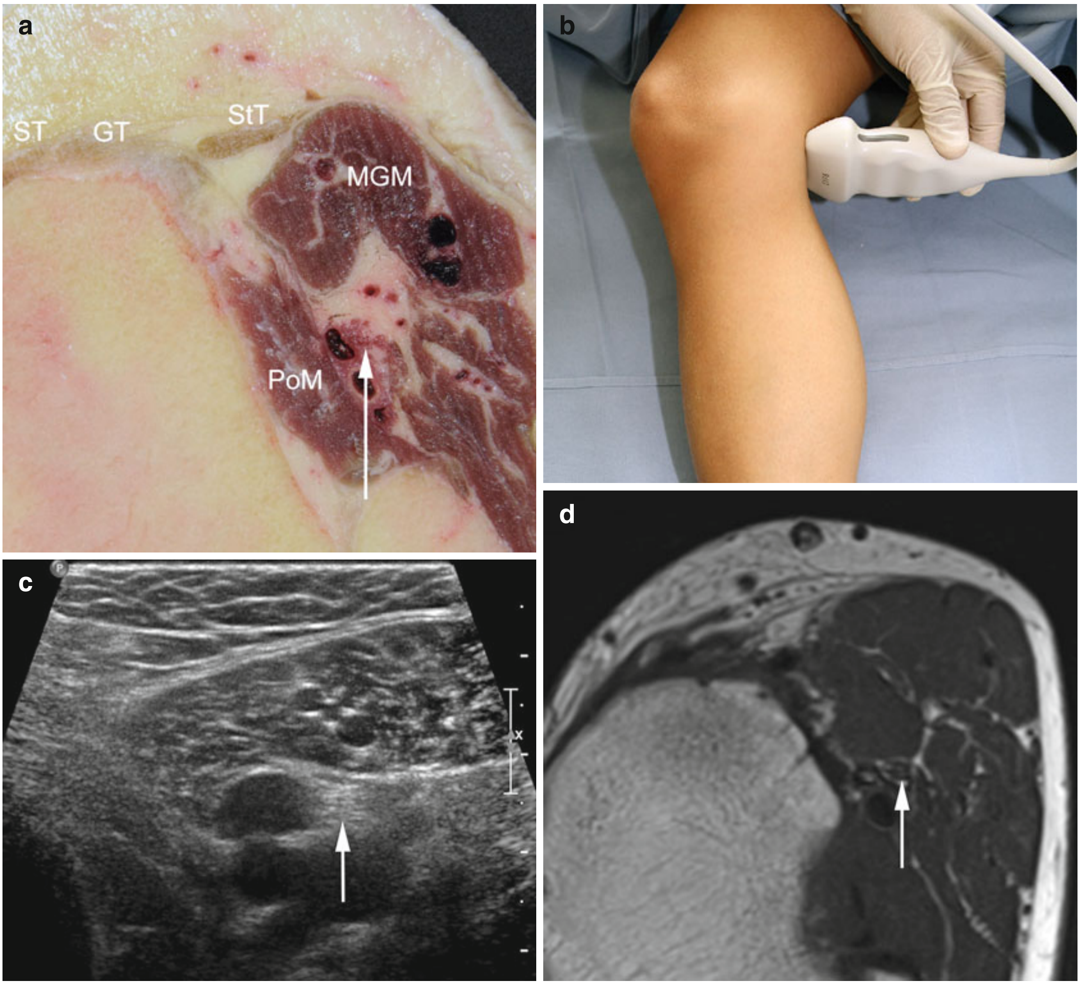

Fig. 5.22 (**a**) Anatomical cross section. (**b**) Transducer position. (**c**) Transverse sonogram. (**d**) Transverse T1-weighted MR image. Tibial nerve (*arrow*) adjacent to posterior tibial vessels and popliteus muscle (*PoM*). *MGM* medial gastrocnemius muscle, *ST* sartorius muscle tendon, *GT* gracilis muscle tendon, *StT* semitendinosus muscle tendon

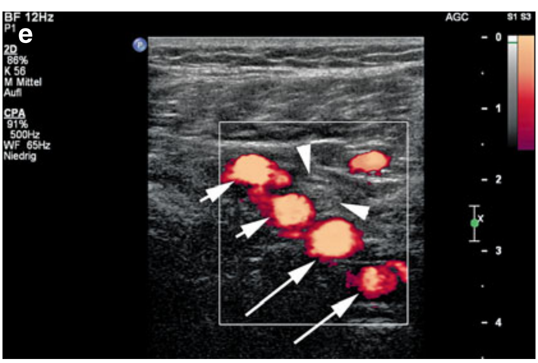

(**e**) Transverse power Doppler sonogram through the proximal shank demonstrating the intimate relationship of the tibial nerve (*arrowheads*) to the posterior tibial (*small arrow*) and anterior tibial (*long arrow*) vessels

5.3.14 Medial Third of Shank Medial Compartment (Tibial Nerve)

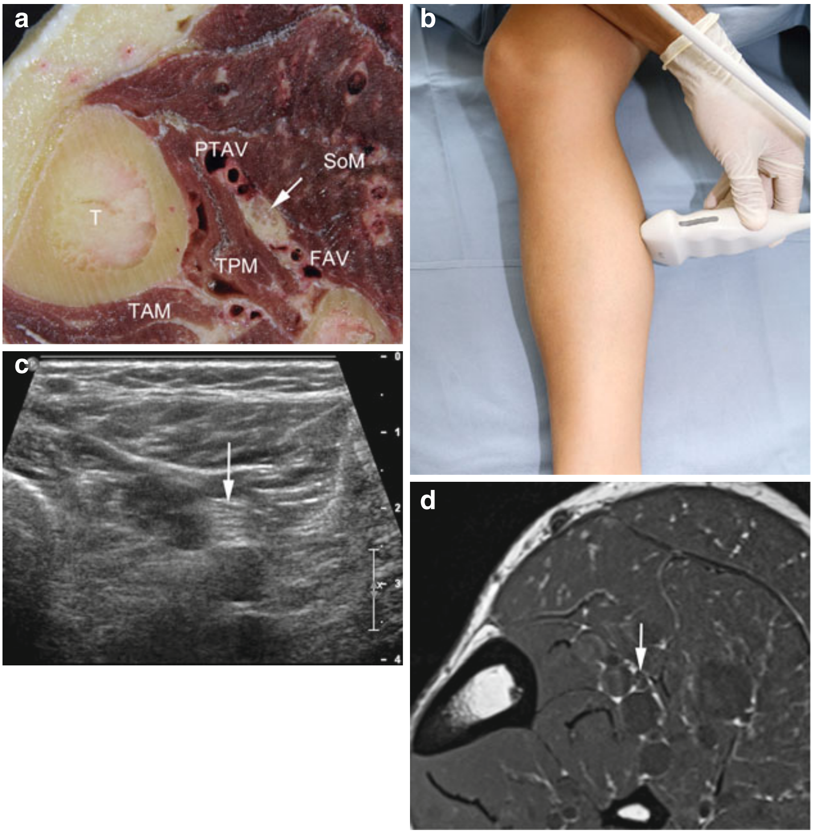

Fig. 5.23 (**a**) Anatomical cross section. (**b**) Transducer position. (**c**) Transverse sonogram. (**d**) Transverse T1-weighted MR image. Tibial nerve (*arrow*) located between posterior tibial vessels (*PTAV*) and fibular vessels (*FAV*). *SoM* soleus muscle, *TPM* tibialis posterior muscle, *TAM* tibialis anterior muscle, *T* tibia

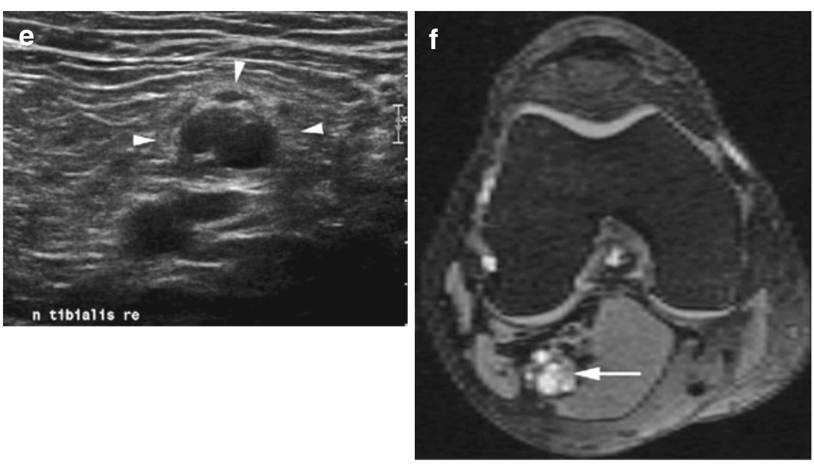

(**e**, **f**) Transverse sonogram (**e**) and corresponding STIR MR image (**f**): the common tibial nerve is markedly enlarged (*arrowheads* in **e**) due to multiple small intraneural cysts. Hypoechoic intraneural ganglia (*arrow* in **f**) are confirmed in the fat-saturated MR image

5.3.15 Nerves Around the Ankle: Topographic Overview

Fig. 5.24 General topographic overview of nerve anatomy around the ankle. Localizer for anatomical cross sections (Fig. 5.25a–d). *Colored lines* correspond to level of cross sections

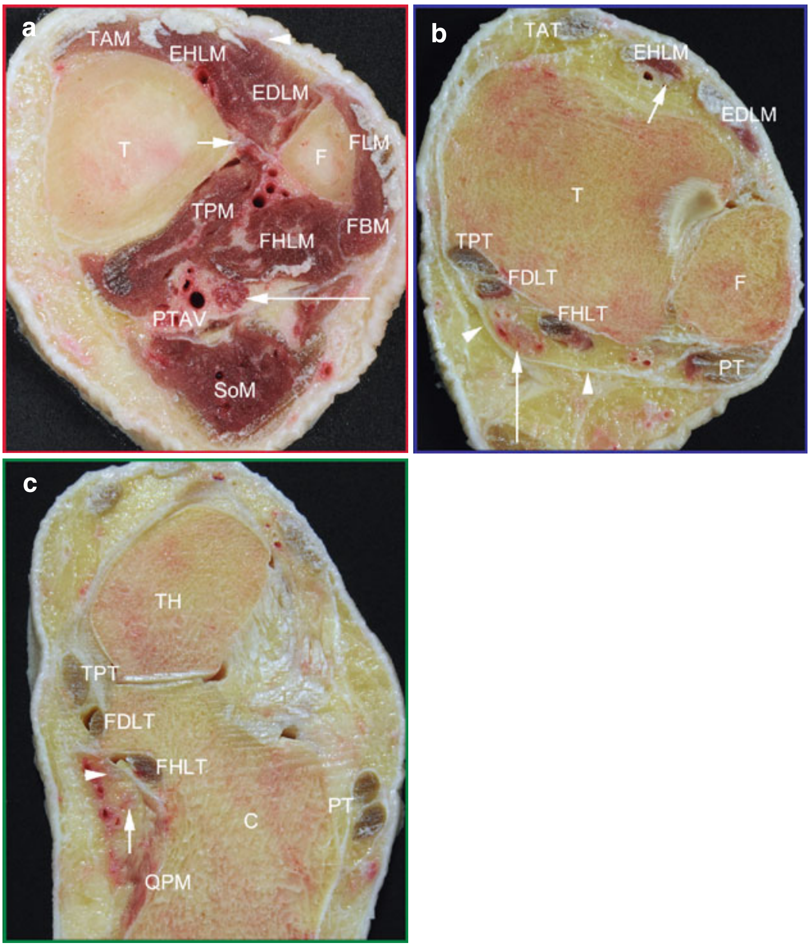

Fig. 5.25 (**a**) Anatomical cross section at the level of the interosseus membrane (*red line* in Fig. 5.24). Tibial nerve (*long arrow*) close to posterior tibial vessels (*PTAV*). Superficial fibular nerve (*arrowhead*) running in subcutaneous fat and deep fibular nerve (*small arrow*) close to edge of tibia. *TAM* tibialis anterior muscle, *EDLM* extensor digitorum longus muscle, *EHLM* extensor hallucis longus muscle, *FLM* fibularis longus muscle, *FBM* fibularis brevis muscle, *FHLM* flexor hallucis longus muscle, *TPM* tibialis posterior muscle, *SoM* soleus muscle, *T* tibia, *F* fibula. (**b**) Anatomical cross section at the level of the lateral malleolus (*blue line* in Fig. 5.24). Tibial nerve (*long arrow*) close to flexor tendon retinaculum (*arrowheads*). Deep fibular nerve (*small arrow*) underneath extensor hallucis longus muscle (*EHLM*). *TAT* tibialis anterior muscle tendon, *EDLM* extensor digitorum longus muscle, *PT* peroneal tendons, *FHLT* flexor hallucis longus muscle tendon, *FDLT* flexor digitorum longus muscle tendon, *TPT* tibialis posterior muscle tendon (**c**) Anatomical cross section through talus head (*green line* in Fig. 5.24). Division of tibial nerve into medial (*arrowhead*) and lateral (*small arrow*) plantar nerve. *TH* head of talus, *C* calcaneus, *TPT* tibialis posterior muscle tendon, *FDLT* flexor digitorum longus muscle tendon, *FHLT* flexor hallucis longus muscle tendon, *PT* peroneal tendons, *QPM* quadratus plantae muscle

5.3.16 Distal Third of Shank Lateral Compartment (Superficial Fibular Nerve)

Fig. 5.26 (**a**) Anatomical cross section. (**b**) Transducer position. (**c**) Transverse sonogram. (**d**) Transverse T1-weighted MR image. Superficial fibular nerve (*arrow*) located between fibularis longus muscle (*FLM*) and extensor digitorum longus muscle (*EDLM*). *EHLM* extensor hallucis longus muscle, *TAM* tibialis anterior muscle, *TPM* tibialis posterior muscle, *FBM* fibularis brevis muscle, *T* tibia, *F* fibula. Deep fibular nerve = *arrowhead*

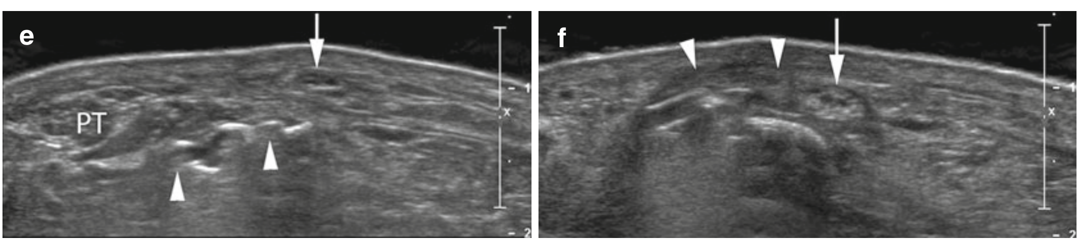

(**e**, **f**) Transverse sonograms through superficial peroneal nerve in a patient with peroneal nerve palsy after surgical fixation of a distal fibular fracture. At the level of the peroneal tendons (**e**) the nerve (*arrow*) looks normal. Note artifact by plate and screws (*arrowheads* in **e**) *PT* peroneal tendons. At a short distance below that level, the nerve (*arrow*) shows a thickened epineurium and compression/traction by a close-lying scar (*arrowheads*)

5.3.17 Tarsal Tunnel (Tibial Nerve)

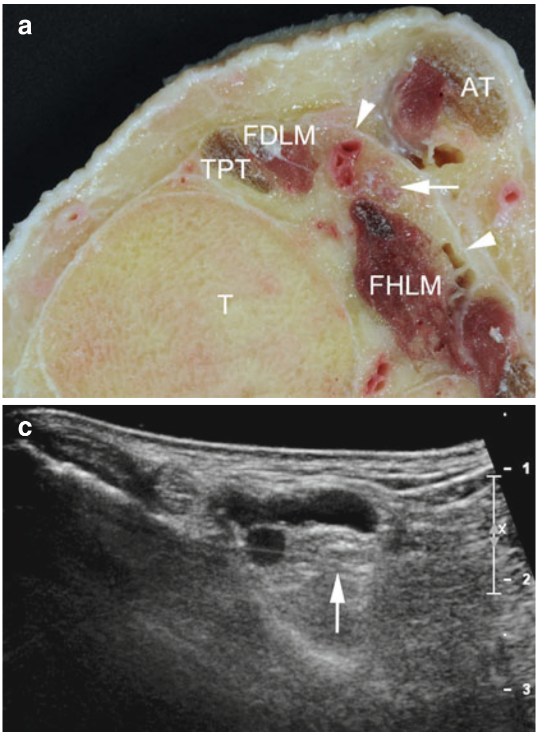

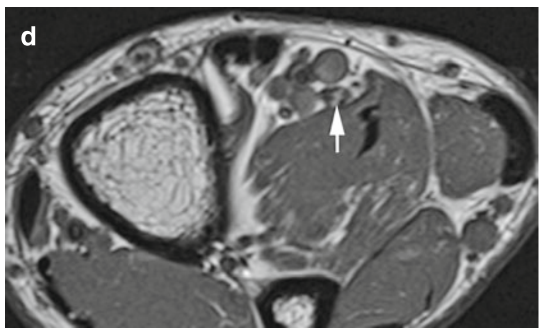

Fig. 5.27 (**a**) Anatomical cross section. (**b**) Transducer position. (**c**) Transverse sonogram. (**d**) Transverse T1-weighted MR image. Common tibial nerve (*arrow*) inside tarsal tunnel bordered superficially by flexor retinaculum (*arrowheads*). *TPT* tibialis posterior muscle tendon, *FDLM* flexor digitorum longus muscle, *FHLM* flexor hallucis longus muscle, *AT* Achilles tendon, *T* tibia

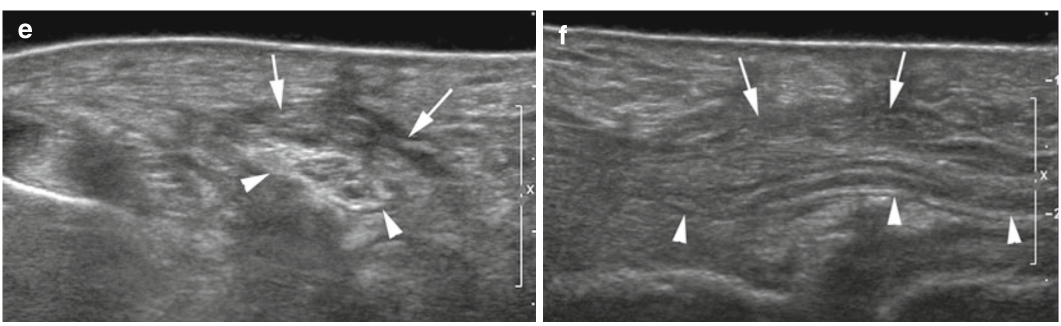

(**e**, **f**) Transverse (**e**) and longitudinal (**f**) sonogram of the tibial nerve at the level of the tarsal tunnel in a patient with poor postoperative outcome after tarsal tunnel release operation for tarsal tunnel syndrome. The nerve (*arrowheads*) is swollen with thickened fascicles and encased by a tight fibrous scar (*arrows*)

5.3.18 Tarsal Tunnel Outlet (Tibial Nerve Division)

Fig. 5.28 (**a**) Anatomical cross section. (**b**) Transducer position. (**c**) Transverse sonogram. (**d**) Transverse T1-weighted MR image. Division of tibial nerve into medial (*small arrow*) and lateral (*long arrow*) plantar nerve. *TPT* tibialis posterior muscle tendon, *FDLT* flexor digitorum longus muscle tendon, *FHLT* flexor hallucis longus muscle tendon, *MM* medial malleolus, (*arrowhead*) distal edge of flexor retinaculum

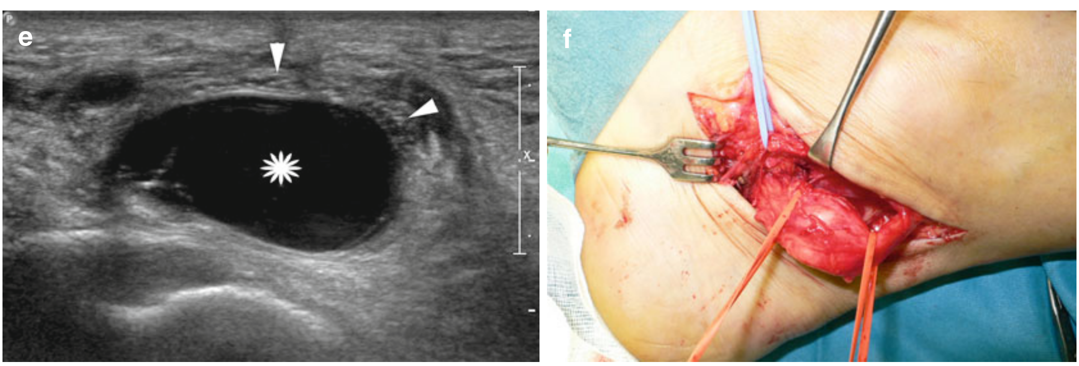

(**e**) Transverse sonogram through the tibial nerve division showing compression/dislocation of the tibial nerve (*arrowheads*) by a large fluid-filled cystic lesion (*asterisk*). (**f**) Surgery confirmed the large intraneural ganglion inside the tibial nerve immediately proximal to its division diagnosed by sonography

5.3.19 Medial Malleolar Compartment (Tibial Nerve Division)

Fig. 5.29 (**a**) Anatomical cross section. (**b**) Transducer position. (**c**) Transverse sonogram. (**d**) Transverse T1-weighted MR image. Medial (*small arrow*) and lateral (*long arrow*) plantar nerve. *TPT* tibialis posterior muscle tendon, *FDLT* flexor digitorum longus muscle tendon, *FHLT* flexor hallucis longus muscle tendon, *QPM* quadratus plantae muscle, *TH* talar head

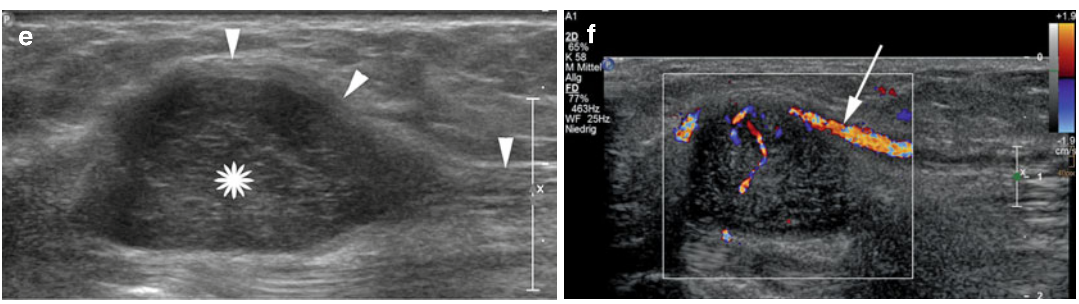

(**e**, **f**) Longitudinal sonogram (**e**) and color Doppler sonogram (**f**) in a patient with a schwannoma of the tibial nerve at the level of the tibial nerve division. On the sonogram, a large mass (*asterisk*) with mixed hypoechoic structure is seen superficially connected to the medial plantar nerve (*arrowheads*). On the color Doppler sonogram (slightly offset to **e**), close proximity of the lesion to the medial plantar artery (*arrow*) and internal vascularization typical for schwannoma are seen

Bibliography

Fornage BD (1988) Peripheral nerves of the extremities: imaging with US. Radiology 167(1):179–182

Gruber H, Peer S, Kovacs P, Marth R, Bodner G (2003) The ultrasonographic appearance of the femoral nerve and cases of iatrogenic impairment. J Ultrasound Med 22(2):163–172

Gruber H, Peer S, Meirer R, Bodner G (2005) Peroneal nerve palsy associated with knee luxation: evaluation by sonography–initial experiences. AJR Am J Roentgenol 185(5):1119–1125

Kopf H, Loizides A, Mostbeck GH, Gruber H (2011) Diagnostic sonography of peripheral nerves: indications, examination techniques and pathological findings. Ultraschall Med 32(3):242–263

Martinoli C, Serafini G, Bianchi S et al (1996) Ultrasonography of peripheral nerves. J Peripher Nerv Syst 1(3):169–178

Netter FH (2010) Atlas of human anatomy, professional edition, 5th edn. Saunders, UK

Peer S, Kovacs P, Harpf C, Bodner G (2002) High-resolution sonography of lower extremity peripheral nerves: anatomic correlation and spectrum of disease. J Ultrasound Med 21(3):315–322

Prakash, Bhardwaj AK, Devi MN, Sridevi NS, Rao PK, Singh G (2010) Sciatic nerve division: a cadaver study in the Indian population and review of the literature. Singapore Med J 51(9):721–773

Silvestri E, Martinoli C, Derchi LE et al (1995) Echotexture of peripheral nerves: correlation between US and histologic findings and criteria to differentiate tendons. Radiology 197(1):291–296

Von Lanz T, Wachsmuth W (1972) Praktische Anatomie, 4th edn. Springer, Berlin/Heidelberg/New York

Walker FO, Cartwright MS, Wiesler ER, Caress J (2004) Ultrasound of nerve and muscle. Clin Neurophysiol 115(3):495–507

6 Nerves in the Trunk and Abdominal Wall

Alexander Loizides, Siegfried Peer,
Werner Judmaier, and Erich Brenner

Contents

A. Loizides (✉) • W. Judmaier
Department of Radiology, Innsbruck Medical University,
Anichstrasse 35, Innsbruck, 6020, Tyrol, Austria
e-mail: alexander.loizides@i-med.ac.at;
werner.judmaier@i-med.ac.at

S. Peer
CTI GesmbH,
Klostergasse 4, 6020 Innsbruck, Tyrol, Austria
e-mail: info@siegfried-peer.at

E. Brenner
Division for Clinical and Functional Anatomy,
Innsbruck Medical University,
Müllerstrasse 59, 6020 Innsbruck, Tyrol, Austria
e-mail: erich.brenner@i-med.ac.at

6.1 Introduction

One of the major advantages of sonography compared to other imaging modalities of peripheral nerves beyond availability and cost-effectiveness is its ability to obtain images in any orientation along the course of a nerve. However, a profound anatomical knowledge of neural topography and especially of crucial landmarks is mandatory for the ultrasonographic (US) localization and assessment of these structures. Compared to extremity nerves pathologies of the nerves in the trunk, abdominal wall and pelvis are rare, and therefore, the assignment of patients for diagnostic US of these nerves is uncommon. Nevertheless procedures for pain management or regional anesthesia, such as ilioinguinal and iliohypogastric nerve blocks for inguinal surgery in children, are often performed under US guidance.

The motor thoracodorsal nerve arises from the brachial plexus and innervates the latissimus dorsi muscle. It includes fibers from the posterior divisions of all three trunks of the brachial plexus. The nerve derives its fibers from the sixth, seventh, and eighth cervical nerve. It follows the course of the subscapular artery, along the

S. Peer, H. Gruber (eds.), *Atlas of Peripheral Nerve Ultrasound*,
DOI 10.1007/978-3-642-25594-6_6,

posterior wall of the axilla to the latissimus dorsi muscle. Isolated injury of the thoracodorsal nerve is very rare, and a deficiency of the latissimus dorsi muscle can be more or less compensated by the pectoralis and major teres muscle. The nerve is easiest identified by sonography in the posterior axillary fold using the subscapular artery (the most prominent branch exiting from the axillary artery) as a landmark.

The intercostal nerves are the ventral divisions of the thoracic spinal nerves of the segments Th1–Th11. Each nerve is connected with the adjoining ganglion of the sympathetic trunk by a ramus communicans. The intercostal nerves spread to the thoracic pleura and abdominal peritoneum and differ from the anterior divisions of the other spinal nerves in that each pursues an independent course without plexus formation. The first two nerves supply fibers to the upper limb in addition to their own nerves, the next four are limited in their distribution to the chest wall, and the lower five supply the walls of the thorax and abdomen. The seventh intercostal nerve terminates at the xiphoid process. The tenth intercostal nerve terminates at the umbilicus. The 12th (subcostal) thoracic spreads to the abdominal wall and groin.

The ilioinguinal and iliohypogastric nerves are small branches of the first lumbar nerve (L1): the larger iliohypogastric nerve is the superior branch of the spinal nerve L1 also receiving fibers from the 12th thoracic nerve. The inferior branch of L1 is the ilioinguinal nerve. This nerve emerges from the lateral border of the major psoas muscle just inferior to the iliohypogastric nerve and passes obliquely across the quadratus lumborum and iliac muscle. Then it perforates the transverse abdominal muscle near the anterior part of the iliac crest and communicates with the iliohypogastric nerve between the transverse and the inner oblique muscle. The ilioinguinal nerve then pierces the inner oblique muscle and innervates it to accompany the spermatic cord through the superficial inguinal ring. Its fibers are then distributed to the skin of the upper and medial part of the thigh. Additionally nerve branches run to the skin over the root of the penis and superior scrotum in males and to the skin covering the mons pubis and labia in females, respectively. The iliohypogastric nerve divides into a lateral and an anterior cutaneous branch after piercing the inner oblique muscle. The lateral cutaneous branch pierces the inner and outer oblique muscle immediately above the iliac crest and spreads to the skin of the gluteal region. The anterior cutaneous branch runs between the inner oblique and transverse muscle and perforates the aponeurosis of the external oblique muscle about 2.5 cm above the subcutaneous inguinal ring to be distributed to the skin of the hypogastric region.

By US the ilioinguinal and iliohypogastric nerve can clearly be identified about 5 cm cranial to the anterior superior iliac spine between the inner oblique and transverse muscle using a scan plane perpendicular to the abdominal muscles.

The lateral femoral cutaneous nerve (LFCN) arises from the dorsal divisions of the second (L2) and third (L3) lumbar nerves. It emerges from the lateral border of the psoas major muscle and crosses the iliacus muscle obliquely, running toward the anterior superior iliac spine. It then passes below the inguinal ligament and above the sartorius muscle into the lateral thigh region, where it divides into an anterior and a posterior branch. In rare cases, the nerve passes through a slit of the inguinal ligament or even through a small channel of the iliac bone. The anterior branch becomes superficial about 10 cm below the inguinal ligament and divides into branches which are distributed to the skin of the anterior and lateral parts of the thigh. The posterior branch pierces the fascia lata and subdivides into filaments which pass backward across the lateral and posterior surfaces of the thigh to supply the skin over the greater trochanter to the middle of the thigh. An irritation of the LFCN can cause pain, tingling, numbness, and paresthesia of the anterolateral thigh. This classic sensory mononeuropathy is called meralgia paresthetica (nocturna). With US the nerve can be localized using defined anatomical landmarks: thereof the most important is the tendinous origin of the sartorius muscle. Typically the nerve lies immediately ventral of the sartorius muscle about 5 cm caudal and 0.15 cm medial of the anterior superior iliac spine. When meralgia paresthetica is diagnosed

clinically, a US-guided therapeutic injection can be performed using a lateral or a medial needle path.

The obturator nerve arises from the ventral divisions of the second (L2), third (L3), and fourth (L4) lumbar nerves. It is responsible for the sensory innervation of the skin of the medial aspect of the thigh and the motor innervation of the adductor muscles including the pectineus muscle. The obturator nerve descends through the psoas major muscle and passes behind the common iliac arteries lateral of the internal iliac artery and usually runs ventrally to the obturator vessels to the upper part of the obturator foramen. Here it enters the thigh via the obturator channel and divides into an anterior and a posterior branch: the anterior branch leaves the pelvis ventrally to the external obturator muscle and descends ventrally to the small adductor and posterior to the pectineus and long adductor muscle. The posterior branch pierces the anterior part of the external obturator muscle to supply it. The residual nerve then runs between the small and large adductor muscle, where it divides into numerous muscular branches. An isolated injury of the obturator nerve is rare. Patients with obturator nerve palsy present numbness and pain radiating to their inner thigh and an additional weakness in thigh adduction.

The pudendal nerve is a mixed motor and sensoric nerve in the pelvic region that innervates the penis or clitoris, the bulbospongious and ischiocavernous muscles, and cutaneous areas around the scrotum, perineum and anus, as well as the sphincters of the bladder and rectum. It arises from ventral division of the second (S2), third (S3) and fourth (S4) sacral nerves and passes between the piriform and coccygeal muscles to dorsally cross the spine of the sciatic bone or the sacrospinous ligament and reenter the pelvis through the lesser sciatic foramen. It is accompanied by the internal pudendal vessels along the lateral wall of the ischiorectal groove. The pudendal nerve initially gives off the inferior rectal nerves. In its further course, it divides into the perineal nerve and the dorsal nerve of the penis (in males) or the dorsal nerve of the clitoris (in females).

An isolated injury of the pudendal nerve is rare. However compression or traction of the pudendal nerve can occur during difficult childbirth, by a pelvic tumor or by bicycling: recurrent or temporary numbness of the genitals and pelvic floor or a disturbance of urination and defecation is the most frequent symptom of a pudendal nerve palsy; however, often more disturbing to the patient is a subsequent neuralgia which is often poorly treatable and recurrent. A pudendal nerve block is a rather common obstetric procedure to anesthetize the perineum during labor: it may also be done from a dorsal (gluteal) access by identifying the nerves course around the sacrospinous ligament.

6.2 Nerves in the Thoracic Wall: Topographic Overview

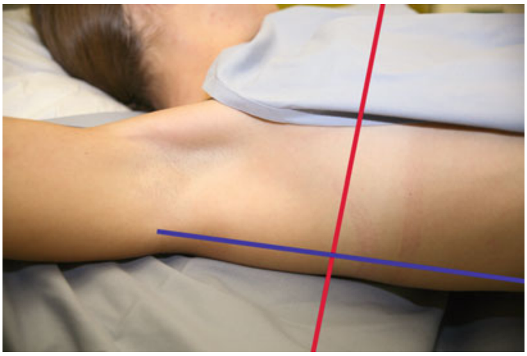

Fig. 6.1 General topographic overview of nerve anatomy in the thoracic wall. Localizer for anatomical cross section (Fig. 6.2a, b)

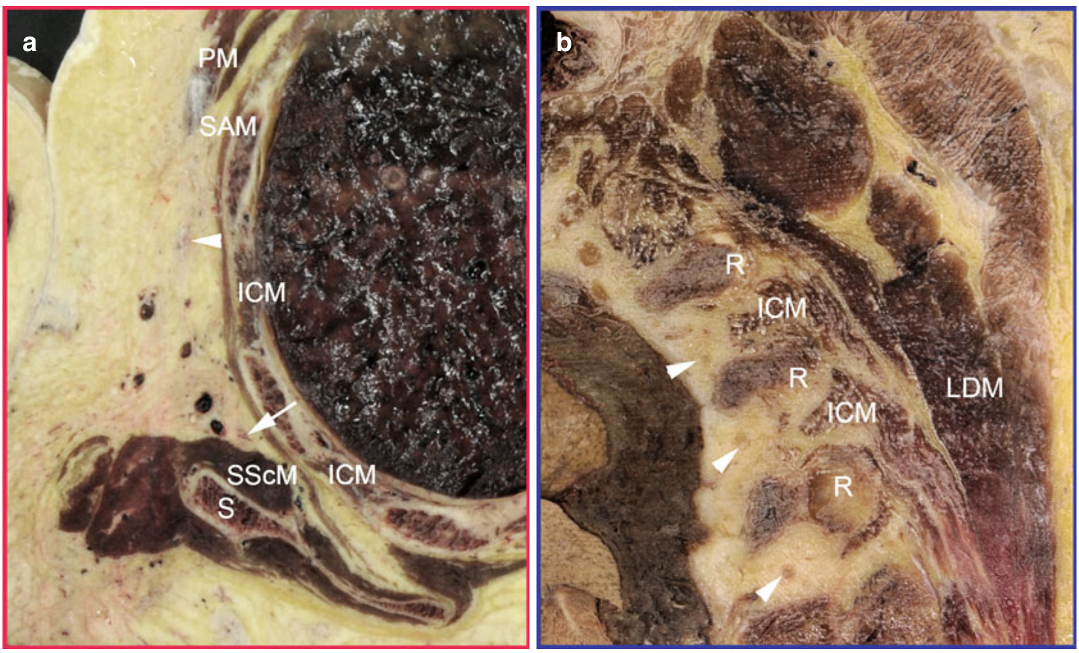

Fig. 6.2 (**a**) Anatomical cross section through the lateral thoracic wall (*red line* in Fig. 6.1). The thoracodorsalis nerve (*arrowhead*) and long thoracic nerve (*arrow*) are seen – the long thoracic nerve is accompanying the long thoracic vessels. *PM* pectoralis major and minor muscles, *SAM* serratus anterior muscle, *ICM* intercostal muscles, *SScM* subscapularis muscle, *S* scapula. (**b**) Sagittal anatomical cross section through the upper intercostal region (*red line* in Fig. 6.1). The intercostal nerves (*arrowheads*) are seen in the individual intercostal space. *ICM* intercostal muscles, *LDM* latissimus dorsi muscle, *R* ribs

6.2.1 Lateral Thoracic Wall (Thoracodorsalis Nerve)

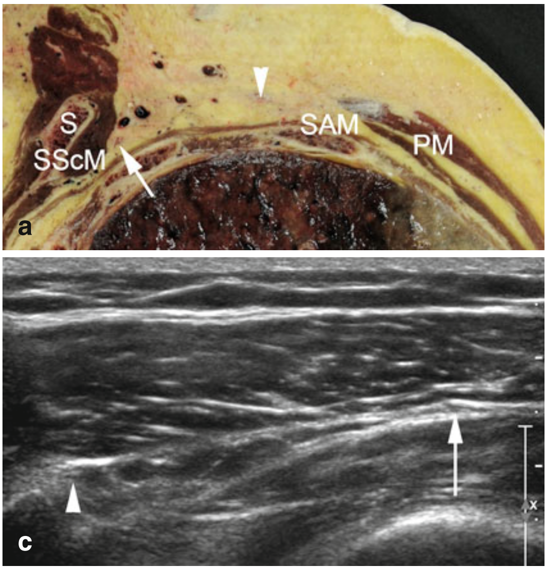

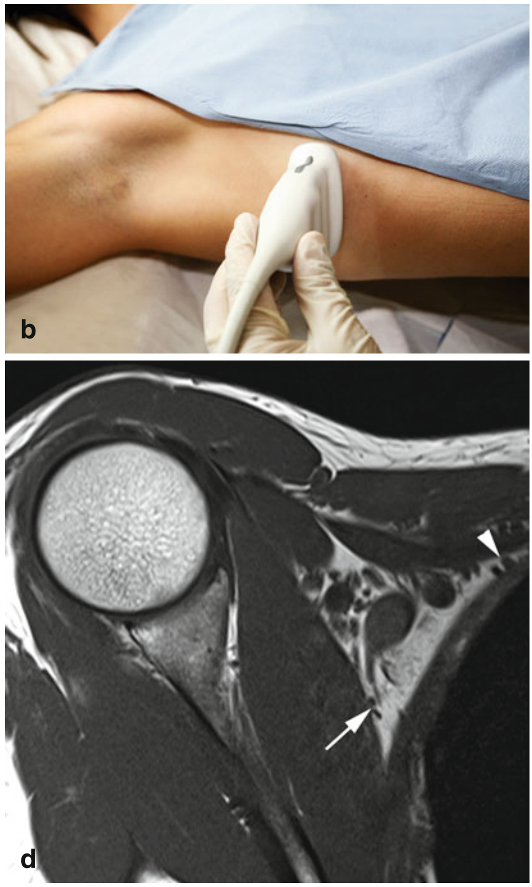

Fig. 6.3 (**a**) Anatomical cross section. (**b**) Transducer position. (**c**) Transverse sonogram. (**d**) Transverse T1-weighted MR image. Thoracodorsalis nerve (*arrowhead*), long thoracic nerve (*arrow*). *SScM* subscapularis muscle, *PM* pectoralis major and minor muscles, *SAM* serratus anterior muscle, *S* tip of scapula

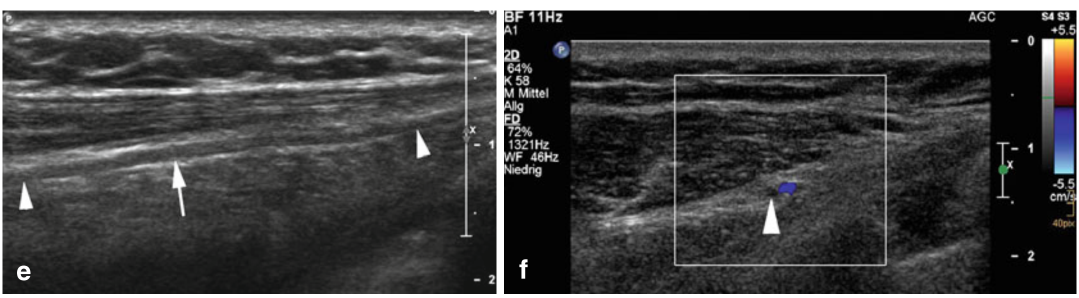

(**e**, **f**) Longitudinal sonogram (**e**) and transverse color Doppler sonogram (**f**) through thoracodorsalis nerve in a patient with paresthesia along the thoracodorsal nerve. The thoracodorsalis nerve (*arrowheads*) is continuous, but on the longitudinal view, a short segment of edema is noted (*arrow* in **e**). The relationship of the nerve to the thoracodorsal artery is depicted in **f**

6.2.1.1 Intercostal Region (Intercostal Nerves)

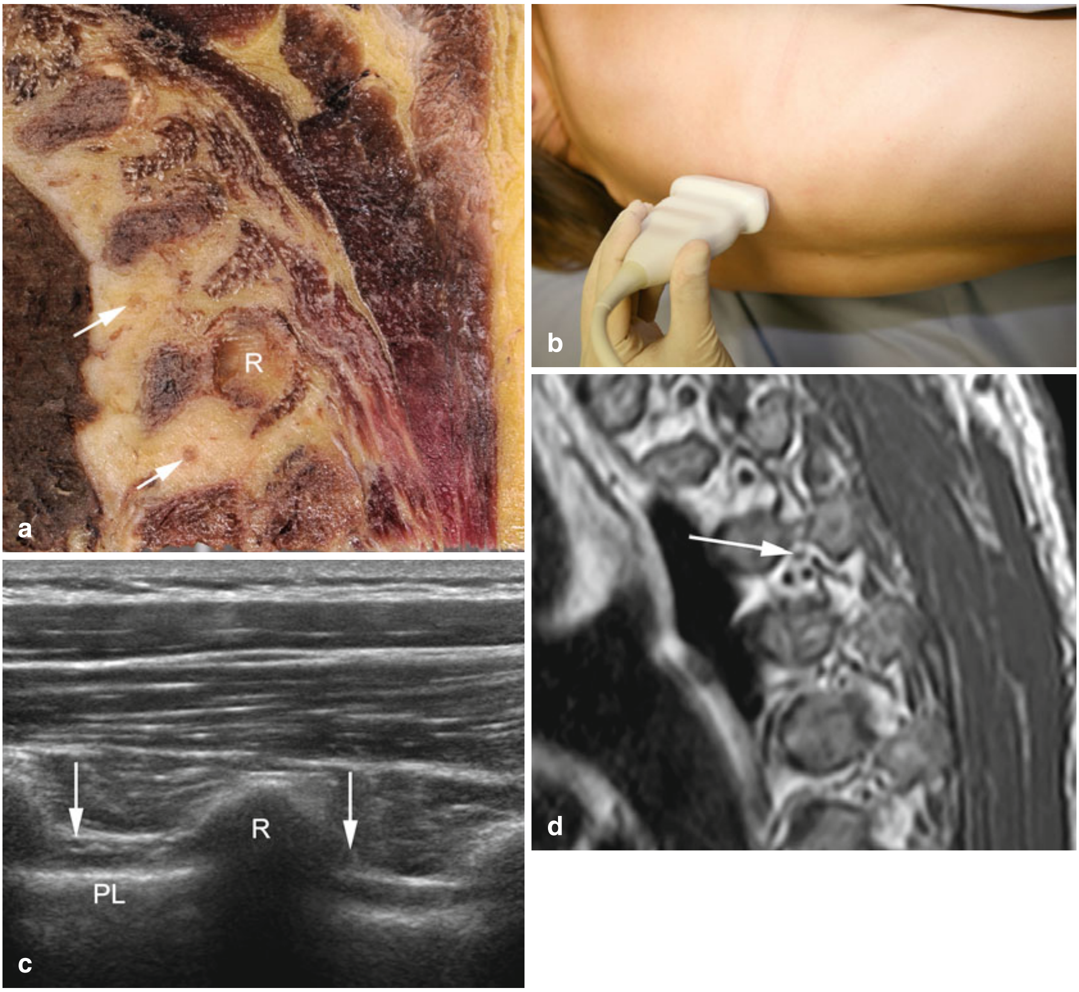

Fig. 6.4 (**a**) Anatomical cross section. (**b**) Transducer position. (**c**) Transverse sonogram. (**d**) Transverse T1-weighted MR image demonstrating intercostal nerves (*arrows*). *R* rib, *PL* pleural line

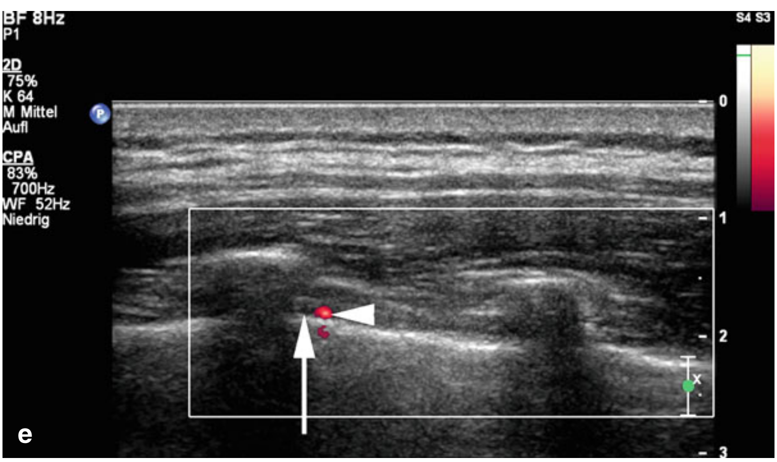

(**e**) Transverse power Doppler sonogram of the intercostal region in a healthy volunteer demonstrating the intimate relationship of the intercostal nerve (*arrow*) and the intercostal artery (*arrowhead*) both lying adjacent to the inferior edge of the rib

6.3 Border Nerves, Abdominal Wall, and Pelvic Outlet: Topographic Overview

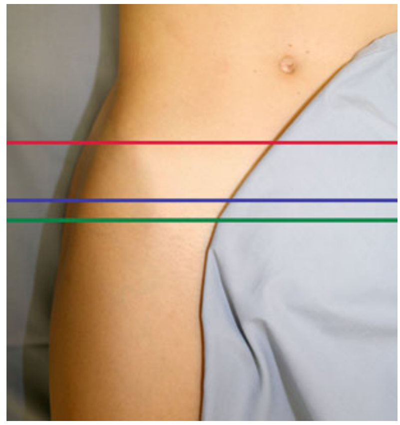

Fig. 6.5 General topographic overview of nerve anatomy in the lower abdominal wall. Localizer for anatomical cross sections (Fig. 6.6a–c). *Colored lines* correspond to level of cross sections

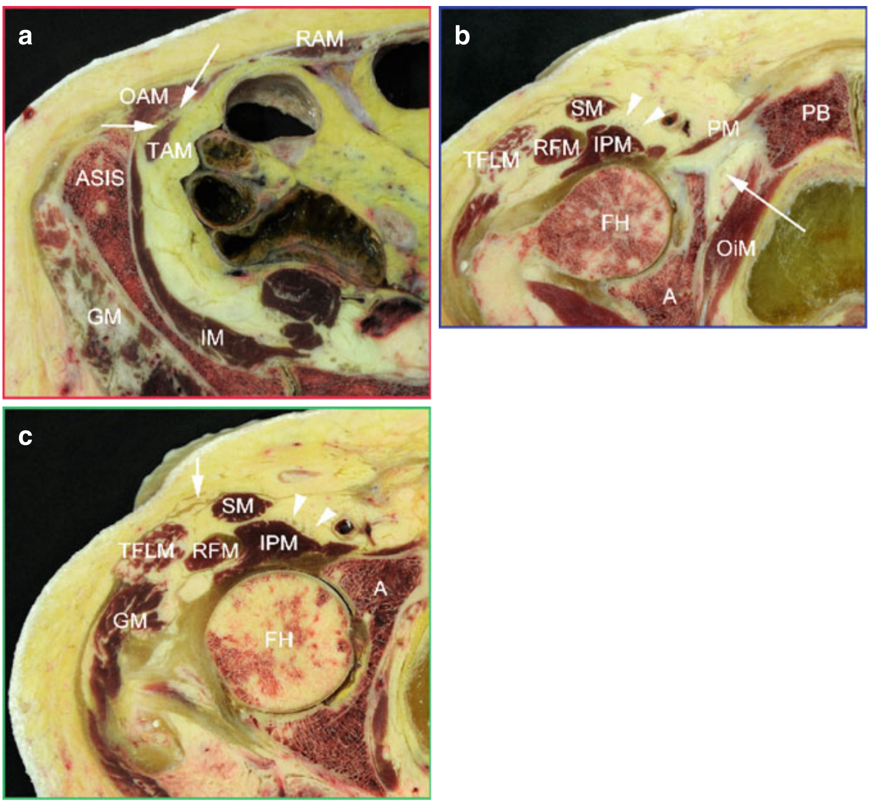

Fig. 6.6 (**a**) Anatomical cross section at the level of the anterior superior iliac spine (*red line* in Fig. 6.5). Ilioinguinal nerve (*short arrow*) positioned in the lateral and iliohypogastric nerve (*long arrow*) in the medial compartment of the plane between the oblique abdominal muscles (*OAM*) and the transverse abdominal muscle (*TAM*). *ASIS* anterior superior iliac spine, *IM* iliac muscle, *GM* gluteal muscles, *RAM* rectus abdominis muscle. (**b**) Anatomical cross section through obturator outlet (*blue line* in Fig. 6.5). Obturator nerve (*long arrow*) below the pubic bone (*PB*) after its exit through the obturator foramen. *OiM* internal obturator muscle, *PM* pectineus muscle, *IPM* iliopsoas muscle, *SM* sartorius muscle, *TFLM* tensor fasciae latae muscle, *FH* femoral head, *A* acetabulum, femoral nerve (*arrowheads*). (**c**) Anatomical cross section through lateral inguinal region (*green line* in Fig. 6.5). Lateral femoral cutaneous nerve (*arrow*) close to sartorius muscle (*SM*). Femoral nerve (*arrowheads*) adjacent to iliopsoas muscle (*IPM*). *TFLM* tensor fasciae latae muscle, *RFM* rectus femoris muscle, *GM* gluteal muscles, *FH* femoral head, *A* acetabulum

6.3.1 Abdominal Wall (Border Nerves = Ilioinguinal and Iliohypogastric Nerve)

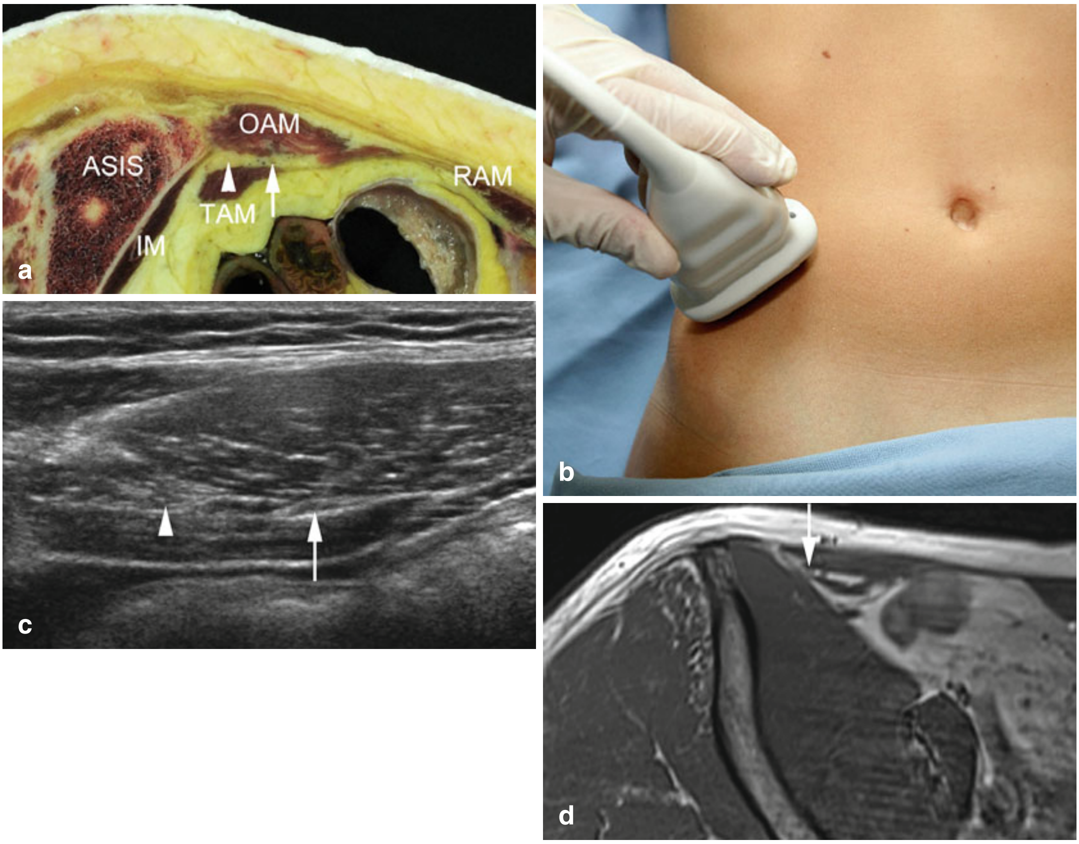

Fig. 6.7 (**a**) Anatomical cross section. (**b**) Transducer position. (**c**) Transverse sonogram. (**d**) Transverse T1-weighted MR image. The ilioinguinal nerve (*arrowhead*) and iliohypogastric nerve (*arrow*) are positioned in the fascial plane between the transverse abdominal muscle (*TAM*) and the oblique abdominal muscles (*OAM*). The nerves are positioned lateral (ilioinguinal nerve) and medial (iliohypogastric nerve) in respect to the vascular bundle. *RAM* rectus abdominis muscle, *IM* iliac muscle, *ASIS* antero superior iliac spine

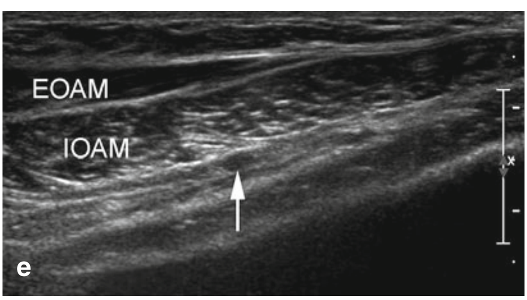

(**e**) Transverse sonogram through the abdominal wall in a patient with painful paresthesia in the lower abdominal wall after surgery. Note edema and thickening of the ilioinguinal nerve (*arrow*). *EOAM* external oblique abdominal muscle, *IOAM* internal oblique abdominal muscle

6.3.2 Obturator Foramen (Common Obturator Nerve)

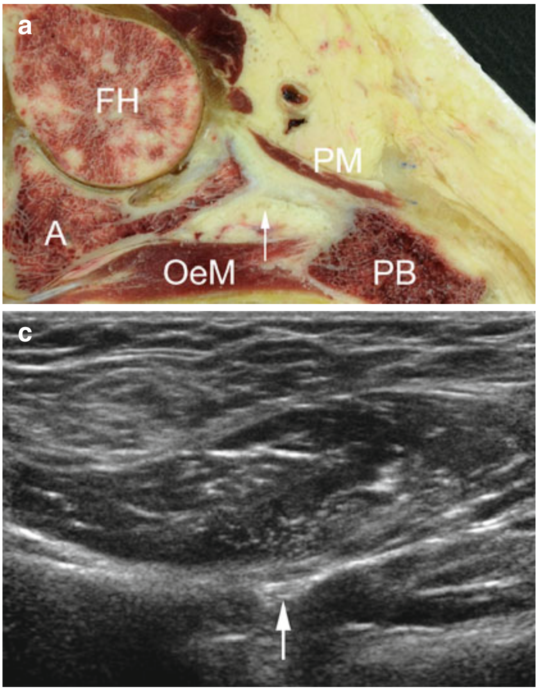

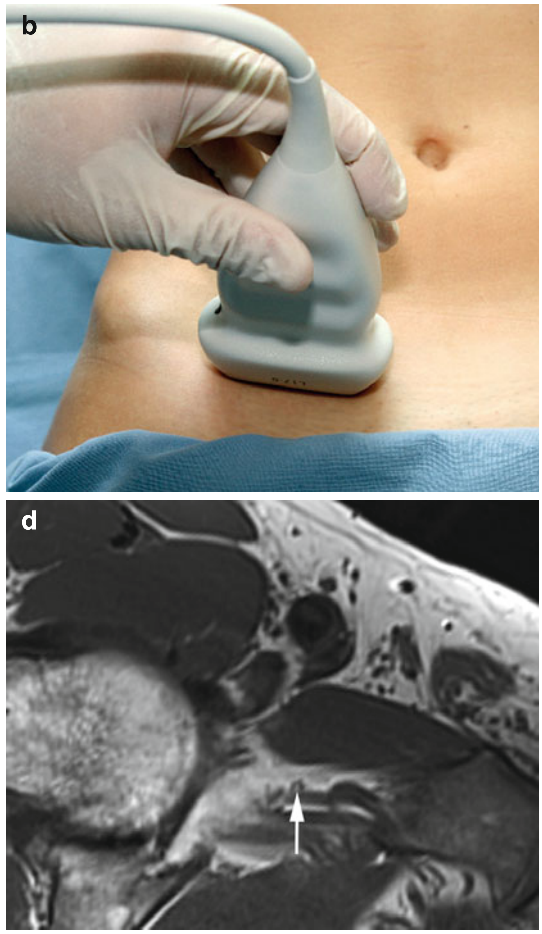

Fig. 6.8 (**a**) Anatomical cross section. (**b**) Transducer position. (**c**) Transverse sonogram. (**d**) Transverse T1-weighted MR image. The obturator nerve (*arrow*) is seen shortly after its exit from the obturator foramen in a plane between the obturator externus muscle (*OeM*) and the pectineus muscle (*PM*). *A* acetabulum, *PB* pubic bone, *FH* femoral head

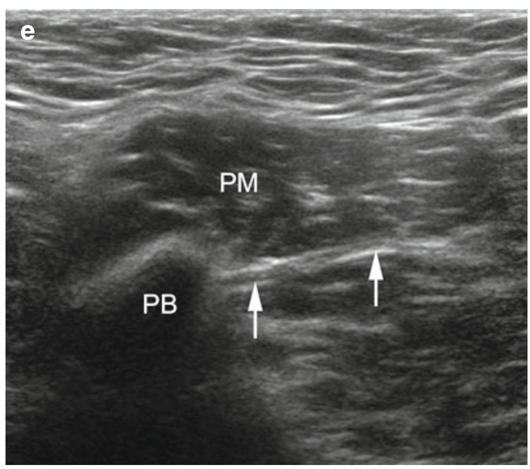

(**e**) Longitudinal view of obturator nerve (*arrows*) immediately after its exit from the obturator foramen. *PM* pectineus muscle, *PB* pubic bone

6.3.3 Lesser Trochanter (Division of Obturator Nerve)

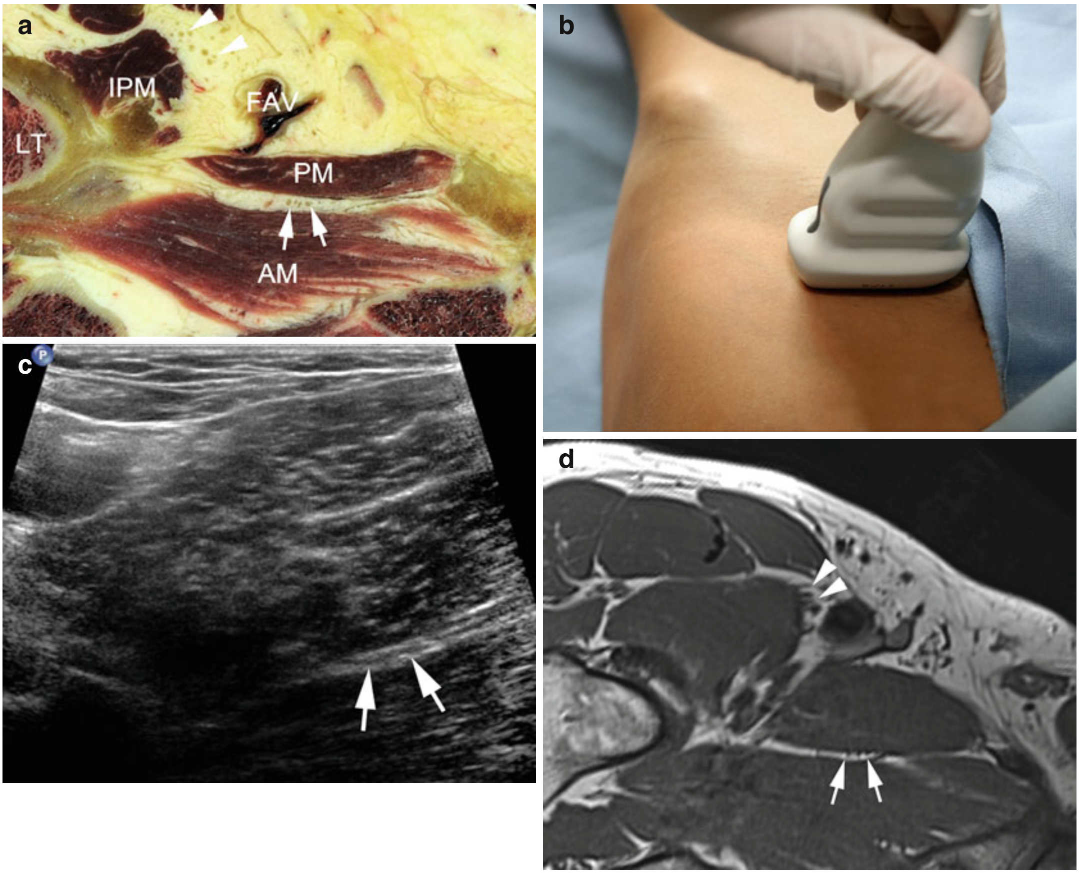

Fig. 6.9 (**a**) Anatomical cross section. (**b**) Transducer position. (**c**) Transverse sonogram. (**d**) Transverse T1-weighted MR image. The obturator nerve (*arrows*) is seen at its division into the anterior and posterior branch. It lies in plane between the pectineus muscle (*PM*) and the adductor muscles (*AM*). The division of the femoral nerve (*arrowheads*) is also seen in the anatomical cross section and the MRI. *LT* lesser trochanter, *IPM* iliopsoas muscle, *FAV* femoral artery and vein

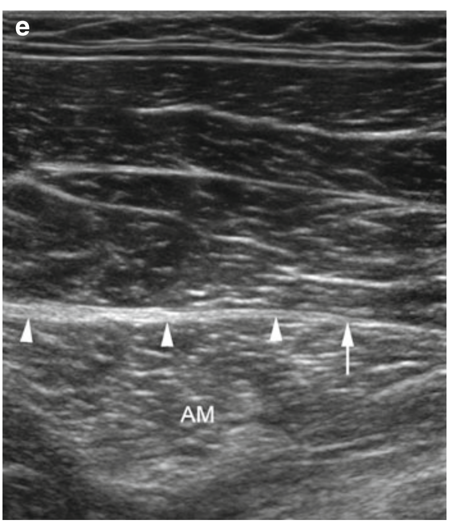

(**e**) Longitudinal sonogram of the obturator nerve division (*arrowheads*) lying on top of adductor muscles (*AM*). Note relatively abrupt distal tapering of nerve in the right side of the image (*arrow*) due to spreading into multiple tiny branches

6.3.4 Lateral Inguinal Region (Lateral Femoral Cutaneous Nerve)

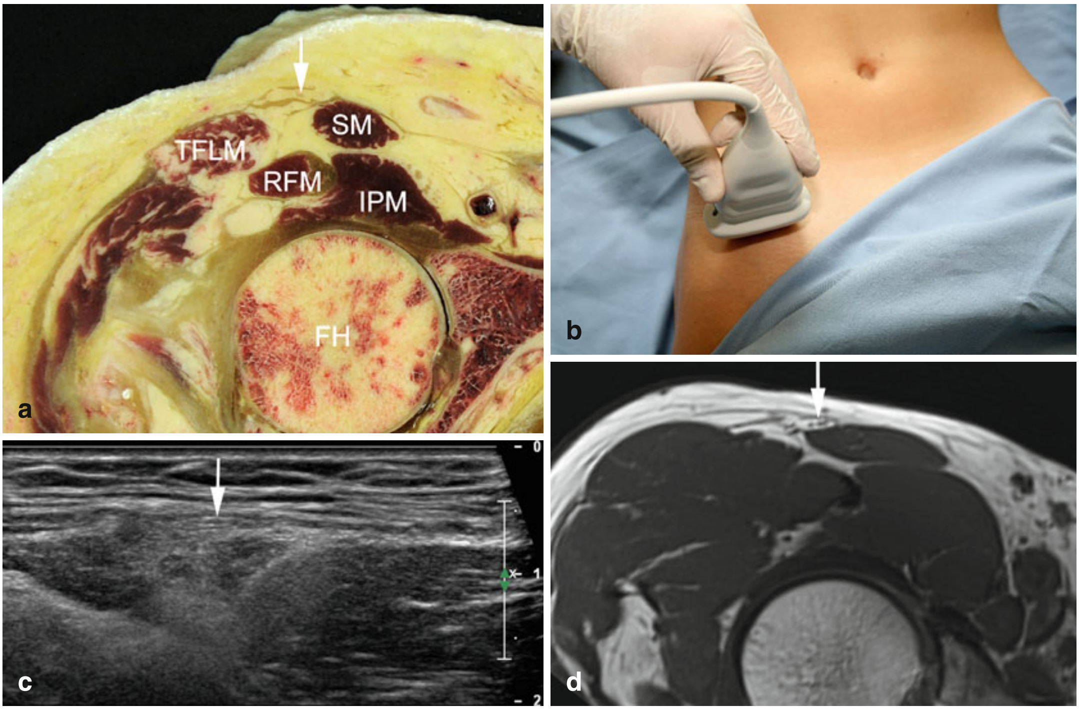

Fig. 6.10 (**a**) Anatomical cross section. (**b**) Transducer position. (**c**) Transverse sonogram. (**d**) Transverse T1-weighted MR image. The lateral femoral cutaneous nerve (*arrow*) is seen in its typical location on top of the sartorius muscle (*SM*). The triangular appearance of the muscle in the transverse sonogram is an important landmark for identification of this tiny nerve. *TFLM* tensor fasciae latae muscle, *RFM* rectus femoris muscle, *IPM* iliopsoas muscle, *FH* femoral head

(**e**) Extended field of view sonogram of the abdominal wall in the inguinal region, demonstrating the relationship of the femoral nerve (*arrow*) and the lateral femoral cutaneous nerve (*arrowhead*)

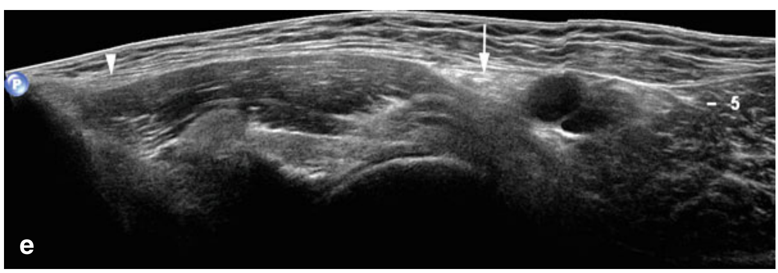

6.4 Gluteal Region: Topographic Overview

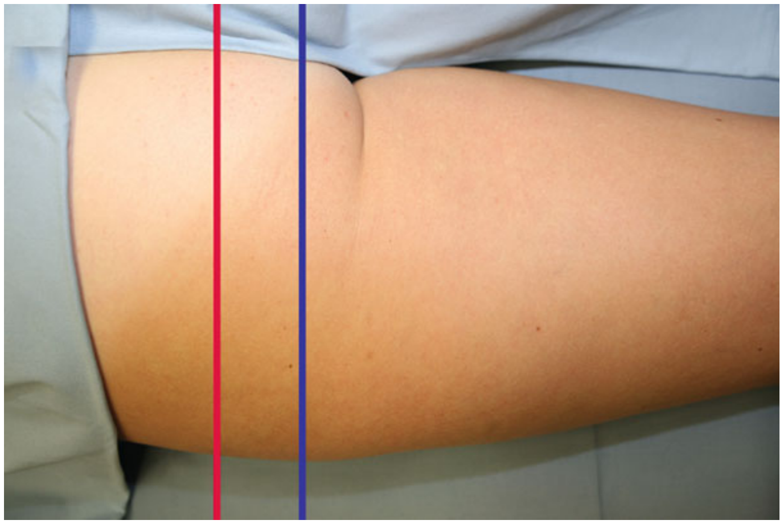

Fig. 6.11 General topographic overview of nerve anatomy in the gluteal region. Localizer for anatomical cross sections (Fig. 6.12a–b). *Colored lines* correspond to level of cross sections

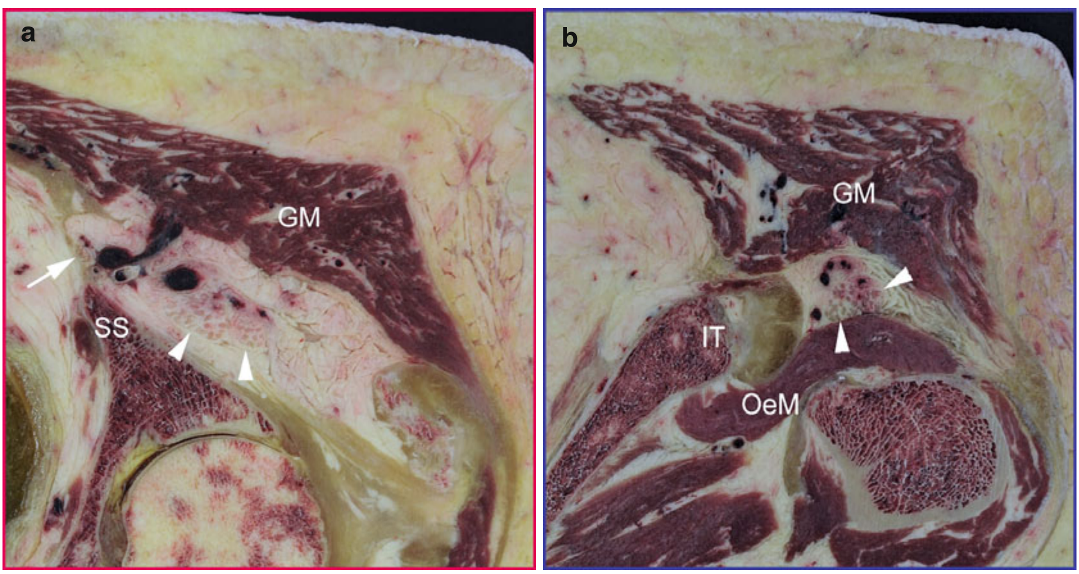

Fig. 6.12 (**a**) Anatomical cross section at the level of the sciatic spine (*red line* in Fig. 6.11). The sciatic nerve (*arrowheads*) is seen posterior to the posterior acetabular pillar. The pudendal nerve (*arrow*) abuts the sacrospinal ligament and the inferior gluteal vessels. *SS* sciatic spine, *GM* gluteal muscles. (**b**) Anatomical cross section at the level of the ischial tuberosity (*blue line* in Fig. 6.11). The sciatic nerve (*arrowheads*) runs close to the external obturator muscle (*OeM*) and the ischial tuberosity (*IT*). *GM* gluteal muscles

6.4.1 Region of the Sciatic Spine (Pudendal Nerve)

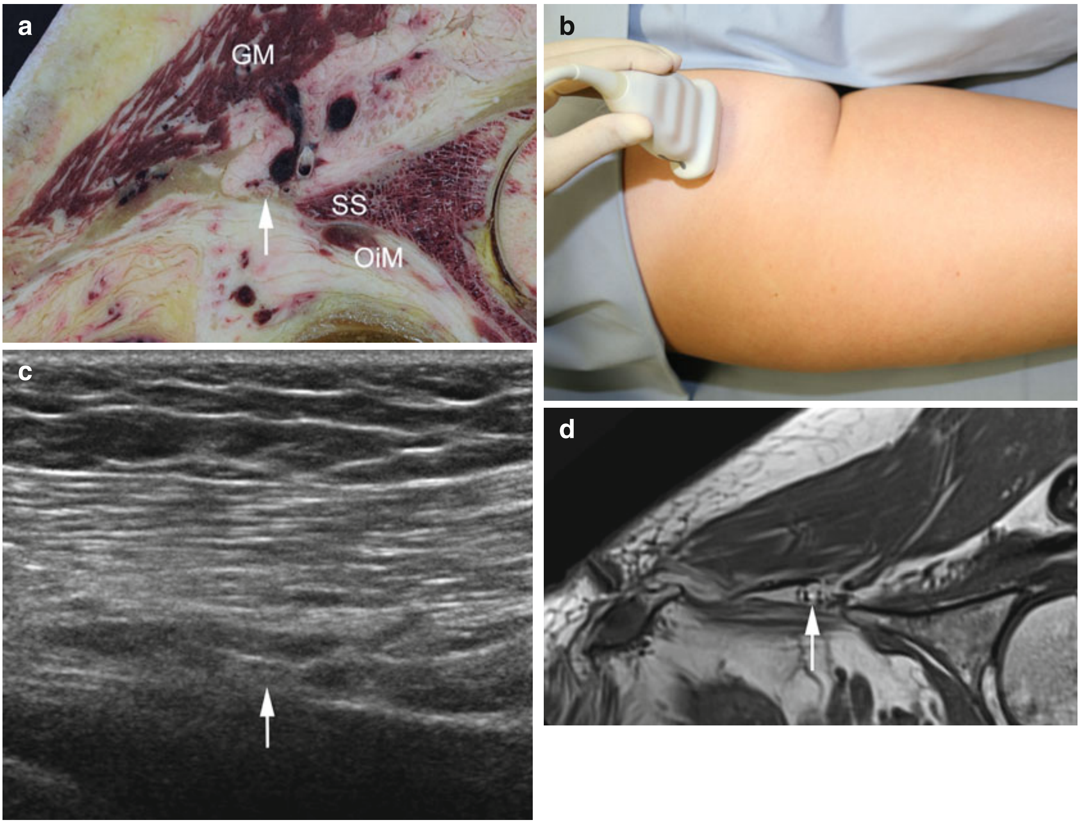

Fig. 6.13 (**a**) Anatomical cross section. (**b**) Transducer position. (**c**) Transverse sonogram. (**d**) Transverse T1-weighted MR image. The pudendal nerve (*small arrow*) is seen lateral to the inferior gluteal artery and close to the sacrospinal ligament. *SS* sciatic spine, *GM* gluteal muscles, *OiM* obturatorius internus muscle

(**e**) Transverse Duplex sonogram through the pudendal nerve (*arrowhead*) at the level of the sciatic spine. The nerve (*arrow*) is seen medial to the accompanying pudendal artery, which is an important landmark for identification of the nerve and ultrasound-guided pudendal nerve block

6.4.2 Region of the Ischial Tuberosity (Proximal Sciatic Nerve)

Fig. 6.14 (**a**) Anatomical cross section. (**b**) Transducer position. (**c**) Transverse sonogram. (**d**) Transverse T1-weighted MR image. Sciatic nerve (*arrowheads*) close to the quadratus femoris muscle (*QfM*) and underneath the gluteal muscles (*GM*). *IT* ischial tuberosity

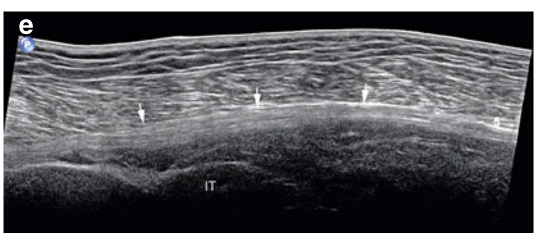

(**e**) Extended field of view sonogram of the sciatic nerve (*small arrows*) in its course from the gluteal region to the posterior thigh. *IT* ischial tuberosity

Bibliography

Abrahams MS, Horn JL, Noles LM, Aziz MF (2010) Evidence-based medicine: ultrasound guidance for truncal blocks. Reg Anesth Pain Med 35(2 Suppl): 36–42

Aravindakannan T, Wilder-Smith EP (2012) High-resolution ultrasonography in the assessment of meralgia paresthetica. Muscle Nerve 45(3):434–435

Aveline C, Le Hetet H, Le Roux A et al (2011) Comparison between ultrasound-guided transversus abdominis plane and conventional ilioinguinal/iliohypogastric nerve blocks for day-case open inguinal hernia repair. Br J Anaesth 106(3):380–386

Bærentzen F, Maschmann C, Jensen K et al (2012) Ultrasound-guided nerve block for inguinal hernia repair: a randomized, controlled, double-blind study. Reg Anesth Pain Med 37(5):502–507

Bischoff JM, Koscielniak-Nielsen ZJ, Kehlet H, Werner MU (2012) Ultrasound-guided ilioinguinal/iliohypogastric nerve blocks for persistent inguinal postherniorrhaphy pain: a randomized, double-blind, placebo-controlled, crossover trial. Anesth Analg 114(6):1323–1329

Cowie B, McGlade D, Ivanusic J, Barrington MJ (2010) Ultrasound-guided thoracic paravertebral blockade: a cadaveric study. Anesth Analg 110(6):1735–1739

Flack S, Anderson C (2012) Ultrasound guided lower extremity blocks. Paediatr Anaesth 22(1):72–80

Ford S, Dosani M, Robinson AJ, Campbell GC et al (2009) Defining the reliability of sonoanatomy identification by novices in ultrasound-guided pediatric ilioinguinal and iliohypogastric nerve blockade. Anesth Analg 109(6):1793–1798

Fornage BD (1988) Peripheral nerves of the extremities: imaging with ultrasound. Radiology 167(1):179–182

Gruber H, Kovacs P, Piegger J, Brenner E (2001) New, simple, ultrasound-guided infiltration of the pudendal nerve: topographic basics. Dis Colon Rectum 44(9):1376–1380

Herring AA, Stone MB, Nagdev AD (2012) Ultrasound-guided abdominal wall nerve blocks in the ED. Am J Emerg Med 30(5):759–764

Kim JE, Lee SG, Kim EJ, Min BW, Ban JS, Lee JH (2011) Ultrasound-guided lateral femoral cutaneous nerve block in meralgia paresthetica. Korean J Pain 24(2):115–118

Kovacs P, Gruber H, Piegger J, Bodner G (2001) New, simple, ultrasound-guided infiltration of the pudendal nerve: ultrasonographic technique. Dis Colon Rectum 44(9):1381–1385

Lee SH, Jeong CW, Lee HJ, Yoon MH, Kim WM (2011) Ultrasound guided obturator nerve block: a single interfascial injection technique. J Anesth 25(6): 923–926

Manassero A, Bossolasco M, Ugues S et al (2012) Ultrasound-guided obturator nerve block: interfascial injection versus a neurostimulation-assisted technique. Reg Anesth Pain Med 37(1):67–71

Martinoli C, Serafini G, Bianchi S et al (1996) Ultrasonography of peripheral nerves. J Peripher Nerv Syst 1:169–174

Miller BR (2011) Combined ultrasound-guided femoral and lateral femoral cutaneous nerve blocks in pediatric patients requiring surgical repair of femur fractures. Paediatr Anaesth 21(11):1163–1164

Paraskeuopoulos T, Saranteas T (2012) Ultrasound-guided obturator nerve block: the importance of the medial circumflex femoral vessels. Reg Anesth Pain Med 37(5):565

Shteynberg A, Riina LH, Glickman LT, Meringolo JN, Simpson RL (2013) Ultrasound guided lateral femoral cutaneous nerve (LFCN) block: safe and simple anesthesia for harvesting skin grafts. Burns 39(1): 146–149

Silvestri E, Martinoli C, Derchi LE et al (1995) Echotexture of peripheral nerves: correlation between US and histologic findings and criteria to differentiate tendons. Radiology 197:291–296

Tagliafico A, Serafini G, Lacelli F et al (2011) Ultrasound-guided treatment of meralgia paresthetica (lateral femoral cutaneous neuropathy): technical description and results of treatment in 20 consecutive patients. J Ultrasound Med 30(10):1341–1346

Walker FO, Cartwright MS, Wiesler ER, Caress J (2004) Ultrasound of nerve and muscle. Clin Neurophysiol 115:495–507

Weintraud M, Lundblad M, Kettner SC et al (2009) Ultrasound versus landmark-based technique for ilioinguinal-iliohypogastric nerve blockade in children: the implications on plasma levels of ropivacaine. Anesth Analg 108(5):1488–1492